



DIPARTIMENTO PER LA INNOVAZIONE NEI
SISTEMI BIOLOGICI AGROALIMENTARI E
FORESTALI - DIBAF

Università degli Studi della Tuscia

Via S. Camillo de Lellis ,01100 Viterbo

TESI SPERIMENTALE

CORSO DI LAUREA MAGISTRALE IN
“SCIENZE FORESTALI E AMBIENTALI” (CLASSE LM-73)

“
Assessing NEE and Carbon Dynamics among 5 European Forest types:
Development and Validation of a new Phenology and Soil Carbon routines
within the process oriented 3D-CMCC-Forest-Ecosystem Model”

RELATORE: Prof. Tommaso Chiti

CANDIDATO: Marconi Sergio

Matr.

CORRELATORE: Dr. Alessio Collalti,

SFA-LM 128

Prof. Riccardo Valentini

ANNO ACCADEMICO 2013/14

“As far as the laws of mathematics refer to reality, they are not certain;
as far as they are certain, they do not refer to reality.”
-- Albert Einstein (1879 – 1955 AD)

“Nature does nothing uselessly.”
-- Aristotle (384-322 BC)

Contents

Abstract (English)	6
Abstract (Italian)	8
CHAPTER 1: OBJECTIVES	10
CHAPTER 2: INTRODUCTION	14
2.1 Carbon Cycle in the Canopy: the aboveground Universe	15
2.1.1 <i>Photosynthesis</i>	15
2.1.2. <i>Respiration</i>	19
2.1.3. <i>Leaf development</i>	20
2.1.4 <i>Leaves coloring and senescence</i>	22
2.2. Carbon Cycle in Soil: the belowground Universe	24
2.2.1. <i>Forest soils</i>	24
2.2.2. <i>Organic matter input: from above and from within</i>	25
2.2.3. <i>Transformed soil Organic Carbon: the humus</i>	26
2.2.4. <i>The microbial Community: habitats and limiting conditions</i>	28
2.2.5. <i>Microfauna: nematodes and protozoa</i>	29
2.2.6. <i>Macrofauna: earthworms</i>	30
2.3. Modeling	31
2.3.1. <i>Deterministic models</i>	33
2.3.1.1. <i>Process Based Models (PBMs)</i>	34
2.3.1.2. <i>Gap Models</i>	36
2.3.2. <i>Stochastic Models</i>	38
2.3.3. <i>Hybrid models</i>	39
CHAPTER 3: THE LATITUDINAL TRANSECT	41
3.1 Area of Study	42
3.2: Climate along the transect.....	44
3.3. Stand Characteristics and Site History	44
3.3.1. <i>Renon forest (Italy)</i>	44
3.3.2. <i>Puechabon forest (France)</i>	45
3.3.3. <i>Hainich (Germany)</i>	46
3.3.4 <i>Sorø (Denmark)</i>	48
3.3.5. <i>Brasschaat (Belgium)</i>	50
3.3.6. <i>Hyytiala (Finland)</i>	52
CHAPTER 4: MATHATERIALS AND METHODS.....	53
4.1. The original version of the model	55

4.2. Improvements on the model: the 5.1 ad 6.1 versions.....	55
4.2.1. Gross primary production	58
4.2.2 Ecosystem water balance.....	60
4.2.3. Ecosystem Respiration.....	64
4.2.4. Soil respiration (SR).....	70
4.2.5. Tree Carbon Dynamics: the Phenology and Allocation routine.....	74
4.2.6. Leaf elongation: introducing the Carbon injection equation for deciduous species.....	76
4.2.7. Normal growth: Deciduous species	78
4.2.8. Senescence and yellowing: a novel semi empirical approach to reproduce leaf yellowing and littering for deciduous species	79
4.2.9. Evergreen leaves turnover: a novel competition based approach to evaluate dynamics of leaves populations.....	85
4.2.10. Tree Carbon Dynamics: littering and turnover routine.....	92
4.3. Model initialization	96
4.3.1. The simples approach.....	96
4.3.2. The Perfect Plasticity Approximation to approach an automated initialization of dominance relations	96
4.3.3. Model initialization: a mixed complex forest in the patchy rural landscape	99
4.4. Model parameterization and simulation.....	101
4.5. Eddy Covariance technique.....	101
4.6. Statistical Analysis	104
4.6.1. Regression analysis: the goodness of fit, linear regression and Coefficient of determination (R^2).....	104
4.6.2. Regression analysis: the trend line	105
4.6.3. Pearson t-test and correlation analysis: the r statistics.....	105
4.6.4. The root-mean-square error (RMSE).....	106
4.6.5. The Normalized root-mean-square error (NRMSE)	106
4.6.6. Nash Sutcliffe efficiency (NSE)	107
4.6.7. Interannual variability	108
4.6.8. Kernel density estimation.....	109
4.6.9. Chi squared normality test	110
4.6.10. Student's two sample t-test	111
4.6.10. Mann-Whitney U-test for equivalence of the median	111
4.6.11. F-Fisher test for variance equality.....	112
CHAPTER 5: RESULTS	114

5.1. Results of GPP modeled	115
5.1.1. Annual and seasonal trends in GPP estimation	115
5.1.2 Validation of 3D-CMCC-Pheno GPP results on daily and monthly temporal resolution ...	121
5.1.3. 3D-CMCC-Pheno FEM Performance for inter monthly, seasonal and annual variability of GPP	126
5.1.4. Comparison with the 5.1 version of 3D-CMCC-FEM	134
5.2. Results of Reco modeled.....	138
5.2.1 Annual and seasonal trends in Reco estimation.....	138
5.2.2 Validation of 3D-CMCC-Pheno Reco results on daily and monthly temporal resolution	143
5.2.3 3D-CMCC-Pheno FEM Performance for inter monthly, seasonal and annual variability of Reco	148
5.2.4. Aboveground and Belowground Autotrophs and Heterotrophic components of Reco	157
5.3. Results of NEE modeled	161
5.3.1 Annual and seasonal trends in NEE estimation	161
5.3.2 Validation of 3D-CMCC-Pheno NEE results on daily and monthly temporal resolution..	165
5.3.3 3D-CMCC-Pheno FEM Performance for inter monthly, seasonal and annual variability of NEE	170
5.4. Soil Carbon dynamics	178
CHAPTER 6: DISCUSSION	181
6.1. Phenology in the 6.1.v 3D-CMCC-FEM:	182
6.2. GPP in the 6.1.v 3D-CMCC-FEM:	185
6.3. Respiration in the 6.1.v 3D-CMCC-FEM.....	187
6.4. NEE in the 6.1.v 3D-CMCC-FEM.....	189
6.5. SOC dynamics in the 6.1.v 3D-CMCC-FEM	190
CHAPTER 7: CONCLUSIONS	192
BIBLIOGRAPHY	195
Appendix 1: Parameterization.....	219
A1.1. <i>Pinus sylvestris</i> (L.) parameters set.....	219
A1.2. <i>Picea abies</i> (L.) parameters set	222
A1.3. <i>Quercus ilex</i> (L.) parameters set	225
A1.4. <i>Quercus robur</i> (L.) parameters set	229
A1.5. <i>Fagus sylvatica</i> (L.) parameters set.....	232
Appendix 2: Initialization sets	236
A2.1. ITRen initialization data	236
A2.2. FRPue initialization data.....	237
A2.3. DEHai initialization data	237
A2.4. DKSor initialization data.....	238
A2.5. BEBra initialization data (Pedunculate Oak stand).....	238
A2.6. BEBra initialization data (Scot Pine stand)	239
A2.7. FIHyy initialization data	240
ACKNOWLEDGEMENTS	241

Abstract (English)

The two main processes involved in forest ecosystems carbon balance are photosynthesis (GPP) and respiration. Ecosystem respiration (Reco) is determined by heterotrophic and autotrophic respiration, the former driven by microbial decomposition of soil organic matter (SOM), the latter by growth and maintenance of plant tissues. By differencing photosynthesis and respiration we have an estimate of the global carbon budget of a forest ecosystem, namely the Net Ecosystem Exchange (NEE).

In this purpose, the aim of this work was to implement the 3D-CMCC-Forest Ecosystem Model (6.1.) to better estimate GPP and assess the C cycle in European forests. We included a new soil Carbon dynamics routine and several modifications in phenology, respiration and littering. Bud burst phenology has been improved with a new “Nonstructural Carbon injection function” representing the quantity of Carbon daily destined to new leaves and fine roots development. Fall phenology has been improved with a novel semi empirical logistic function to simulate leaf falling. Evergreen leaves turnover has been completely redesigned following an intra-crown competition logic. Soil carbon dynamics through the Residues, Microbial and Humus pools have been developed following a zero order kinetics equation, representing microbial decomposition activity. Autotrophic respiration has been implemented with a soil water potential factor to represent stomata closure when drought occurs. A new canopy vertical structure initialization rationale has been developed using the Perfect Plasticity Approximation algorithm; unfortunately it could be tested only on sites where dendrometric data were available.

3D-CMCC-FEM 6.1.v was validated against 6 EddyCovariance CarboEurope towers, representing 5 of the most diffuse forest ecosystems in Europe. The sites have been chosen to represent a climatic and longitudinal transect trough the European continent, so that the model could be tested on different critical boundary conditions. The GPP, Reco and NEE fluxes were validated for about 10 years at each site.

To evaluate the model efficiency we tested daily and monthly correlation, Nash-Sutcliffe Model Efficiency, Goodness of Fit to a mono parametric linear regression. The model’s plasticity and ability in representing observed anomalies was determined by analyzing inter annual, month and seasonal variability following published methods. We then statistically inferred the relationships between expected and observed frequency distributions of the anomalies.

The results were quite encouraging; GPP r^2 was averagely 0.74 (daily) and 0.89 (monthly), the RMSE of about $1\text{gC m}^{-2} \text{d}^{-1}$, the NSE greater than 0.7. Anomalies results were very good too; the NRMSE was averagely of $1.2 \text{gC m}^{-2} \text{d}^{-1}$ and their distribution were always significantly consistent with the observed ones. Reco r^2 was averagely 0.59 (daily) and 0.69 (monthly), the RMSE of about $0.83 \text{gC m}^{-2} \text{d}^{-1}$, the NSE greater than 0.54 (daily) and .75 (monthly). Anomalies results were very good too; the NRMSE was averagely of $1.2 \text{gC m}^{-2} \text{d}^{-1}$, their sign was captured for about 70% of the times and their distribution were always significantly consistent with the observed ones. The propagation of uncertainties resulted in NEE r^2 averagely of 0.56

(daily) and 0.89 (monthly) (0.66 and 0.82 excluding the Mediterranean forest), the RMSE of about $1.5 \text{ gC m}^{-2} \text{ d}^{-1}$, the NSE greater than 0.51 excluding the negative value of the Q. ilex stand. Anomalies results were acceptable and in line with the other PBMs in literature. Even though the NRMSE was averagely of $1.3 \text{ gC m}^{-2} \text{ d}^{-1}$ the frequency distribution of the anomalies distribution coincided with the observed ones just for half the sites.

The model showed interesting improvements from the 5.1. version (in prep.), even more from the published 4.0 version. The model showed its weakness in representing the Mediterranean Forests, probably because of the over simplistic way to represent soil water dynamics and stresses. The use of the water potential RA limiting factor apparently confirmed this hypothesis, since Reco was significantly improved and gave even better results than GPP after its implementation.

In conclusion this work positively achieved its objectives. The model now reliably estimate all the components of the C cycle for the main European forest ecosystems. The new functions resulted in better GPP and RA estimation, finally allowed the model to simulate RH, Reco and NEE, and introduced new ideas to the forest modeling international panorama. The 6.1. version thus has wider perspectives and applicability and may be taken into account for several different applications; from predicting the net C cycle on regional scale, to assisting future forest management on finer scales up to 1 hectare.

Abstract (Italian)

I due principali processi coinvolti nel bilancio del Carbonio in ecosistemi forestali sono fotosintesi e respirazione. La respirazione ecosistemica è determinata dalla somma tra la componente eterotrofa ed autotrofa; la prima è guidata dai processi di decomposizione della sostanza organica del suolo (SOM), la seconda dalla respirazione di crescita e di mantenimento dei tessuti vegetali. Pertanto è estremamente importante quantificare in modo affidabile ogni componente della respirazione ecosistemica per stimare il bilancio globale del carbonio di un ecosistema forestale, cioè la Net Ecosystem Exchange (NEE).

Lo scopo del presente lavoro è stato quello implementare una nuova versione di 3D-CMCC-Forest Ecosystem Model (6.1), al fine di migliorarne l'efficienza nella stima della GPP, e renderlo in grado di simulare il ciclo del Carbonio nelle foreste Europee. Contestualmente sono stati sviluppati un modello di dinamica del Carbonio nel suolo e diverse modifiche nel riprodurre fenologia, respirazione e formazione della lettiera.

La fase di schiusura delle gemme primaverili è stata migliorata con una nuova funzione "Non structural Carbon injection", sviluppata per determinare la quantità giornaliera di Carbonio destinato allo sviluppo dei germogli fogliari e delle radici fini. La fenologia autunnale è stata migliorata con una nuova funzione logistica semi empirica per simulare la fase di caduta delle foglie. Il ricambio fogliare nelle specie sempreverdi è stato completamente ridisegnato. Il nuovo modello di dinamica fogliare segue la logica di un modello teorico di concorrenza all'interno della corona. La dinamica del carbonio del suolo entro i compartimenti di "Lettiera", "Biomassa microbica" e "Sostanze umiche" è stato sviluppato a partire da un modello cinetico di ordine zero, e rappresenta la decomposizione della SO ad opera della biomassa microbica. Alla respirazione autotrofa è stato aggiunto un nuovo fattore limitante legato alla differenza di potenziale idrico tra suolo e pianta, per rappresentare l'effetto della chiusura stomatica in caso di siccità. È stata sviluppata una nuova funzione di inizializzazione della struttura verticale della foresta, integrando l'algoritmo "Perfect plasticity approximation"; al momento è utilizzabile solo per i siti di cui sono disponibili misure dendrometriche.

Per valutare questi miglioramenti 3D-CMCC-FEM 6.1. è stato validato usando i dati di 6 torri Eddy Covariance (siti CarboEurope), che rappresentano i 5 ecosistemi forestali più diffusi in Europa. I siti sono stati scelti lungo un transetto climatico e longitudinale del continente, in modo da testare il modello nelle più disparate condizioni di criticità. I flussi di GPP, Reco e NEE sono stati validati per circa 10 anni per sito. Per valutare l'efficienza del modello abbiamo testato i risultati delle simulazioni su scala giornaliera e mensile, valutando il grado di correlazione con i dati EC, l'indice di efficienza di Nash-Sutcliffe, il grado di fitting con una relazione lineare di tipo uniparametrico. Per valutare la plasticità e la capacità del modello di rappresentare le anomalie osservate abbiamo quantificato la variabilità inter annuale, mensile e stagionale come da letteratura. Abbiamo anche testato statisticamente il grado di omogeneità tra la distribuzione di frequenza delle anomalie attese e osservate.

I risultati sono incoraggianti; l' r^2 per la GPP è stato mediamente di 0,74 (scala giornaliera) e 0.89 (mensile), l'RMSE di circa $1\text{gC m}^{-2} \text{d}^{-1}$, la NSE maggiore di 0,7. Risultati relativi alle anomalie sono apparsi buoni; l'NRMSE era mediamente di 1,2

$\text{gC m}^{-2} \text{ d}^{-1}$ e la loro distribuzione significativamente coerente con le anomalie osservate. Reco r^2 era mediamente 0,59 (giornaliera) e 0,69 (mensile), l' RMSE di circa $0,83 \text{ gC m}^{-2} \text{ d}^{-1}$, la NSE superiore a 0,54 (giornaliero) e 0,75 (mensile). Risultati relativi alle anomalie sono apparsi buoni; l'NRMSE era mediamente di $1,2 \text{ gC m}^{-2} \text{ d}^{-1}$, il segno delle anomalie osservate è stato catturato circa il 70% dei casi e la loro distribuzione sempre significativamente coerente. La propagazione delle incertezze ha influito sui risultati meno buoni di NEE, con r^2 mediamente di 0,56 (giornaliero) e 0,89 (mensile) (0,66 e 0,82 escludendo la foresta mediterranea), RMSE di circa $1,5 \text{ gC m}^{-2} \text{ d}^{-1}$, NSE maggiore di 0,51 escluso il negativo valore della lecceta. I risultati della riproduzione delle anomalie erano in linea con gli altri PBMs testati in letteratura. Tuttavia, nonostante gli NRMSE mediamente di $1,3 \text{ gC m}^{-2} \text{ d}^{-1}$ la distribuzione delle anomalie osservate e simulate sono risultate significativamente dissimili per la metà dei casi.

In conclusione, il modello ha mostrato interessanti miglioramenti dalla versione 5.1. (in prep.), ancor più evidenti rispetto alla versione 4.0 pubblicata. Il modello si è però mostrato debole nel rappresentare le foreste mediterranee, probabilmente a causa del modo troppo semplicistico di rappresentare il ciclo dell'acqua nel suolo e li stress idrici. L'utilizzo del nuovo fattore limitante la respirazione autotrofa confermerebbe questa ipotesi, in quanto, dopo averlo integrato, la Reco è stata significativamente migliorata e ha dato risultati anche migliori rispetto a GPP.

In conclusione, il presente lavoro ha raggiunto positivamente i suoi obiettivi. Il modello ora simula in modo affidabile tutte le componenti del ciclo del Carbonio per i principali ecosistemi forestali europei. Le nuove funzioni hanno portato al miglioramento della stima di GPP e RA, permettono di quantificare RH, Reco ed NEE, ed hanno introdotto nuove idee nel panorama internazionale della modellistica forestale ed ecologica.

La presente versione ha quindi più ampie prospettive e applicabilità e può essere presa in considerazione per diverse applicazioni; dalla previsione del ciclo netto del Carbonio su scala regionale, all'assistenza per le pratiche di gestione forestale su scala ridotta fino a 1 ettaro.

CHAPTER 1: OBJECTIVES

Passing from a monthly time scale to a finer daily scale in simulating C fluxes within a forest imply several problems need to be solved. The 4.0 version of 3D-CMCC FEM (Collalti et al., 2014) was allowed to have a very simplistic phenology routine, respiration was considered as a constant proportion of GPP and soil C dynamics could be ignored. With the 5.1. version we introduced more complex respiration and phenology routines, mainly integrating the ones of the Biome Family models (Collalti et al., in prep). However these routines in our opinion were still over simplistic. Respiration was mainly driven by empirical relations, tree C turnover functions were not accompanied by strong theoretical/mathematical analyses (i.e. leaves/roots littering, represented as a linear constant decay of the previous year biomass). These simplifications implied a wide number of artifacts (i.e. bud burst anomalous respiration) which could mine the quality of the modeled gross Carbon production and estimation of variability.

Moreover 3D-CMCC-FEM main novelty was the ability of represent the stand vertical structure; but when/how a more complex structure should be considered? In a previous work or ours (Marconi et al., 2013) we compared simulations with different levels of canopy complexity and concluded that the use of a multilayer canopy may not be always useful. Thus the development of a system able to automatically and not arbitrarily infer the difference in height between different cohorts would be fundamental to initialize the quantity of height layers at the beginning of each year of simulation.

Finally up to the 5.1.v the model was able to quantify only Gross Primary Production (GPP) and Net primary production, which was

sufficient for a Forest yield model. However in the context of the biogeochemical C cycle it is extremely important to determine the total Ecosystem Respiration and thus quantify the net Ecosystem Carbon Exchange. As a consequence it was determinant to be able to evaluate soil Carbon dynamics, fresh organic matter supply, and microbial population dynamics.

These considerations led to the development of the 6.1.version, the modeling work presented in this dissertation. To improve leaf/fineroots turnover, forest littering, soil C dynamics and tree phenology I coupled different theoretical, ecophysiological, mathematical and statistical techniques. Another important objective for the next future resides in making the 3D-CMCC usable on regional scale. Thus the model was yet parameterized on a species specific basis, but validated against the main European forest ecosystems, to check its potential ability to simulate C net fluxes, forest structure and dynamics on diametrical different ecosystems and continental scale.

The resulted model structure was holistic, thus the results should be seen in the perspective of the whole forest ecosystem, and not as separate responses in individual compartments of the forest. Results from changes in the biomass, soil chemistry and organic matter along with the structure of vegetation community should be considered as indicators of the status of the forest ecosystem as a 3 whole.

The main aims of this thesis resides in developing, parameterizing, validating and presenting the dynamic Ecosystem and Soil model 3D-CMCC-FEM 6.1 (Marconi et al., in prep), to describe its use, and to evaluate its strengths and weaknesses compared with the 5.1 version

(Collali et al., in prep). The model structure and assumptions are presented and evaluated, with the objective of providing a transparent picture of the model.

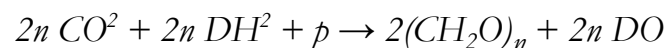
CHAPTER 2: INTRODUCTION

2.1.1 Photosynthesis

Photosynthesis is a process used by plants and other organisms to convert light energy, normally from the Sun, into chemical energy that can be later released to fuel the organisms' activities. This chemical energy is stored in carbohydrate molecules, such as sugars, which are synthesized from carbon dioxide and water (Lehninger et al., 2008).

Carbon fixation is an endothermic redox reaction, so photosynthesis needs to supply both a source of energy to drive this process, and the electrons needed to convert carbon dioxide into a carbohydrate. This addition of the electrons is a reduction reaction. In general outline photosynthesis is the opposite of cellular respiration, in which glucose and other compounds are oxidized to produce carbon dioxide and water. However, the two processes take place through a different sequence of chemical reactions and in different cellular compartments.

The general equation for photosynthesis is therefore:



(Eq. 2.1.)

Photosynthesis occurs in two stages, generally referred as the light and dark phases.

The process always begins when energy from light is absorbed by the reaction centers that contain green chlorophyll pigments; these proteins reside in the chloroplasts, mainly in leaves. In the light-dependent reactions some energy is used to strip electrons from suitable substances

such as water, producing O₂, reduced Nicotinamide Adenine Dinucleotide Phosphate (NADPH) and Adenosine Triphosphate (ATP). As a matter of fact, one molecule of the pigment chlorophyll absorbs one photon and loses one electron. The photons are captured in the light-harvesting antenna complexes of photosystem II by chlorophyll and other accessory pigments. When a chlorophyll molecule at the core of the photosystem II reaction center obtains sufficient excitation energy from the adjacent antenna pigments, an electron is transferred to the primary electron-acceptor molecule, pheophytin, through a process called photo induced charge separation. These electrons are shuttled through an electron transport chain, the so called Z-scheme shown in the diagram (Fig. 2.1.).

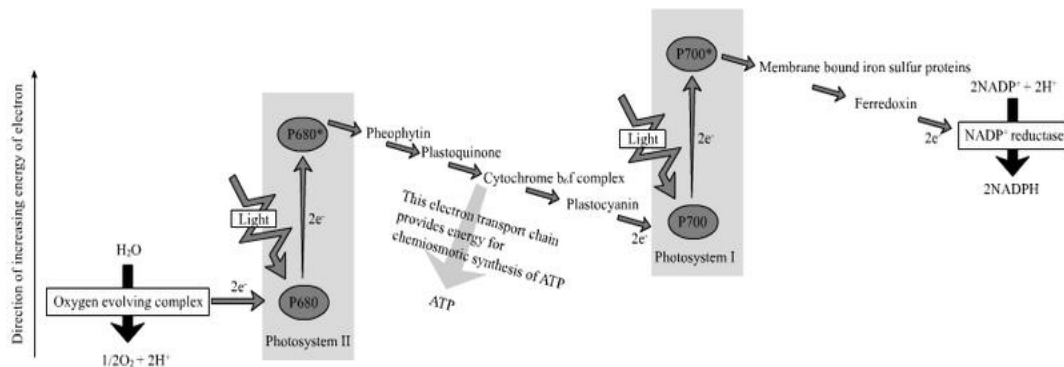
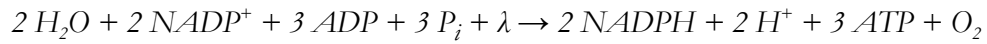


Fig. 2.1 Representation of the Z-scheme of Photosynthesis light phase

This flow of electrons down an electron transport chain leads to the ultimate reduction of NADP to NADPH, and creates a proton gradient across the chloroplast membrane, whose dissipation is used to reduce further ATP. The chlorophyll molecule regains the lost electron from a water molecule through a process called photolysis, releasing O₂. Thus the overall equation for the light-dependent reactions under the

conditions of non-cyclic electron flow in green plants follows Raven et al. (2005):

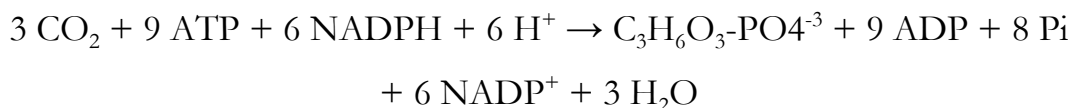


The source of electrons in green-plant photosynthesis is water. Two water molecules are oxidized by four successive charge-separation reactions by photosystem II to yield a molecule of diatomic oxygen and four hydrogen ions; the electron yielded in each step is transferred to a redox-active tyrosine residue.

The photosynthetic action spectrum depends on the type of accessory pigments present; the action spectrum in green plants resembles the absorption spectrum for chlorophylls and carotenoids with peaks for violet-blue and red light.

Sugars are produced by a subsequent sequence of light-independent reactions called the Calvin cycle (Fig. 1.2.); in this chain of reactions the atmospheric carbon dioxide is incorporated into already existing Organic Carbon compounds (Reece et al., 2006). During the Calvin Cycle the ATP and NADPH produced by the light-dependent reactions get oxidized to reduce carbohydrates such as glucose.

In the reactions, the enzyme RuBisCO captures CO₂ from the atmosphere and releases three-carbon sugars in a process that requires the newly formed NADPH. These primordia molecules are later combined to form sucrose and starch. The overall equation for the light-independent reactions in green plants is:



(Eq. 2.2.)

The fixation or reduction of carbon dioxide is a process in which carbon dioxide combines with a five-carbon sugar, Ribulose 1,5-bisphosphate (RuBP), to yield two molecules of a three-carbon compound, glycerate 3-phosphate (GP). ATP and NADPH formerly reduced drive the reduction of GP into Glyceraldehyde 3-phosphate (G3P). 5 out of 6 produced molecules of G3P are used to regenerate RuBP, the last one is used to ultimately yield sucrose, starch and cellulose. These sugars finally yield carbon skeletons that can be used for other metabolic reactions like the production of amino acids and lipids.

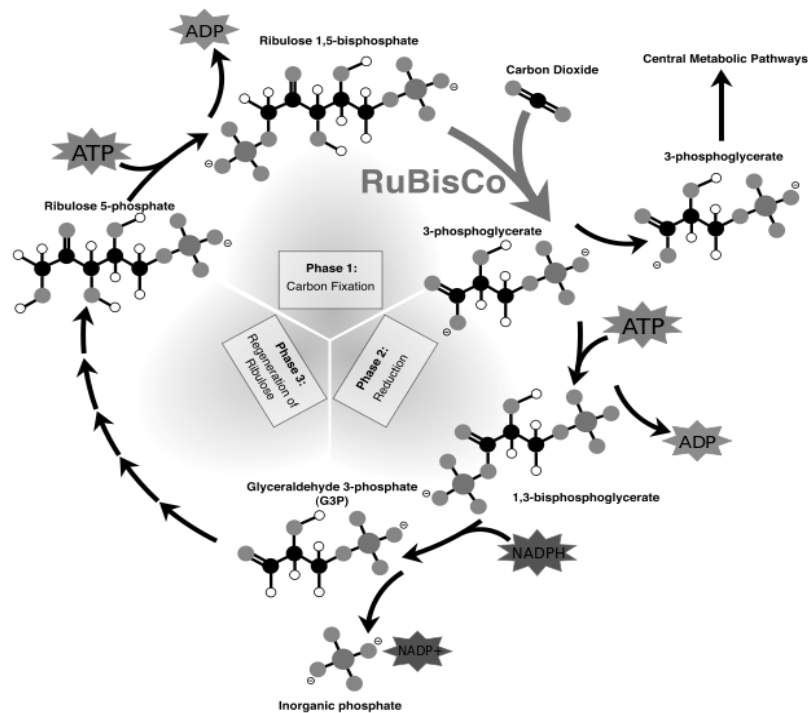


Fig. 2.1 Calvin Cycle

Plants usually convert light into chemical energy with a photosynthetic efficiency of 3–6% (Maxwell et al., 2000). The rest of the absorbed light is dissipated primarily as heat or re-emitted as chlorophyll fluorescence (1-2%). Actual plants' photosynthetic efficiency varies with the frequency

of the light being converted, light intensity, temperature and proportion of carbon dioxide in the atmosphere, and can vary from 0.1% to 8%.

2.1.2. Respiration

Cellular respiration is the set of metabolic reactions and processes that take place in the cells of organisms to convert biochemical energy from nutrients into adenosine triphosphate (ATP), and then release waste products. The reactions involved in respiration are catabolic reactions, which break large molecules into smaller ones, releasing energy in the process as "high-energy" bonds are replaced by stronger bonds in the products. Respiration is one of the key ways a cell gains useful energy to fuel cellular activity. Cellular respiration is considered an exothermic redox reaction which releases heat. The overall reaction occurs in a series of biochemical steps, most of which are redox reactions themselves. Although cellular respiration is technically a "combustion" reaction, it clearly does not resemble one when it occurs in a living cell due to slow release of energy from the series of reactions.

Plant cellular respiration is usually divided into growth and maintenance respiration. Growth respiration is essentially the one involved in cellular division, elongation and differentiation. Maintenance is the one involved in the generation of usable energy (mainly ATP, NADPH, and NADH) and metabolic intermediates used for (Penning de Vries, 1975; Lambers et al., 1983, 1989; Amthor, 2000):

1. re-synthesis of compounds that undergo renewal (turnover) in the normal process of metabolism (examples are enzymatic proteins, ribonucleic acids, and membrane lipids);

2. maintenance of chemical gradients of ions and metabolites across cellular membranes that are necessary for cellular integrity and plant health;
3. operation of metabolic processes involved in physiological adjustment (i.e., acclimation) to a change in the plant's environment.

The metabolic costs of the repair of injury from biotic or abiotic stress may also be considered a part of maintenance respiration (Penning de Vries, 1975).

Maintenance respiration is essential for biological health and growth of plants. It is estimated that about half of the respiration carried out by terrestrial plants during their lifetime is for the support of maintenance processes (Amthor, 1989). It is clear then that it is a key component of most physiologically based mathematical models of plant growth, including models of crop growth and yield and models of ecosystem primary production and carbon balance (Canell et al., 2000; Amthor et al., 2001; Thornley et al., 2007).

2.1.3. Leaf development

A leaf is an organ of a vascular plant and is the principal lateral appendage of the stem (Esau, 1953). The leaves and stem together form the shoot (Cutter, 1971).

Typically a leaf is a thin, dorsiventrally flattened organ, borne above ground and specialized for photosynthesis. Most leaves have distinctive upper (adaxial) and lower (abaxial) surfaces that differ in color, hairiness, number of stomata and other features. The primary site of

photosynthesis in most leaves (palisade mesophyll) almost always occurs on the upper side of the blade or lamina of the leaf (Esau, 1953) but in some species palisade occurs on both sides and the leaves are said to be isobilateral.

Many types of leaves are adapted to have different shapes: succulents and conifers leaves are usually not flat; in other species some leaves lose their major photosynthetic function (e.g. cataphylls, and spines).

Typically leaves structure aims to maximize the surface area directly exposed to light and promoting photosynthetic function (Terashima et al., 2011). They are arranged on the plant to expose their surfaces to light as efficiently as possible without shading each other, but there are many exceptions and complications. Some leaf forms are adapted to modulate the amount of light they absorb to avoid or mitigate excessive heat, ultraviolet damage, or desiccation. For xerophytes the major constraint is not light flux or intensity, but drought (Willet et al., 1992)

Gas exchange is controlled by stomata, which open or close to regulate the exchange of carbon dioxide, oxygen, and water vapor with the atmosphere.

Leaves shape and structure varies considerably from species to species; it largely depends on their adaptation to climate and light, grazers, nutrients availability, and ecological competition. Considerable changes in leaf type occur within each individual too (James et al, 2000). Other factors include the need to balance water loss at high temperature and low humidity against the need to absorb atmospheric carbon dioxide (Gunasekera et al., 1992; Mott et al., 1991; Schulze et al, 1973). In most plants leaves also are the primary organs responsible for transpiration and guttation (Raven et al., 2005).

Leaves represent heavy investment on the part of the plants bearing them, and their retention or disposition are the subject of elaborate strategies for dealing with pest pressures, seasonal conditions, and protective measures such as the growth of thorns and the production of phytoliths, lignin, tannins and poisons.

Deciduous plants in frigid or cold temperate regions typically shed their leaves in autumn, whereas in areas with a severe dry season, some plants may shed their leaves until the dry season ends. In either case the shed leaves may be expected to contribute their retained nutrients to the soil where they fall.

2.1.4 Leaves coloring and senescence

In late summer, as daylight hours shorten and temperatures cool, the veins that carry fluids into and out of the leaf are gradually closed off; in effect a layer of special cork cells forms at the base of each leaf. As this cork layer develops, water and mineral intake into the leaf is reduced, slowly at first, and then more rapidly. It is during this time that the chlorophyll begins to decrease (Wang et al., 2003).

During fall the LHC II complex (the one where light is captured and most of the chlorophyll is located) degrades. Horie et al. (2009) suggest that the beginning of chlorophyll degradation is catalyzed by Chlorophyll B Reductase, which reduces chlorophyll b to chlorophyll A. This is believed to destabilize the complex, resulting in the protein breakdown (Zelisko et al., 2005).

Chlorophylls degrade into colorless tetrapyrroles known as Nonfluorescent Chlorophyll Catabolites (NCCs) (Hortensteiner, 2009);

the amino acids released from degradation of light harvesting complexes are stored all winter in the tree's roots, branches, stems, and trunk until next spring when they are recycled to re-leaf the tree.

As the chlorophylls degrade, the hidden pigments of yellow Xanthophylls and orange beta-carotene are revealed. These pigments are present throughout the year, but the red pigments, the Anthocyanins, are synthesized de novo once roughly half of chlorophyll has been degraded. These pigments are not present in the leaf throughout the growing season, but are actively produced towards the end of summer in the sap of leaf cells (Archetti et al., 2011). Their formation depends on a complex conjugation of internal and external factors; according to Davies and Kevin (2004), the Anthocyanins synthesis is stimulated by the breakdown of sugars in the presence of bright light as the level of phosphate in the leaf is reduced. Phosphate in fact is highly concentrated in summer, and has a vital role in the breakdown of the sugars manufactured by chlorophyll. During fall, phosphate moves out of the leaf into the stem of the plant; thus the sugar-breakdown process changes, leading to the production of anthocyanin pigments.

Deciduous plants are traditionally believed to shed their leaves in autumn primarily because the high costs involved in their maintenance would outweigh the benefits from photosynthesis during the winter period of low light availability and cold temperatures (Thomas and Stoddart, 1980). Moreover according to the photoprotection theory, anthocyanins protect the leaf against the harmful effects of light at low temperatures (Lee et al., 2002; Lee and Gould, 2002). Even though the leaves are about to fall and therefore it is apparently unimportant to protect them, Photo-oxidation and Photo-inhibition make the process of reabsorbing

nutrients less efficient, especially at low temperatures. By shielding the leaf with anthocyanins, according to the photoprotection theory, the tree manages to reabsorb nutrients (especially nitrogen) more efficiently.

2.2. Carbon Cycle in Soil: the belowground Universe

2.2.1. Forest soils

Soils placed under forest vegetation can be considered to cover approximately one-half of the Earth's land surface area. Essentially, all soils except those of tundra, marshes, grasslands, and deserts were developed under forest cover and have acquired some distinctive properties as a result. (Brinkley et al., 2012). However about one-third of former forest soils are now devoted to agricultural, urban, or industrial use.

In spite of the common origin of soils, forest cover and its resultant litter layer (Organic horizon), provide a microclimate and a spectrum of organisms very different from those associated with cultivated soils or horticultural plantations. Such dynamic processes as nutrient cycling among components of the forest community and the formation of soluble organic compounds from decaying debris, with the subsequent eluviation of mineral ions and organic matter, give a distinctive character to soils developed beneath forest cover (Brinkley et al., 2012). In the following paragraphs we will discuss of some of the most important factors which have to be considered in modeling Carbon dynamics in soil.

2.2.2. Organic matter input: from above and from within

Forests drop massive amounts of dead leaves, twigs, and branches each year, generally adding one-half to one kg of material to each m² of ground area (Brinkley et al., 2012). The death of a tree leads to the input of a very concentrated mass of organic matter onto a portion of the soil surface. Across decades and centuries, the episodic addition of organic matter in woody boles of dead trees may be similar to the more regular, annual inputs of smaller materials. Most of this material is relatively rapidly transformed into CO₂ and lost to the atmosphere, and some is transformed into longer-lasting soil organic matter. The transformed soil organic matter may reside within the Organic horizon, or may be transferred to the mineral horizons if animals mix the soil, or as soluble organic matter leaching out of the Organic horizon. A portion of Organic horizon material moves into the topsoil (A horizon) via percolating water.

Soil food webs are fueled by both aboveground litterfall and belowground inputs. Soil animals, and the food webs they weave, have been thought to rely largely on aboveground detritus. The annual input of litterfall arrives to the O horizon where many decomposers are concentrated. On the other hand, animals may frequent more than one location in soils, and isotopic tracer studies have shown that much of the soil animal community feeds on belowground roots and detritus within the mineral soil (Pollierer et al., 2007).

2.2.3. Transformed soil Organic Carbon: the humus

In soil science, humus refers to the fraction of soil organic matter that is amorphous and without the "cellular structure characteristic of plants, micro-organisms or animals"(Whitehead and Tinsley 1963). Humus significantly influences the bulk density of soil and contributes to moisture and nutrient retention.

The process of "humification" occurs naturally in forest soils. The importance of chemically stable humus relies in the fertility provided by humic organic compounds, in both a physical and chemical sense (Hargitai, 1993). Humus helps the soil retain moisture (Hogan, 2010) by increasing microporosity (De Macedo et al., 2002) and encourages the formation of soil structure (Hempflig et al., 1990). The incorporation of oxygen into large organic molecular assemblages generates many active, negatively charged sites that bind to positively charged ions (cations) of plant nutrients, making them more available to the plant by way of ion exchange (Szalay, 1964). Humus allows soil organisms to feed and reproduce, and is often described as the "life-force" of the soil (Elo et al., 2006).

It is difficult to define humus precisely; it is a highly complex substance, which is still not fully understood. Humus should be differentiated from decomposing organic matter. The latter is rough-looking material and remains of the original plant are still visible. On the other hand, humified material, has a uniform dark, spongy, jelly-like appearance, is amorphous and may remain in the soil from century to millennia (Di Giovanni et al., 1998). Despite humified organic matter has no determinate shape, structure or character, when examined under the microscope may reveal

tiny plant, animal or microbial remains that have been mechanically, but not chemically, degraded (Bernier and Ponge, 1994). This suggests a fuzzy boundary between humus and organic matter. In most literature, humus is considered an integral part of soil organic matter.

Plant remains (including those that passed through an animal gut and were excreted as feces) contain organic compounds: sugars, starches, proteins, carbohydrates, lignin, waxes, resins, and organic acids. The process of organic matter decay in the soil begins with the decomposition of sugars and starches from carbohydrates, which break down easily as detritivores initially invade the dead plant organs. The remaining cellulose and lignin break down more slowly (McClaugherty, 2007). Simple proteins, organic acids, starches and sugars break down rapidly, while crude proteins, fats, waxes and resins remain relatively unchanged for longer periods of time. Lignin, which is quickly transformed by white-rot fungi, is one of the main precursors of humus, together with by-products of microbial and animal activity (Gonzales-Perez et al., 2008; Knicker et al., 1995; Muscoloa et al., 1999). The end-product of this process, the humus, is thus a mixture of compounds and complex life chemicals of plant, animal, or microbial origin that has many functions and benefits in the soil.

Much of the humus in soils can persist for more than a century (rather than having been decomposed to CO₂), and can be considered stable—this is organic matter that has been protected from decomposition by microbial or enzyme action because occluded inside soil aggregates or tightly attached to clays (Dungait et al., 2012). Most humus that is not protected in this way is decomposed within ten years and can be regarded as less stable or more labile. Thus stable humus contributes

little to the pool of plant-available nutrients in the soil, but it does play a part in maintaining its physical structure (Odaes, 1984).

2.2.4. The microbial Community: habitats and limiting conditions

Soil air is important primarily as a source of oxygen for aerobic organisms, including tree roots. Soil air composition, like air volume, is constantly changing in a well-aerated soil. Oxygen is used by plant roots and soil microorganisms, and Carbon Dioxide is liberated in root respiration and by aerobic decomposition of organic matter.

Gaseous exchange between the soil and the atmosphere takes place primarily through diffusion. Consumption of Oxygen by respiration in the soil leads to a gradient from relatively high Oxygen in the ambient air to the low-Oxygen soil air. The Oxygen content of air in well-drained surface soils seldom falls much below the 20% found in the atmosphere, but oxygen deficits are common in poorly drained, fine-textured soils. Under these conditions, gas exchange is very slow because of the high percentage of water-filled pore spaces. In wet soils if the soil water is moving, it may have a reasonably high content of Oxygen brought in through mass flow; on the contrary soils saturated with stagnant water are low in Oxygen, and they are very important in the context of Green House Gases (GHGs) emissions. Soil air usually is much higher in water vapor than is atmospheric air, and it may also contain a higher concentration of such gases as Methane and Hydrogen Sulfide, formed during organic matter decomposition. Oxygen concentrations in soil air as low as 2% are generally not harmful to most trees for short periods.

2.2.5. Microfauna: nematodes and protozoa

The soil microfauna include nematodes, rotifers, and many types of protozoa. Nematodes are nearly microscopic, non-segmented roundworms that commonly occur O horizons (e.g. mull humus type) and upper mineral soil. Densities of more than 100 individuals per m² are not uncommon, and their populations can expand rapidly as soil conditions change. Only about a tenth of the 10000 or so known nematodes are soil inhabitants. Although the populations of nematodes are always highest in the vicinity of plant roots, only a few appear to be root parasites. Most prey on bacteria, algae, fungi, protozoa, rotifers, or other nematodes. Nematodes can be important as population regulators and nutrient concentrators in the soil ecosystem. The impact of their parasitism versus their role in decomposition is poorly understood (Benckiser, 1997).

Protozoa are the most abundant soil fauna; Brinkley reported that their number varied from 1500 to 10 000 per grain of forest soil. These one-celled organisms may exist in either an active or a cyst stage, but they are generally aerobic and occur in the upper soil horizons. Their diet consists largely of decomposing organic materials and bacteria. Soil conditions that favor their development are similar to those that favor bacteria. They are found in soils supporting both hardwood and coniferous forests. In a strict sense, they are the only major group of soil fauna classified as microorganisms.

2.2.6. Macrofauna: earthworms

The ordinary earthworm is probably the most important component of soil macrofauna (Edwards, 1998). A high population of earthworms is generally associated with mull humus formation, and this is particularly true of *Lombricus terrestris*, which may make up as much as 80% of the total soil fauna by weight. These earthworms feed on fallen leaves and organic debris and pass it, together with fine mineral particles, through their bodies. Each year, earthworms have been estimated to pass more than 30Mg soil ha⁻¹ through their bodies, where it is subjected to digestive enzymes and to a grinding action. Earthworm casts are higher in total and nitrate nitrogen, available phosphorus, potassium, calcium, magnesium, and cation exchange capacity and lower in acidity than is the soil proper. Earthworms mix bits of organic materials into the mineral soils, and they promote soil structure formation and aeration through their burrowing action. As a result of this transporting and mixing action, the upper layer of certain O horizons takes on the crumbly structure of the so-called earth-worm mull. The concentration of earthworms in forest soils has been estimated to be from 0.5 million to more than 2 million per hectare, the actual numbers depending on several climatic and soil factors. Although earthworms are present in acid soils, highly acid soils support fewer earthworms than less acid soils, with the optimum range being about pH 6.0 to 8.0. Sandy soils and soils that dry excessively are not favorable habitats for earthworms.

They are active in forest soils of Europe and North America and are particularly important in the development of hardwood mull humus type. The smaller worms also devour organic debris, thereby improving

the physical and chemical properties of the surface soil. Because of their smaller size, they have not been considered as important as the other worms in forest soil formation. However, since these Enchytraeidae have less stringent environmental requirements than their larger relatives, they may be approximately as numerous in mor as in mull humus type layers.

Assemblages of European earthworms convert former mor O horizons into mull types. The exotic earthworm biomass can exceed the biomass of native soil animals, changing almost every aspect of soil structure and chemistry, even altering the vegetation (Szlavec et al., 2011).

2.3. Modeling

Following Parker et al. (1995), the need to predict long-term responses of terrestrial ecosystems to anthropogenic environmental change at stand, regional, and global level underscores the importance of understanding the carbon balance of forest ecosystems. Extrapolating from small-scale measurements of photosynthesis to estimates of canopy and stand-level photosynthesis is difficult for a variety of reasons:

- ecological and physiological differences among species;
- leaf-to-leaf variation within a species through the canopy;
- influences of canopy architecture on leaf microclimate;
- nonlinearities in the response of photosynthesis to resource levels.

In this context, during the last 30 years a large number of computer based approaches were developed to describe ecological processes under a complex mathematical framework; the Ecosystem models.

A model can be described as a symbolic representation of certain aspects of a real-world object or phenomenon, i.e. an expression or formula written following the rules of the symbolic system from which this representation stems. In all cases, it should be clear that the model does not constitute an end in itself, but is simply a tool in the scientist's toolbox. The biological problem always comes before the methodological development; that said modeling may assist in the creation of a theory, bringing out concepts (Fig.1.3.).

Modeling is the approach which leads to the creation of a model; it takes into account:

- carry out formalization activities in correspondence with the writing of the model;
- manipulate this model within the formal system to render it more "useable" (for example to obtain an integrated expression from a differential equation) and to study its properties;
- establish relationships with other representations (for example, the graph of a function, or the computer program which will allow users to calculate numerical values);
- interpret and compare the different representations obtained in the formal world with the biological reality (this reality is generally seen through experimental data).

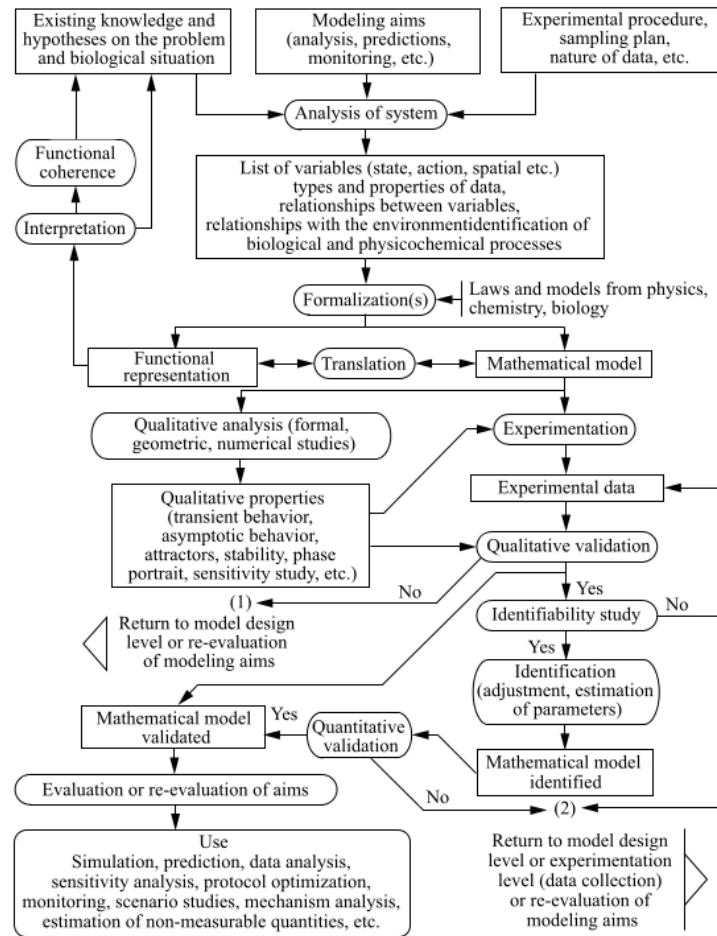


Fig.2.2. Theoretical scheme followed in developing an Ecosystem Model (Parker et al., 1995)

There are many different modeling approaches in investigating Forest Ecology. In this study we will discuss just the approaches which are consistent with the 3D-CMCC-FEM modeling rationale.

2.3.1. *Deterministic models*

Deterministic models describe phenomena making use of the fundamental relations governing the mechanics of the ecosystems. The theoretical rationale is the resolution of Partial Differential Equations describing the phenomena using the method of characteristics

(Moorcroft and Medvigy, 2002); thus the model is divided in sub modules and simpler functions which are easily calculated. Process based, theoretical and Gap models belong to this family of Ecosystem models.

2.3.1.1. Process Based Models (PBMs)

Process models and process-based system models are essential scientific tools, providing formalized statements of hypotheses and a framework that encapsulates disparate pieces of information and knowledge (Mäkelä et al. 2000). Process models are considered to embody too many uncertainties and to require too many poorly known parameters for their projections to be as reliable in practice as those of empirical models (Mohren and Burkhardt 1994).

“Most of the process-based growth and yield models developed toward management applications start with photosynthesis; either treating it as the basic growth process underlying the carbon balance independence or using it as an independent predictor variable” (Mäkelä et al. 2000). Following Mäkelä, modeling forest growth in terms of carbon balance involves calculating assimilation of carbon and its distribution at different levels of organization in the stand. The primary effect of environmental factors is on net assimilation rate, either directly, through factors such as light and temperature, or indirectly. Tree growth is described as a dynamic process where stand structure affects the distribution of the environmental driving variables in the canopy.

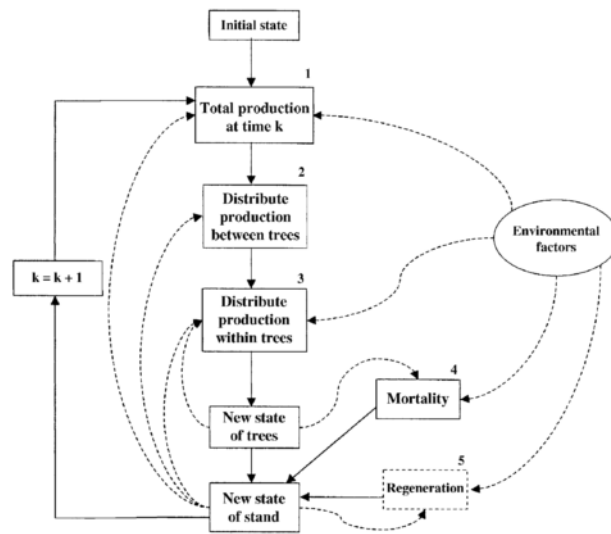


Fig. 2.3 scheme of the feedbacks processes in stand models (Makela et al., 2000)

Process Models focused on stand-level primary productivity typically use weather data and data on soil structure and chemistry as inputs, Long-term stand-level dynamics are hence irrelevant, and the stand can be specified at a certain stage of development. Because models of this class have tight connections to the basic ecophysiology of trees and forests, they are used primarily to make quantitative predictions of the productivity of different sites and the variation in productivity between years and climates (McMurtrie et al. 1994).

On the other hand, stand-level models focus on the long-term dynamics of productivity, concentrating on the effects of different feedback processes (shown by dashed-line arrows in Figure 1.4); these models consider growth, senescence and mortality as stand average dynamic processes and apply a simplified treatment of the metabolic processes. They are often more theoretically oriented, aiming at developing the general principles of growth modeling. Many models of this type include

a nutrient balance, deriving characteristics of stand dynamics from carbon–nitrogen interactions.

Ecosystem Process models are derivations of the PBMs; they simulate the processes on the leaf scale (usually m^2), upscale the result on the spatial resolution of the geographic matrix into consideration, for each grid cell of the matrix. They are successfully used also in Forestry because of their integrability with remote sensing data; these data may also be used for wide spatial scale validation. The spatial scale at which they work is placed in an intermediate between gap models and global models, aiming to the representation of the characteristics of forest structure and physiognomy (Collalti et al., 2012). Examples of Ecosystem process models are MAESTRO (Wang & Jarvis, 1990), FOREST-BGC (Running & Coughlan, 1988), CENTURY (Parton et al., 1988), 3PG (Landsberg & Waring, 1997; Sands, 2004); DNDC (Li et al., 1992).

In another area of growth and yield modeling, the emphasis has been on interactions between individual trees in stands related to carbon allocation; the gap models.

2.3.1.2. Gap Models

In the gap models, the establishment, growth and mortality of individual trees on small patches of land are simulated as a function of biotic (competition) and abiotic factors (climate and soils). The mortality of a large, dominating tree produces a gap in the forest, which leads to the release of suppressed trees and increased tree recruitment rates, both of which drive succession; thus the name ‘gap’ models. Vegetation

dynamics were strictly related to competition and environmental conditions.

Classic gap models (Botkin et al., 1972b) were based on 4 general assumptions (Bugmann 2001):

1. The forest stand is abstracted as a composite of many small patches of land, where each can have a different age and successional stage;
2. Patches are horizontally homogeneous, i.e. tree position within a patch is not considered;
3. The leaves of each tree are located in an indefinitely thin layer (disk) at the top of the stem;
4. Successional processes can be described on each of those patches separately (no interactions between patches).

The strength of these models is in the ability to reliably estimate both horizontal and vertical competition between individuals; their weakness resides in usability on regional scale, since they usually are individual based models which require lots of data and the explicit spatial position of each tree (Collalti, 2011).

2.3.1.3. Dynamic Global Vegetation Models, DGVMs

These models simulate shifts in potential vegetation and their associated biogeochemical and hydrological cycles as a response to shifts in climate. DGVMs use time series of climate data and, given constraints of latitude, topography, and soil characteristics, simulate monthly or daily dynamics of ecosystem processes. They are used most often to simulate the effects

of future climate change on natural vegetation and its carbon and water cycles.

DGVMs generally combine biogeochemistry, biogeography, and disturbance submodels. Disturbance is often limited to wildfires, but in principle could include any other, like land management decisions, insect or ozone damage and so on. DGVMs usually "spin up" their simulations from bare ground to "equilibrium" vegetation to establish realistic initial values for their various "pools": carbon and nitrogen in live and dead vegetation, soil organic matter, etc. corresponding to a documented historical vegetation cover. They are usually spatially distributed, with simulations carried out for thousands of homogeneous cells. Simulations are carried out across a range of spatial scales, from global to landscape. Cells are usually arranged as lattice points; the distance between adjacent lattice points may be as coarse as a few degrees of latitude or longitude, or as fine as 30 arc-seconds.

Several DGVMs appeared in the middle 1990s. The first were apparently IBIS (Foley et al., 1996) and VECODE (Brovkin et al., 1997), followed by several others such as LPJ(Sitch et al., 2003), CLM-DVGM (Lews et al., 2004) and ED (Moorcroft & Medvigy, 2001; Medvigy, 2009).

2.3.2. Stochastic Models

The second family of models used in Ecology is usually referred as the Stochastic or Empirical Models. Following Collalti et al. (2012) an empirical model is defined by a set of variables dependent of a parameter "t" which usually represents time. Referring to a statistical basis, they

take into consideration the dynamics of the variables, giving back probability of occurrence as results.

The initialization of the variables takes into account the knowledge of their probability density functions, fitted on data previously collected. Hence the stochastic model simulates the variation in time of each variable probability density function, obtaining as a result a new probabilistic space for each variable itself.

These models generally have a more complex structure with respect to deterministic models; an example is the Monte Carlo statistical method used to simulate real phenomena. The method is based on an algorithm generating a series of values following the expected probability distribution of the i th variable.

Regression models too are empirical models. According to Prentice (1992) these models may be of scarce interest in for estimation of forest growth dynamics, because the conditions leading to the present empirical relation may change with environmental changes due to modifications in the tradeoffs between processes and state variables.

2.3.3. Hybrid models

Hybrid models couple the concepts of the two model families described above (e.g. deterministic and stochastic models). Following Collalti (2012) the compromise is reached by using the strengths of deterministic models in simulating chemical compounds balance and dynamics, along with the strengths of stochastic models in representing chaotic processes (i.e. seeds dispersion). 3D-CMCC –FEM belongs to this family of

models, even though it is mainly oriented to the deterministic compound.

CHAPTER 3: THE LATITUDINAL TRANSECT

Under the auspices of the CarboEurope-IP an extensive set of eddy covariance flux measurement towers has been established all over Europe, supporting ecosystem level research on energy and mass transfer processes (Aubinet et al., 2000). From this network a set of six sites was chosen for the current study.

They were chosen to represent a latitudinal and climatic transect through Europe, containing both conifer and broadleaf stands and depicting the most widely spread European Forest Ecosystems (Fig. 3.1). Thus a *Quercus ilex* forest was chosen in the Mediterranean region, a Norway spruce stand (*Picea abies*) in the Alpine region, an old growth beech (*Fagus sylvatica*) forest in the continental plains of Germany, a small beech forest in the rural context of Copenhagen, a patchy mixed forest next to the town of Brasschaat, in Belgium (*Quercus robur* and *Pinus sylvestris*) and a Scots pine forest (*Pinus sylvestris*) in Finland. (Tab. 3.1).

Tab. 3.1. CarboEurope sites characteristics

SITE_	Stand type	Biome	YoS	n years
IT-Ren	3 layers , unevenaged structure determined with the PPA algorithm (<i>Picea abies</i>)	Alpine Taiga	2006-2010	6
FR-Pue	Uni layer uni age (<i>Quercus ilex</i>)	Medit	2000-2011	11
DE-Hai	Uni layer (<i>Fagus sylvatica</i>)	Temperate dry	2000-2007	8
DK-Sor	Uni layer uni age (<i>Fagus sylvatica</i>)	Temperate humid	2001-2009	9
BE-Bra	Mixed, unevenaged, 3 canopy layers (<i>Q. robur</i> + <i>P. sylvestris</i>)	Temperate humid	2001-2010	10
FI-Hyy	Uni layer uni age (<i>Pinus sylvestris</i>)	Taiga	2001-2011	11

3.2: Climate along the transect

The climatic conditions along the gradient vary from Boreal in Finland, humic continental at the Mid European sites, to montane Meditterrenenan in Italy, to strictly Meditterreanean in France.

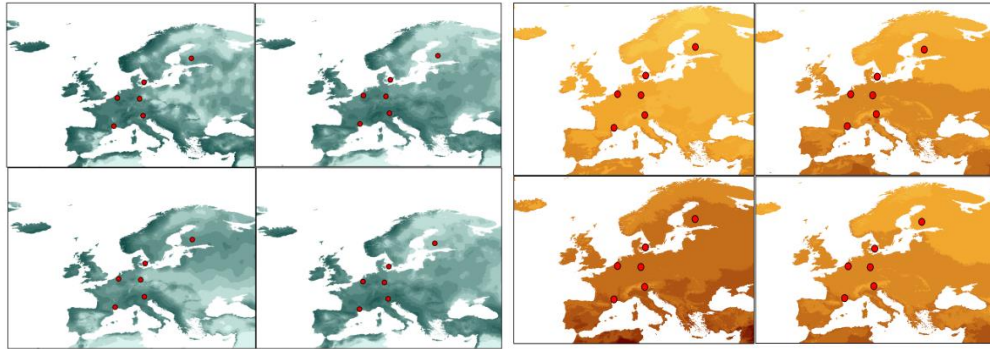


Fig. 3.2. Average seasonal precipitations (left, in green) and Temperatures (right, in red); climate data were taken from the WordClim project, on a spatial resolution of 1km².

3.3. Stand Characteristics and Site History

3.3.1. Renon forest (Italy)

As described by Montagnani et. al.(2009), the study site of Renon-Selva Verde (46°25' N, 11°17' E, elevation about 1735 m asl) is located in northeast Italy, on the southern side of the Alps at a distance of 12.2 km north- northeast from the town of Bolzano. The site is placed on a porphyric plateau that is part of the irregular slopes of “Cima del Lago Nero” (2069 m) and is between the wide Isarco river valley and the narrow and steep Sarentino river valley. The nearest peaks are “Corno di Renon” (2259 m asl) at about 3.7 km north-northeast and “Cima di Villandro” (2509 m asl) at about 8.2 km north-northwest. The vegetation is of natural origin and is used for wood production. It consists of an

unevenly aged coniferous forest with gaps between groups of older and younger trees. The main forest species is spruce (*Picea abies* (L.) corresponding to about the 85% of the cover, followed by cembran pine (*Pinus cembra* L., 12%) and larch (*Larix decidua* Mill., 3%). Reported net ecosystem production is $450 \text{ gC m}^{-2} \text{ a}^{-1}$ (Valentini et al., 2000). Different forest types are present in the area: mesophilous mature forest covers 52.3% of the surface, waterlogged mature forest 21.0%, young forest 12.0%, while clearings cover 14.7% of the area. The canopy is irregular with maximal height of 29 m.

The leaf area density, measured along the measurement towers, showed two peaks: the first at understory level, the second at 2/3 of maximal canopy height. Outside the reference area, at a distance of 80 m northwest of the central tower, tree density decreases and the forest is replaced by ample pastures with sparse trees.

3.3.2. Puechabon forest (France)

The forest of Puechabon is dominated by the evergreen tree species *Quercus ilex* (L.) and is situated in the French Mediterranean region of Languedoc Roussillon. The stand is located within the Puéchabon State Forest; the site has been continuously monitored since 1984 for ecophysiological measurements from leaf scale (Limousin et al. 2010; Misson et al. 2010) to stand or ecosystem scales (Rambal et al. 2003; Limousin et al. 2009; Misson et al. 2010b). Mean annual temperature was of 13.4°C while average annual precipitation was of 907mm (temporal

series 1984 to 2009). Meteorological data were obtained using a fully equipped weather station, located on site.

This forest is located on hard Jurassic limestone. Because of the large amount of rocks and stones in the mineral soil, available soil water, cumulated over a 5 m depth, does not exceed 150 mm. Mean annual rainfall and mean annual air temperature over the 1984-1992 period were 778 mm and 13.4 °C, respectively. The Puéchabon State Forest has been managed as a coppice for many centuries and the last clear-cut was performed in 1942 (Floret et al, 1989). The coppice stand was thus 59 years old at the beginning of the study in 2001. Mean tree height of *Q ilex* was about 4.5 m, stem density was $977 \pm 71 \text{ ha}^{-1}$ (diameter at breast height [DBH] > 7.5 cm) and $10\,316 \pm 616 \text{ ha}^{-1}$ (DBH > 1 cm) (Cartan Son et al, 1992). (Joffree et al., 1995).

3.3.3. Hainich (Germany)

The old unmanaged Hainich mixed beech site is located within the Hainich National Park, near the city of Eisenach. Following Knohl et al. (2003) the Hainich National Park was established in 1997 to protect one of the largest beech forests in Central Europe and covers an area of about 7600 ha. Because of its history as a military base for over 40 years prior to 1997, a large part of the forest had been taken out of regular management and left relatively undisturbed. In earlier centuries, the forest at the Hainich tower site was used as a coppice with some older-growth trees cut for timber ('coppice-with-standards'). From 1872 until the end of the 1940s it was subject to selective cutting by the local population and none of the area has been clear felled. Consequently, the forest displays characteristics typical of an unmanaged old-growth forest,

with a wide range of age classes (from 1 to 250 years), comparatively large dead wood pools, canopy gaps, and a vertically structured canopy. The forest is dominated by beech (*Fagus sylvatica*, 65%), co-dominated by ash (*Fraxinus excelsior*, 25%), and maple (*Acer pseudoplatanus* and *A. plantanoides*, 7%), with some European hornbeam (*Carpinus betulus*), and elm (*Ulmus glabra*).

Flux measurement at the site began in October 1999. Flux data of this site were investigated in detail with regard to site quality in combination with footprint modeling (Reithmaier, 2003; Rebmann et al., 2004b).

In the surroundings of the tower, the tree density is about 330 trees ha⁻¹ (stem diameter >7 cm), resulting in above-ground stem carbon pool of about 130tC ha⁻¹ (Anthoni et. al., 2004). Maximum tree height varies between 30 and 35m with a maximum leaf area index (LAI) of 5.0 m² m⁻² and a diverse structured canopy (3.5% gaps). The Hainich tower site is located in suboceanic/subcontinental climate (long-term annual means: 7.5–8 °C for air temperature, 750–800mm precipitation) on a gentle north facing slope (2–3° inclination). The forest surrounding the tower site has an extension of more than 3 km in the prevailing wind direction. The closest change in surface land use is a small clearing located about 800m perpendicular to the prevailing wind, with only 5% contribution to the overall wind distribution. The typical forest phenology during the year is characterized by a dormant season from November to March, a forest floor covered completely with understory vegetation from April to October, and leafed trees from May to October. Bud break of the leaves based on field observations starts about the period between the 25th of April and the 8th of May. Soils are fertile

cambisols on limestone bed rock with a depth of 50–60 cm. The soil is characterized by large clay content (40%, sand 4%) and a thin litter layer. Soil carbon pools were 5.3 tC ha⁻¹ in the organic layer and 124 tC ha⁻¹ in the mineral horizons (Knohol et al., 2003).

3.3.4 Sorø (Denmark)

The site, Lille Bøgeskov Forest (MAN), is an even-aged and homogenous mature 80-year old stand (55°29'N, 11°38'E) near Sorø, on the island of Zealand. It is believed that the forest has never been under cultivation and that beech trees have been dominating in the area since 2500 B.C. As a matter of fact the stand is the typical conventionally managed beech forest. A tower allows meteorological measurements in up to 57m height (Pilegaard et al. 2003). Roots were observed in the upper 0.85 m of the soil (Ladekarl et al. 2001). The mean annual air temperature is 8.1°C (1987–97, Laursen et al. 1999). The mean annual is about 650 mm precipitation (1961–90, Frich et al. 1997).

The soils in the area are brown soils classified after the American Soil Taxonomy system as either Alfisols or Mollisols (depending on a base saturation under or over 50%) with a 10–40 cm deep organic layer. The Mollisols are rich in clay (8–23%), having field capacity of 31.5 vol % (0–1.5m depth) and groundwater table fluctuations between 0.2 m in winter and 2 m in summer below the soil surface (Ladekarl et al. 2001). The carbon pool in the soil (down to 1 m depth) is 20 kg m⁻². The C/N ratio is about 20 in the upper organic soil layers falling to about 10 in the lower mineral layers. The parent material is relatively rich in lime (25%–50%). However most of this is leached from the upper horizons of the

forest soil, resulting in a low pH (4–5) and a lower base-saturation (Østergård 2000).

The trees around the station were 82-year-old in 2001 with an average tree height of 25 m. Average tree diameter was 38 cm, the stand density was about 283 stems ha⁻¹ and the wood increment calculated on the basis of yield tables (Møller 1933) was approximately 11 m³ ha⁻¹ yr⁻¹. The peak leaf area index of the canopy was about 5 m² m⁻² at mid-summer. The terrain was flat and there was a homogeneous fetch of 0.5–1 km depending on direction. The main part of the surrounding forest is beech forest of varying age but there are also scattered stands of conifers (mainly *Picea abies*) as well as single trees of other conifers such as European. In total, conifers constitute about 20% of the footprint area. In April before bud-break there is flourishing forest floor vegetation mainly composed of *Anemone nemorosa* L. and *Mercurialis perennis* L. Later in summer the forest floor vegetation mainly consisted of patches of grasses.

The general climate at the Sorø site is determined by its geographical location in the northern temperate zone on the western side of the European landmass, close to the North Sea. The temperature is influenced by the warm Gulf Stream. Therefore, the station has a maritime temperate climate dominated by westerly winds and frequent passes of frontal systems. As a result the usual weather is characterized by cool and unsteady summers and warm and changeable winters. Occasionally the easterly winds carry to the station severe winters and hot summers of the continent (Pilegaard et al. 2003).

3.3.5. Brasschaat (Belgium)

The study was carried out on the 150-ha mixed coniferous–deciduous De Inslag forest. The forest is located in Brasschaat, in the Campine region of the province of Antwerpen, Belgium (51°18'3" N and 4°31'14" E, altitude 16 m a.s.l, orientation NNE; De Pury and Ceulemans 1997). The stand is part of the European CARBO-EUROFLUX network and is a level-II observation plot of the European program for intensive monitoring of forest ecosystems (EU/ICP Forests) managed by the Institute for Forestry and Game Management, Flanders, Belgium. The site is almost flat (slope 0.3%) and belongs to the plateau of the northern lower plain basin of the Scheldt River. The climate at the site is moist sub-humid, rainy and mesothermal. Long-term (30-year average) mean annual and growing season temperatures at the site are 9.8 and 13.7 °C, respectively. Mean temperatures of the coldest and warmest months are 3 and 18 °C, respectively. Mean annual and growing season precipitations are 767 and 433 mm, respectively (Xiao et al. 2003). Mean annual and growing season potential evapotranspiration values are 670 and 619 mm, respectively (Èermák et al. 1998). The site has a moderately wet sandy soil with a distinct humus or iron B-horizon, or both (Baeyens et al. 1993) and is classified as umbric regosol in the FAO classification. The upper soil layer is about 1.8 m thick and consists of aeolian northern Campine cover sand. Beneath this sand layer, at a depth between 1.5 and 2 m, lies a shallow clay layer, below which there's another sand layer (Pretiglian; Baeyens et al. 1993). The soil is typically moist, but rarely saturated because of the high hydraulic conductivity of the upper sandy

layers. A detailed report of the physical and chemical properties of the topsoil is presented by Roskams et al. (1997) and Janssens et al. (1999).

The original climax vegetation in the area was a Querceto– Betuletum (Tack et al. 1993). The site was a low productive heathland in the 18th century (Gemeentekrediet 1965), up to the beginning of the 20th century when the stand was planted. The relatively high SOC stock of the stand, 172.6 Mg ha⁻¹, is due to substantial human-induced additions of organic material under the pine stand (Chiti et al., 2011). According to Chiti et al. (2009) in the soil under pine the organic horizon comprises mainly “modern” C (fixed after the 1950s) while the mineral soil contains prevalently “old” C, with a recycle time of more than a millennia in the A1 and A2 horizons. Opposite, under oak the soil showed ¹⁴C concentrations largely influenced by modern C, both in the organic layer and the mineral ones. It is plausible that organic material from drained peatlands could have been brought to the pine soil and not to the oak one (Bastiaens and van Mourik, 1994).

The experimental Scots pine stand was planted in 1929, and was 73 years old at the time of the present study (i.e., 2001). The evergreen stand canopy was sparse, with a projected leaf area index (LAI) in 1997 between 1.9 in late spring (before bud burst) and 2.4 in early autumn before leaf fall (Gond et al. 1999). Scots pine trees at the study site have only two needle classes (current-year and 1-year-old needles; Janssens et al. 1999).

3.3.6. Hyytiälä (Finland)

The EC station is located in a homogeneous Scots pine stand (*Pinus sylvestris* L.), planted in 1962 next to the Hyytiälä forest station in southern Finland (61°51'N, 24°17'E, 181 m above sea level). As 29% of the forests in southern Finland, the Scots pine forest in Hyytiälä is of medium site quality (Cajander 1909) and has a typical growth rate of 8 m³ ha⁻¹ yr⁻¹.

The forest is half way through the rotation time for this site type, which is about 80 years. Scots pine forests dominate about 56% of the forest area in southern Finland. Regeneration and growth of the forest have been performed along standard silvicultural guidelines (Peltola 2001). The height of the dominant stand is around 14 m and the all-sided needle area was of about 8 m² m⁻² (2002). Total tree biomass was 68 t ha⁻¹ (Ilvesniemi and Liu 2001). The homogeneous fetch in the prevailing wind direction (230°) is 250 m (Vesala et al. 1998). The soil is composed of sandy and coarse silty glacial till. The annual mean temperature in 1961–1990 was +2.9 °C and the annual mean precipitation 709 mm. (Suni et al. 2003).

CHAPTER 4: MATERIALS AND METHODS

The achievement of the objectives of this work requested the acquisition of several informatics competences and mastery of different software packages and programming languages. The 5.1 (Collalti et al., in prep) and 6.1 versions (Marconi et al., in prep) of the model were written in C-programming language, and corrected using the Eclipse CDT tool debugger (<https://www.eclipse.org/>) under UNIX environment. The mathematical analysis of the new functions was assisted by the use of Mathematica™ (evaluation license) and web based Wolfram-Alpha **tools** (Wolfram Research, Inc., 2014). The statistical analyses were entirely performed in Matlab™ (student edition) (2013a, MathWorks, Inc., 2013), using its proprietary programming language for scripting:

- input-formatting-output framework of the model outputs (from .txt to .mat files) to be correctly utilized during the statistical analysis, filtering missing data and creating different temporal resolution matrices;
- the estimators and statistics not included in the set of Matlab core functions (NMRSE, NSE, etc.);
- the whole “deciduous yellowing/senescence sub module” to be validated against a wide set of MODIS data

The initialization and evaluation of partial results was developed in Microsoft Excel 2010 Professional. The Perfect Plasticity based “height structure discrimination” algorithm was developed in MS Excel VBA programming language (Microsoft Inc., 2010). Mapping of sites and evaluation of general climatic and vegetative characteristics were developed by using ESRI ArcMap™ software package (evaluation license) (Esri Inc.,2014).

4.1. The original version of the model

The 3D-CMCC FEM is “a hybrid Process Based Model coupled with the concepts of the canopy layer models for analysis of forest dynamics, Functional–Structural Tree Models and empirical models” (Collalti et al. 2014). It was partially inspired by existing models such as 3-PG (Almeida et al., 2004; Landsberg and Waring, 1997; Nightingale et al., 2008; Nolè et al., 2009; Sands and Landsberg, 2002; Tickle et al., 2001), Sortie (Pacala et al., 1996), BIOME family (Haxeltine and Prentice, 1996; Running and Hunt, 1993; Thornton, 2010) and LPJ (Sitch et al., 2003, 2008).

The model introduced a novel routine simulating trees competition for light and had a spatialized version to be used for regional analyses (Collalti et al. 2013). Unfortunately it worked only for monthly temporal resolution, and respiration quantification and soil dynamics were not taken into account. Thus it wasn't able to perform NEE estimation. Its core was the light use efficiency model (LUE) of Montheith (1972, 1977), which postulated that NPP could be treated as a constant fraction of the product between the Absorbed Photosynthetic Active Radiation (APAR) and quantum yield (Waring, Landsberg, and Williams 1998).

4.2. Improvements on the model: the 5.1 ad 6.1 versions

The 5.1 version of 3D-CMCC-Forest Ecosystem Model aimed to describe Forest Ecosystem Dynamics in structure, productivity and

respiration on a daily time step (Collalti et al., in prep). The 6.1 version aimed to improve the model with soil Carbon dynamics, Net Ecosystem Exchange estimation, better littering, turnover and Phenology routines, automated height dominance initialization, and other minor corrections (e.g. stress related respiration modifiers) out of the 5.1 version. From now on we will refer to the 6.1 version as the object of this study, since it was the one completely developed by the author.

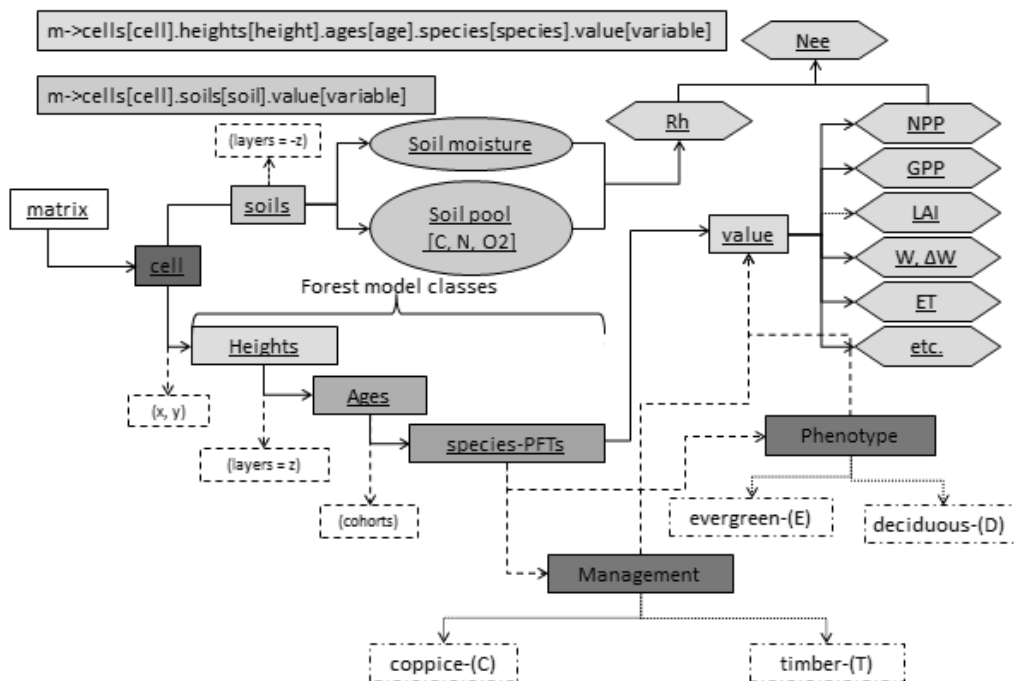


Fig. 4.1. 3D-CMCC-FEM 6.1. general flowchart. The code is structured repartitioning the aboveground cohorts and soil layers in a set of nested structures. In this way the model neatly records the process variables and updates them as a result of the place specific constitutive relations.

The core of the model was the quantification of the Net Ecosystem Exchange (NEE) in a generic forest context. Theoretically Net Carbon

Exchange follows a mass conservation equation, which can be expressed in its simplest version as

$$NEE = GPP - R_A - R_H \quad (\text{Eq. 4.1})$$

These variables depend on a large amount of state conditions, which are related to the tree position in space, on its genotype and age related maturity. Thus we ideally represented the forest structure in the *itb* instant *t* to be described as the hyper volume of 5 dimensions in which the two “age” (A) and “species” (SP) dimensions were bounded to the three spatial ones (Fig 3.1).

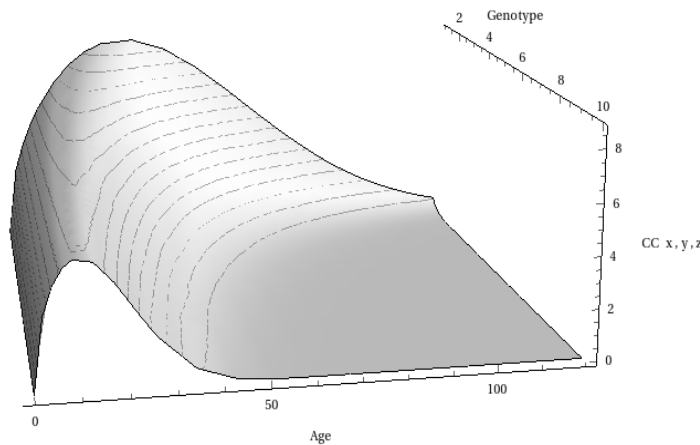


Fig 4.2. Graph representation of growth rates on 5d for a theoretical generic set of trees throughout a gradient of 10 species for 120 age units. CC stands for the Crown Cover along the three spatial dimensions x,y,z.

The theoretical rationale was that every genotype had its phenotypic plasticity and replied uniquely to the Environment, Age decline and Competition stimuli (Schlichting, 1986).

The GPP calculation followed the Light Use Efficiency (LUE) approach (Montheith, 1994), which assumes that Gross photosynthesis at time *t* may be calculated as the product between the Absorbed Photosynthetic Active Radiation (APAR) and an efficiency factor which may be a function of age (Ryan et al., 2007), leaf specific adaptation to light (Tyree

et al., 1997), genotype and period of the year (Bordeau, 1959). The potential GPP described so far is however reduced by competition for light and nutrients, and limited by environmental constrains (Thornton, 2010).

Competition for light (Collalti et al., 2014) had the double role to reduce the amount of light reaching a characteristic height surface and encouraged growth along the height dimension. The other environmental factors had impact on potential gross photosynthesis and respiration, and drove competition for nutrients. These factors were treated as reduction coefficients, and estimated following the original 3D-CMCC-FEM rationale (Collalti et al., 2010).

4.2.1. Gross primary production

The forest GPP for a known surface in a known day should ideally be calculated as:

$$GPP_t = \int_0^H \int_0^A \int_0^{SP} \bar{\alpha}(h, a, sp, t) \cdot \overline{CC}(h, a, sp, \rho) \cdot \overline{APAR}(S_R, L, h, C) \cdot \bar{f}_E(swc, T, ice, phys) \delta h \delta a \delta sp \quad (\text{Eq. 4.2})$$

Where a is the quantum yield efficiency function, CC represents the Canopy Cover intended as the population of leaves on a plane, $APAR$ the quantity of net light transmitted from above and absorbed by the plane $\delta h, f_E$ the Environmental factors reducing actual GPP.

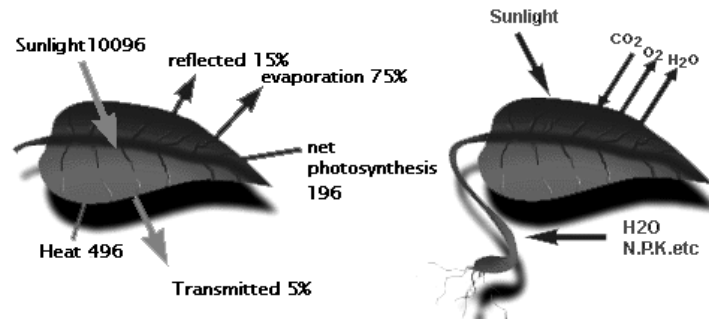


Fig. 4.3. Light intercepting the canopy only partially enters the photosynthesis routine. As a matter of fact part of the light gets reflected outside of the system, partly is transmitted through the canopy, a large amount is degraded into thermic radiation (Picture taken from Wikipedia).

To calculate the integral, the canopy was divided into up to three layers representing the emergent, dominant and dominated trees (Fig 4.4.). This discretization into the different layers was dependent on an arbitrary parameter, representing their difference in average height, which was set constant throughout the simulation. In our opinion this approach may lead to inadequate representations of the canopy structure on the long period. Thus we started to work on a more dynamic approach, based on the z^* concept (Adams et al. 2007; Purves et al., 2008 Strigul et al. 2008) upscaling cell *DBHs* and heights densities at the end of each year to recompute the modified prefect plasticity approximation algorithm described in the initialization section.

The genotype plasticity was discretized assuming the “species” as the elementary level of genetic diversity. Age integral was discretized by progressively increase age count at the beginning of the year of simulation on the first of January. Once the classes were defined, all the trees belonging to the *ith* height layer, the *jth* age class and *kth* species cohort, were treated as having the biometric characters of the average individual.

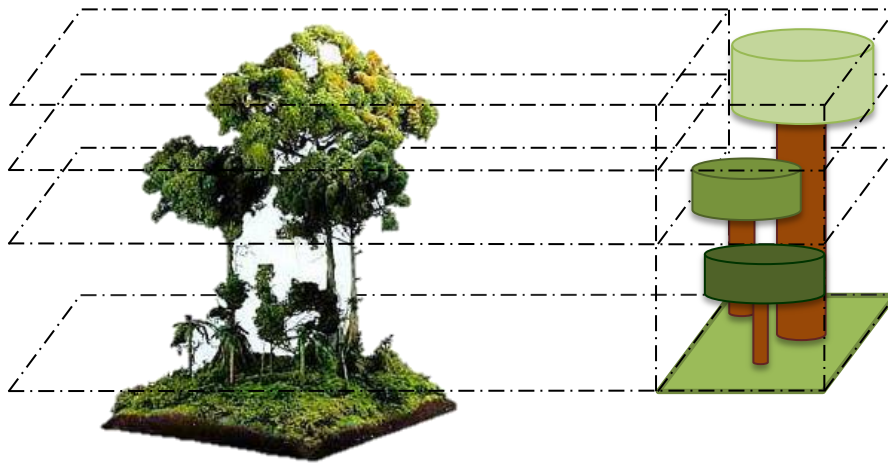


Fig. 4.4. The canopy structure is discretized by the model in up to 3 height classes and an indefinite number of age and species specific cohorts (usually 3). In each “box” the canopy is treated as a set of equally spaced and characterized plants with a disk like crown shape. The quantity of light reaching the height layer below is determined by following Collalti et al., 2014.

4.2.2 Ecosystem water balance

Water is essential for forest growth dynamics and is implicated in a large number of constitutive relations linking state and process variables both in the aboveground and belowground (Nobel 1999). Idealistically assuming the forest ecosystem as a closed one over the punctual surface $U(\delta x, \delta y)$ and open on $\mathcal{Z}(\mathcal{z}, H + \delta i)$ on its upper limit $H + \delta i$, water may enter the system just as rain and leave it as vapor from the very same upper limit. Thus the quantity of new water reaching the upper soil, ignoring lateral flux and instantaneous evaporation in atmosphere ideally follows the Eq.:

$$w(h_0, t_{24}) = \int_{t=0}^{24} \int_{h=z}^{H+\delta i} \left(r(t) \cdot \int_{h_c=h}^H CC(h_c) \cdot \Omega(L) \delta h_c \right) \delta h \delta t$$

(Eq. 4.3)

where t represents the temporal resolution (e.g. day), z the maximum soil depth, $H + \delta i$ the canopy height plus the infinitesimal upper limit through which rain enters the system; CC is the canopy cover assumed constant in time but varying in h , Ω the canopy resistance to water movement, $r(t)$ the net water gain variable.

The water reaching the soil boundary layer moves into the soil column z following the vector w_s :

$$w_s(z) = g(z) + J(z) - E(z) - R(z)$$

(Eq. 4.4.)

Where $g(z)$ represents the gravimetric movement along the soil column, $J(z)$ the matrix diffusion, $E(z)$ the Evapotranspiration and R lateral runoff. Thus the total amount of water along the soil profile should be represented by the integral:

$$w_t = \int_{z=0}^z (w(z) + g(z) + J(z) - E(z) - R(z)) \partial z$$

(Eq. 4.5.)

Water infiltrates into soil because of the gradient of water pressure and the force of gravity. These two components are strictly related to the physical steady state of the soil layer δz in the instant δt . Thus,

considering the water movement constrained on the z dimension, and defining the boundary conditions in Eq.4.6b., the gravimetric and diffusivity influence on water infiltration may follow the Eq. 3.6a. (JY Parlange, 1971)

$$\frac{\partial z}{\partial t} + \frac{\partial}{\partial t} \cdot \left[\frac{D}{\partial z / \partial \theta} \right] = \frac{\partial K}{\partial \theta}$$

(Eq. 4.6.a)

$$\begin{cases} t = 0, & z > 0 & \theta = 0 \\ t > 0, & z = 0 & \theta = 1 \end{cases}$$

(Eq. 4.6.b)

where D is the diffusivity, K the conductivity, $z(\theta, t)$ the depth of the point with moisture θ at time t .

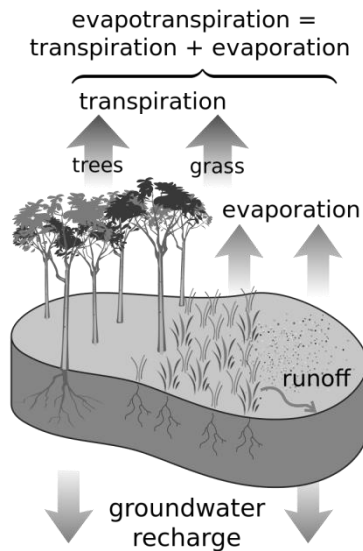


Fig. 4.5. Schematic representation of a terrestrial ecosystem Ecohydrology

3D-CMCC-Pheno-FEM still doesn't account this physical component, and in fact the water dynamics into the soil profile are assumed merely as a function of evaporation, transpiration and runoff (Manabe, 1969).

Thus the Eq. 3.5 becomes:

$$w_t = \int_{z=0}^Z (w(z) - E(z) - R(z)) \partial z$$

(Eq. 4.7.)

with $E(z)$ assumed as the sum of the soil evaporation and water uptake from roots at depth δz due to canopy transpiration.

The evapotranspiration is defined as the sum of the soil water evaporation and canopy transpiration (Fig. 4.5.). Canopy conductance and stand transpiration was modeled following the Biome approach (Thornton, 2010):

$$CT_t = \int_0^H \frac{E_{20} \cdot R_N(h) + \rho \cdot \lambda \cdot VPD \cdot Bl_k(s)}{\lambda \cdot (1 + E_{20} + Bl_k(s)/CK_M(L))} \delta h$$

(Eq. 4.8.)

Assuming that all the rain intercepted by the canopy got lost due to canopy evaporation following the Eq. 4.3., the total amount of system evaporation can be assumed as the sum of the Soil evaporation and the water dissipated by $\Omega(L, b)$.

Soil evaporation (S_E) is a process occurring at the boundary layer with the atmosphere. This process is related to the net radiation transmitted through the canopy and reaching the surface, along with the water concentration in the boundary layer for the thickness δz . Assuming the process to be independent to time ($dS/dt = 0$) daily Soil Evaporation was determined by the following:

$$S_E = \frac{E_{20} \cdot N_{rd_s}}{(E_{20} + \varphi_c) \cdot \lambda} \cdot \varepsilon \cdot \theta(z) \cdot \left(1 - \int_0^H CC(h) \delta h \right) \cdot D_l + S_{sbl}$$

(Eq. 4.9.)

4.2.3. Ecosystem Respiration

Respiration is the process of mineralization of organic carbon which determines the Ecosystem Carbon loss, along with forest management (Schulze et al., 2002). Defined in this way it is ideally determined by the sum of each biological entity respiration (above and belowground), plus the carbon oxidation due inorganic respiration and combustion. Assuming that these two are negligible in ecosystems with no fire passage (Fig 3.6), the *Reco* may be described by:

$$\begin{aligned}
 Reco_t = & \int_0^H \int_1^A \int_1^{SP} \int_1^{Pa} AR_A([N](h, a, sp, cl), T_t, CC(h, a, sp, \rho), C_t) \delta h \delta a \delta sp \delta cl \\
 & + \int_0^Z \int_1^{Bsp} \int_1^S HR(f_S(clay, bd, hc, z), Ts(z, Lit), \varepsilon(Bsp), Cp) \delta z \delta Bsp \delta cp \\
 & + \int_0^Z \int_1^A \int_1^{SP} \int_1^{Pa} AR_B([N](h, a, sp, cl), T_t, CC(h, a, sp, \rho), C_t) \delta h \delta a \delta sp \delta cl
 \end{aligned}
 \tag{Eq. 4.10.}$$

where RA is the autotrophic respiration of a specific tissue of the aboveground (RA_A) or belowground (RA_B) portion of a specific tree, while HR is the heterotrophic respiration of the microbes living in the δz portion of soil.

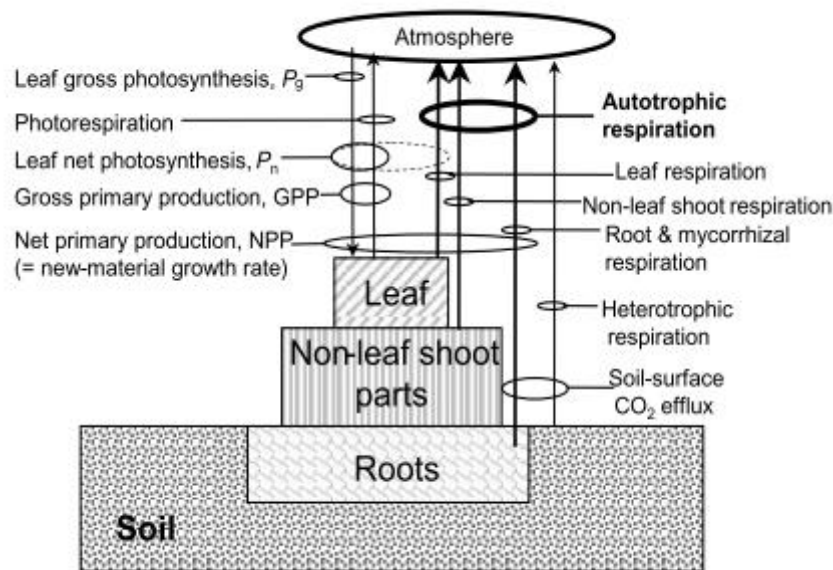


Fig. 4.6. Schematic representation of the several components contributing to the Ecosystem Respiration (Gifford, 2003).

How to model the autotrophic respiration has been an argument widely discussed and still under debate. A few years ago Gifford (1995) proposed an empirical solution assuming that the ratio of respiration and photosynthesis (R:P) may be relatively constant, ranging from 0.40 to about 0.45. This ratio was independent to temperature (Gifford, 2003). Other studies confirmed this finding by demonstrating that R:P on the long period was necessarily constrained between quite narrow bounds, albeit for not biological reasons but mathematical ones. However the R:P was no longer constrained to small values modeling the process on daily temporal resolution (Van Oijen, Schapendonk, and Höglind 2010).

“At least nine plant processes can be separated which require energy: growth (Penning de Vries et al., 1983; Thornley and Johnson, 1990); nitrate reduction, symbiotic dinitrogen fixation; root N-uptake; other ion uptake; phloem loading, protein turnover; maintenance of cell ion

concentrations and gradients; and apparently wasteful, heat producing respiration following the alternative (cyanide resistant) pathway or futile cycles” (Cannell & Thornley, 2000).

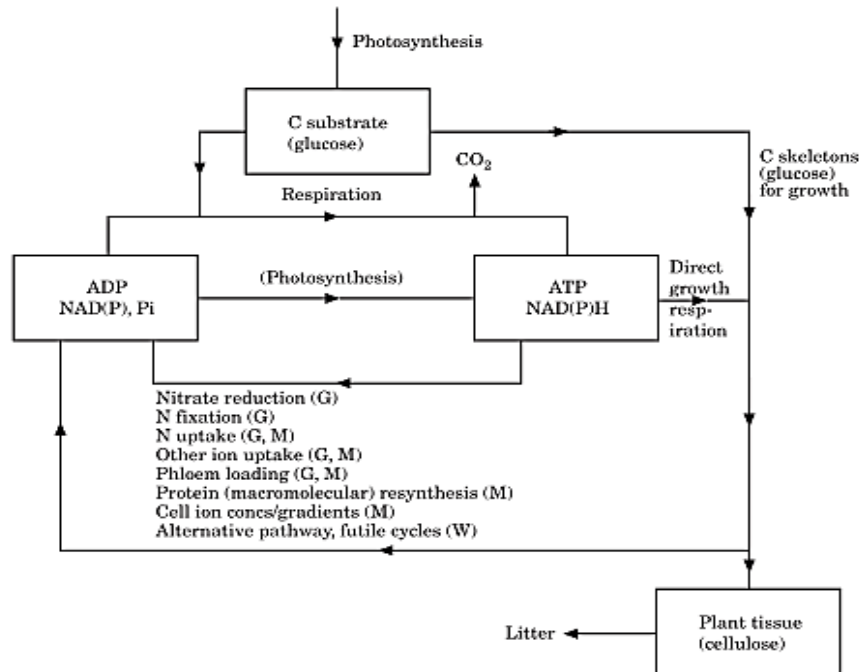


Fig. 4.7. The flowchart representing the rationale of the Autotrophic respiration process (Cannell & Thornley, 2002).

Since the constitutive relations between these components have not been identified yet, respiration models usually unify these processes in Growth (GR) and Maintenance (MR) respiration. Solutions for these two process variables are determined by using empirical relations. By the way the growth-maintenance paradigm is valuable, but there is no rigorous division between the two components.

The current version of 3D-CMCC-FEM determines MR and GR following the theoretical partitioning of McCree (1970) and Thornley (1970):

$$R_{A,t} = \int_{c_p=0}^{c_p} \left(\frac{(1 - Y_G(c_p))}{Y_G(c_p)} \cdot \frac{\partial C(c_p)}{\partial t} + m \cdot \frac{\partial}{\partial t} C(c_p) \right) \delta c_p$$

(Eq. 4.11)

where c_p stands for the specific tissue Carbon pool. The integral is simplified by the model by aggregating each Carbon unit (gC) in five different biomass compartments (Collalti et al., 2014).

The first term of the Eq. 4.11. represents Growth respiration. Y_g , the biosynthetic efficiency, was parameterized following Biome (Thornton, 2010). $C'(c_p)$ was determined by taking into account the NPP of the specific Biomass Compartment for the previous day.

Maintenance respiration was represented by the second term of the equation; it is the most responsive of the functional components of respiration to environmental change, because the processes of protein synthesis and replacement, membrane repair and maintenance of gradients of ions and metabolites vary exponentially with temperature (M. G. Ryan 1991). Thus estimate MR correctly is essential to reliably estimate AR dynamics and realistically reproduce its inter temporal variability. Unfortunately this task is tricky and still in debate.

“The nature of MR has long been a controversial concept. Many may doubt the existence of a separate process which could be dubbed ‘maintenance’. It is difficult to represent an MR process in crop and ecosystem models directly and effectively – such efforts easily give rise to unacceptable behavior or ad hoc assumptions being introduced into the model”(Thornley, 2011).

Rates of enzymatic processes of respiration increase with temperature and thus environmental physiologists often express respiration rates in terms of Q_{10} , the change in MR rate with a 10°C change in Temperature (Ryan, 1991). Thus the maintenance coefficient was expressed as

$$m(T_t) = Q_{10}^{((T_t-20)/10)}$$

(Eq. 4.12)

where T_t was the Temperature in °C of the medium at the specific time t . For simplicity, average daytime and nighttime temperatures were used when the medium was the atmosphere; daily average soil temperature was used for both night and day when the medium was the soil.

According to Ryan (1991) MR is better correlated with the Nitrogen content dynamics rather than Carbon of the specific tissue; thus the $C'(c_p)$ of the second term was replaced by $N'(c_p)$ as follows:

$$R_{A,t} = \sum_{c_p=0}^{c_p} \left(\frac{(1 - Y_G(c_p))}{Y_G(c_p)} \cdot \frac{\partial C(c_p)}{\partial t} + m \cdot \eta \cdot \frac{\partial}{\partial t} N(c_p) \right)$$

(Eq. 4.13.)

Where η is the slope of the empirical relation between $N(c_p)$ and $RM(c_p)$.

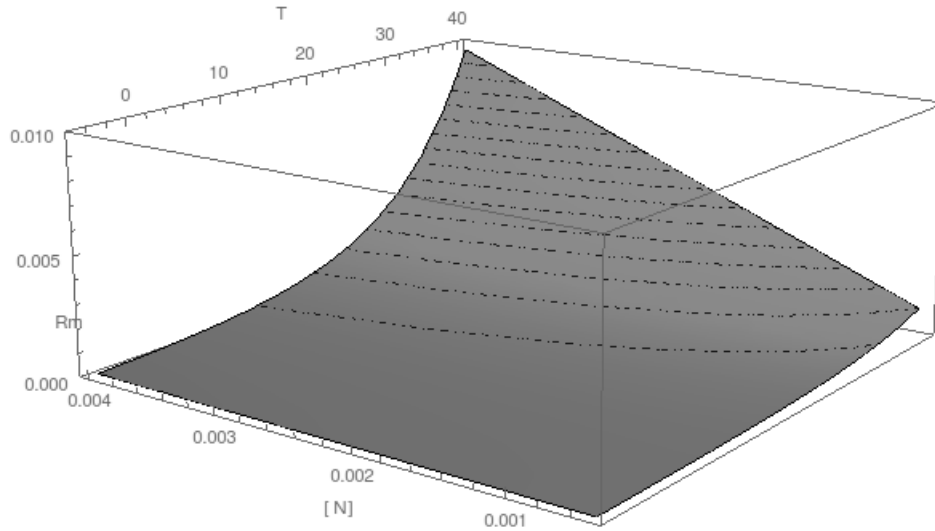


Fig. 4.8. The rationale used to represent Maintenance Respiration (MR) considers it to be determined by an exponential function of Temperature, whose slope is directly proportional to tissue [N]. This method is strongly dependent on tissue N content, which however is grossly quantified from a constant C:N ratio.

Soil water content strongly affects substrate diffusion and thus indirectly affects their availability for respiration. Moreover at water contents below desiccation stress threshold (usually matric potential < 1.5 MPa) loss of tissue turgor, stomatal closure and leaf shedding occur (Davidson et al. 2006). In addition the metabolic reactions involving cell respiration is inhibited under a minimum temperature usually referred as the biological zero. To take these two reduction factors into account a new version of maintenance coefficient have been introduced and the Eq. Xi was modified into:

$$m(T_t) = Q_{10}^{\left(\frac{(T_t-20)}{10}\right)} \cdot f_{\varphi}(swc) \cdot f_{T_0}(sp)$$

(Eq. 4.14.)

where $f_{\varphi}(swc)$ was the soil matric potential reduction factor :

$$\left\{ \begin{array}{l} f_{\varphi}(swc) = \frac{1}{1 + \left(1 - \theta / \alpha_{sw}(sp)\right)^{\beta_{sw}(sp)}} \\ \varphi_{sat}(txt) \cdot \left(W_{vc} / W_{vc_{sat}}\right)^{\frac{\partial}{\partial t} \left(\frac{\ln(\varphi)}{\ln(rwc)}\right)} < \varphi_D \end{array} \right.$$

(Eq. 4.15.)

where $\beta_{sw}(sp)$ and $\alpha_{sw}(sp)$ are parameters depending on species. $f_{T_0}(sp)$ represented the biological zero biochemical inhibition factor, and was considered a constant limiter of 0.1 for all species.

$$\left\{ \begin{array}{l} f_{T_0}(sp) = 0.1 \\ T_t \leq T_0(sp) \end{array} \right.$$

(Eq. 4.16.)

4.2.4. Soil respiration (SR)

During the decomposition processes of SOC (e.g. from fresh organic matter (FOM) to humic organic carbon (HUM)), part of the energy gets lost in atmosphere as mineral Carbon (mainly CO₂) (Changsheng 2007) because of the metabolic activity of soil biota. Theoretically each organic compound has a different stability which makes it more or less difficult to be attacked by fungi, bacteria or arthropods. According to Sollins et al. (1996) SOC stability is just partly related to its chemical recalcitrance, while it is mainly determined by its accessibility, and interaction with clays, especially in deeper portions of the profile (Eusterhues et al. 2005).

As a matter of fact SOC reacts with the inorganic fraction and gets incorporated in aggregates which make the organic compound inaccessible to most of the microbes (Quiquampoix et al., 2002; Tietjen and Wetzel, 2003). Moreover microbial activity and population dynamics are strictly related to the ever-changing environmental conditions.

For what discussed so far the soil respiration process ideally follow the pattern of a typical prey-predator relation:

$$\begin{cases} \frac{\partial C_z}{\partial t} = \alpha \cdot C_z(t) - \delta \cdot C_z(t) \cdot B_z(t) \\ \frac{\partial B_z}{\partial t} = \gamma \cdot B_z(t) + \delta \cdot C_z(t) \cdot B_z(t) \end{cases}$$

(Eq. 4.17.)

where $\frac{\partial C_z}{\partial t}$ is the CO₂ efflux, $C_z(t)$ the quantity of the specific Organic Compound family, $B_z(t)$ the microbial whole population competing for the $C_z(t)$. The factors α , γ , δ respectively represent the littering process, the microbial turnover and the SOM “predation” factor. The α and γ constitutive relations will be discussed in the littering processes and soil carbon dynamics sections respectively.

The predation factor is related to both the specific SOM family stability and the micro environmental conditions.

$$\delta(cp, z) = \mu_T \cdot \mu_M \cdot \mu_A \cdot k_{cp}$$

(Eq. 4.18.)

$$\left\{ \begin{array}{l} \mu_T = -a \cdot T^2 + b \cdot T + c \\ \mu_M = -a \cdot \theta^3 + b \cdot \theta^2 + c \cdot \theta - d \\ \mu_D = 0.6 \cdot z_i^{-0.136} \cdot (-0.02 \cdot clay_{\%} + DRF) \\ \mu_A = \mu_D \cdot \frac{\log(0.14 \cdot clay_{\%}^{-1}) + 1}{2.3026} \\ k_{cp} = a(sp) \end{array} \right.$$

(Eq. 4.19.)

where μ_T represents the temperature factor, μ_M the moisture factor, μ_A the accessibility, k_{cp} the recalcitrance; μ_D a clay dependent depth factor (Fumoto et al. 2008a). Since aggregation with clay is negligible in litter, the μ_A factor is simplified as the only μ_D component by 3D-CMCC-Soil Routine. The k_{cp} factor was treated as a specific parameter dependent on the biomass compartment.

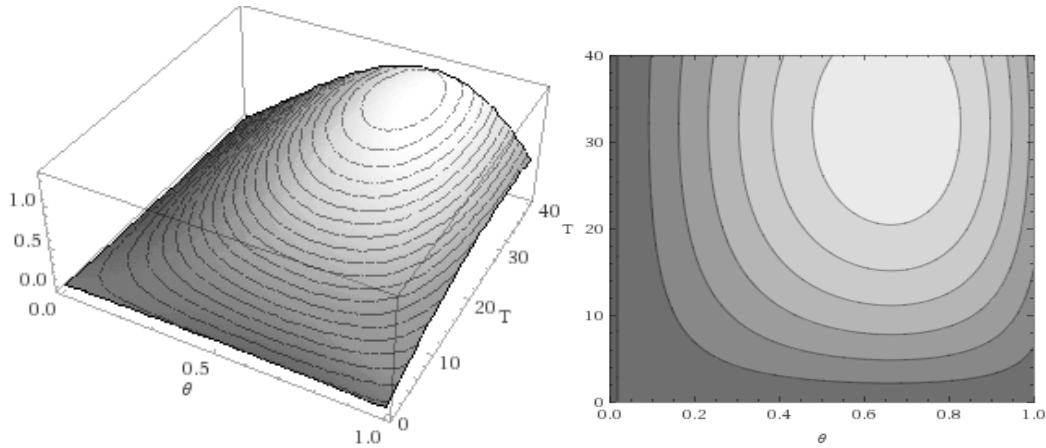


Fig. 4.9. Influence of T and θ on SOM decomposition and SR. The two components act as a paraboloid, following the boundaries of the theoretical and actual niche of microbial populations (θ), and the boundaries of minima and maxima reaction rates.

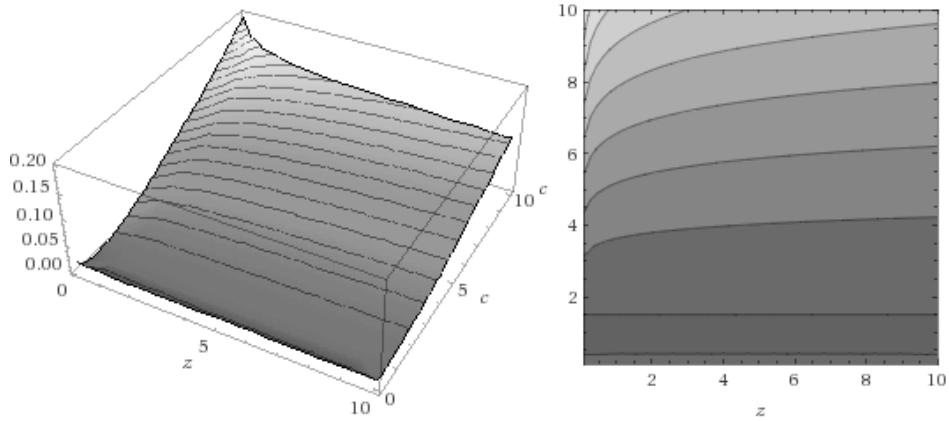


Fig. 4.10. Influence of soil depth on SR.

The specific C pool mineralization dynamics could be solved as a zero-order kinetics with respect to the active microbial biomass (Molina et al. 1983). The difference between the actual and potential rates of residue decomposition reflects the availability of N (Molina et al. 1983). Thus the actual respiration rate of the whole soil profile for a single point in $U(x,y)$ may be computed as the sum from the boundary to the deepest soil layer, from the most labile to the most recalcitrant SO compound of the profile:

$$\frac{\partial C}{\partial t} = \int_0^z \int_0^{cp} (\mu_{w\&T} \cdot \mu_N \cdot \mu_L \cdot \mu_A \cdot k(cp) \cdot C_t) \delta cp \delta z$$

$$+ \int_0^{zL} \int_0^L \left(\mu_{w\&T} \cdot 0.01 \cdot C_t - \frac{\partial C_F}{\partial t} \right) \delta cp \delta z$$

(Eq. 4.20.)

For simplicity the 3D-CMCC Soil Routine represented the SOC in three families and eight sub families (C pools) with average chemical characteristics. The characteristics and dynamics of these C pools will be discussed below in the Soil Carbon Dynamics section.

4.2.5. Tree Carbon Dynamics: the Phenology and Allocation routine

Phenological transitions drive the seasonal progression of vegetation through stages of dormancy, active growth, and senescence. Phenology influences both spatial and temporal (at seasonal-to-inter-annual time scales) variability in ecosystem productivity (Richardson et al., 2012). Phenology and allocation drive the Carbon dynamics throughout the aboveground and belowground C pools, and thus respiration and competition processes. Furthermore it affects hydrology and atmospheric feedbacks (Richardson et al., 2012).

Unfortunately a lot of processes involving phenology are still obscure and represented simplistically so that terrestrial ecosystem models overly result in biased predictions (Kucharik et al., 2006; Ryu et al., 2008; Richardson et al., 2013b).

Several phenological bud burst models have been published for tree species, but their application have so far been applied either to data sets of limited size for single species, small data sets from a geographically limited region or to clones (Schaber and Badeck 2003).

3D-CMCC-FEM uses one of the most simplistic and widely used approaches to reproduce bud burst, the so called thermal growing degree (GDD) approach (Wang , 1960). Thus new leaves emergence for both evergreen and broadleaves occurred when:

$$GDD_{Max} - \max_{T_0(sp) \leq T_{day} \leq \infty} (T_{day} - T_0(sp)) - GDD_d \leq 0$$

(Eq. 4.21.)

Leaf ecology from emergence to senescence is obviously different in evergreen and deciduous species. We considered two phenological classes (Evergreen and Deciduous), and discerned each one into two sub classes (broadleaves and needle-leaves). The 3D-CMCC-FEM 6.1 major modifications were developed on the class level. Deciduous species maintained the same partition in five phenological phases of the 5.1 (Collalti et al., in prep, Thonrton et al., 2010), evergreen phenology was modified to be discretized in 4 different phases (Tab 3.1)

Tab. 3.1. Phenology routine scheme for Evergreen (needle/broadleaves) and Deciduos (needle/broadleaves) species.

<i><u>Deciduos</u></i>		<i><u>Evergreen</u></i>	
<i><u>Phase</u></i>	<i><u>Trigger</u></i>	<i><u>Phase</u></i>	<i><u>Trigger</u></i>
Bud Burst	GDD treshold	Bud Burt	GDD treshold
Leaf development	PeakLai/2	PeakLai	Pipe model
PeakLai	Pipe model	Leaffall	Daylength treshold
Leaffall	Daylength treshold		
Unvegetative	Delpierre		

The main novelties for deciduous species phenology were;

- the development of a Carbon injection equation to simulate the use of non-structural reserve C for leaves and fine roots growth during the budburst phase;
- the innovative yellowing and senescence sub model.

4.2.6. Leaf elongation: introducing the Carbon injection equation for deciduous species

Soon after bud burst shoots internodes elongation occurs, and then leaves primordia start to grow. Cell division predominate during early stages while subsequent expansion determines the development of leaves final shape (Pallardy 2008). In the context of this fraction of annual developmental cycle most of the metabolized Carbon comes from Carbohydrates reserves (e.g. “nonstructural Carbon pool” B_R), especially during the early stage (Carbone et al., 2013; Richardon et al., 2013). Moreover it is widely recognized that in this stage most of the net primary production is destined to shoots, leaves and fine root development. Thus idealistically the total B_R Carbon injection into early development of shoots leaves and fine roots could be represented by the following first order ordinary linear differential equation (ODE):

$$\frac{\delta B_R}{\delta t} - R_{S\&F\&R}(t) \cdot B_R(t) = 0$$

(Eq. 4.22.)

where $R_{S\&F\&R}(t)$ is the instantaneous proportion of Reserve Carbon demand for shoots & foliage growth. Assuming that the tree system potentially extends the total amount of B_R for new fine roots & leaves, the potential total fractional B_R loss at the end of this phenological stage would be equal to 1. We expect that actual Carbon request may exponentially decrease with increasing leaf maturity (Keel et al., 2010), while the demand should increase with increasing number of leaf primordia. For simplicity we assumed that the two components resulted in a linear function. Thus

$$\frac{R_{S\&F\&R}}{BB_T} = 1 = \int_0^t \frac{B_0 \cdot t}{BB_T} \delta t$$

$$R_{S\&F\&R}(t) = \frac{2t}{BB_T^2}$$

(Eq. 4.23.)

The two components which influence the actual Carbon request are finally determined resolving the ODE by substituting $R_{S\&F\&R}(t)$.

$$\frac{\delta B_R}{\delta t} = \frac{B_0 \cdot e^{2t+2/BB_T^2} \cdot e^{-t^2/BB_T^2}}{BB_T} \cdot \frac{2t}{BB_T^2}$$

(Eq. 4.24.)

where e^{2t+2/BB_T^2} is the biomass dependent and e^{-x^2/BB_T^2} the maturity dependent factor. From now on we will refer to the Eq.Xi as the Carbon Injection Equation.

Daily gain in foliage biomass (B_L) and fine root biomass is determined as follows

$$\left\{ \begin{array}{l} \frac{\delta B_L}{\delta t} = \frac{\delta B_R}{\delta t} \cdot \frac{(\delta t)}{BB_T} \cdot \mu_L + \left(\frac{\delta GPP}{\delta t} - \frac{\delta R_A}{\delta t} \right) \\ \frac{\delta B_{Roots}}{\delta t} = \frac{\delta B_R}{\delta t} \cdot \frac{(\delta t)}{BB_T} \cdot (1 - \mu_L) + \left(\frac{\delta GPP}{\delta t} - \frac{\delta R_A}{\delta t} \right) \end{array} \right.$$

(Eq. 4.25.)

being μ_L a species specific parameter reflecting the fraction of $B_R'(t)$ reserved to leaf growth.

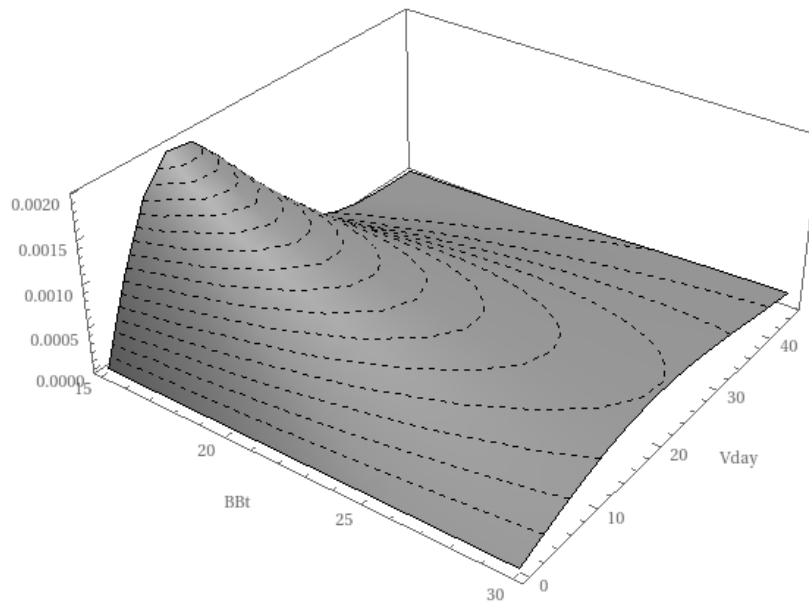


Fig. 4.11. Graphic representation of the Carbon injection function.

4.2.7. Normal growth: Deciduous species

Even though Reserve Biomass could all be destined to the elongation phase, it is usually not necessary. This phase ends with the canopy reaching an amount of foliage biomass equal to half of the maximum theoretical carrying capacity. Maximum B_L is determined as a function of sapwood and crown area following the pipe model approach (Köstner et al., 2002).

$$Pk_L = SW_A \cdot B_{Sw} / B_L \cdot C_A^{-1}$$

(Eq. 4.26.)

Before reaching the maximum canopy capacity, the model allocates all daily NPP to foliage and fine roots biomass, using the very same μ_L parameter as before. After reaching the Pk_L new Carbon allocation and repartitioning follows the same approach of the previous version of 3D-CMCC-FEM (Collalti et al. 2013; Arora & Boer 2005).

4.2.8. Senescence and yellowing: a novel semi empirical approach to reproduce leaf yellowing and littering for deciduous species

Leaf senescence is of primary importance in determining heterotrophic (and therefore ecosystem) respiration dynamics (Hibbard et al., 2005; Knohl et al., 2003), as leaf litter represents half of annual litter input. To date, understanding the processes behind leaf senescence is still a challenge. Though some of the implied molecular agents of senescence have been identified and related to stress-responses pathways, environmental triggers and their interactions are still far from clear

(Delpierre et al. 2009a). The original version of 3D-CMCC-FEM represented the senescence process by linearly decreasing leaves biomass for a time lapse which was a parameterized fraction of the vegetative period. Thus part of our energies were invested in improving fall phenology and senescence routine. We collected LAI (MOD15A2) and LST (MOD11A2) data from MODIS Global Subsets program for a period of 13 years and about 15 cells (1km x 1km) extracted from the European Forest Institute (EFI) Forest Map with dominant deciduous species. The data observed followed a logistic function with positive $\beta(t)$. Assuming for hypothesis that all leaves inhabiting the tree ecosystem get lost at the end of the senescence season, variation in LAI (L) may follow:

$$\frac{\partial L}{\partial t} = L(t) - \left(0, \frac{\alpha(h,a,sp)}{1+e^{t-\beta(t)/\gamma(t)}} \right)$$

(Eq. 4.27.)

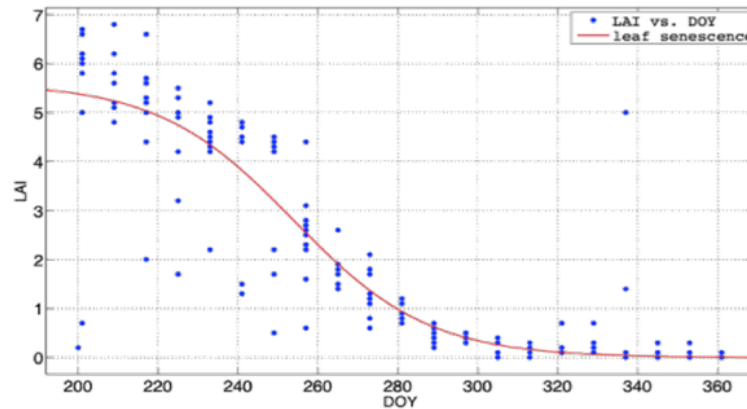


Fig. 4.12. regression fitting of the MODIS LAI 8day data for a beech forest (Italy). The pattern shown was revealed for the other analyzed sites, thus we suspect it may be generalized at least to continental level. It is evident that the use of the VPsat threshold as a trigger may be used to determine a slight reduction rather than the sigmoid function itself.

Where $a(t)$, $\beta(t)$, $\gamma(t)$ are parameters which have specific mathematical characters bounded to the general properties of the logistic function. In fact it can be demonstrated that:

$$\left\{ \begin{array}{l} \alpha(h, a, sp) = L_{0+\delta t}(h, a, sp) \\ \beta(s) = t_0(s) + \frac{\Delta t(s)}{2} \\ \gamma(s) \cong \frac{\Delta t(s)}{\ln(0.1) - \ln(10(\beta(s) - 0.1))} \end{array} \right.$$

(Eq. 4.28.)

Thus, assuming $L_{0+\delta t}$ the value of peakLai (Eq. i) the senescence algorithm for the vertical column in $U(\delta x, \delta y)$ could be determined as:

$$\frac{\partial L}{\partial t} = \int_{h=0}^H \int_{a=0}^A \int_{sp=0}^{sp} \left(L(h, a, sp) - \frac{Pk_L(h, a, sp)}{1 + e^{\frac{t - t_0(s) + \frac{\Delta t(s)}{2}}{\gamma(s)}}} \right)$$

(Eq. 4.29.)

It is clear that the algorithm is strictly dependent to the function $\Delta t(s)$ (e.g. senescence phase time span) and $t_0(s)$ (e.g. the first day of senescence), which however are tricky to be determined (Salk, 2011). We used the framework exposed in a former modeling work (Delpierre et al. 2009; Vitasse et al. 2011) as basis to determine $\Delta t(s)$. Leaf senescence period was achieved when a temperature and photoperiod dependent function (e.g. $R_{sen}(t)$) reached a threshold value (Y_c). Thus we modelled the time derivative of the state of coloring and senescence on a daily basis as:

$$\left\{ \begin{array}{l} R_{sen}(t) = (T_M(s) - T(t)) \cdot \left(\frac{D_L(t)}{D_L(0)} \right)^2 \\ \Delta t(s) = \sum_{R_{sen}(t)=0}^{R_{sen}(t) < Y_c} R_{sen}(t) \end{array} \right.$$

(Eq. 4.30.)

Where T_M was a specific parameter representing the maximum temperature at which senescence processes were effective, $D_L(0)$ the photoperiod of the first day of senescence, $D_L(t)$ the photoperiod of the i_{th} day of the year. When this approach failed a fraction of the vegetative period was used instead following BIOME scheme (Thornton, 2010).

Determination of senescence starting date is an argument on debate, but still there are molecular evidences that it may be related to the reaching of a maximum night length (Woo et al., 2003; Lim et al., 2007). Therefore we assumed senescence $D_L(0)$ to be triggered by a predetermined minimum photoperiod, consistently to previous Model version. **(Collalti et al., in prep.)**. However we suspected that vapor pressure deficit could have a role in triggering reduction of Leaf area angle in summer, as effect of stomata closure, loss in turgor and partial yellowing (Shao et al., 2008; Huemmrich, 2013). For this reason we determined vapor pressure saturation by using LST MOD11A2 data following Hashimoto (2011); we extracted ten points in Italy of known dominant species class (*Quercus robur/petrea* and *Fagus sylvatica*) and canopy cover greater than 20% from the EFI Forest Map (Brus et al. 2012). Observing the patterns of LAI and VPsat we noticed that summer reduction in LAI averagely started the period in which the Gaussian

distribution function fitting daily VP_{sat} reached its maximum ($VP_{sat}'(t) = 0$) (unpublished data).

Nevertheless we decided not to use this $VP_{sat}'(t)$ threshold to determine LAI reduction activation, since we still needed to validate the relation on a wider range of data points and need confirmation from data collected on field. As a matter of fact the improvements observed correlating the model's outputs with MODIS data were not consistent with those obtained by contrasting model outputs with field data collected for Collelongo CARBOEUROPE site (ITCol) using LI-COR 2000 in 2005 (D'Andrea, personal communication) (Fig. 4.13). Thus we suspect that the VPD influence on LAI reduction may trigger a slight reduction of LAI, which however starts to strongly decrease only after reaching the minimum daylength. Since we are still debating on the reliability of this intuition and on the magnitude of this summer reduction, we have decided to use the former "photoperiod only dependent" approach of 5.1 model version.

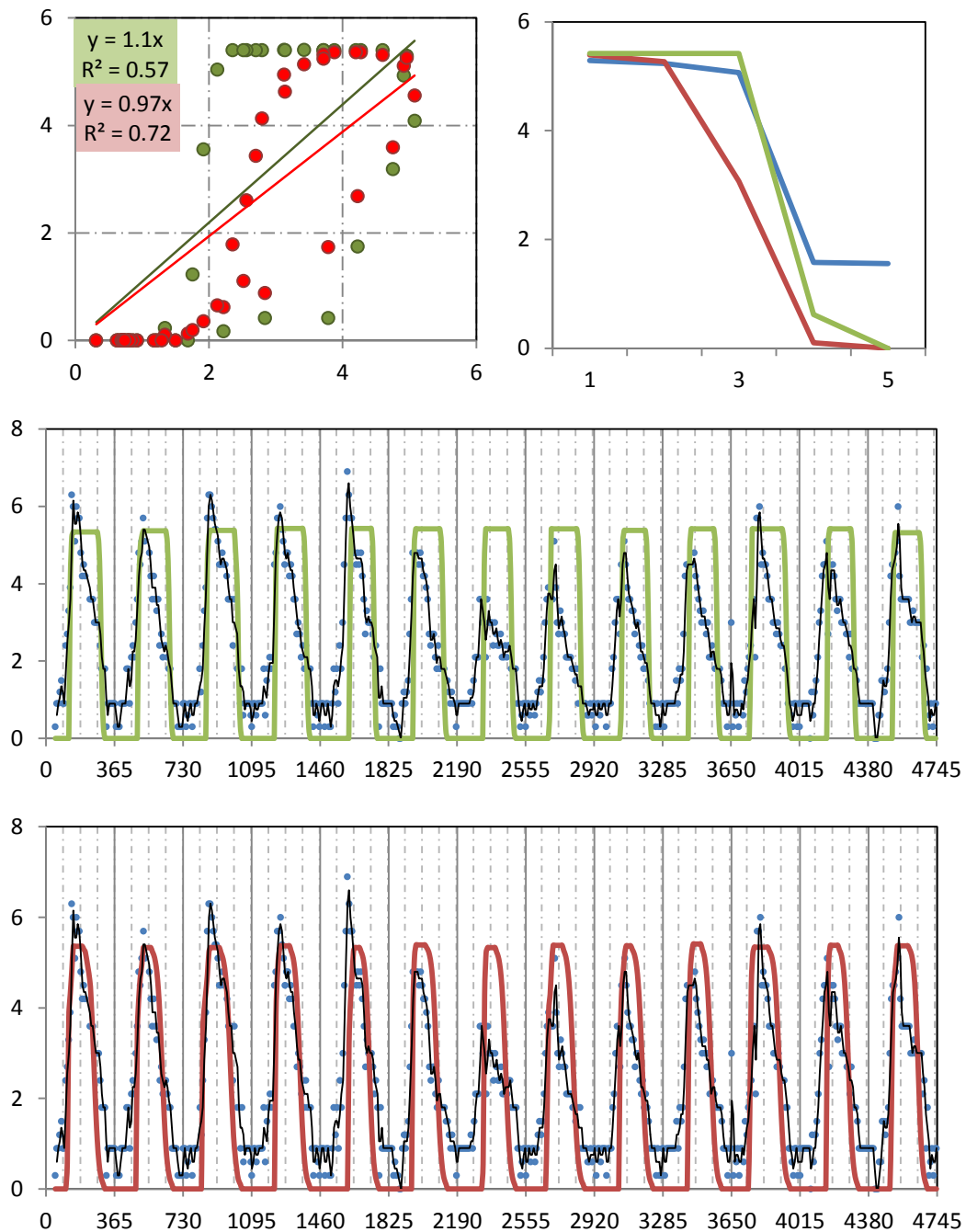


Fig.4.13. Comparison between the two versions of the new leaf fall equation (the photoperiod based in green; the VPsat based in red). Data refer to the Collelongo beech forest CarboEurope site. Box (a) shows the correlation with MODIS 8day data; the use of the VPsat as a trigger of LAI reduction resulted in a significant improvement in both correlation, goodness of fit and estimation error. However box (b) shows that according to field captured data the LAI reduction may be overestimated. Boxes (c) and (d) represents MODIS and Modeled trends throughout the simulation The sensation is that the red version gives better results, and that this relationship should be further investigated.

4.2.9. Evergreen leaves turnover: a novel competition based approach to evaluate dynamics of leaves populations.

While leaves populations of deciduous stands all face death within the year, evergreen canopies follow a very different pattern. Most of the BGMs models simplify evergreen canopy turnover by linearly reducing the foliar biomass acquired the year before throughout current year (Thornton, 2010; Collalti et al, 2013). However we suspected this approach to be too simplistic. As a matter of fact many species have leaf life span exceeding two years, and thus this approach may underestimate or overestimate leaf littering consistently to patterns in inter-annual variability of leaf carbon allocation. Moreover leaf turnover seems to be concentrated in specific annual windows consistently to new leaf emergence (spring) and approaching of photosynthetic inefficient season (fall) (Devi et al., 2013; Chabot et al., 1982; Nitta et al., 1997). In addition conifers photosynthetic rate is age-dependent, declining in a quasi-exponential fashion (Chabot and Hicks 1982). For these reasons we developed an attempt to reproduce leaves dynamics in evergreen canopies without increasing the number of parameters and conserving a simplistic framework.

We assumed the canopy to be a population of leaves in competition for nutrients and light, which cannot move from their position and are disposed so that elder are constrained to a more and more shaded position. In this framework, competition between leaves within a crown may be represented as the simplest version of the “Competition for one Resource” conceptual model of Grace & Tilman (1990):

$$\left\{ \begin{array}{l} \frac{\partial B_i(t)}{\partial t} B_i(t)^{-1} = f_i(R) - f_i(m_i) \\ f_i(R) = \frac{r_i \cdot R}{(R + K_i)} \\ R_i^* = \frac{m_i \cdot Y_i}{(r_i - m_i)} \end{array} \right.$$

(Eq. 4.31.)

In this model, originally developed to simulate algae competitions, the (R_i^*) is the concentration of available resource that a leaf generation requires to survive in the canopy habitat, r_i the max photosynthetic rate, m_i is the competition independent loss rate (which we considered to be Maintenance Respiration), Y_i Carbon yield. Thus according to Tilman's conceptual model the R^* was the key variable to evaluate a species (or a generation in this case) survivorship (S^*). As a matter of fact S^* may be quantified as $f_i'(R_i^*)$

But how do R^* change through generations? In the context of a tree crown, ignoring water asymmetric upwelling, leaves compete just for light. For hypothesis, older leaves live in the shaded portions of the canopy, where light transmitted is reduced following Lambert Beer's exponential decay equation (Vose et al., 1995); thus the more they are old, the more they are shaded. As to max photosynthetic rate, we expect an age dependent quasi exponential decay in leaf quantum efficiency (Chabot and Hicks 1982). Consequently, being growth rate directly proportional to both a and $APAR$, we expect a more than exponential decay in r_i .

Nutrient content (and thus Nitrogen) in older leaves is often lower than in younger leaves, indicating withdrawal from segments of the plant with low productivity and transfer to new leaves of higher productivity (Chabot and Hicks 1982). That implies, following Ryan's assumptions on maintenance respiration (Ryan, 1997), that an exponential reduction in Maintenance costs occur too. For hypothesis we assumed that Y_i constancy (Waring, Landsberg, and Williams 1998) may be valid within a single tree, as the conjunctive effect of reduction in respiration rate and quantum yield efficiency. We assumed though that the three components of the Eq.Xi may have the following shapes:

$$\begin{cases} m_i = m_0 \cdot e^{-k_\eta \cdot t} + m_m \\ r_i = (\alpha_0 \cdot e^{-k_\alpha \cdot t} + \alpha_m) \cdot (\lambda_0 \cdot e^{-k_\lambda \cdot t} + \lambda_m) \\ k_{i=const} \end{cases}$$

(Eq. 4.32.)

where m_0, α_0, λ_0 are the MR, quantum yield and APAR at the end of the most favorable period (i.e. the first day of bud burst at the second year of life). m_m, α_m, λ_m are the theoretical minima values to grant leaf survivorship in a non-competition context. $k_\eta, k_\alpha, k_\lambda$ are the exponential parameters for the three functions, shaping the magnitude of their decay.

On the basis of these hypotheses the Eq 4.31. becomes:

$$R_i^* = \frac{(m_0 \cdot e^{-k_\eta \cdot t} + m_m) \cdot k_i}{(\alpha_0 \cdot e^{-k_\alpha \cdot t} + \alpha_m) \cdot (\lambda_0 \cdot e^{-k_\lambda \cdot t} + \lambda_m) - (m_0 \cdot e^{-k_\eta \cdot t} + m_m)}$$

(Eq. 4.33.)

A strong simplification was the hypothesis that the three exponential functions varied with the same magnitude in time and thus:

$$k_\eta = k_\alpha = k_\lambda = \xi$$

So the Eq. 4.33. became the positive logistic function in Eq. 4.34.

$$R_i^* = \frac{(m_0 k_i) \cdot e^{-\xi} + (m_m \cdot k_i)}{(\alpha_0 \lambda_0) \cdot e^{-2\xi} + (\alpha_0 \lambda_m + \alpha_m \lambda_0 - m_0) \cdot e^{-\xi} + (\alpha_m \lambda_m - m_m)}$$

(Eq. 4.34.)

Following the theoretical assumption that the denominator has to be greater than zero for the *i*th generation to survive (Tilman et al., 1997), it can be demonstrated that:

$$(\alpha_0 \lambda_m)^2 \leq 2\alpha_0 \lambda_0 m_m - (\alpha_m \lambda_0)^2$$

(Eq. 4.35.)

And thus, considering that $2\alpha_0 \lambda_0 m_m \rightarrow 0$ the R_i^* can be calculated for species where:

$$\frac{\alpha_0}{\alpha_m} \leq \frac{\lambda_0}{\lambda_m}$$

The model described so far can be graphically represented as in Fig. 4.14.

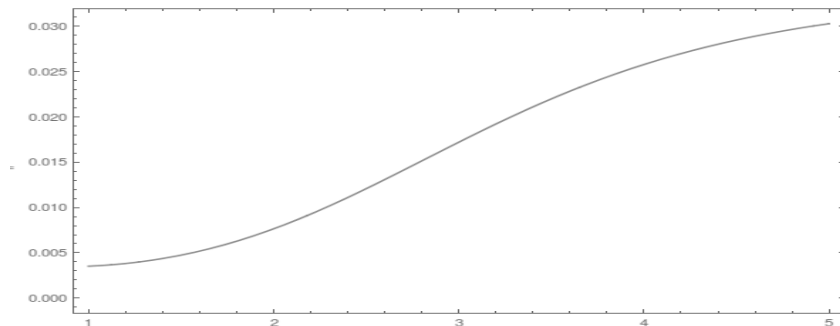


Fig. 4.14. Shape of the R^* function as a result of the theoretical assumptions

For simplicity we decided to use the following parabolic function as a kernel to represent $S^*(t)$ of each i th foliar generation:

$$S_i^*(t) = \frac{1}{2}t^2 - \frac{2BF_{LS(i)} + 1}{2}t + BF_{LS(i)}$$

(Eq. 4.36.)

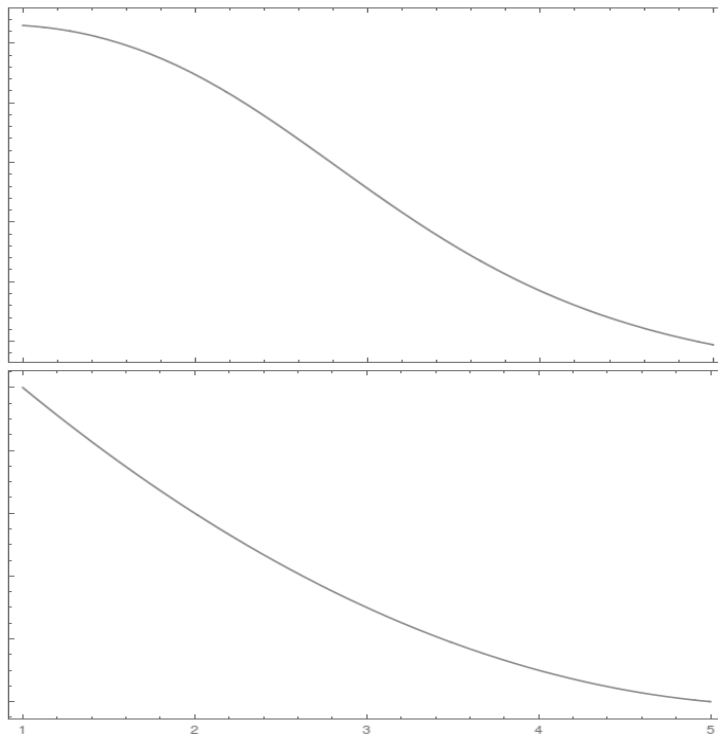


Fig. 4.15. simplification of the theoretical sigmoidal function with the parabolic expression described in Eq. 4.36. As it is, the equation slightly overestimates the number of leaves dying at the end of the first year. However it can be considered a good compromise between easy computation and similarity with the expected

According to this model the theoretical maximum age of each generation ($BF_{LS(i)}$) should correspond to the year in which the R^* almost reached its asymptote. However in the context of light competition potential leaf longevity should theoretically be equal to the time necessary “to replace the leaf when the net gain by a leaf per unit time over the entire life span is maximum” (Kikuzawa 1991). Following this reasoning a tree should replace leaves when:

$$g_M = t^{-1} \left(\int_0^f r(t) \delta t + \int_1^{1+f} r(t) \delta t + \dots + \int_{[t]}^t r(t) \delta t - \int_0^t m(t) \delta t - K \right)$$

(Eq. 4.37.)

where K is the total construction cost of the leaf. The different integrals refer to each t_i year favorable (f) and unfavorable ($1-f$) periods during the leaf life span. By substituting the equations of $r(t)$, K and $m(t)$ into equation (i) and by differentiating with respect to t , we'd obtain the t_{opt} which represents the theoretical leaf longevity. However we considered the calculation of t_{opt} avoidable, since it can be substituted with a parameter widely used in literature (Collalti, personal communication).

For simplicity we discretized the Eq. 4.36. so that t may represent the specific generation biomass for the beginning of the i th year. Therefore we used it to quantify the total amount of annual biomass loss for each specific generation.

That total amount was subtracted during two specific temporal windows. The former was in spring, when elder leaves lose their competition with newborn; the latter in fall, when the amount of PAR and Temperatures were reduced. We simplistically assumed that about 60% of the annual leaf biomass destined to litter was lost during spring, the leftover in autumn.

During the bud burst season new leaves take place in the sparse crown thinned during fall and winter. They of course also progressively shade part of the older leaves. Idealistically considering the crown aiming to the crowding equilibrium, old leaves biomass turnover shouldn't exceed new

leaf biomass allocation; the two quantities however would reach dynamic equilibrium once the crown gets fully populated again:

$$\frac{\partial B_0}{\partial t} \geq \frac{\partial B_1}{\partial t} + \frac{\partial B_2}{\partial t} + \dots + \frac{\partial B_i}{\partial t}$$

(Eq. 4.38.)

In fall we simplistically considered no secondary growth occurrence, which means that no Biomass allocation counterbalanced old leaves turnover. Leaf biomass reduction was then determined by linearly decreasing each B_i to the quantity predicted by the specific parabolic decay for the end of the year (Fig. 4-16).

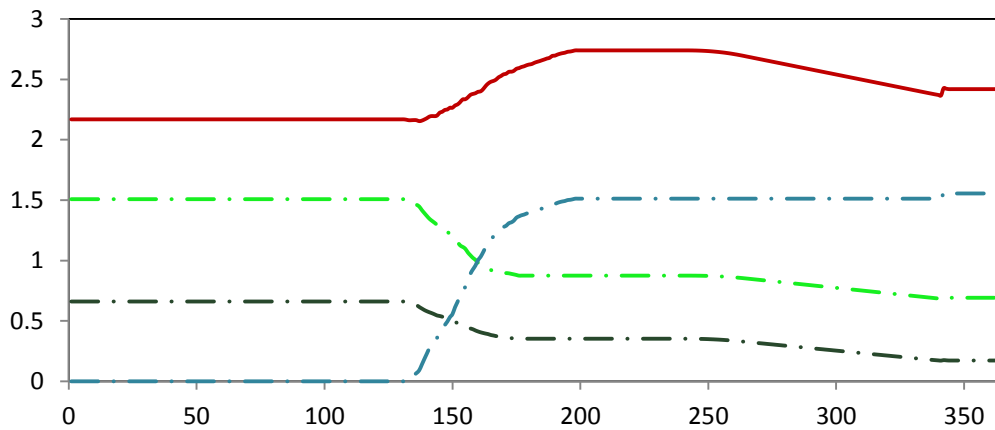


Fig. 4.16. graphical representation of the yearly leaves turnover for the Hyttiala forest. We assumed *Pinus sylvestris* needles to survive about three years. The dark green dotted line represents needles from 2 to 3 years old; the bright green one from 1 to 2 years old; the blue one the leaves emerged the current year. The red line represents the total amount of leaves in for units of space. Here leaves are referred as Biomass ($\text{gC m}^{-2} \text{d}^{-1}$).

4.2.10. Tree Carbon Dynamics: littering and turnover routine

“For most terrestrial ecosystems litter incorporation is almost the sole source of SOC. During or after the plant growing season, the plant litter or residue can be incorporated into the local soils through senescence or harvest/tillage practice”(Changsheng 2007).

Littering for woody tissues was similar to that introduced in the 5.1 version (Collalti et al., in prep) but was slightly modified to correctly follow the rationale of BIOME-BGM family (Thornton et al. 2002). Leaves and fine root turnover were treated as parallel processes and followed the patterns described above. Biomass coming from the aboveground deposited on the very first soil layer, and partly reached deeper portions because of earthworm activity (SOC leaching was not represented yet). In the framework of a multi strata approach fine and coarse roots Carbon were supplied in deeper layers as a function of roots depth and density distribution.

Litter Carbon pool was discretized in three sub-pools representing metabolic very labile C (e.g. carbohydrates, proteins, nucleic acids and lipids) structural labile C (e.g. cellulose) and structural resistant C (e.g. lignin and complex secondary metabolites). To represent these sub-pools without the use of massive calculations or increased number of parameters, we used a modification of DNDC approach (Fumoto et al. 2008b). Litter partitioning in the three sub pools was determined as a function of Carbon and Nitrogen content for the specific fallen tissue as follows:

$$\left\{ \begin{array}{l} \frac{\partial}{\partial t} C_{i+1} = \frac{(CN_{lt}^{-1} - CN_i^{-1})}{(CN_i^{-1} - CN_{i+1}^{-1})} \cdot C_{lt} \\ \frac{\partial}{\partial t} C_i = \frac{\partial}{\partial t} C_{lt} - \frac{\partial}{\partial t} C_{i+1} \\ CN_i < CN_{lt} < CN_{i+1} \end{array} \right.$$

(Eq. 4.39.)

Where C_{lt} represents the Carbon included in litter and earlier belonging to one of the 5 different structural Carbon compartments of the plant. Its relative C and N were distributed to the two litter sub pools with proximal C:N; the former, C_{i+1} , was the one with higher recalcitrance. When CN_{lt} was higher than any litter sub pool, all the new C was added to the structural resistant pool; otherwise, if CN_{lt} was lower than the CN of the metabolic pool, all its C and N were added to that very labile sub pool.

Litter Carbon dynamically move from a pool to another. Microbes absorb and partially immobilize litter C in their biomass, free it again in the mean as ecto-enzymes or after their lysis, co-operate in the humification processes (Liang et al., 2010). To simulate these dynamics we decided to use the approach of DNDC as a framework (Y. Zhang et al. 2002a).

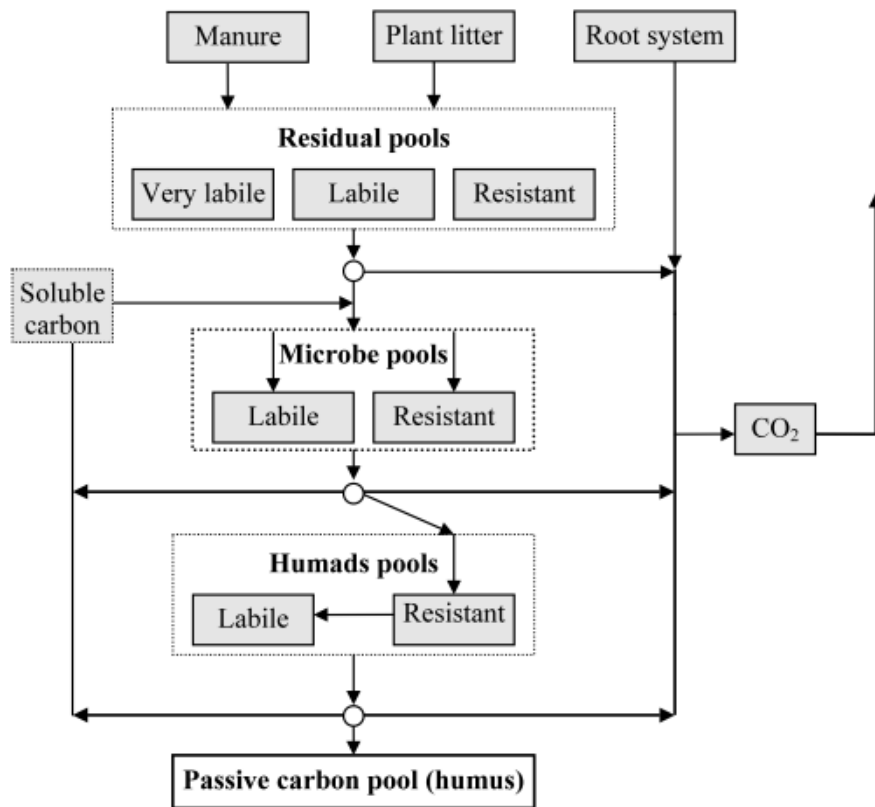


Fig. 4.16. Flowchart of the soil C routine (Zheng, 2003). Each soil layer is composed of three macro pools and each one is divided into two or three subpools. The key pool is the Microbial Biomass, since decomposition activity is mediated by microbes metabolism. The equation set followed to quantify the C dynamics from a pool to another follow the same logic described for soil respiration.

The litter C decomposed by microbial activity was partially mineralized as CO₂ (Eq. above), partly stored into Microbial metabolic Biomass (labile), partly in structural Microbial Biomass (resistant). We assumed that Microbial Carbon Efficiency (MUE) was constant and specific for each Carbon substrate family. Thus we calculated this amount as a proportion of the CO₂ produced.

Microbial Biomass and clay content were the principal drivers in determining the humic substances turnover. Humic pool (Humads) was divided into a more labile (Fulvic Acids) and a more resistant sub-pool

(Humic Acids). Depth was taken into account in case of a multilayer approach. Humads too were decomposed, even though at very low rates with respect to litter and biomass pools. Inert Organic Matter (IOM) was calculated following Coleman & Jenkinson (1999).

We also developed a parallel empirical routine to estimate heterotrophic respiration and C allocation in three different C pools following the RothC rationale (Fig. 4.17); the modeling framework of this routine was exactly the same of Coleman & Jenkinson (1999). This routine was developed to eventually grant more agile simulations on regional scale if a lower resolution was acceptable (e.g. monthly input time step). As a matter of fact it was included mainly to estimate soil organic C content for the next 50 years on a national scale, as an extension of the regional work of Sirca et al. (2014). However we won't discuss of its results in this dissertation.

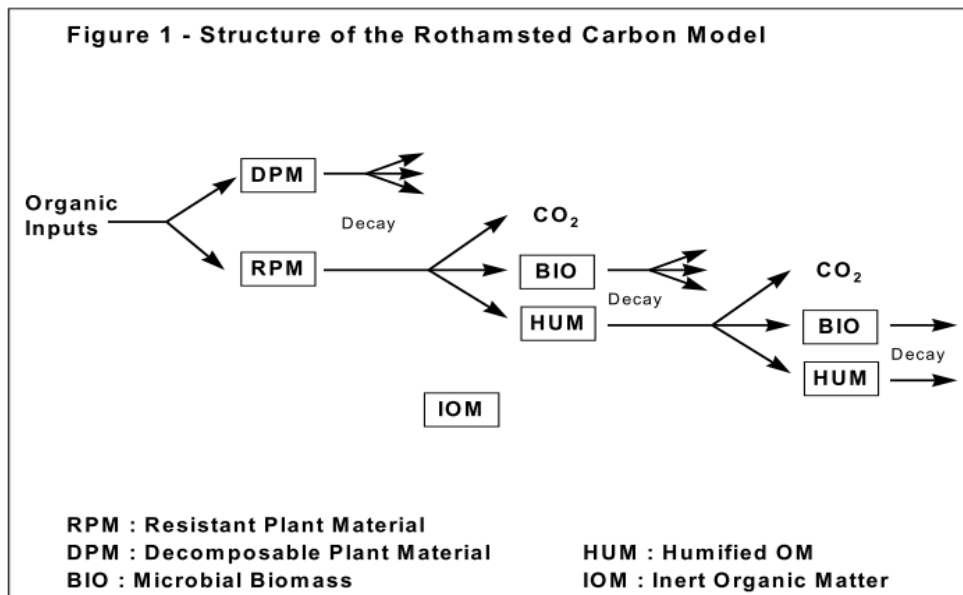


Fig. 4.17. Scheme of the soil C dynamics following Jenkinson (1999). The scheme is simple, empirical, low parameters demanding and validated for monthly data and time step. Even if this rationale is much more simplistic than the other one returns acceptable results, especially in the framework of a regional study.

4.3. Model initialization

4.3.1. The simples approach

Four of the six simulations (i.e. FRPue, DKSor, DEHai and FIHyy) were initialized with the simplest modeling approach. The canopy was assumed as a single layer, thus competition for light was not taken into account. This choice was obliged since no information about the forest structure could be found in literature. This problem was especially true for the FRPue case of study, for which we expected a division between two canopy levels, but we found only generic and partly inconsistent information in literature.

Soil was always tested as a single layer model, using the daily turnover approach. Initialization data were derived from literature; the repartition between the three major pools was calculated starting from literature data when available. Data used for initialization are summarized in Appendix 1.

4.3.2. The Perfect Plasticity Approximation to approach an automated initialization of dominance relations

In the case of the ITRen case of study we had the dendrometric characteristics of the forest for about two hectares around the flux tower. Since the stand was a complex uneven aged one we proposed a novel initialization approach to determine dominance relations between the canopy layers. Before this attempt the definition of the canopy

structure was arbitrary, and thus its reliability strictly dependent to the user's knowledge of the site area.

The theory under the approach is that crown plasticity causes forest stands to develop a regular spatial canopy in closed-canopy forest. The actual crowns occur at heterogeneous heights because of heterogeneous spacing of trees, heterogeneous tree size, and heterogeneity among the potential shapes among species (Fig. xx) (Strigul et al. 2008).

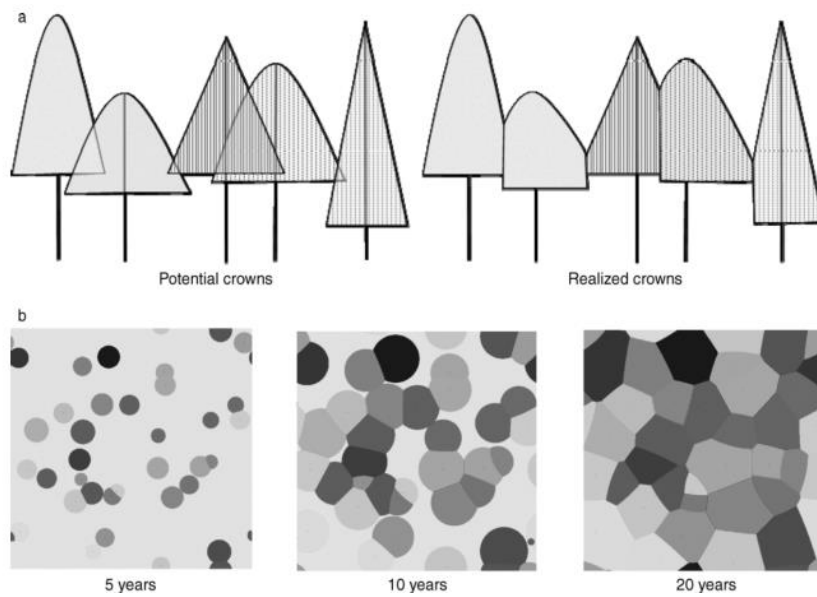


Fig.4.18. PPA rationale in simulating crown competition (Strigul et al., 2008). The realized tree crown for each tree is given by the portion of the tree's potential crown that is taller than the potential crowns of all neighboring trees. (a) Potential (left) and realized (right) crown in a hypothetical stand. (b) Realized crowns at 5, 10, and 20 years.

Thus, known the theoretical crown volumetric shape for each single tree of species k , in the elementary plot \mathcal{A} :

$$1 = \sum_{j=1}^k \int_{z^*}^{\infty} N_j(z) \cdot A_j(z^*, z) \delta z$$

(Eq. 4.40.)

where $N_j(z)$ is the number of trees of the j th species reaching height z , $A_j(z^*, z)$ their specific projected potential crown area at height z . “The perfect plasticity approximation (PPA) states that the sunlight portion of every tree of species j is simply equal to $A_j(z^*, z)$. Thus, all trees shorter than z^* are fully shaded. We can also define a second threshold z^{**} at which the lower and upper limits of integration in Eq. 2 are, respectively, z^{**} and z^* ” (Strigul et al. 2008).

Based on this theoretical assumption, we used the PPA algorithm to determine at which height the emergent ($z^* < H < \infty$) and dominant ($z^{**} < H < z^*$) layers closed, and then determined the number of trees and average biometric characteristics for each class. We calculated the z^* and z^{**} (Fig XX) assuming that the Crown Shape of *Picea abies* was outlined by the rotation of the parabola:

$$r_i(z) = CR_i^2(sp) \cdot \left(1 - \frac{4z}{CH_i(sp)}\right)$$

(Eq. 4.41)

where $r_i(z)$ was the potential Crown Radius at height $CH_i - z$, CH_i was the maximum Crown Height of the i th tree, CR_i was the Crown Radius at the crown basis. These two were calculated following Widłowski et al. (2003)

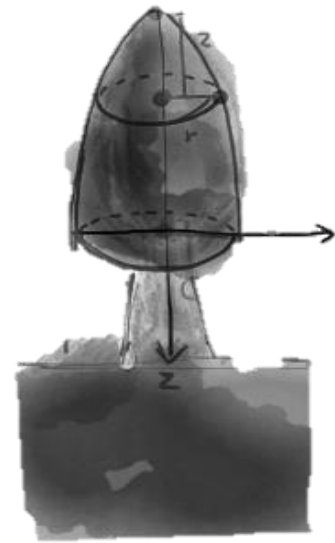


Fig. 4.19. Crown area and representation using a parabola whose vertex is in the origin and the vertical axis “z” is negative.

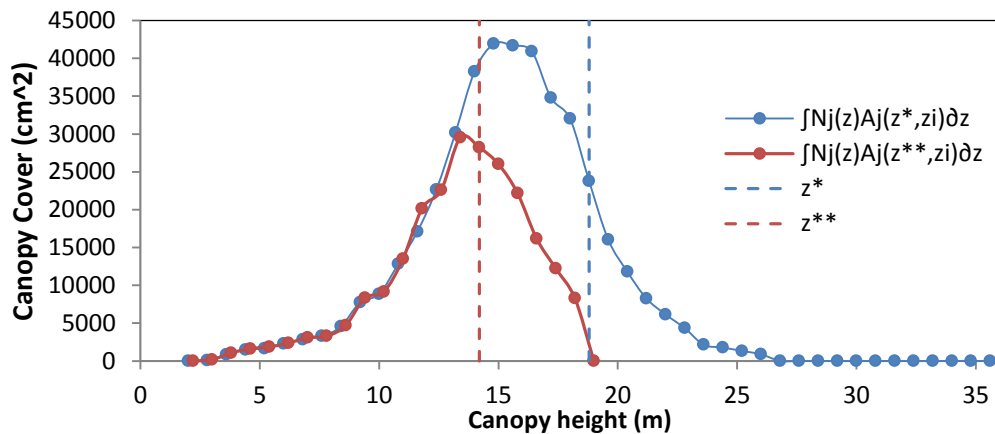


Fig. 4.20. Application of the PPA algorithm to the ITRen simulation initialization. The blue line represents the area covered by the emergent layer; the red one by the dominant. dotted vertical lines represent the minimum height of the trees afferent to the specific layer.

4.3.3. Model initialization: a mixed complex forest in the patchy rural landscape

The BEBra case of study was initialized considering the *Pinus sylvestris* and *Quercus robur* stands as two different forests one next to the other. The oak stand was treated as a three layers forest, as inferred by Yuste et al. (2005). On the other hand the pine stand was even aged and its structure justified the use of a single layer approach. A brief analysis of the preliminary evaluation of which of the initialization set could represent the best approach for the site can be found in Marconi et al. (2013).

The two stands soils were treated separately because of the different soil history and land use described before (Appendix 1).

To reduce EC data noise, we filtered the tower's data by following the footprint adjusting method already applied on the same site (Nagy et al.

2006). “The surroundings around the flux tower were divided into twelve wind sectors (about 308 range each) (Fig. 4.21.). In a few sectors all data were rejected either because of an insufficient fetch or an undesired vegetation type (e.g. grassland, or recently afforested area). In each of the remaining wind sectors all data obtained under stable conditions were rejected. In these sectors, different j thresholds were applied according to the fetch in that direction. Where the fetch was large enough, also fluxes obtained under neutral conditions were maintained. Where the fetch was intermediate, the j threshold was set at 0. Where sector borders split a matrix cell, the matrix values were divided proportionally to the area of the matrix cell within each wind sector”.

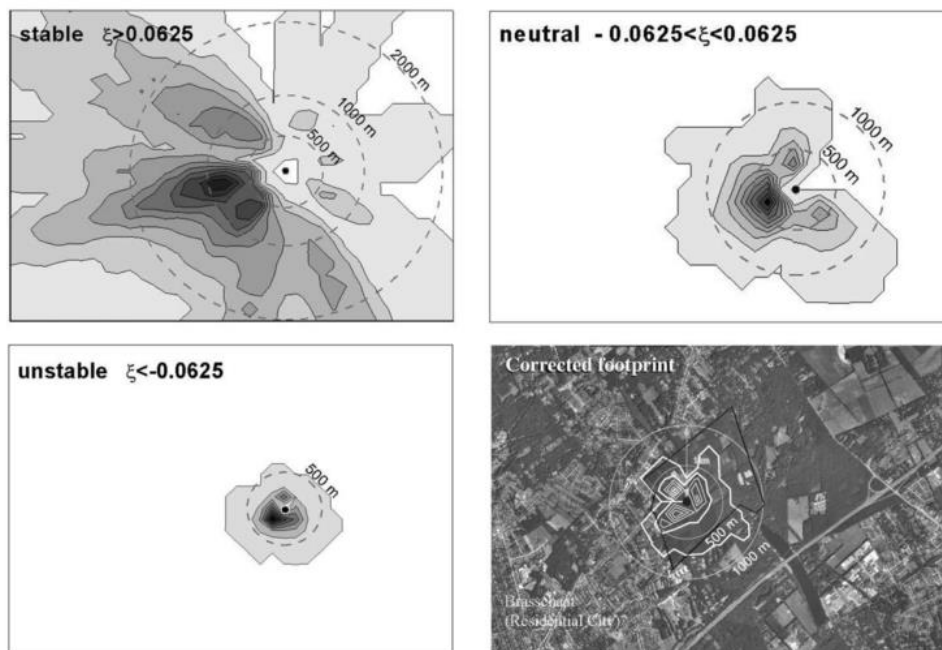


Fig. 4.21. Spatial contribution to the total flux in case of different classes of turbulence; in stable conditions the landscape outside the forest highly influence the data

Thus we obtained a subset of 874 days extracted from a set of Lv 3 Eddy Covariance data.

4.4. Model parameterization and simulation

The model calibration and parameterization was performed by using a range of published data. The aim was to create a parameterization set which was generally species specific and site independent. This objective was mostly achieved with the only exception of thermic sum threshold, which was calibrated specifically for each site. The present study proposes the parameterization for five different species, tested on ten CarboEurope IP sites (even though we will present the results just for a subset of six). The resulting parameterization and bibliographic references are summarized in Appendix 2.

The model was tested for a number of years ranging from 7 to 13 (Tab 3.3). We used a daily temporal resolution, and thus the daily soil C routine.

4.5. Eddy Covariance technique

The eddy covariance method provides measurements of gas emission and consumption rates, and also allows measurements of momentum, sensible heat, and latent heat (e.g. evapotranspiration, evaporation water loss, etc.) fluxes integrated over areas of various sizes. Fluxes of H₂O, CO₂, CH₄, N₂O and other gases are characterized above soil, and plant canopies. This method evaluates vertical flux densities of scalars between the forest and atmosphere by measuring the mean covariance between

vertical velocity (w') and scalar (c') fluctuations of the measured flux (Baldocchi, 1997).

In conditions of turbulent flow, assuming that air density (ρ_d) fluctuations and mean vertical flow to be negligible in horizontal homogeneous terrain, vertical flux can be represented by the equation (Baldocchi, 2003)

$$F \approx \overline{\rho_d} \cdot \overline{w' s'}$$

(Eq. 4.42)

In addition other important assumptions in the eddy covariance method are:

- Measurements at a point are assumed to represent an upwind area;
- Measurements are assumed to be done inside the boundary layer of interest, and inside the constant flux layers;
- Fetch and footprint are assumed adequate, so flux is measured from the area of interest;
- Flux is fully turbulent;
- Terrain is horizontal and uniform;
- Air density fluctuations are negligible;
- Flow divergences and convergences are negligible;
- The instruments can detect very small changes at very high frequency;
- Mean air flow and turbulence at the measurement point are not appreciably distorted by the installation structure or the instruments themselves.

Following Burba (2013) The degree to which some of these assumptions hold true depends on proper site selection and experimental setup. Measurements are of course never perfect, due to assumptions, physical phenomena, instrument problems, and specifics of the particular terrain or setup. As a result, there are a number of potential flux errors, but they can be prevented, minimized, or corrected out.

First, there is a family of errors called frequency response errors. They include errors due to instrument time response, tube attenuation, path and volume averaging, sensor separation, sensor response mismatch, low and high pass filtering, and digital sampling.

Time response errors occur because instruments may not be fast enough to catch all the rapid changes that result from the eddy transport.

Tube attenuation error is observed in closed-path analyzers, and is caused by attenuation of the instantaneous fluctuation of the concentration in the sampling tube.

Path averaging error is caused by the fact that the sensor path is not a point measurement, but rather is an integration over some distance; therefore, it can average out some of the changes caused by eddy transport.

Sensor separation errors occur due to the physical separation between the places where wind speed and concentration are measured, so covariance is computed for parameters that were not measured at the same point.

There can also be frequency response errors caused by sensor response mismatch, and by filtering and digital sampling.

In addition to frequency response errors, other key sources of errors include spikes and noise in the measurements, unlevelled anemometer, wind angle of attack, sensor time delay (especially important in closed-path analyzers with long intake tubes), sonic heat flux errors, the Webb-Pearman-Leuning density terms, spectroscopic effects (for LASER-based measurements), band-broadening effects (for NDIR measurements), oxygen sensitivity, gas flux storage, and data filling errors”.

In this study we only made use of C fluxes measurements. The EC tower directly measured Net Ecosystem Exchange fluxes (NEE), which were partitioned in GPP and Reco using the standard Carboeurope-IP methodology described in Papale et al., 2006 and Moffat et al., 2007.

4.6. Statistical Analysis

We made use of a commonly utilized set of estimators and statistics to validate the model against EC data and evaluate its performance.

4.6.1. Regression analysis: the goodness of fit, linear regression and Coefficient of determination (R^2)

The goodness of fit of a model describes how well it fits a set of observations. Measures of goodness of fit typically summarize the discrepancy between observed values and the values expected under the model in question. In statistics, the coefficient of determination (R^2) is a

number that indicates how well data fit a statistical model – sometimes simply a line or curve.

$$R^2 = 1 - \frac{\sum_i^n (y_i - \bar{y})^2}{\sum_i^n (y_i - f_i)^2}$$

(Eq. 4.43)

In this context it is a statistic used in to provide a measure of how well observed outcomes are replicated by the model, as the proportion of total variation of outcomes explained by the model (Glantz et al., 1990).

4.6.2. Regression analysis: the trend line

In statistics, linear regression is an approach for modeling the relationship between a scalar dependent variable y and one or more explanatory variables denoted X . The case of one explanatory variable is called simple linear regression.

4.6.3. Pearson t -test and correlation analysis: the r statistics

In statistics, the Pearson product-moment correlation coefficient (referred to as the Pearson's r) is a measure of the linear correlation (dependence) between two variables X and Y , giving a value between $+1$ and -1 inclusive. It is widely used in the sciences as a measure of the degree of linear dependence between two variables: 1 is total positive

correlation, 0 is no correlation, and -1 is total negative correlation. (Cox et al., 1974; Pearson, 1895)

$$\rho_{X,Y} = \frac{\text{cov}(X,Y)}{\sigma_X \sigma_Y}$$

4.6.4. The root-mean-square error (RMSE)

The root-mean-square error (RMSE) is a frequently used measure of the differences between values predicted by a model or an estimator and the values actually observed. Basically, the RMSE represents the sample standard deviation of the differences between predicted values and observed values. These individual differences are called residuals when the calculations are performed over the data sample that was used for estimation, and are called prediction errors when computed out-of-sample. The RMSE serves to aggregate the magnitudes of the errors in predictions for various times into a single measure of predictive power. RMSE is a good measure of accuracy, but only to compare forecasting errors of different models for a particular variable and not between variables, as it is scale-dependent.

$$RMSE = \sqrt{\frac{\sum_{t=1}^n (y_t - \hat{y}_t)^2}{n}}$$

(Eq. 4.45)

4.6.5. The Normalized root-mean-square error (NRMSE)

Model- data agreement for inter-annual variability in annual flux sums was assessed in terms of the normalized root mean squared error (NRMSE). The NRMSE represents the RMSE normalized by the magnitude of observed variability at the site (T. F. Keenan et al. 2012). Lower values indicate less residual variance.

$$NRMSE = \frac{RMSE}{\sigma(y_t)}$$

(Eq. 4.46)

Where $\sigma(y_t)$ is the standard deviation of observed interannual variability at the site.

4.6.6. Nash Sutcliffe efficiency (NSE)

The Nash-Sutcliffe efficiency is a normalized statistics that determines the relative magnitude of the residual variance (“noise”) compared to the measured data variance (“information”) (Nash & Sutcliffe, 1970). NSE indicates how well the plot of observed versus simulated data fits the 1:1 line. NSE is computed as shown in the equation:

$$NSE = 1 - \left[\frac{\sum_{i=1}^n (Y_i^{obs} - Y_i^{sim})^2}{\sum_{i=1}^n (Y_i^{obs} - \bar{Y})^2} \right]$$

(Eq. 4.47)

where Y_i^{obs} is the i th observation for the constituent being evaluated, Y_i^{sim} is the i th simulated value for the constituent being evaluated, \bar{Y} is the mean of observed data for the constituent being evaluated, and n is the total number of observations. NSE ranges between $-\infty$ and 1.0 (inclusive), with $NSE = 1$ being the optimal value.

Values between 0.0 and 1.0 are generally viewed as acceptable levels of performance, whereas values <0.0 indicates that the mean observed value is a better predictor than the simulated value, which indicates unacceptable performance (Moriasi et al. 2007). NSE was recommended because it is very commonly used, thus it can be used to compare the model with others in literature.

4.6.7. Interannual variability

To assess inter annual variability, we normalized the measured/modeled values of NEE, GPP, and Reco by subtracting the long-term year measured/modeled mean for each site from individual site-year flux values. By comparing the long-term calendar year mean of measured and modeled fluxes, we also identified biases in model estimates; model- data agreement for inter annual variability in annual flux sums was assessed in terms of the normalized root mean squared error (T. F. Keenan et al. 2012).

$$F_i = \Phi_i - \bar{\Phi}_i$$

(Eq. 4.48)

Inter annual variability is commonly derived by short periods of anomalous fluxes within the year (Krishnan et al., 2008, 2009; Chen et al., 2009; le Maire et al., 2010). We therefore also assessed model performance for variability on a monthly and seasonal scale. The variability of monthly/seasonal fluxes was calculated in the same way as annual variability, as the difference between the observed or modeled value and the associated long-term mean. By differencing the observed and predicted monthly variability (referred as Variance Residuals or VRs) specific periods during the year at which the models under- or over-represent the observed variability can be identified (T. F. Keenan et al. 2012).

We finally defined periods of systematic model error the months or seasons in which the model showed the same-signed bias in variance residuals for the 90% of times.

4.6.8. Kernel density estimation

In statistics, kernel density estimation (KDE) is a non-parametric way to estimate the probability density function of a random variable. Kernel density estimation is a fundamental data smoothing problem where inferences about the population are made, based on a finite data sample. Kernel density estimates are closely related to histograms, but can be endowed with properties such as smoothness or continuity by using a suitable kernel. The bandwidth of the kernel is a free parameter which exhibits a strong influence on the resulting estimate.

Let (x_1, x_2, \dots, x_n) be an independent and identically distributed sample drawn from some distribution with an unknown density f . We are interested in estimating the shape of this function f . Its kernel density estimator is:

$$\hat{f}_h(x) = \frac{1}{n} \sum_{i=1}^n K_h(x - x_i) = \frac{1}{nh} \sum_{i=1}^n K\left(\frac{x - x_i}{h}\right),$$

(Eq. 4.49)

Unlike histogram in the KDE a normal kernel with known variance is placed on each of the data points; then they are summed to make the kernel curve. The smoothness of the kernel density estimate is evident compared to the discreteness of the histogram, since they converge faster to the true underlying density for continuous random variables (Ward et al., 1995).

4.6.9. Chi squared normality test

The Chi squared normality test returns a decision for the null hypothesis that the data in vector x comes from a normal distribution with a mean and variance estimated from x . The alternative hypothesis is that the data does not come from such a distribution. The result is 1 if the test rejects the null hypothesis at the 5% significance level, and 0 otherwise.

The chi-square goodness-of-fit test groups the data into bins, calculating the observed and expected counts for those bins, and computing the chi-square test statistic

$$\chi^2 = \sum_{i=1}^N \frac{(O_i - E_i)^2}{E_i}$$

(Eq. 4.50)

where O_i are the observed counts and E_i are the expected counts based on the hypothesized distribution. The test statistic has an approximate chi-square distribution when the counts are sufficiently large.

4.6.10. Student's two sample t-test

A t-test is any statistical hypothesis test in which the test statistic follows a Student's t distribution if the null hypothesis is supported. It can be used to determine if two sets of data are significantly different from each other, and is most commonly applied when the test statistic would follow a normal distribution if the value of a scaling term in the test statistic were known.

4.6.10. Mann-Whitney U-test for equivalence of the median

In statistics, the Mann–Whitney U test (also called the Wilcoxon rank-sum test) is a nonparametric test of the null hypothesis that two

populations are the same against an alternative hypothesis especially that a particular population tends to have larger values than the other. It has greater efficiency than the t-test on non-normal distributions, such as a mixture of normal distributions, and it is nearly as efficient as the t-test on normal distributions. The Wilcoxon rank-sum test is not the same as the Wilcoxon signed-rank test, although both are nonparametric and involve summation of ranks.

The test involves the calculation of a statistic, usually called U , whose distribution under the null hypothesis is known. For sample sizes above ~ 20 approximations using the normal distribution is fairly good. Some books tabulate statistics equivalent to U , such as the sum of ranks in one of the samples, rather than U itself.

Following Mann (1947) the U is easily calculated by arranging all the observations into a single ranked series, which means rank all the observations without regard to which sample they are in. The sample for which the ranks seem to be smaller gets chosen; that would be the "sample 1," while the other is the "sample 2." For each observation in sample 1, the number of observations in sample 2 that have a smaller rank is counted; the sum of these ranks is U .

4.6.11. F-Fisher test for variance equality

The two-sample F-test is used to test if the variances of two populations are equal. The alternative hypothesis is that they come from normal distributions with different variances. The result h is 1 if the test rejects

the null hypothesis at the 5% significance level, and 0 otherwise. The test statistic is

$$F = s^2_1 / s^2_2$$

(Eq. 4.51)

where s_1 and s_2 are the sample standard deviations. The test statistic is a ratio of the two sample variances. The further this ratio deviates from 1, the more likely you are to reject the null hypothesis. Under the null hypothesis, the test statistic F has a F -distribution with numerator degrees of freedom equal to $N_1 - 1$ and denominator degrees of freedom equal to $N_2 - 1$, where N_1 and N_2 are the sample sizes of the two data sets.

CHAPTER 5: RESULTS

5.1. Results of GPP modeled

5.1.1. Annual and seasonal trends in GPP estimation

The results of the six 3D-CMCC-Pheno-FEM simulations were compared with daily data of Eddy Covariance (EC) flux measurements for the available years from 2000 to 2011, as described in methods. On average the model showed good estimation of daily trends of Gross Primary Production (GPP) throughout the six different forest ecosystems of the latitudinal transect (Fig 5.1).

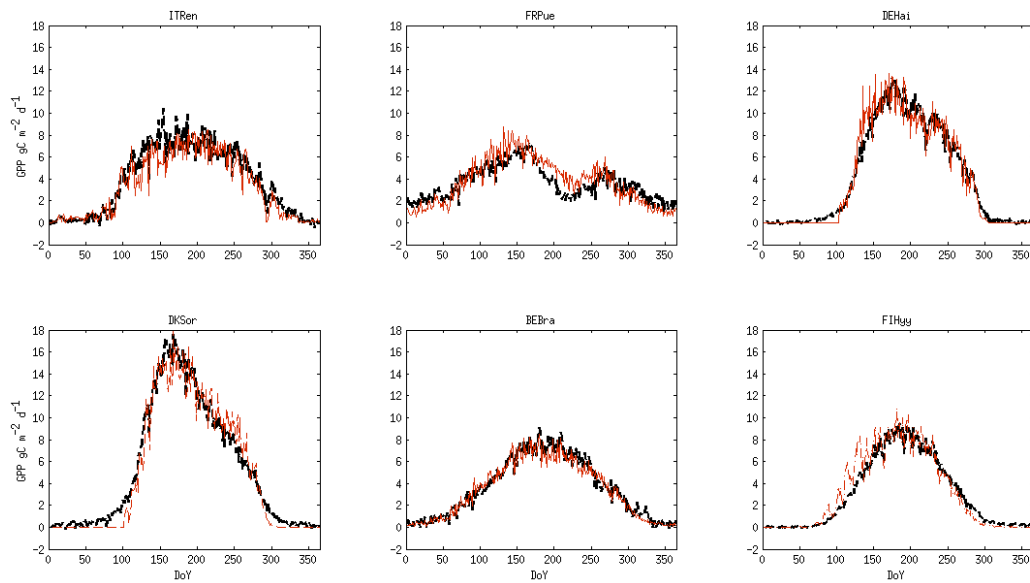


Fig. 4.1. GPP ($\text{gC m}^{-2} \text{d}^{-1}$) trends for the six study cases. Red dotted lines represent 3D-CMCC-FEM 6.1. simulations, black lines the EC data.

Deviations from expected values occurred in different seasons for the different sites. Winter trends resulted well represented for all sites with the exception of a slight underestimation in the *Quercus ilex* stand

(FRPue). The use of the thermic sum method to determine bud burst date apparently determined a source of uncertainty for deciduous species, as inferred by Fig 5.2.

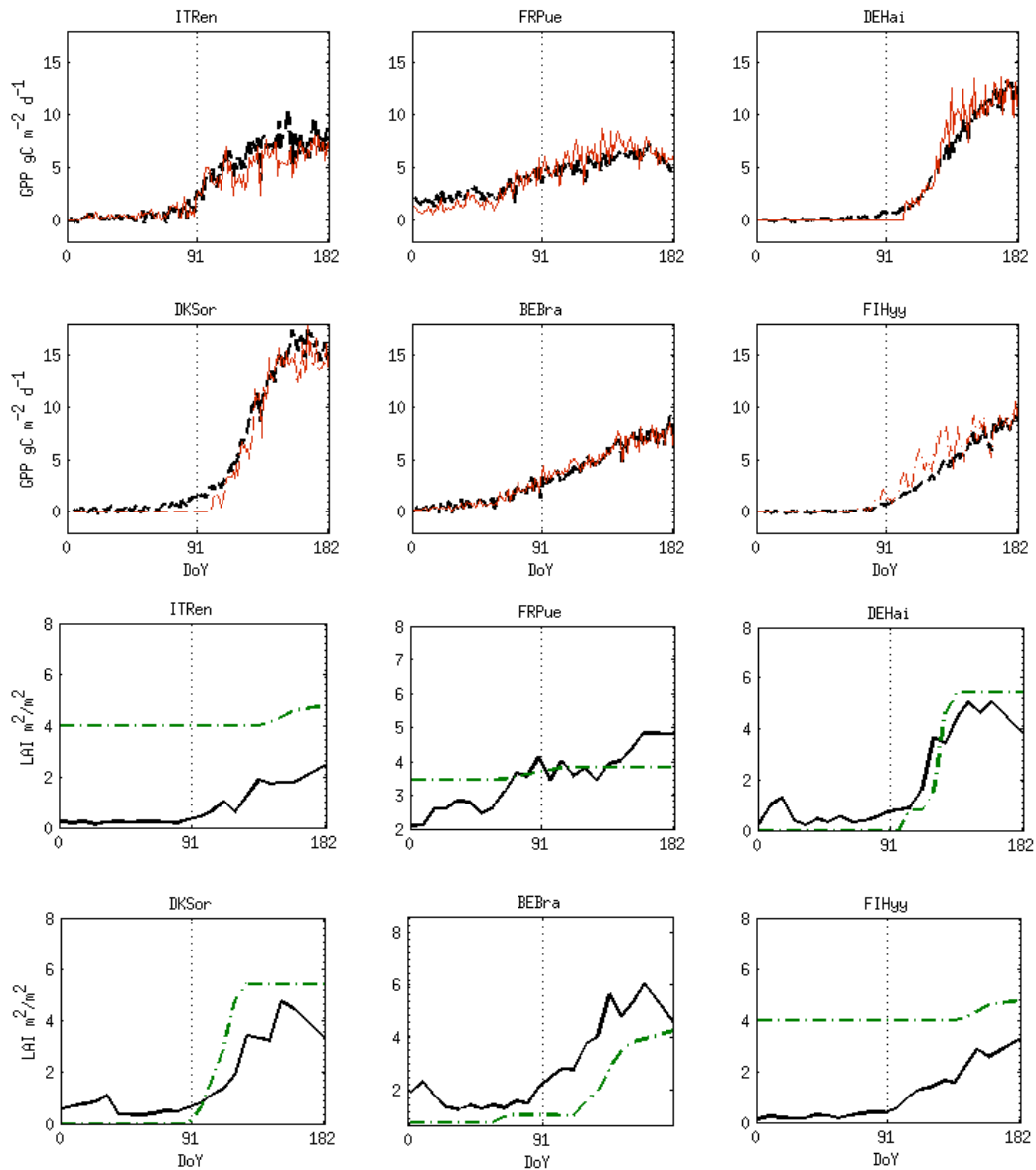


Fig. 5.2. GPP ($\text{gC m}^{-2} \text{d}^{-1}$) trends for winter and spring seasons along with dynamics of cumulated LAI ($\text{m}^2 \text{m}^{-2}$). Red line in box (a) represents simulated GPP, black line the EC data. Green dotted line in box (b) represents 3D-CMCC-FEM LAI, black line the MODIS LAI data at 8 days temporal resolution. In observing the phenological shifts for Evergreen it is important to consider that LAI strongly increased after most of the dying leaves already fell.

As a matter of fact a slight underestimation in GPP occurred at the very beginning of spring for both DEHai and Sorø. Nevertheless this underestimation may be related to the early growth of pioneer species which are not considered in this study (Kiuizawa, 1991). The same can be noticed in the simulation of new leaf emergence for Evergreen stands. On Renon, where the canopy reached the maximum of LAI on late spring, GPP trends were slightly underestimated during most of the season. The opposite occurred at FRPue, where leaf turnover happened at the beginning of spring. Early spring GPP trends were slightly overestimated in FIHyy Scots pine stand too, probably because the model didn't take into account any influence of snow coverage onto the dynamics of the Carbon fluxes (Starr et al., 2003; Ichii et al., 2008).

GPP trends during summer appeared well simulated for most of the evergreen ecosystems. A significant exception was the Mediterranean forest of FRPue, in which GPP was averagely overestimated during the season. Summer trends appeared more uncertain for deciduous forests, probably as a consequence of the constant LAI and canopy cover values expected by the pipe model (Waring et al., 1984).

Trends of LAI and foliage coverage were mostly different to the ones remotely estimated by MODIS reference data (Tab. 5. 1), but resulted

consistent to data collected on field (Montagnani et al., 2009; Goerner et al., 2009; Anthoni et al., 2004; Pilegaard et al., 2011; Janssens et al., 1999; Kramer et al., 2002). The most evident difference occurred in inter seasonal dynamics of evergreen species, with MODIS showing a much steeper seasonality than 3D-CMCC-PhenoFEM.

Tab. 5.1 Peak LAI ($\text{m}^2 \text{m}^{-2}$) for the six sites as it has been simulated by 3D-CMCC-FEM, MODIS satellite data and LiCOR based field measurements. Model's LAI was calibrated to better fit field data.

	ITRen	FRPue	DEHai	DKSor	BEBra	FIHyy
LAI Model	5.1 ± 0.3	3.7 ± 0.3	5.41 ± 0.1	5.4 ± 0.1	4.0 ± 0.4	4.21 ± 0.4
LAI Modis	2.29 ± 1.6	3.6 ± 1.4	4.74 ± 0.4	5.9 ± 0.4	5.8 ± 0.4	4.78 ± 0.4
LAI Cited	5.1 ± 0.4	2.8 ± 0.4	5.0 ± 0	4.5 ± 0.5	2.25 ± 0.15	5.0 ± 0.0

The new Phenology routine well represented GPP trends for all the six sites during leaf yellowing and senescence period (Fig 5.3). Again there was a strong mismatch between MODIS data and model simulation in LAI.

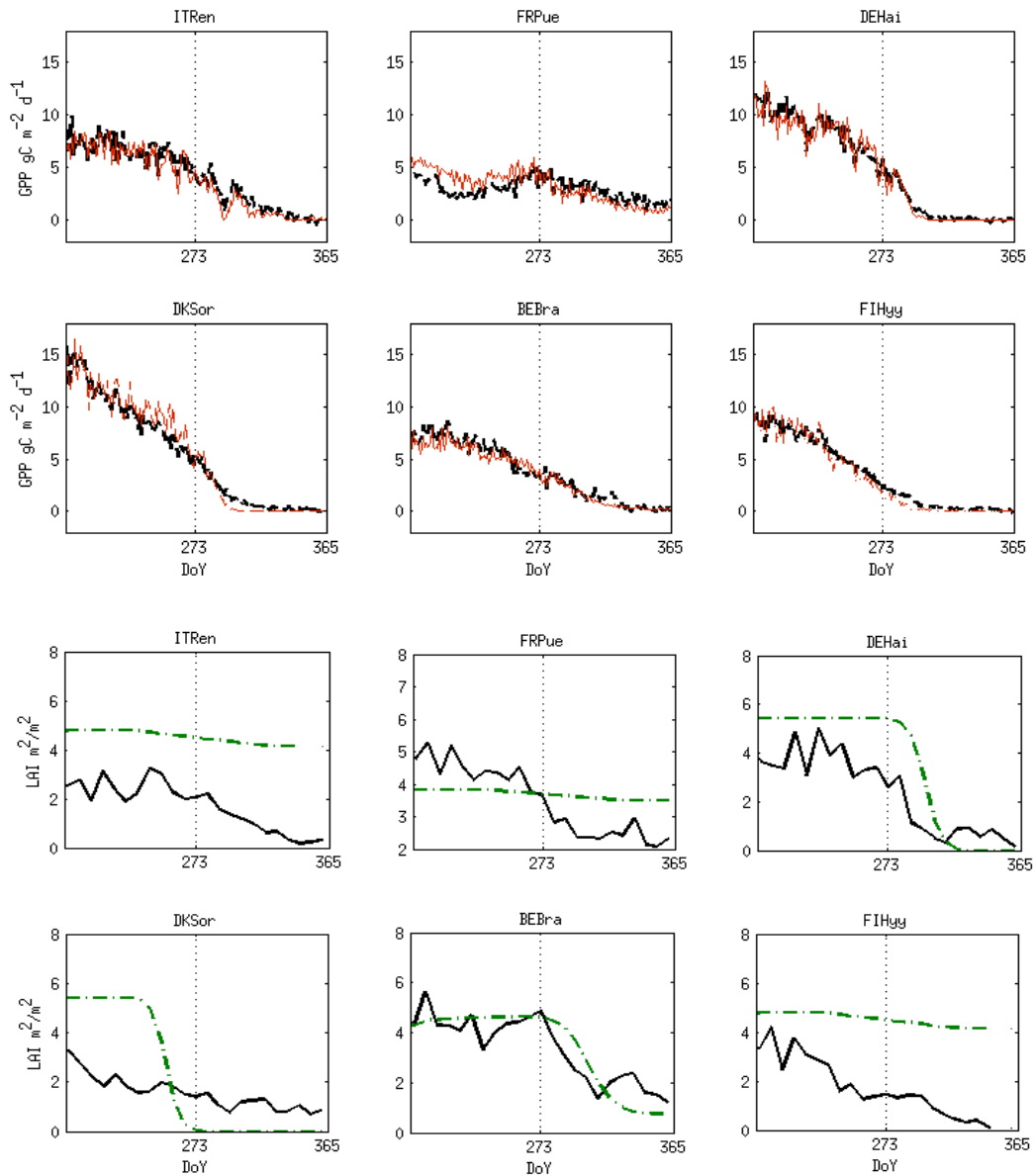


Fig. 5.3 GPP ($\text{gC m}^{-2} \text{d}^{-1}$) trends for summer and fall seasons along with dynamics of cumulated LAI ($\text{m}^2 \text{m}^{-2}$). Red line in box (a) represents simulated GPP, black line the EC data. Green dotted line in box (b) represents 3D-CMCC-FEM LAI, black line the MODIS LAI data at 8 days temporal resolution. Deciduous species showed shifts in the beginning of leaf senescence and falling as expected (no VPsat influence in starting data approach).

As a matter of fact, MODIS LAI began to slightly decrease at about the end of July, while 3D-CMCC-FEM remained constant until fall, when a photoperiod threshold was the only trigger in senescence activation.

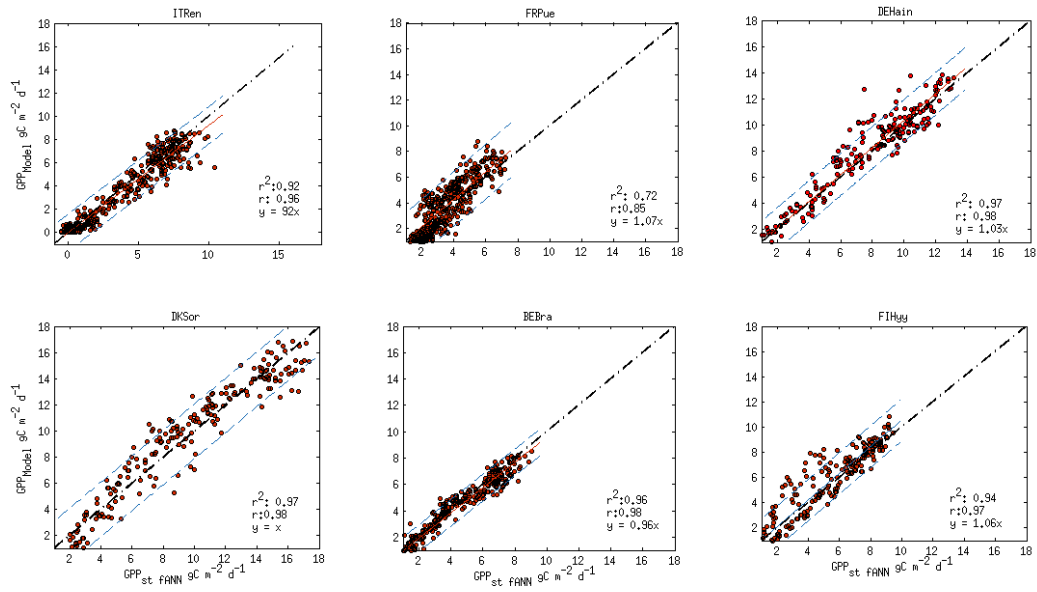


Fig. 5.4 Daily trends of simulated GPP plotted against EC data for the six sites. The black dotted lines represent the 1:1 ratio (perfect fit), red lines the actual mono parametric regression lines. The slopes of these lines represent the average over/underestimation. Azure dotted lines are the 95% expected bonds. The r is the Pearson's correlation statistic.

To quantitatively infer the goodness of fit, correlation and efficiency of the model, GPP trends were plotted against EC data as described in methods. Fig 5.4 and Tab 5.3. show the results of these analyses. The GPP trends showed high goodness of fit [0.72; 0.97], correlation coefficient [0.85; 0.98] and Model Efficiency coefficient [0.48; 0.94]. The RMSE was reduced of about a half for all the six ecosystems compared

to daily results. The fluctuation among the 1:1 line was further reduced of about 6% (from -11% to -8% and from +6 to +3%).

Tab. 5.2 Statistics of the daily average observed-simulated GPP ($\text{gC m}^{-2} \text{d}^{-1}$). The table reports for each site: the regression goodness of fit estimator (r^2), the Pearson's correlation estimator; the RMSE ($\text{gC m}^{-2} \text{d}^{-1}$); the Nash Sutcliffe model efficiency estimator; the slope of the mono parametric linear regression; the range of the parameter using a Levenberg-Marquardt algorithm.

Site	Var	r^2	r	RMSE	NSE	a	a-range
ITRen	GPP - Trends	0.92	0.96	0.81	0.92	0.92	(0.9, 0.94)
FRPue	GPP - Trends	0.78	0.8	1.08	0.62	1.04	(1.02, 1.07)
DEHain	GPP - Trends	0.97	0.98	0.82	0.94	1.035	(1.02, 1.05)
DKSor	GPP - Trends	0.97	0.98	1.06	0.92	0.9848	(0.97, 1.00)
BEBra	GPP - Trends	0.96	0.98	0.51	0.89	0.7145	(0.70, 0.73)
FIHy	GPP - Trends	0.94	0.97	0.84	0.91	1.207	(1.18, 1.23)

5.1.2 Validation of 3D-CMCC-Pheno GPP results on daily and monthly temporal resolution

Fig. 5.5 Shows daily correlation between Model outputs and the Eddy Covariance tower GPP fluxes ($\text{gC m}^{-2} \text{d}^{-1}$). The regression had a strong correlation (t-test p value < 0.0001 and r [0.63; 0.91]) in all cases, and showed a good agreement for each set of values, with an r^2 ranging from 0.38 to 0.91 (Tab 5.3).

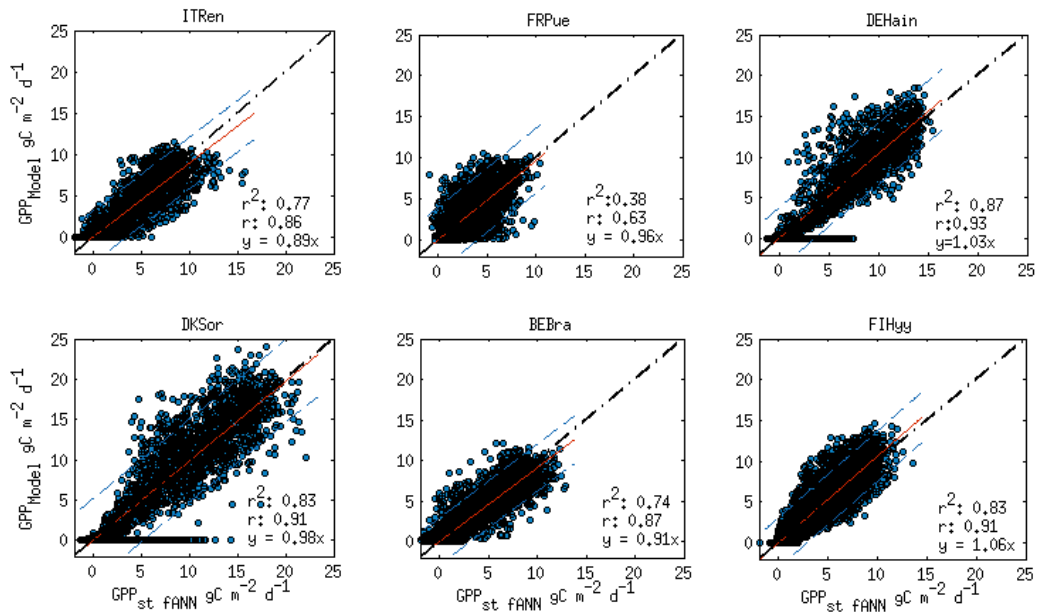


Fig. 5.5 Daily simulated GPP plotted against daily EC data for the six sites. Days for which no EC data were available were discarded. Otherwise days with simulated GPP = 0 were taken into account. The black dotted lines represent the 1:1 ratio (perfect fit), red lines the actual mono parametric regression lines. The slope of this line represents the average over/underestimation. Azure dotted lines are the 95% expected bonds. The r is the Pearson's correlation statistic.

As expected, the lowest correlation occurred for FRPue forest, due to both a systematic overestimation in summer and underestimation in autumn and winter gross photosynthesis. Thus the lowest value of Nash-Sutcliffe model efficiency coefficient was in the Mediterranean forest ecosystem (0.03). The other five simulations resulted in very good NSE, ranging from 0.8 and 0.9. RMSE ranged from 1.57 to 2.62 $\text{gC m}^{-2} \text{d}^{-1}$, with highest values associated to broadleaves and lowest to needle leaves. On average the modeled daily GPP fluctuated on an 11%

underestimation to a 6% overestimation, as inferred by the values of the “a” parameter (Tab X.3).

Tab. 5.3 Statistics of the daily observed-simulated GPP ($\text{gC m}^{-2} \text{d}^{-1}$). The table reports for each site: the regression goodness of fit estimator (r^2), the Pearson’s correlation estimator; the RMSE ($\text{gC m}^{-2} \text{d}^{-1}$); the Nash Sutcliffe model efficiency estimator; the slope of the mono parametric linear regression; the range of the parameter using a Levenberg-Marquardt algorithm.

Site	Var	r^2	r	RMSE	NSE	a	a-range
ITRen	GPP - daily	0.77	0.86	1.59	0.72	0.89	(0.87, 0.9)
FRPue	GPP - daily	0.41	0.65	1.96	0.09	0.96	(0.95, 0.98)
DEHain	GPP - daily	0.86	0.91	1.91	0.96	1.024	(0.99, 1.06)
DKSor	GPP - daily	0.83	0.91	2.62	0.8	1.24	(1.21, 1.27)
BEBra	GPP - daily	0.74	0.87	1.48	0.75	1.05	(1.04, 1.05)
FIHyy	GPP - daily	0.83	0.91	1.57	0.76	1.059	(1.05, 1.07)

Figure 5.6 shows the correlation between EC data and Model outputs on a monthly time scale, Tab. 5.4 the statistics of the validation. Monthly outputs showed better results compared with daily GPP.

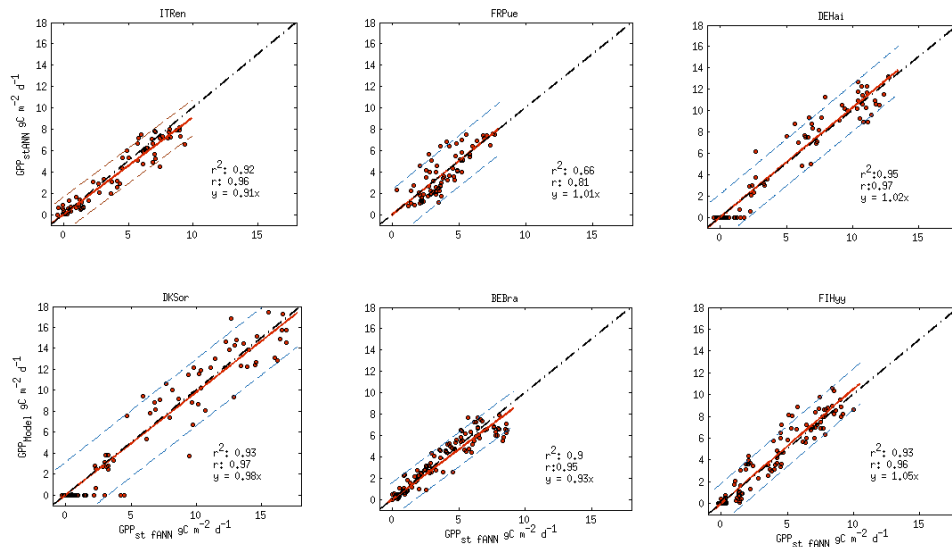


Fig.5.6. Monthly simulated GPP plotted against monthly EC data for the six sites. The black dotted lines represent the 1:1 ratio (perfect fit), red lines the actual mono parametric regression line. The slope of these lines represents the average over/underestimation. Azure dotted lines are the 95% expected bonds. The r is the Pearson's correlation statistic.

Excluding the exception of FRPue (r^2 0.66, NSE 0.44), NSE and r^2 were always greater than 0.9. RMSE and “a” parameter values were of the same magnitude of that observed for the average daily trends. Again the GPP estimation for FRPue site improved significantly compared with daily resolution.

Tab. 5.4 Statistics of the monthly observed-simulated GPP ($\text{gC m}^{-2} \text{d}^{-1}$). The table reports for each site: the regression goodness of fit estimator (r^2), the Pearson's correlation estimator; the RMSE ($\text{gC m}^{-2} \text{d}^{-1}$); the Nash Sutcliffe model efficiency estimator; the slope of the mono parametric linear regression; the range of the parameter using a Levenberg-Marquardt algorithm.

Site	Var	r^2	r	RMSE	NSE	a	a -range
ITRen	GPP - Monthly	0.92	0.96	0.82	0.91	0.91	(0.87, 0.95)
FRPue	GPP - Monthly	0.71	0.81	1.09	0.56	1.00	(0.95, 1.06)
DEHain	GPP - Monthly	0.97	0.97	0.82	0.98	1.03	(1.02, 1.05)
DKSor	GPP - Monthly	0.93	0.97	1.60	0.96	0.84	(0.84, 0.85)
BEBra	GPP - Monthly	0.90	0.95	0.81	0.96	0.91	(0.90, 0.92)
FIHyy	GPP - Monthly	0.93	0.96	0.93	0.92	1.03	(1.02, 1.04)

GPP correlation for FRPue significantly improved switching the temporal resolution, mainly because of the strong reduction of the residuals variability (Fig 5.7).

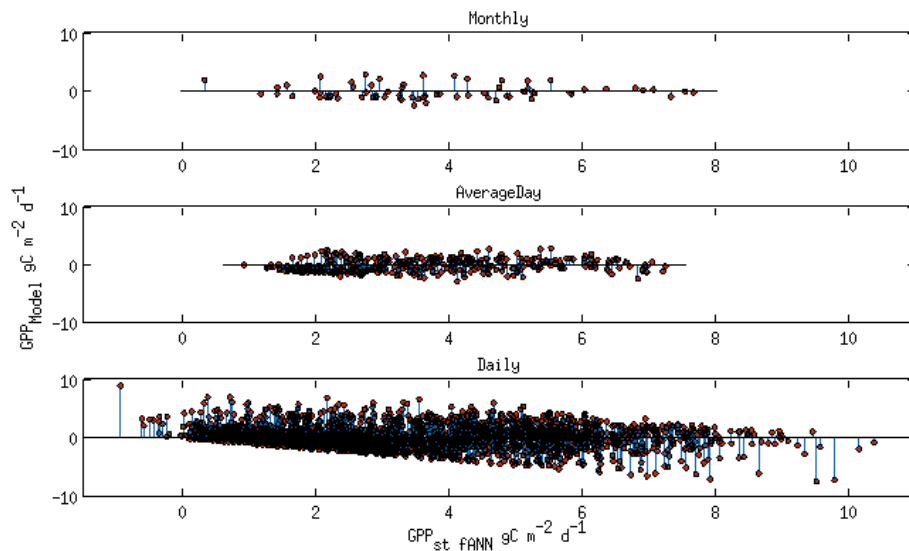


Fig. 5.7 FRPue Residuals distribution among the 1:1 line for simulated against EC GPP (monthly, daily and daily trends). Daily errors compensate and thus are strongly reduced on a monthly time scale.

5.1.3. 3D-CMCC-Pheno FEM Performance for inter monthly, seasonal and annual variability of GPP

Monthly and annual data were normalized by subtracting respective mean totals from individual totals in order to quantify inter annual (IAV), inter monthly (IMV) (Keenan et al., 2012) and inter seasonal variability (ISV). The presence of periods of systematic error was evaluated by differencing observed and predicted monthly variability (e.g. Variance Residuals VRs). The magnitude of modeled IAVs in GPP flux was on average of the same order of the observed ones (Fig. 5.8), proving enough flexibility to reproduce the observed range of variability.

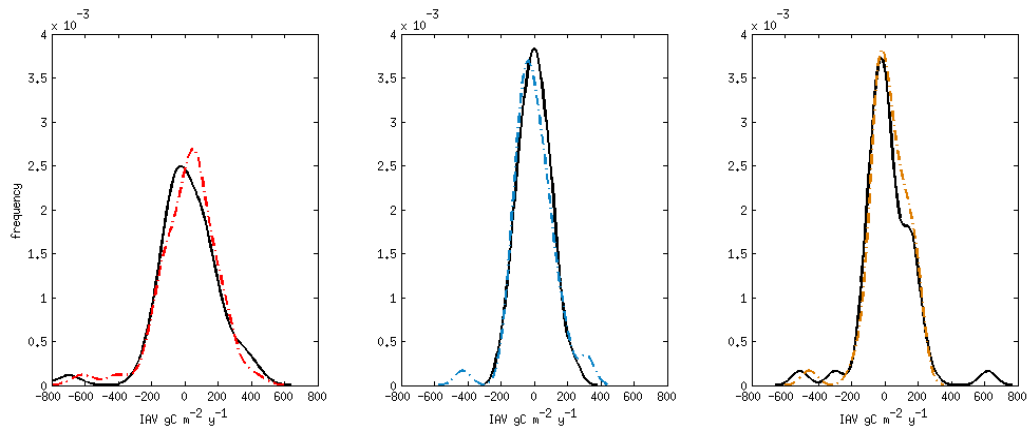


Fig. 5.8 Whole dataset distribution of the IMVs for simulated GPP (red dotted line), Reco (yellow) and NEE (azure). Black lines show the EC respective IMVs. The density functions have been calculated by using kernel density estimation.

Fig 5.9 shows annual anomalies for each simulated forest. The model resulted to be able to capture about 67% of the anomalies for the total set of 52 years.

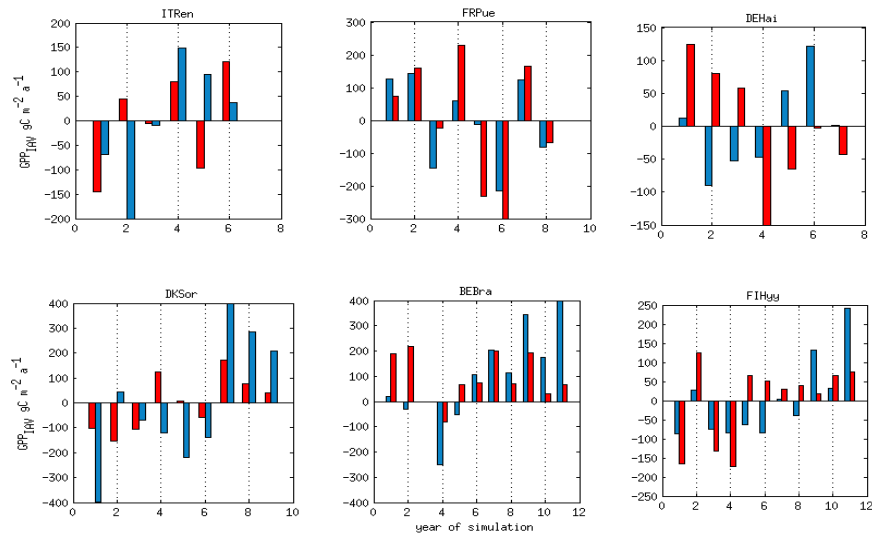


Fig. 5.9. Inter annual GPP variability for the 6 simulations ($\text{gC m}^{-2} \text{d}^{-1}$). Red bars represent EC based anomalies; blue ones the 3D-CMCC-FEM anomalies.

The Normalized root mean square error (NRMSE) was calculated to quantitatively evaluate the biases for each site (Tab 5.5). NRMSEs evidenced that the highest errors were associated to deciduous forests (e.g. beech stands at DEHai and DKSor).

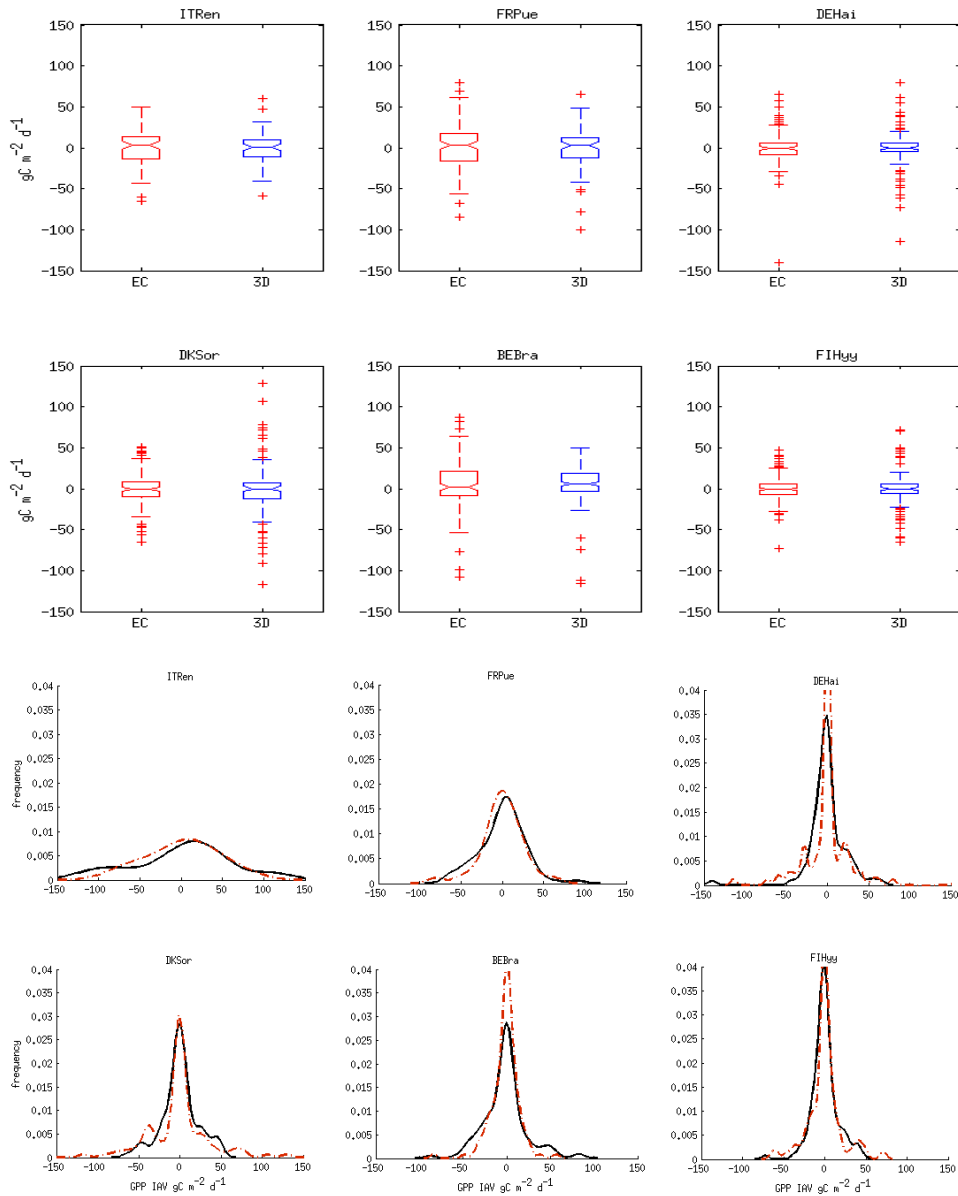


Fig. 5.10. IMVs of measured and simulated GPP for the 6 simulations. Boxplots in (a) (Red EC data, Blue 3D-CMCC simulations) represent median, upper-lower interquartile, lower and upper bounds. Red crosses represent IMVs extreme values. Graphs in (b) represent the distribution of the frequencies of GPP IMVs resulted from a kde estimation; red dotted line represent simulated data, black lines EC data.

Tab. 5.5. Statistics of the GPP anomalies (IMVs, ISVs and IAVs). IMVs results of the statistic tests of normality (χ^2 GOF) and equivalency of the central tendency (CET). 0 values imply H_0 acceptance, that is respectively that “the distribution of the IMVs is normal” and/or “the expected and observed distributions are statistically equal”. The CET t-test was performed for normally distributed IMVs, Mann–Whitney U if not. The CET H_0 was automatically rejected if expected and observed IMVs had different χ^2 GOF outcome.

		ITRen	FRPue	DEHai	DKSor	BEBra	FIHyy
NRMSE	IAVs	1.12	0.34	1.22	1.82	0.74	0.95
NRMSE	ISVs	0.96	0.93	1.48	1.8	0.99	1.23
NRMSE	IMVs	1.09	1.09	1.26	1.84	0.97	1.23
χ^2 GOF	IMVs	0	0	1	1	1	1
CET	IMVs	0	0	0	0	0	0

GPP IMVs showed anomalies very similar in magnitude and density functions, even though simulated IMVs appeared more highly concentrated around the average for both BEBra and DEHai (Fig 5.10). The analysis of the VRs resulted in no significant persistent bias in any month for any case of study (Fig. 5.11).

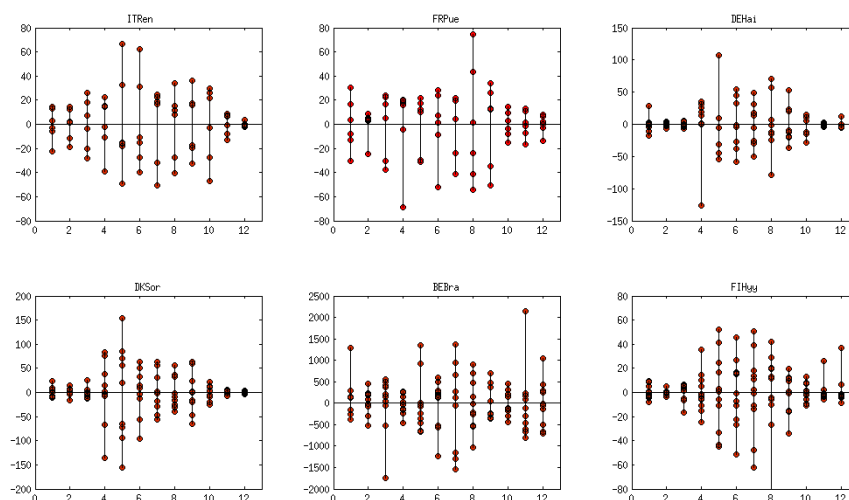


Fig. 5.11. Residuals (predicted-observed) of GPP monthly variability. Positive values indicate higher variability in the observations than in the model. When more than 90% of a specific month residuals were positive/negative systematic errors were detected.

In general the model resulted to be able to capture about 70% of the biases for the months observed (417 over 600 months). Again evergreen forests showed better VRs and lower NRMSE, with the exception of FIHyy spruce forest.

Nevertheless, the model showed its limits in simulating summer IMVs, especially in forests dominated or co-dominated by deciduous broadleaf species. This appeared especially true for beech forests (e.g. DEHai and DKSor) where only 30% of the observed IMVs were captured (Fig. 5.12); hence IMVs magnitude of inter month variability was well reproduced, but not the timing.

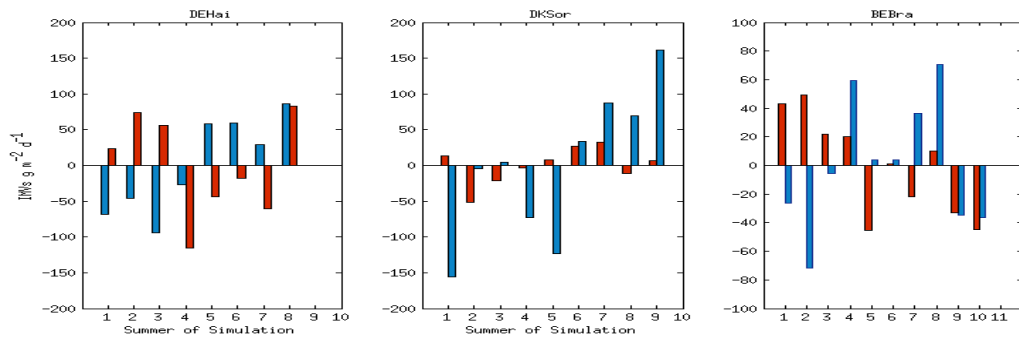


Fig. 5.12. Summer IMVs ($\text{gC m}^{-2} \text{d}^{-1}$) for the 3 simulations having deciduous species dominating or codominating the ecosystem canopy. Red bars represent EC based anomalies; blue ones the 3D-CMCC-FEM anomalies.

The new Phenology routine gave different results in spring anomalies (Fig 5.13); it was able to capture ISVs very well (about 80%) for 5 ecosystems on 6, but gave awful results in the Mediterranean one (0/6).

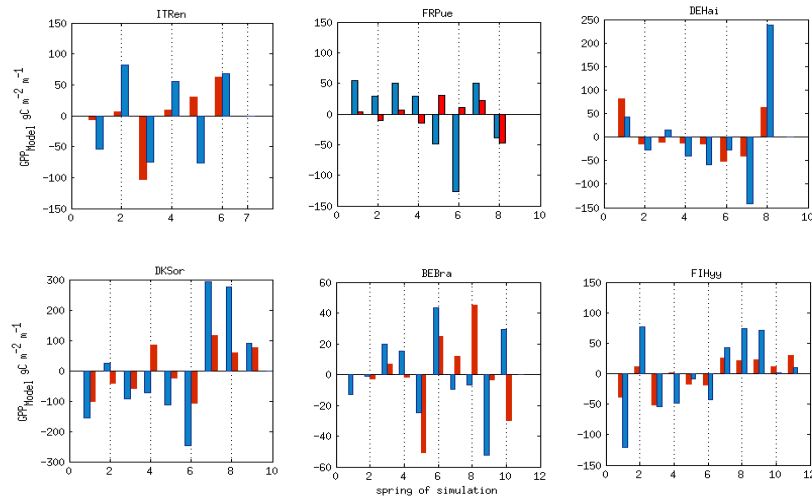


Fig. 5.13 Inter seasonal GPP variability for the 6 simulations during spring ($\text{gC m}^{-2} \text{d}^{-1}$). Red bars represent EC based anomalies; blue ones the 3D-CMCC-FEM anomalies.

On the other hand the new Phenology routine gave more constant results in autumn ISVs, but averagely captured only 70% of the ISVs (Fig 5.14), with best result in FIHyy, worst in ITRen.

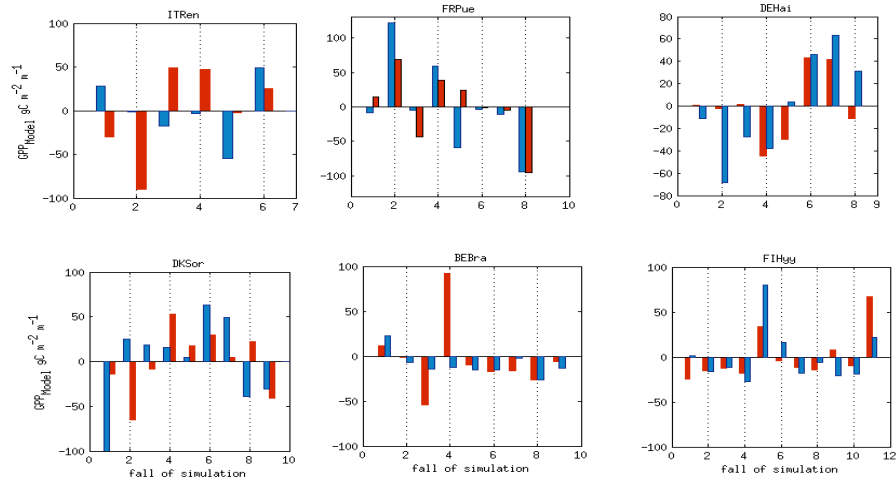


Fig. 5.14 Inter seasonal GPP variability for the 6 simulations during fall ($\text{gC m}^{-2} \text{ d}^{-1}$). Red bars represent EC based anomalies; blue ones the 3D-CMCC-FEM anomalies.

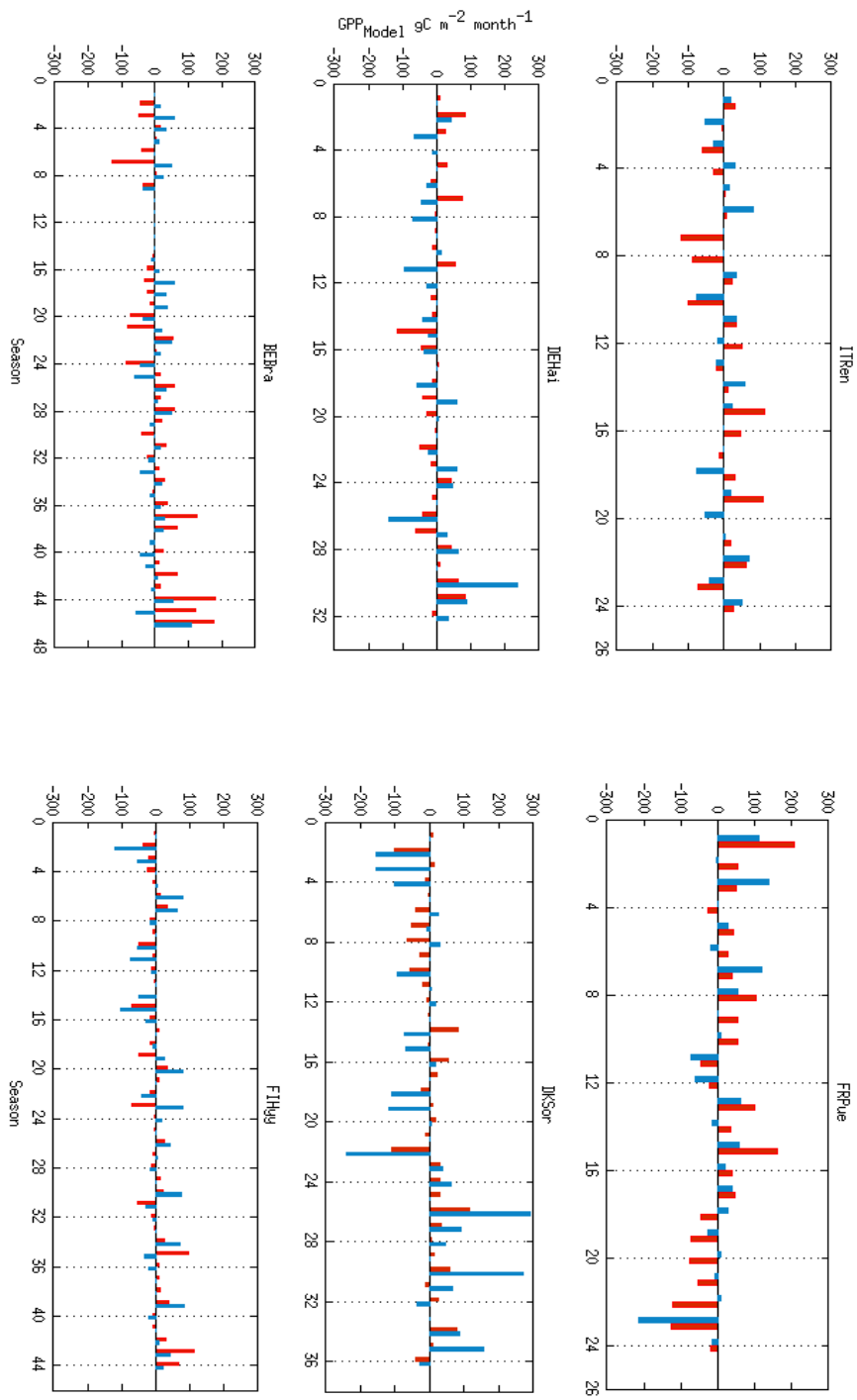


Fig. 5.15 Inter seasonal GPP variability for the 6 simulations ($\text{gC m}^{-2} \text{d}^{-1}$). Red bars represent EC based anomalies; blue ones the 3D-CMCC-FEM anomalies.

5.1.4. Comparison with the 5.1 version of 3D-CMCC-FEM

The modifications in the 6.1 version resulted in overall better agreement with the EC daily data. The new phenology routine resulted in higher correlation and goodness of fit, with the exception of FRPue (Tab. 5.6); in any case the NSE was significantly higher in the 6.1 version, even for FRPue. Gaps too were generally lower in the 6.1, as inferred by contrasting the two code versions average RMSE (Collalti et al., in prep).

Tab. 5.6. Comparison between 5.1.v and 6.1.v estimators resulted by the validation against EC data.). The table reports for each site: the regression goodness of fit estimator (r^2), the Pearson's correlation estimator and the Nash Sutcliffe model efficiency estimator.

	Version	ITRen	FRPue	DEHai	DKSor	BEBra	FIHy	Avg
Daily r^2	5.1	0.66	0.67	0.85	0.80	0.60	0.83	0.73
	6.1	0.77	0.41	0.86	0.83	0.74	0.83	0.74
Monthly r^2	5.1	0.91	0.41	0.94	0.94	0.83	0.93	0.83
	6.1	0.92	0.71	0.97	0.93	0.90	0.93	0.89
Daily r	5.1	0.82	0.82	0.92	0.89	0.77	0.91	0.85
	6.1	0.86	0.65	0.91	0.91	0.87	0.91	0.85
Monthly r	5.1	0.95	0.64	0.97	0.97	0.91	0.96	0.90
	6.1	0.96	0.81	0.97	0.97	0.95	0.96	0.94
Daily trends r^2	5.1	0.94	0.87	0.94	0.96	0.90	0.95	0.93
	6.1	0.92	0.78	0.97	0.97	0.96	0.94	0.92
Daily RMSE	5.1	2.09	1.52	1.85	2.96	1.59	1.56	1.93
	6.1	1.59	1.96	1.91	2.62	1.48	1.57	1.86
Monthly RMSE	5.1	0.97	1.01	1.07	1.47	0.91	0.91	1.06
	6.1	0.82	1.09	0.82	1.60	0.81	0.93	1.01
Daily NSE	5.1	0.61	-0.54	0.84	0.74	0.58	0.87	0.52
	6.1	0.72	0.09	0.96	0.8	0.75	0.76	0.68
Monthly NSE	5.1	0.91	-0.11	0.94	0.93	0.82	0.91	0.73
	6.1	0.91	0.56	0.98	0.96	0.96	0.92	0.88

Encouraging results were obtained by analyzing the anomalies distribution and normalized errors. The NRMSE was averagely lower in the 6.1 version at each temporal resolution; moreover it never rose over 2gC m-2 d-1, differently from the 5.1 (Tab. 5.7.).

Tab. 5.7. NRMSE (gC m2 d-1) between 5.1.v and 6.1.v estimators resulted by the validation against EC data.) for IMVs, ISVs and IAVs.

	Version	ITRen	FRPue	DEHai	DKSor	BEBra	FIHyy	Avg
Annual	5.1	1.31	0.63	2.41	1.83	0.95	2.74	1.65
NRMSE	6.1	1.12	0.34	1.22	1.82	0.74	0.95	1.03
Seasonal	5.1	1.35	1.08	1.32	4.26	0.78	3.48	2.05
NRMSE	6.1	0.96	0.93	1.48	1.8	0.99	1.23	1.23
Monthly	5.1	0.99	1.13	1.68	2.75	0.55	1.19	1.38
NRMSE	6.1	1.09	1.09	1.26	1.84	0.97	1.23	1.25

The distribution of the anomalies was somehow similar for deciduous stands (no significance differences). On the contrary the new evergreen turnover and phenology routines resulted in significantly improved ability to collect inter month variation (Fig. 5.16). As a matter of fact the F test for needle leaves species resulted in a consistent equality in variance between EC and the 6.1v, condition which was not reached between the EC and 5.1v data. Evergreen broadleaves in the 5.1 version showed consistency in variance but not in the average (two-sample t-test). Again the 6.1 IMVs distribution showed better results (equality in both variance and average).

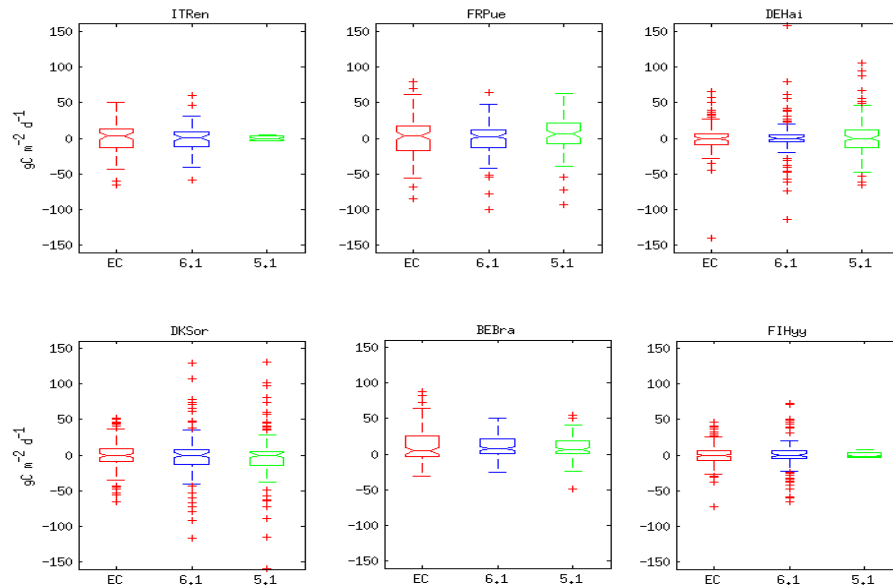


Fig. 5.16. IMVs of measured and simulated GPP for the 6 simulations. Red boxplots represent EC data, blue one the 3D-CMCC 6.1. simulations data, green ones the 3D-CMCC-FEM 5.1. simulations data. Each boxplot represent median, upper-lower interquartile, lower and upper bounds. Red crosses represent IMVs extreme values.

The use of the new C injection function resolved the occurrence of artifacts which mined the Autotrophic Respiration and thus C loss during bud burst (Fig. 5.17.). The use of the new fall phenology may have contributed in significantly reducing the NRMSE in deciduous stands; nevertheless even though p-value were higher in the 6.1v the F-test resulted in the rejection of the null hypothesis for both the 5.1 and 6.1 simulations. Important implications caused by the fall phenology modifications rely in the daily “fluxes” of FOM littered in autumn; however the 5.1 model version didn’t explicitly take into account either littering or RH, thus we couldn’t compare the results of the two versions.

The use of the PPA granted results in line with the manually calibrated ones, even though the biometric characteristics of the two simulations were different. This represented an advantage in the perspective of the integration of the algorithm to yearly determine the dominance relations in the canopy height layers, which will be discussed below.

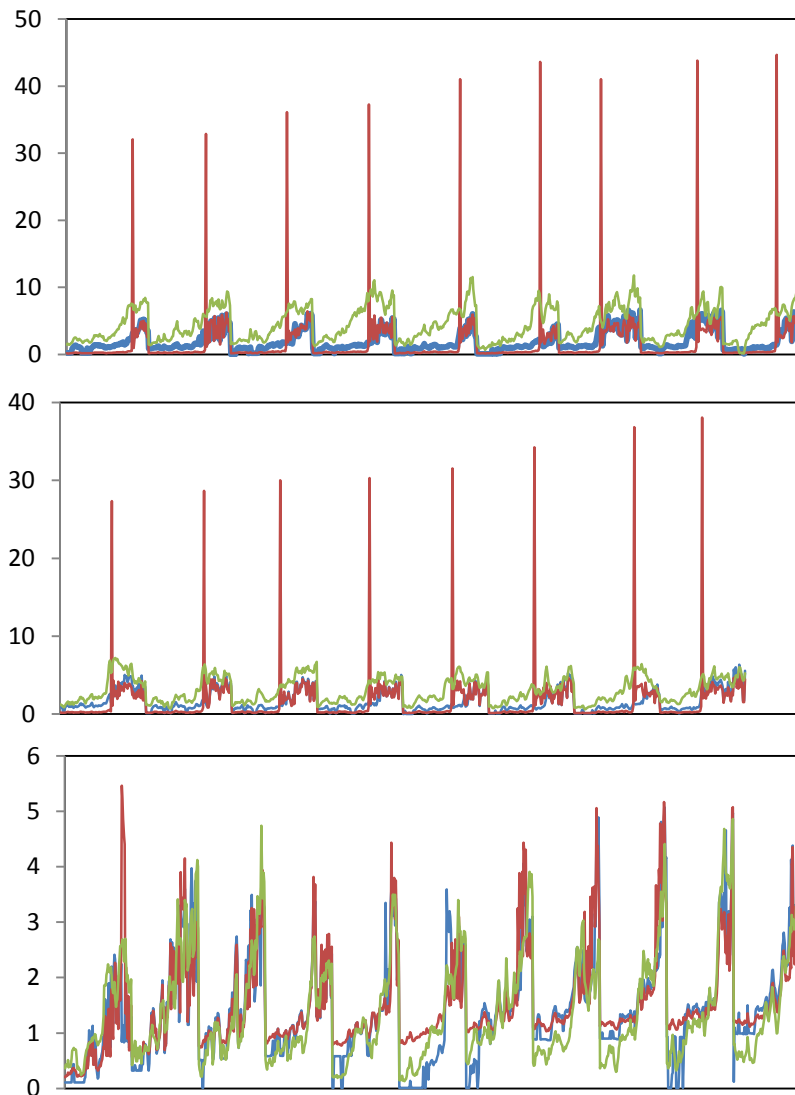


Fig. 5.17. Autotrophic Respiration in March, April and May for DKSor (a), DEHai (b) and FIHyy (c). Redo lines represent 5.1.v AR, blue lines 6.1.v AR. Green line srepresent EC Reco (FANN). The artifact in 5.1.v AR during budburst was resolved in the 6.1.v.

5.2. Results of Reco modeled

5.2.1 Annual and seasonal trends in Reco estimation

The 3D-CMCC-Pheno-FEM model was ran simplifying the whole soil as a single layer with average characteristics and total soil organic C in it; nonetheless the model well represented Reco trends of the EC sites (Fig 5.18). In contrast with GPP the Reco was generally represented in a noisier way, but the trends were respected in all the 6 sites, including the Mediterranean FRPue forest.

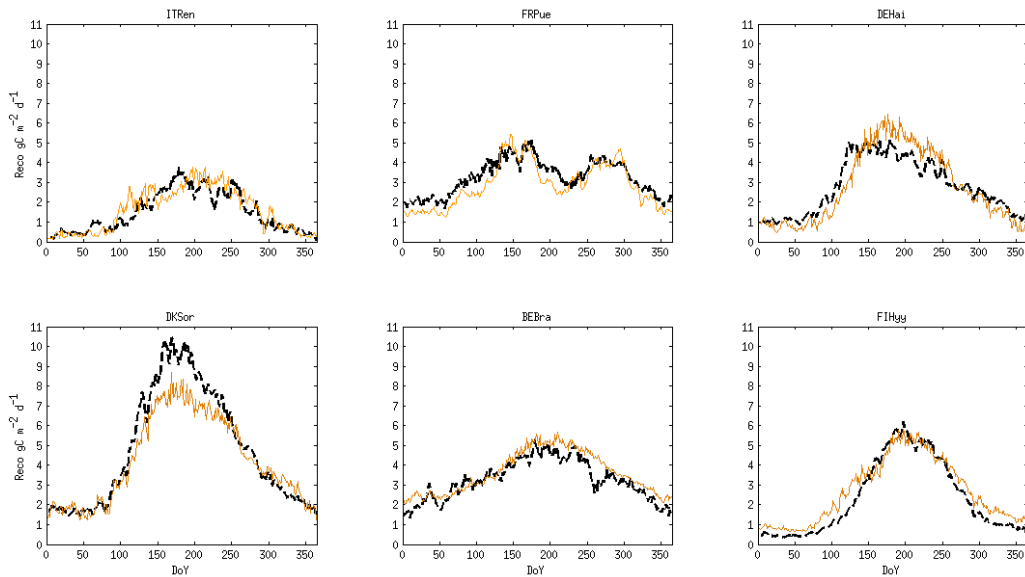


Fig. 5.18 Reco ($\text{gC m}^{-2} \text{d}^{-1}$) trends for the six study cases. Yellow dotted lines represent 3D-CMCC-FEM 6.1. simulations, black lines the EC data.

Winter trends resulted well represented for all sites. Good replication of winter trends occurred in deciduous forests, suggesting that soil respiration may be properly represented in those ecosystems during the period of no plant activity. Reco estimation appeared more uncertain during spring (Fig 5.19); indeed spring appeared to be the most critical season in determining the accuracy of the Reco assessment. This statement was especially valid for the two beech dominated forests of DKSorand DEHai. The former showed the same patterns for observed and modeled Reco, but evident underestimation of late spring fluxes; the latter even displayed two different patterns, with the result of low respiration in early spring whilst too high in late spring. An overestimation in early spring respiration can be noticed again in high altitude or latitude ecosystems (e.g. ITRen and FIHyy), where the influence of snow cover on the Carbon fluxes may not be ignored (Luus et al., 2013).

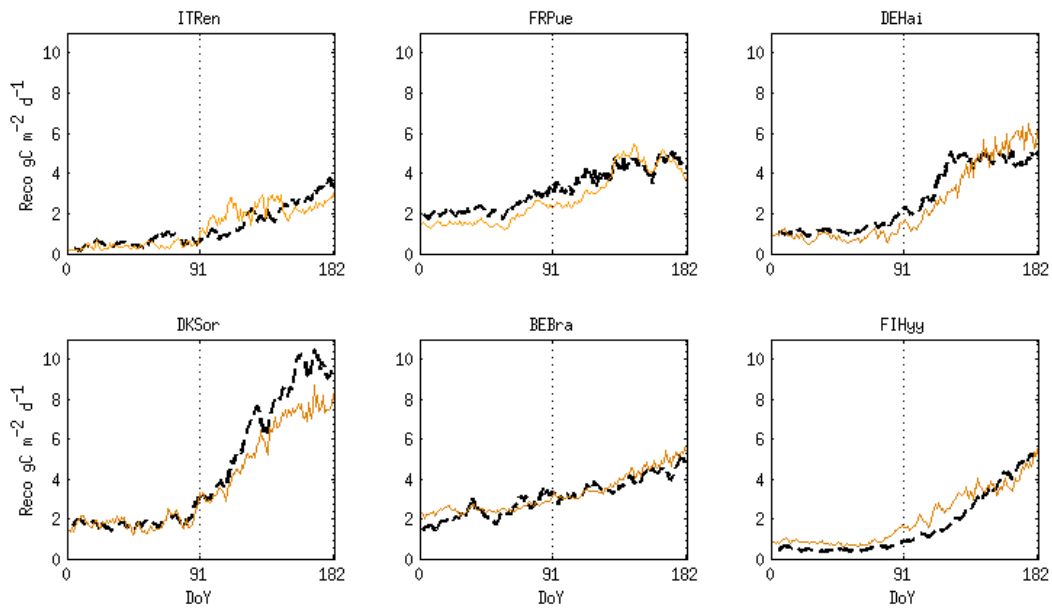


Fig. 5.19. Reco ($\text{gC m}^{-2} \text{d}^{-1}$) trends for winter and spring seasons along with dynamics of cumulated LAI ($\text{m}^2 \text{m}^{-2}$). Yellow lines represent simulated Reco, black line the EC data.

Even though they were clearly influenced by spring biases, Reco trends during summer followed the observed patterns in a more consistent way. An interesting exception occurred in late summer respiration at BEBra; this inconsistency may be related to the overestimation of the heterotrophic respiration under the pine stand, because of the very high Carbon content in the A2 soil horizon (Chiti et al., 2009) merged here in the average layer. Moreover the use of the soil water potential limiter on tree respiration resulted in a significant improvement in the assessment of autotrophic respiration in Mediterranean habitats.

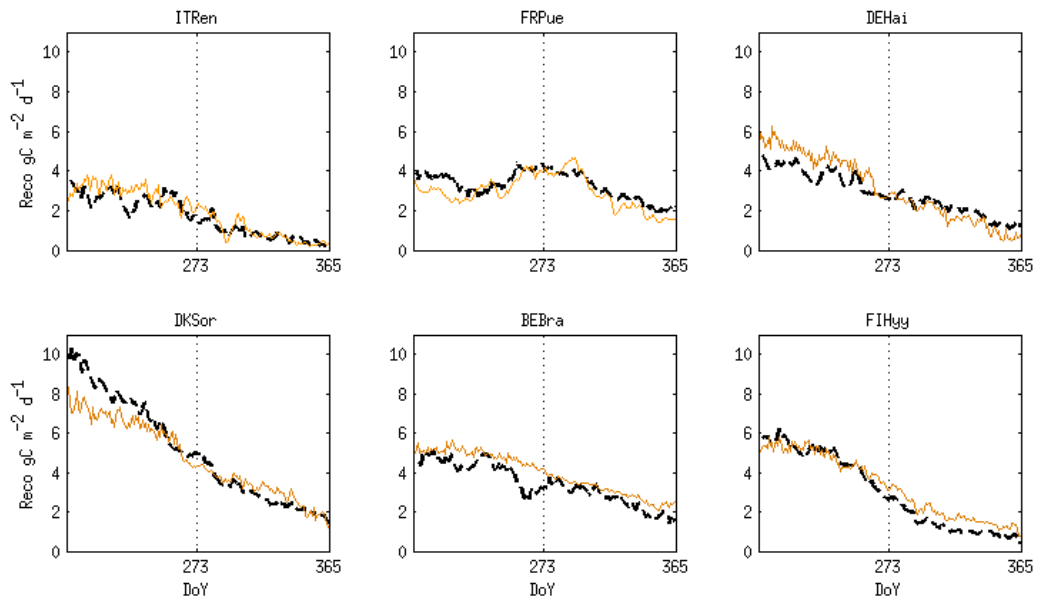


Fig. 5.20 Reco ($\text{gC m}^{-2} \text{d}^{-1}$) trends for summer and fall seasons along with dynamics of cumulated LAI ($\text{m}^2 \text{m}^{-2}$). Yellow line represent simulated GPP, black line the EC data.

The use of the new Phenology and Carbon turnover routines gave encouraging results as to fall respiration too (Fig. 5.20). As a matter of fact trends in Autumn Reco resulted consistent in all the 6 ecosystems. Even though the correlation between modeled and EC ecosystem respiration was generally worse than the GPP one, the 3D-CMCC-Pheno FEM returned encouraging results in its first simplified version. The results of Reco trends correlation is summarized in the Fig. 5.21 and Tab. 5.8. The trends showed high goodness of fit [0.66; 0.93], correlation coefficient [0.88; 0.98] and Model Efficiency [0.57; 0.88].

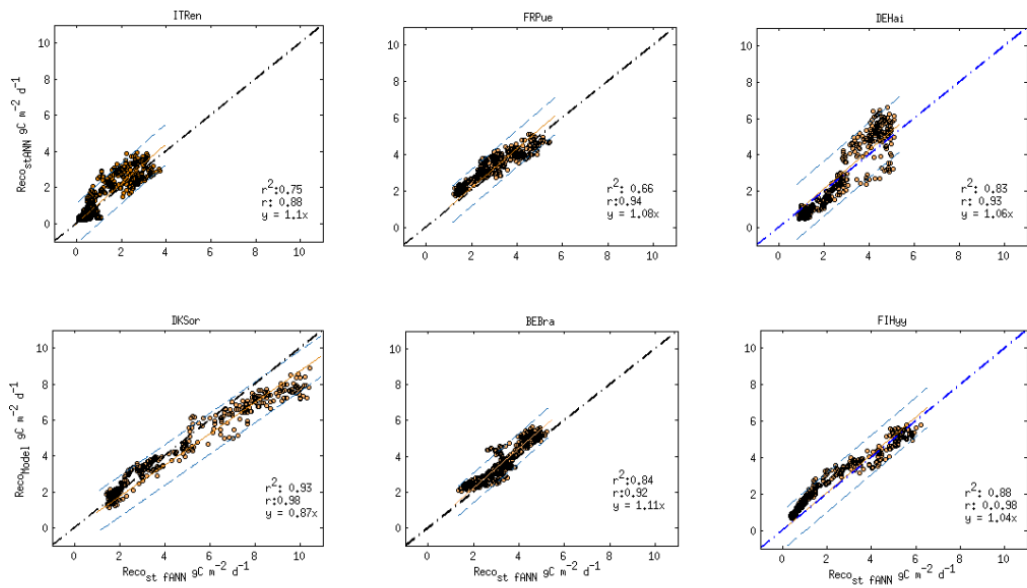


Fig. 5.21 Daily trends of simulated Reco plotted against EC data for the six sites. The black dotted lines represent the 1:1 ratio (perfect fit), yellow lines the actual mono parametric regression lines. The slopes of these lines represent the average over/underestimation. Azure dotted lines are the 95% expected bonds. The r is the Pearson's correlation statistic.

Like for GPP trends, the RMSE was reduced of about a half for all the six ecosystems compared to daily results. The fluctuation among the 1:1 line was higher than GPP's, implying an average bias ranging from -13% to +11%.

Tab. 5.8 Statistics of the daily average observed-simulated Reco ($\text{gC m}^{-2} \text{d}^{-1}$). The table reports for each site: the regression goodness of fit estimator (r^2), the Pearson's correlation estimator; the RMSE ($\text{gC m}^{-2} \text{d}^{-1}$); the Nash Sutcliffe model efficiency estimator; the slope of the mono parametric linear regression; the range of the parameter using a Levenberg-Marquardt algorithm.

Site	Var	r^2	r	RMSE	NSE	a	a-range
ITRen	Reco - Trends	0.75	0.88	0.56	0.71	1.10	(01.07, 1.13)
FRPue	Reco - Trends	0.67	0.94	0.50	0.57	1.08	(1.04, 1.10)
DEHain	Reco - Trends	0.83	0.98	0.77	0.63	1.06	(1.03, 1.09)
DKSor	Reco - Trends	0.93	0.98	0.58	0.88	0.87	(0.85, 0.89)
BEBra	Reco - Trends	0.84	0.98	0.42	0.68	1.11	(1.09, 1.12)
FIHyy	Reco - Trends	0.88	0.97	0.55	0.83	1.04	(1.02, 1.06)

5.2.2 Validation of 3D-CMCC-Pheno Reco results on daily and monthly temporal resolution

Fig. 5.22 shows daily correlation between Model outputs and the EC Reco fluxes ($\text{gC m}^{-2} \text{d}^{-1}$). The regression showed a very significant correlation ($p < 0.0001$ and $r [0.69; 0.90]$), and good agreement for each sets of values, with an r^2 ranging from 0.36 to 0.73 (Tab 5.9). The use of the new limitation factor for respiration under water stress significantly improved Reco estimation for broadleaves species, especially in the Mediterranean ecosystem, where summer drought stress is typical.

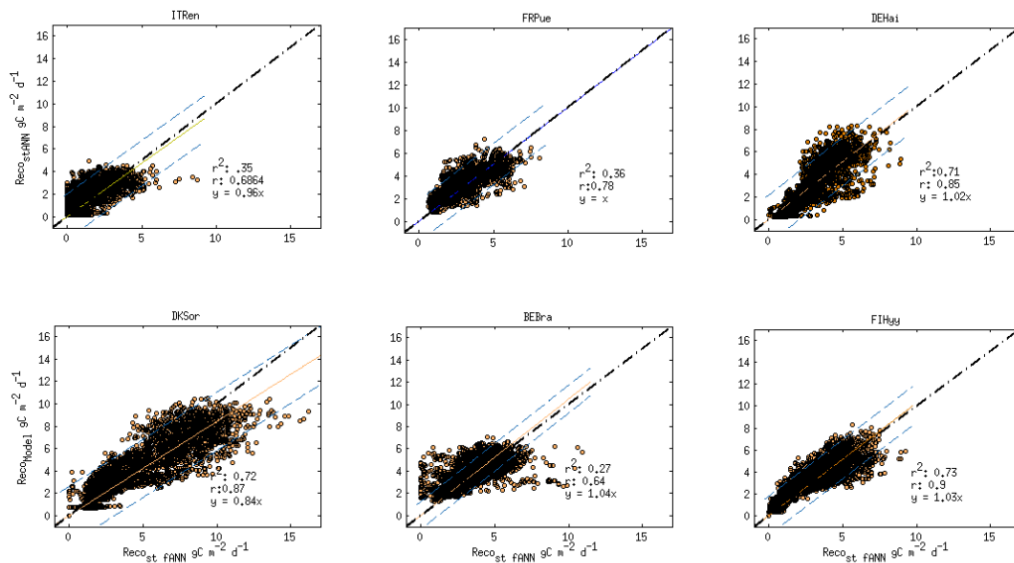


Fig. 5.22 Daily simulated Reco plotted against daily EC data for the six sites. Days for which no EC data were available were discarded. Otherwise days with simulated Reco = 0 were taken into account. The black dotted lines represent the 1:1 ratio (perfect fit), yellow lines the actual mono parametric regression lines. The slope of these lines represent the average over/underestimation. Azure dotted lines are the 95% expected bonds. The r is the Pearson's correlation statistic.

However the lowest correlation and Model Efficiency occurred in the spruce forest of ITRen (e.g. r^2 of 0.42, NSE of 0.35). In contrast the model generally gave better results at higher latitudes. The NSE coefficient value was unexpectedly low for the BEBra simulation, presumably because of the noisy EC data for the 2011 (Fig. 5.23); the efficiency coefficient is in fact sensitive to extreme values and might yield suboptimal results when the dataset contains large outliers (Moriassi et al. 2007).

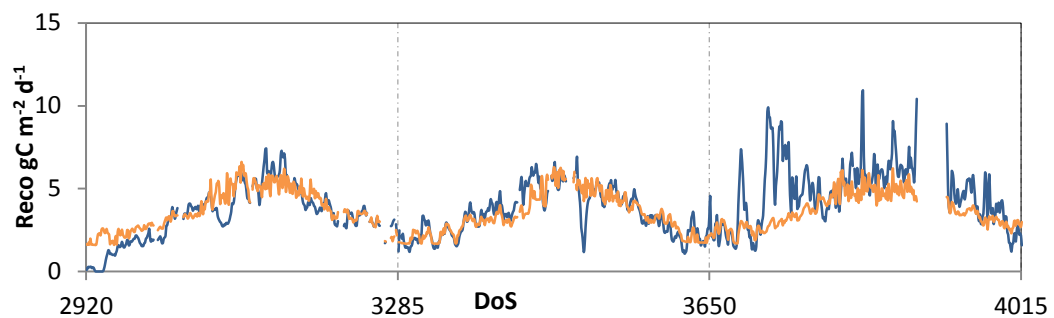


Fig. 5.23. Daily trends of Reco (gC m⁻² d⁻¹) in the years 2009, 2010 and 2011 for BEBra simulation. Yellow line represents simulated data, blue one measured data. Apparently there is some artifacts in the EC data for the last year of simulation which mined the quality of the correlation.

Thus the lowest values of NSE coefficient were in BEBra and ITRen simulations (0.33 and 0.35). Best results were in FIHyy and DKSor, ranging from 0.71 and 0.77. RMSE was considerably low, ranging from 0.66 to 1.33 gC m⁻² d⁻¹. According to the regression model “y = ax”, the modeled daily Reco fluctuated from a 16% of underestimation to a 4% of overestimation (Tab 5.9). These values were in line with daily GPP (Tab 5.3).

Figure 5.24 shows the correlation between EC data and Model outputs on a monthly time scale, Tab. 5.10 its principal statistics. Monthly outputs showed better results compared with daily Reco. No significant improvement was obtained in the BEBra simulation, where RMSE,

Tab. 5.9 Statistics of the daily observed-simulated Reco ($\text{gC m}^{-2} \text{d}^{-1}$). The table reports for each site: the regression goodness of fit estimator (r^2), the Pearson's correlation estimator; the RMSE ($\text{gC m}^{-2} \text{d}^{-1}$); the Nash Sutcliffe model efficiency estimator; the slope of the mono parametric linear regression; the range of the parameter using a Levenberg-Marquardt algorithm.

Site	Var	r^2	r	RMSE	NSE	a	a-range
ITRen	Reco - daily	0.42	0.79	0.91	0.35	0.96	(0.94, 0.98)
FRPue	Reco - daily	0.36	0.63	0.92	0.57	1.00	(0.98, 1.02)
DEHai	Reco - daily	0.71	0.91	1.09	0.51	1.02	(1.01, 1.05)
DKSor	Reco - daily	0.72	0.91	1.33	0.71	0.84	(0.80, 0.88)
BEBra	Reco - daily	0.63	0.64	0.63	0.33	1.04	(1.04, 1.05)
FIHyy	Reco - daily	0.73	0.91	0.91	0.77	1.03	(1.02, 1.04)

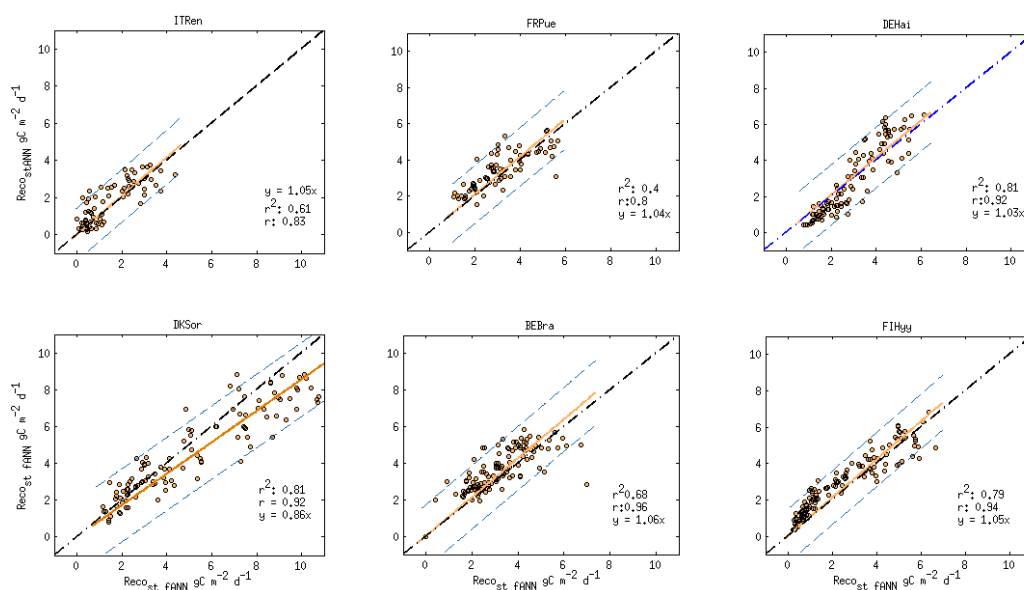


Fig. 5.24. Monthly simulated Reco plotted against monthly EC data for the six sites. The black dotted lines represent the 1:1 ratio (perfect fit), yellow lines the actual mono parametric regression line. The slopes of these lines represent the average over/underestimation. Azure dotted lines are the 95% expected bonds. The r is the Pearson's correlation statistic.

NSE and r^2 were similar to those referred to daily temporal resolution (r^2 0.68, RMSE 0.88, NSE 0.4). As to the other sites, the reduction in residuals dispersion determined the reduction of the RMSE of about 30%, and the improvement of the Goodness of fit of about 0.1. NSE resulted significantly higher, ranging from 0.74 to 0.91.

Tab. 5.10 Statistics of the monthly observed-simulated Reco ($\text{gC m}^{-2} \text{d}^{-1}$). The table reports for each site: the regression goodness of fit estimator (r^2), the Pearson's correlation estimator; the RMSE ($\text{gC m}^{-2} \text{d}^{-1}$); the Nash Sutcliffe model efficiency estimator; the slope of the mono parametric linear regression; the range of the parameter using a Levenberg-Marquardt algorithm.

Site	Var	r^2	r	RMSE	NSE	a	a-range
ITRen	Reco - Monthly	0.61	0.96	0.71	0.77	1.05	(0.95, 1.13)
FRPue	Reco - Monthly	0.44	0.81	0.80	0.74	1.04	(0.98, 1.08)
DEHain	Reco - Monthly	0.81	0.97	0.84	0.76	1.03	(1.01, 1.08)
DKSor	Reco - Monthly	0.81	0.97	1.00	0.90	0.86	(0.86, 0.88)
BEBra	Reco - Monthly	0.68	0.95	0.88	0.40	1.06	(1.09, 1.12)
FIHyy	Reco - Monthly	0.79	0.96	0.75	0.92	1.05	(1.02, 1.05)

Fluctuations around the 1:1 ratio were in line with daily ones. Moreover it appeared that the model slightly overestimated Reco monthly fluxes in all sites except DKSor.

5.2.3 3D-CMCC-Pheno FEM Performance for inter monthly, seasonal and annual variability of Reco

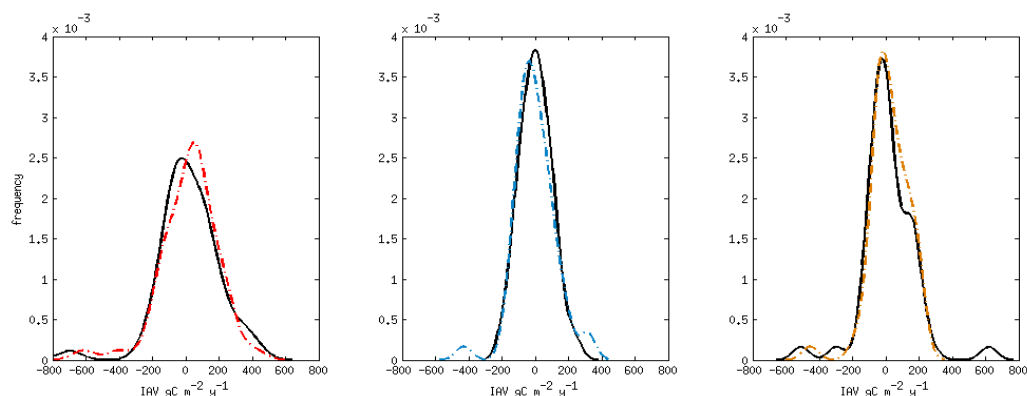


Fig. 5.25. Whole dataset distribution of the IMVs for simulated GPP (red dotted line), Reco (yellow) and NEE (azure). Black lines show the EC respective IMVs. The density functions have been calculated by using kernel density estimation.

The magnitude of modeled IAVs in Reco fluxes was again of the same order of the observed ones (Fig. 5.25). Fig 5.26 shows annual anomalies for each simulated forest. The model resulted to be able to capture about 64% of the anomalies for the total set of 52 years, 73% excluding the DKSor simulation. As a matter of fact the model badly simulated summer Reco in DKSor, with implications in its poor capability to reproduce inter annual anomalies.

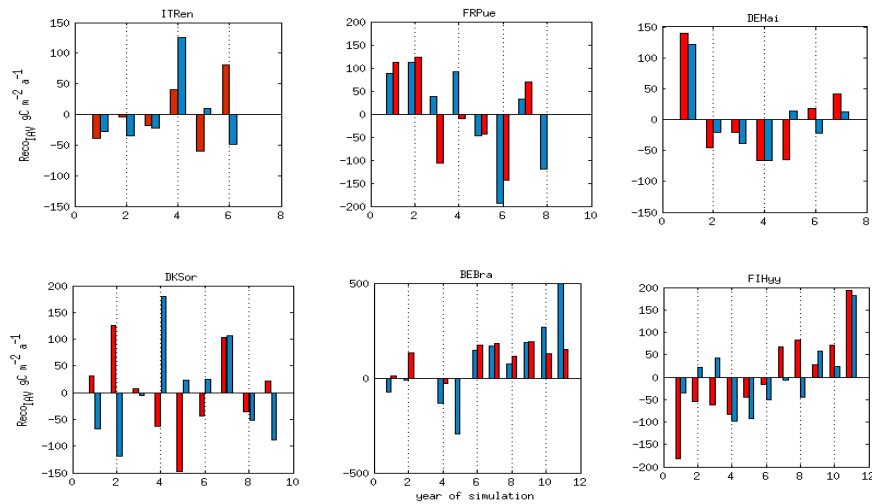


Fig. 5.26. . Inter annual Reco variability for the 6 simulations ($\text{gC m}^{-2} \text{d}^{-1}$). Red bars represent EC based anomalies; blue ones the 3D-CMCC-FEM anomalies.

That said the model’s ability in capturing IAVs resulted higher for Reco than GPP, as inferred by comparing the respective NRMSE indexes showed in Tab.5 and Tab 5.10 (Tab 5.11).

Tab. 5.11. Difference between anomalies in Reco and GPP. Positive values mean that Reco NRMSE is lower than the one it is compared to.

		ITRen	FRPue	DEHai	DKSor	BEBra	FIHyg
ΔNRMSE	Annual	0.01	0.06	0.63	0.38	-0.02	-0.04
ΔNRMSE	Seasonal	0.00	0.13	0.69	0.57	0.21	-0.06
ΔNRMSE	Monthly	-0.1	0.22	0.25	0.47	0.08	0.07

Reco IMVs showed anomalies similar in magnitude but generally different density functions (Fig 5.27).

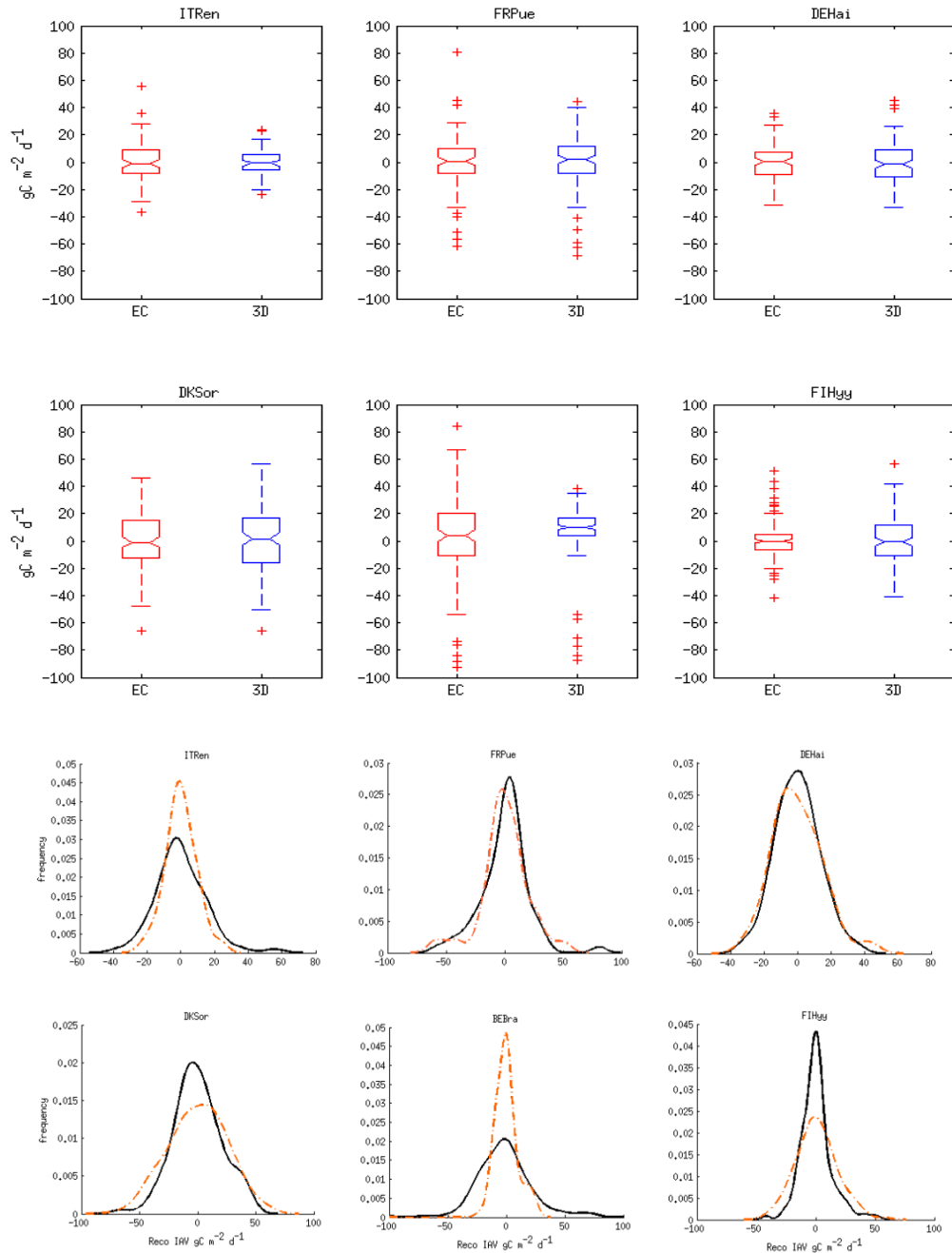


Fig. 5.27. IMVs of measured and simulated Reco for the 6 simulations. Boxplots in (a) (Red EC data, Blue 3D-CMCC simulations) represent median, upper-lower interquartile, lower and upper bounds. Red crosses represent IMVs extreme values. Graphs in (b) represent the distribution of the frequencies of GPP IMVs resulted from a kde estimation; yellow dotted lines represent simulated data, black lines EC data.

Excluding the FRPue and DEHai cases, which still had biased modal values, the distribution of IMVs for the other four ecosystems showed a similar shape but narrower (BEBra and ITRen) or wider distributions (DKSor ad FIHy). No persistent biases were found in evaluating Reco VRs in any month for any case of study (Fig 5.28 and Tab. 5.12).

Tab.5.12. Statistics of the Reco anomalies (IMVs, ISVs and IAVs). IMVs results of the statistic tests of normality (χ^2 GOF) and equivalency of the central tendency (CET). 0 values imply H0 acceptance, that is respectively that “the distribution of the IMVs is normal” and/or “the expected and observed distributions are statistically equal”. The CET t-test was performed for normally distributed IMVs, Mann–Whitney U if not. The CET H0 was automatically rejected if expected and observed IMVs had different χ^2 GOF outcome.

		ITRen	FRPue	DEHai	DKSor	BEBra	FIHy
NRMSE	Annual	1.09	0.34	1.22	1.82	0.74	0.95
NRMSE	Seasonal	1.08	0.93	1.48	1.8	0.99	1.23
NRMSE	Monthly	1.04	1.09	1.26	1.84	0.97	1.23
χ^2 GOF	Monthly	0	0	0	1	1	1
CET	Monthly	0	0	0	0	0	0

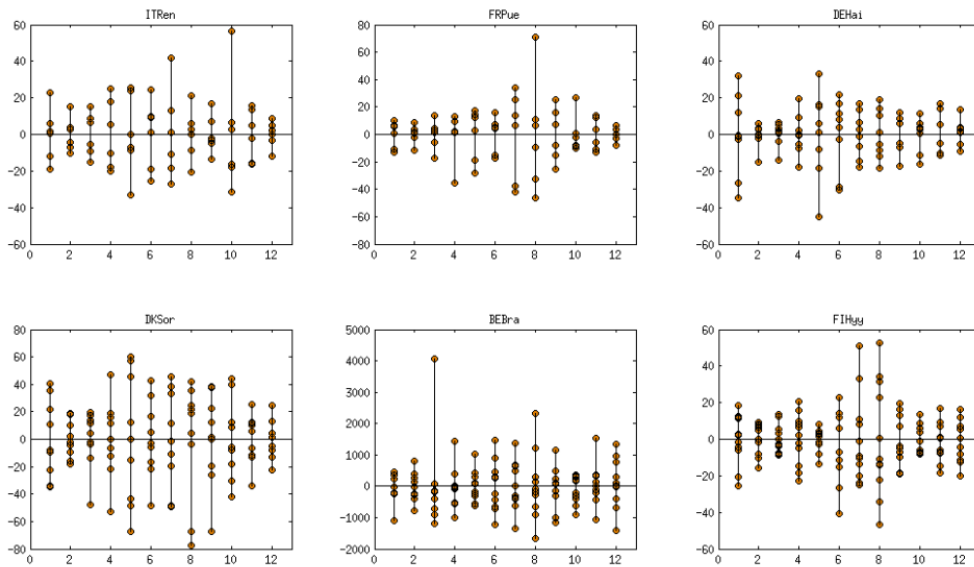


Fig. 5.28. Residuals (predicted-observed) of Reco monthly variability. Positive values indicate higher variability in the observations than in the model. When more than 90% of a specific month residuals were positive/negative systematic errors were detected.

ISVs during summer (Fig. 5.29) were in proportion the worst reproduced on a seasonal resolution (30/52 summers, capturing about 58% of the anomalies).

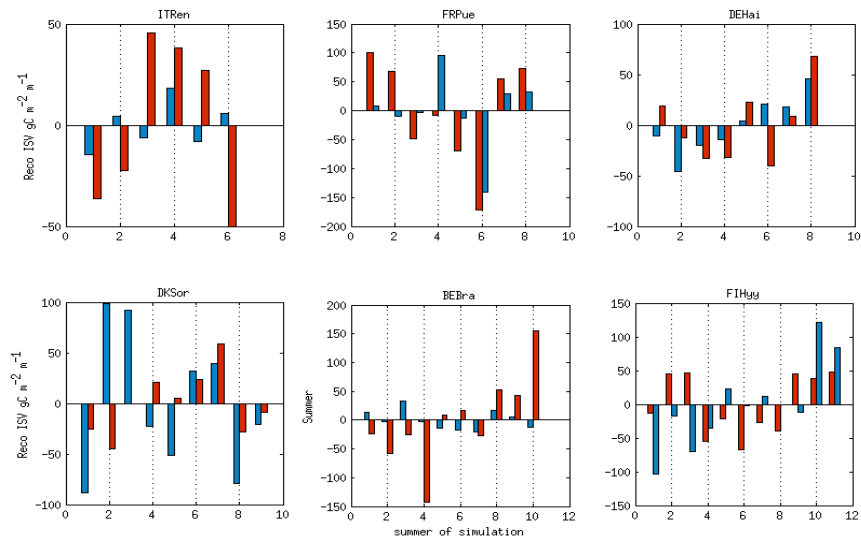


Fig. 5.29. Summer Reco IMVs ($\text{gC m}^{-2} \text{d}^{-1}$) for the 3 simulations having deciduous species dominating or codominating the ecosystem canopy. Red bars represent EC based anomalies; blue ones the 3D-CMCC-FEM anomalies.

Apparently needleleaf species performed worse. DKSor had the highest NRMSE between the six sites (Tab.5.12) mainly because of the high biases in 2001, 2002 and 2003.

In general the model resulted to be able to capture about 66% of the biases for the months observed (396 over 600 months). Again evergreen forests showed better VRs and lower NRMSE, with the exception of FIHyg spruce forest. The new Phenology routine gave good results in detecting spring and fall anomalies (Fig 5.30).

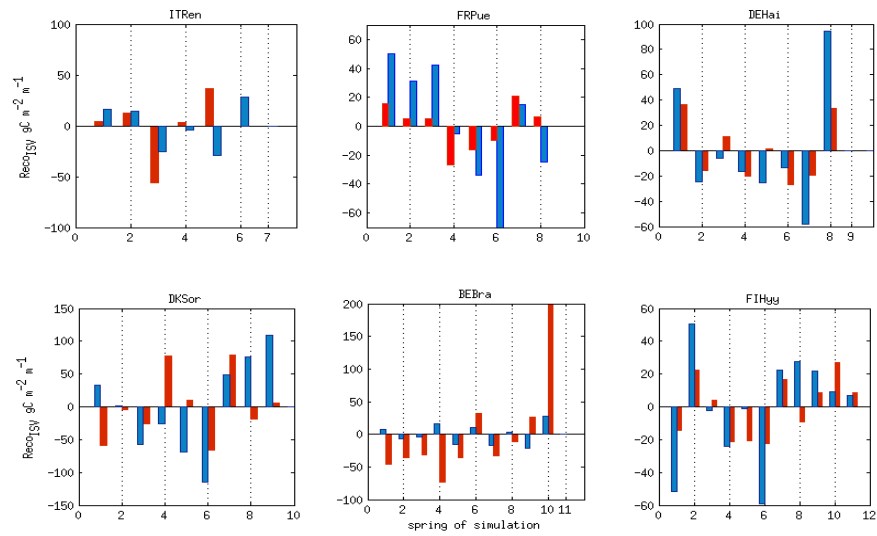


Fig. 5.30. Inter seasonal Reco variability for the 6 simulations during spring ($\text{gC m}^{-2} \text{d}^{-1}$). Red bars represent EC based anomalies; blue ones the 3D-CMCC-FEM anomalies.

The model captured about 70% of the spring ISVs, and gave the best results for FRPue (6/6). Again the worst results were at DKSor (4/9 springs, with about 44% of the anomalies captured).

Fig. 6

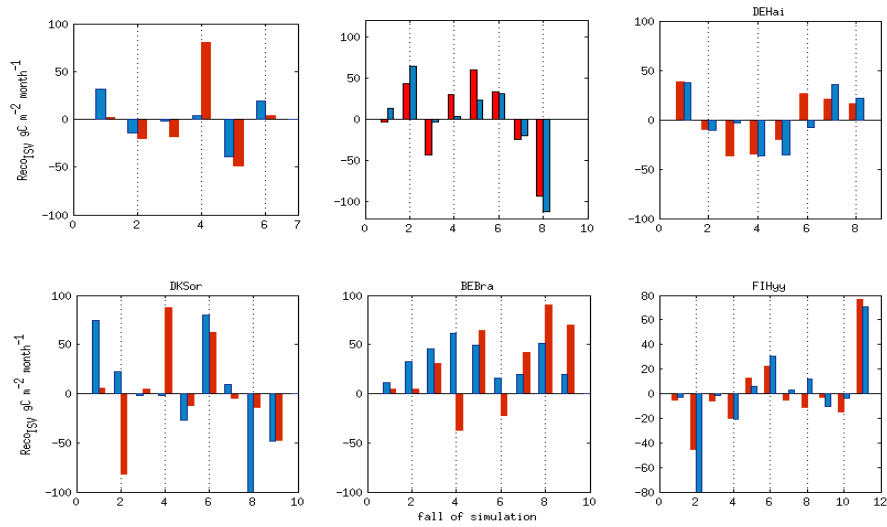


Fig. 5.31. Inter seasonal Reco variability for the 6 simulations during fall ($\text{gC m}^{-2} \text{d}^{-1}$). Red bars represent EC based anomalies; blue ones the 3D-CMCC-FEM anomalies.

Fall and Winter ISVs (Fig. 5.31) were the most well captured (respectively about 80% and 84% of the seasonal anomalies). This information was interesting also because of its biological meaning. As a matter of fact autumn and winter were the seasons in which the autotrophic component of the Ecosystem respiration was minimal. Thus the model's ability to reproduce ISVs in this period of the year may be partially considered an indicator of its ability in reproducing microbial respiration variability during these seasons.

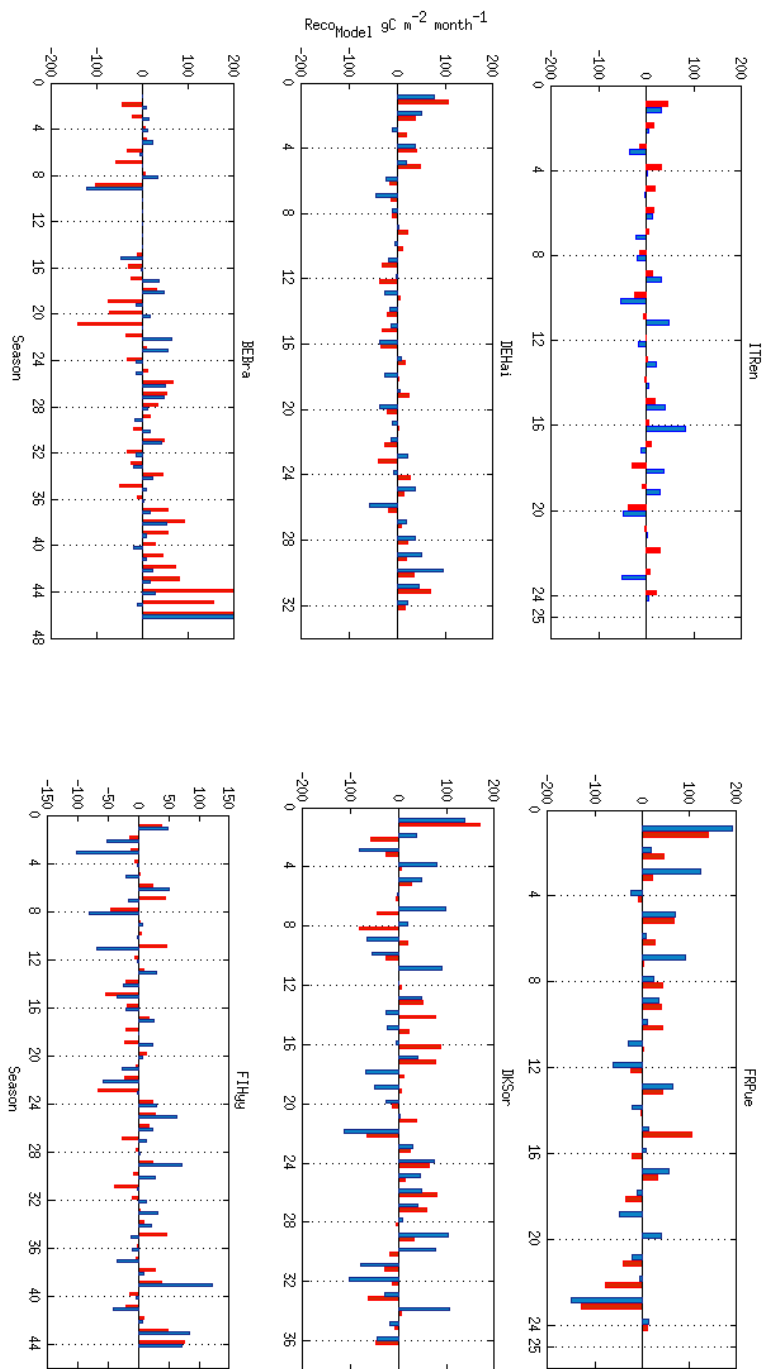


Fig. 5.32. Inter seasonal Reco variability for the 6 simulations ($\text{gC m}^{-2} \text{d}^{-1}$). Red bars represent EC based anomalies; blue ones the 3D-CMCC-FEM anomalies.

5.2.4. Aboveground and Belowground Autotrophs and Heterotrophic components of Reco

Fig. 5.33 shows the model's fractioning of Reco in its Autotrophic and Heterotrophic components.

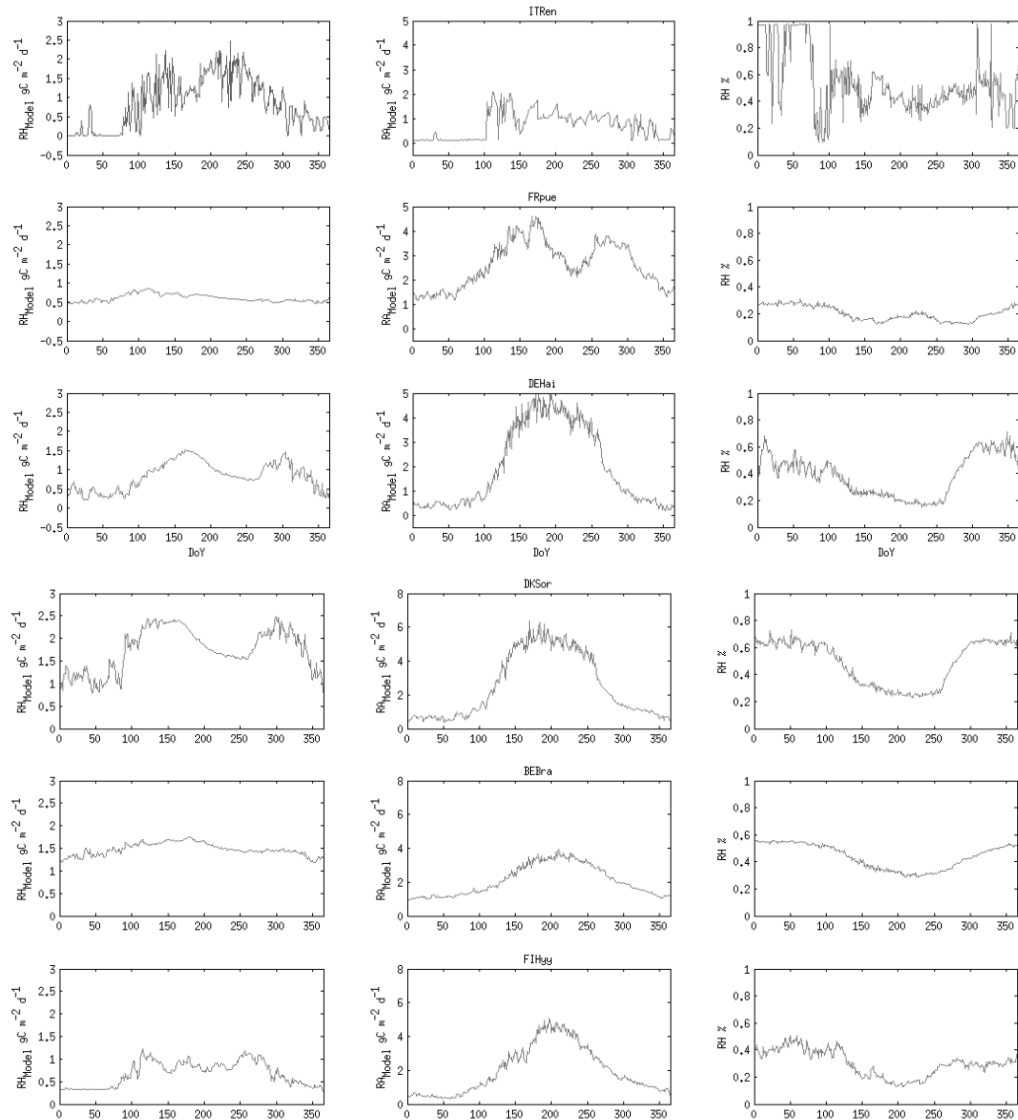


Fig. 5.33. Fractioning of the Reco into the Autotrophic (RA) and heterotrophic (RH) respiration. The first column represents average daily RA ($\text{gC m}^{-2} \text{d}^{-1}$), column 2 average daily RH ($\text{gC m}^{-2} \text{d}^{-1}$). Column 3 represents relative average daily fraction of RH on Reco.

Heterotrophic respiration (RH) appeared very low in FRPue (averagely 25% of the Reco) throughout the year, while Autotrophic Respiration (RA) was very low in ITRen during winter (representing about 5% of the Reco). Generally the RH represented about 60% of the total winter and fall Reco, and about 40% during spring and summer.

Fig. 5.34 shows how Soil Respiration (SR) was distributed in its RH and RA components. On average Roots Respiration (RR) represented about 43.5% of SR, ranging from 25 to 58% (Tab.5.13). These results were consistent with other published works, where RR formed about 50% of the average annual SR (Nakane et al., 1996, Epron et al., 2001, Andersen et al. 2005).

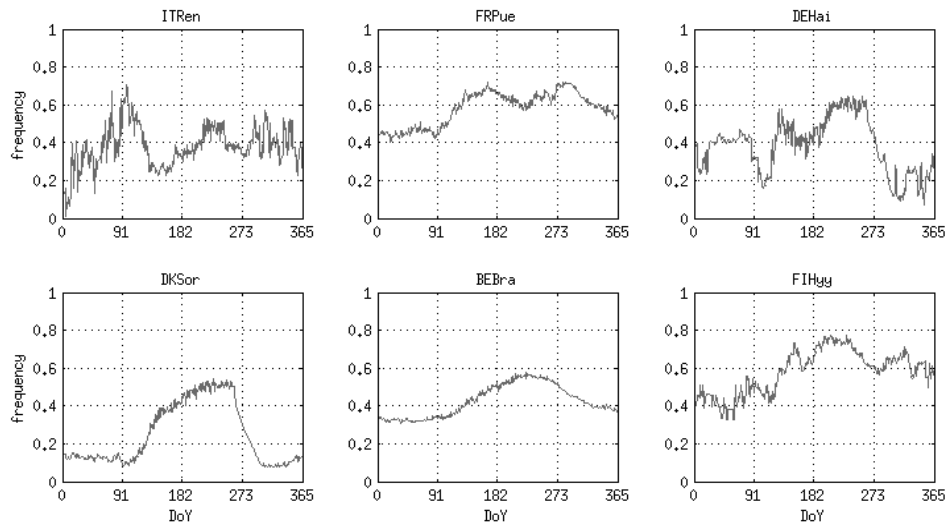


Fig. 5.34. Daily trends of NPP:GPP ratios throughout the solar year.

The Carbon Use efficiency (CUE) was calculated for the days with active Net Primary Production. It ranged from 0.37 to 0.68 and averaged at 0.53, showing a decrease with increasing average temperatures. These results matched with those of DeLucia et al. (2007) who showed that the slope of the relationship between NPP and GPP (CUE) is generally 0.53, ranging from 0.23 to 0.83. Model's CUEs ranged within the domain [0.41; 64] and overall respected the estimated features related to vegetation production shown in Ito et Oikawa (2004). According to Ito et Oikawa (2004) CUE was relatively low in FIHyy, suggesting that the overestimation in Reco previously described may be ascribable to excesses in RA.

Tab. 5.13. Average NPP:GPP and Root Respiration: Soil Respiration ratios.

	ITRen	FRPue	DEHai	DKSor	BEBra	FIHyy
RR/(RS)	0.38	0.58	0.39	0.25	0.43	0.58
Y	0.68	0.37	0.58	0.57	0.5	0.49

The NPP:GPP ratio was quite high in ITRen, probably because of unmatched trends in maintenance respiration (MR). To check it, the model's results of 2001 were compared with the data published by Matteucci et al., (2000) (Fig. 5.35). It resulted that MR was peaking during the periods in which daily Reco trends were overestimated (90th

to 120th DoY; 210th to 240th) while was relatively low during spring and summer, when GPP was higher.

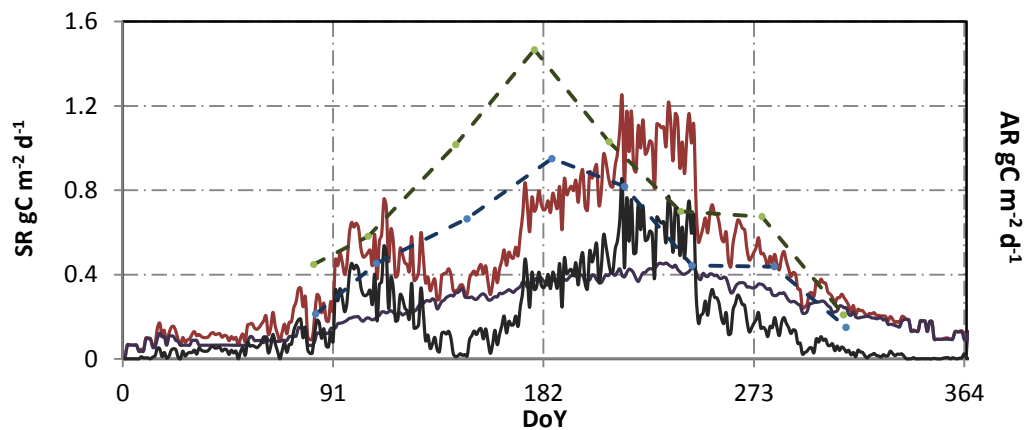


Fig. 5.35 Growth (purple), maintenance (black) and total autotrophic roots respiration (red) in 2006 at ITRen. Dotted lines represent maximum and minimum measured soil respiration for 2001 (Matteucci et al., XX). Maintenance respiration anomalous peak was responsible of summer SR overestimation.

Even though FRPue showed a value of NPP:GPP below 0.41, the ratio was in line with the values found by Sabate et al. (2002), DeLucia et al. (2007), (Ranbal et al., 2014). CUE tended to decrease more slightly in response to drought than GPP and NPP, probably due to drought-acclimation of autotrophic respiration (Ranbal et al., 2014)

5.3. Results of NEE modeled

5.3.1 Annual and seasonal trends in NEE estimation

NEP was calculated by difference between GPP and Reco, and assumed as the same value of the negative of NEE; herein NEE will be referred as equaling NEP. NEE daily trends (Fig 5.36) were overall respected even though seasonal biases could be identified in the ecosystems analyzed.

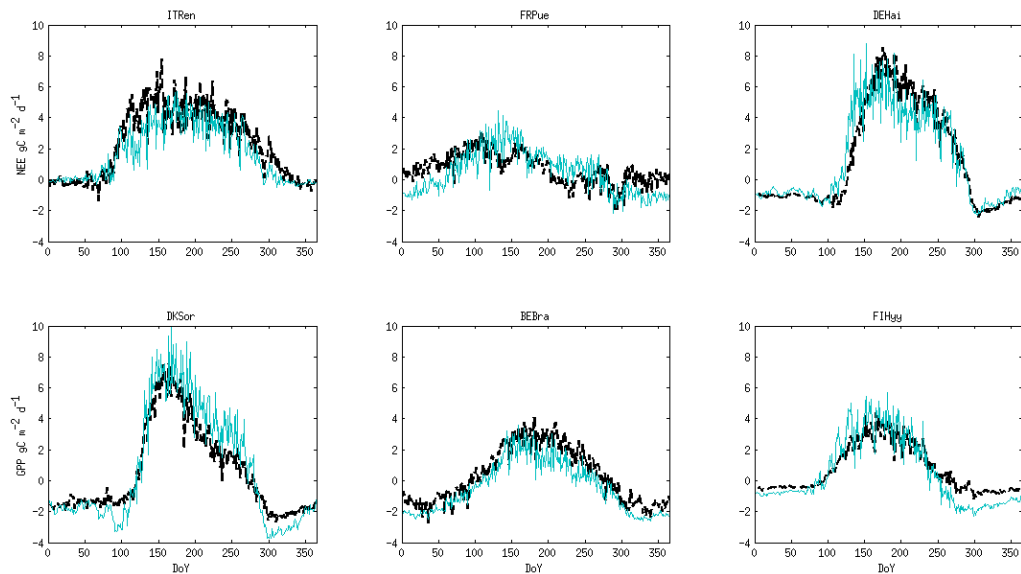


Fig. 5.36. NEE ($\text{gC m}^{-2} \text{d}^{-1}$) trends for the six study cases. Azure dotted lines represent 3D-CMCC-FEM 6.1. simulations, black lines the EC data.

Winter trends resulted well represented for most of the sites; the exception was at FRPue, where the underestimation was slightly higher

in GPP rather than in Reco, resulting in a bias of about $1 \text{ gC m}^{-2} \text{ d}^{-1}$. Nevertheless most of the biases occurred during spring (Fig. 5.37). Even though trends were respected, NEE at ITRen was on average 2-4 $\text{gC m}^{-2} \text{ d}^{-1}$ less than measured until late spring, as effect of the overestimation in maintenance respiration and GPP.

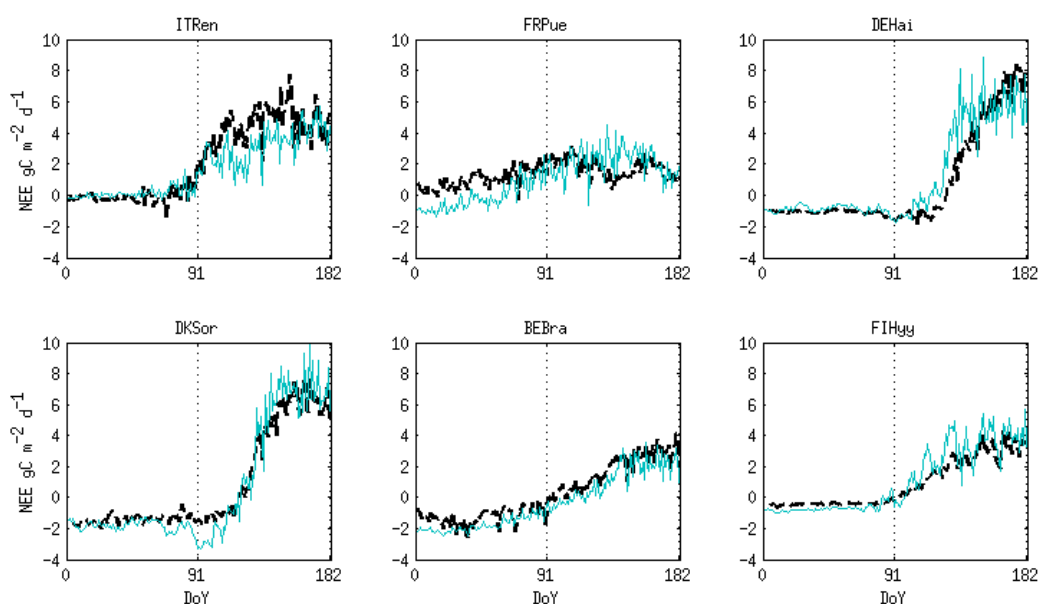


Fig. 5.37 NEE ($\text{gC m}^{-2} \text{ d}^{-1}$) trends for winter and spring seasons. Azure lines represent simulated Reco, black line the EC data.

Since NEE trends in FRPue followed the GPP patterns, they were badly represented where the model failed to reproduce them. FIHyg case of study evidenced similar results. Higher GPP combined with the Reco delay resulted in high NEE at DEHai (about $4\text{-}5 \text{ gC m}^{-2} \text{ d}^{-1}$). Moreover

the discrepancy in late spring Reco resulted on average in a slight NEE underestimation in June (about $1 \text{ gC m}^{-2} \text{ d}^{-1}$). Delay in bud burst determined an anomalous reduction in NEE at DKSor in early spring. No evident biases were found in BEBra simulation.

NEE trends during summer and fall were much more consistent with the measured ones (Fig. 5.38). During these seasons the biases appeared mostly related to falls in Reco estimation.

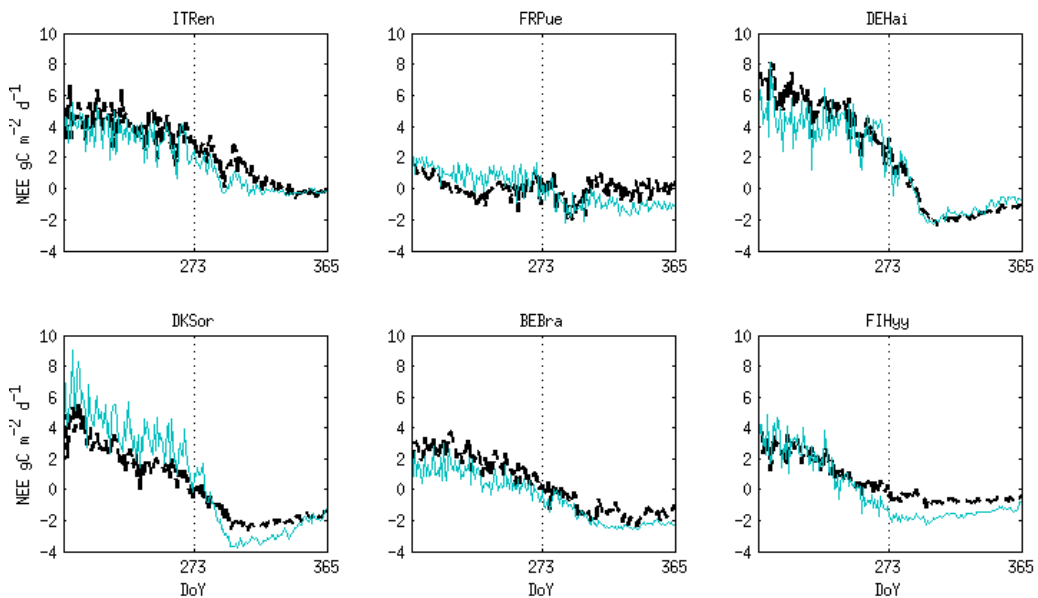


Fig. 5.38. NEE ($\text{gC m}^{-2} \text{ d}^{-1}$) trends for summer and fall. Azure line represent simulated GPP, black line the EC data.

Thus discrepancies in DKSor NEE patterns appeared mainly the consequence of summer low Reco and slightly hasten leaf senescence. High Reco and low GPP determined the average underestimation of

about $1 \text{ gC m}^{-2} \text{ d}^{-1}$ in FIHyy. NEE daily trends showed high goodness of fit [0.76; 0.93], correlation coefficient [0.91; 0.98] and Model Efficiency coefficient [0.63; 0.87] in 5 ecosystems over 6 (Fig. 5.39).

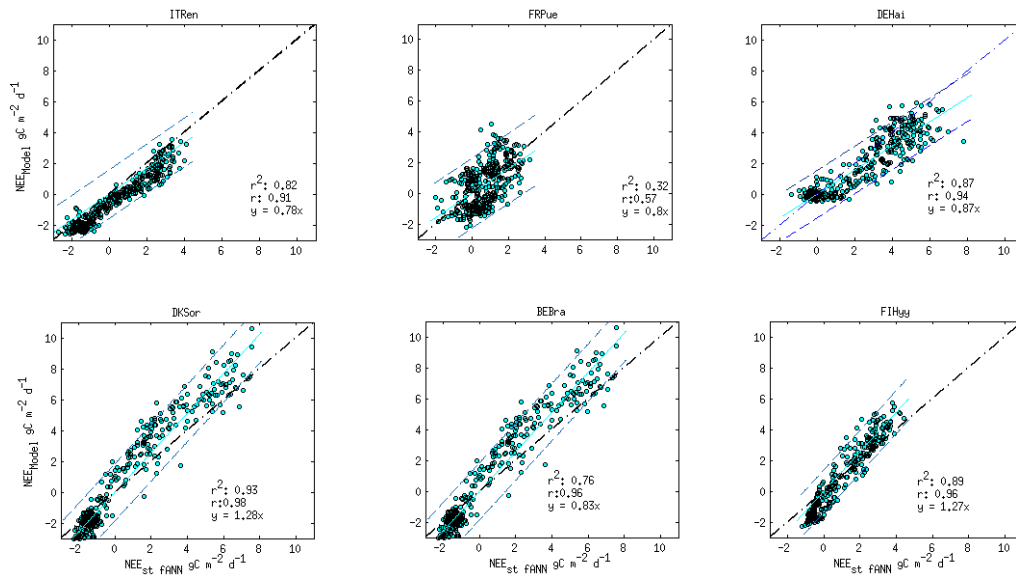


Fig. 5.39. Daily trends of simulated NEE plotted against EC data for the six sites. The black dotted lines represent the 1:1 ratio (perfect fit), azure lines the actual mono parametric regression lines. The slopes of these lines represent the average over/underestimation. Azure dotted lines are the 95% expected bonds. The r is the Pearson's correlation statistic.

FRPue was the only exception, since the model resulted both scarcely efficient ($\text{NSE} < 0$) and in low goodness of fit (r^2 0.32); however the results showed very significant correlation with EC data (r of 0.57, $p < 0.0001$) (Tab. 5.14).

Tab. 5.14 Statistics of the average daily observed-simulated NEE ($\text{gC m}^{-2} \text{d}^{-1}$). The table reports for each site: the regression goodness of fit estimator (r^2), the Pearson's correlation estimator; the RMSE ($\text{gC m}^{-2} \text{d}^{-1}$); the Nash Sutcliffe model efficiency estimator; the slope of the mono parametric linear regression; the range of the parameter using a Levenberg-Marquardt algorithm.

Site	Var	r^2	r	RMSE	NSE	a	a-range
ITRen	NEE - Trends	0.83	0.91	1.52	0.51	0.72	(0.70, 0.74)
FRPue	NEE - Trends	0.35	0.57	1.04	-0.36	0.5	(0.65, 0.83)
DEHain	NEE - Trends	0.87	0.94	1.04	0.87	0.89	(0.84 – 0.93)
DKSor	NEE - Trends	0.93	0.98	0.94	0.70	1.24	(1.21, 1.27)
BEBra	NEE - Trends	0.76	0.96	0.80	0.70	0.85	(0.80, 0.93)
FIHyy	NEE - Trends	0.89	0.96	0.71	0.76	1.28	(1.24, 1.30)

The RMSEs were similar to those observed for both GPP and Reco. Otherwise fluctuations among the 1:1 line were significantly higher, ranging from about -22% to +28%.

5.3.2 Validation of 3D-CMCC-Pheno NEE results on daily and monthly temporal resolution

Fig. 5.40 Shows daily correlation between Model outputs and the NEE fluxes measured by the EC towers ($\text{gC m}^{-2} \text{d}^{-1}$).

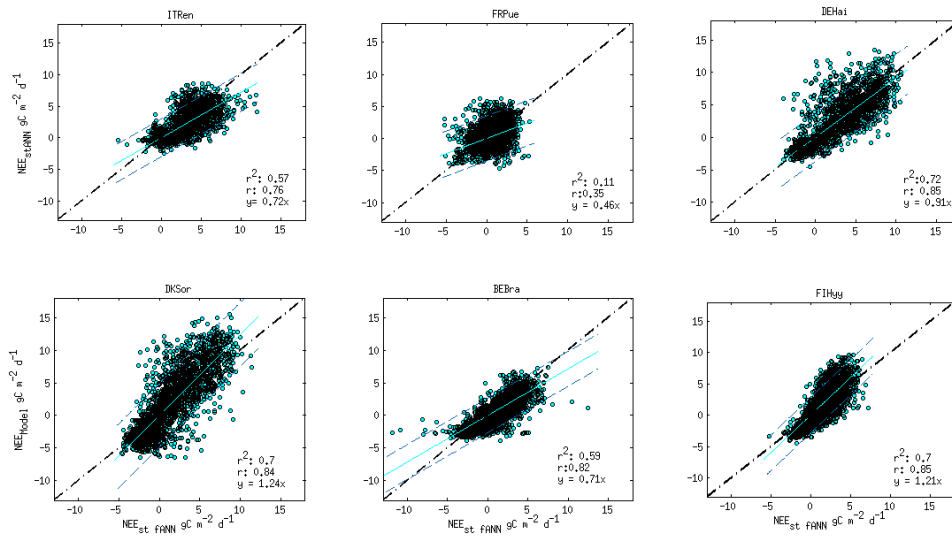


Fig. 5.40. Daily simulated NEE plotted against daily EC data for the six sites. Days for which no EC data were available were discarded. Otherwise days with simulated NEE = 0 were taken into account. The black dotted lines represent the 1:1 ratio (perfect fit), azure lines the actual mono parametric regression lines. The slope of these lines represent the average over/underestimation. Azure dotted lines are the 95% expected bonds. The r is the Pearson's correlation statistic.

The regression had a strong correlation ($p < 0.0001$ and r [0.75; 0.85]) in every case except FRPue, for which it was still strong ($p < 0.0001$) but had a very low r (0.35). The five sites showed good agreement for each set of values, with an r^2 ranging from 0.57 to 0.72 (Tab X.13).

Tab. 5.14 Statistics of the daily observed-simulated NEE ($\text{gC m}^{-2} \text{d}^{-1}$). The table reports for each site: the regression goodness of fit estimator (r^2), the Pearson's correlation estimator; the RMSE ($\text{gC m}^{-2} \text{d}^{-1}$); the Nash Sutcliffe model efficiency estimator; the slope of the mono parametric linear regression; the range of the parameter using a Levenberg-Marquardt algorithm.

Site	Var	r^2	r	SSE	RMSE	NSE	a	a-range
ITRen	NEE - Daily	0.57	0.76	5053.99	1.53	0.51	0.72	(0.70, 0.74)
FRPue	NEE - Daily	0.11	0.35	8956	1.75	- 0.71	0.48	(0.42, 0.50)
DEHain	NEE - Daily	0.72	0.85	10318.66	1.89	0.88	0.89	(0.84, 0.90)
DKSor	NEE - Daily	0.71	0.84	20422.09	2.45	0.32	1.24	(1.14, 1.33)
BEBra	NEE - Daily	0.59	0.82	5803.09	1.35	0.56	0.85	(0.77, 0.94)
FIHyy	NEE - Daily	0.70	0.85	8228.98	1.44	0.28	1.21	(1.15, 1.32)

Mediocre agreement resulted by fitting the $\text{NEE}_{3\text{D-CMCC}}$ with NEE_{EC} through the regression model “ $y = a x$ ”. This inconsistency was mainly determined by excesses in AR during fall and winter which caused systematic mismatches with expected NEE (Fig. 5.41).

The consequence was the negative value of the NSE (-0.7). NSE for the other sites was always positive, and ranged from 0.28 to 0.88. The low values at FIHyy (0.28) and DKSor (0.32) were respectively the consequence of the high GPP variance and the systematic underestimation of Reco during summer.

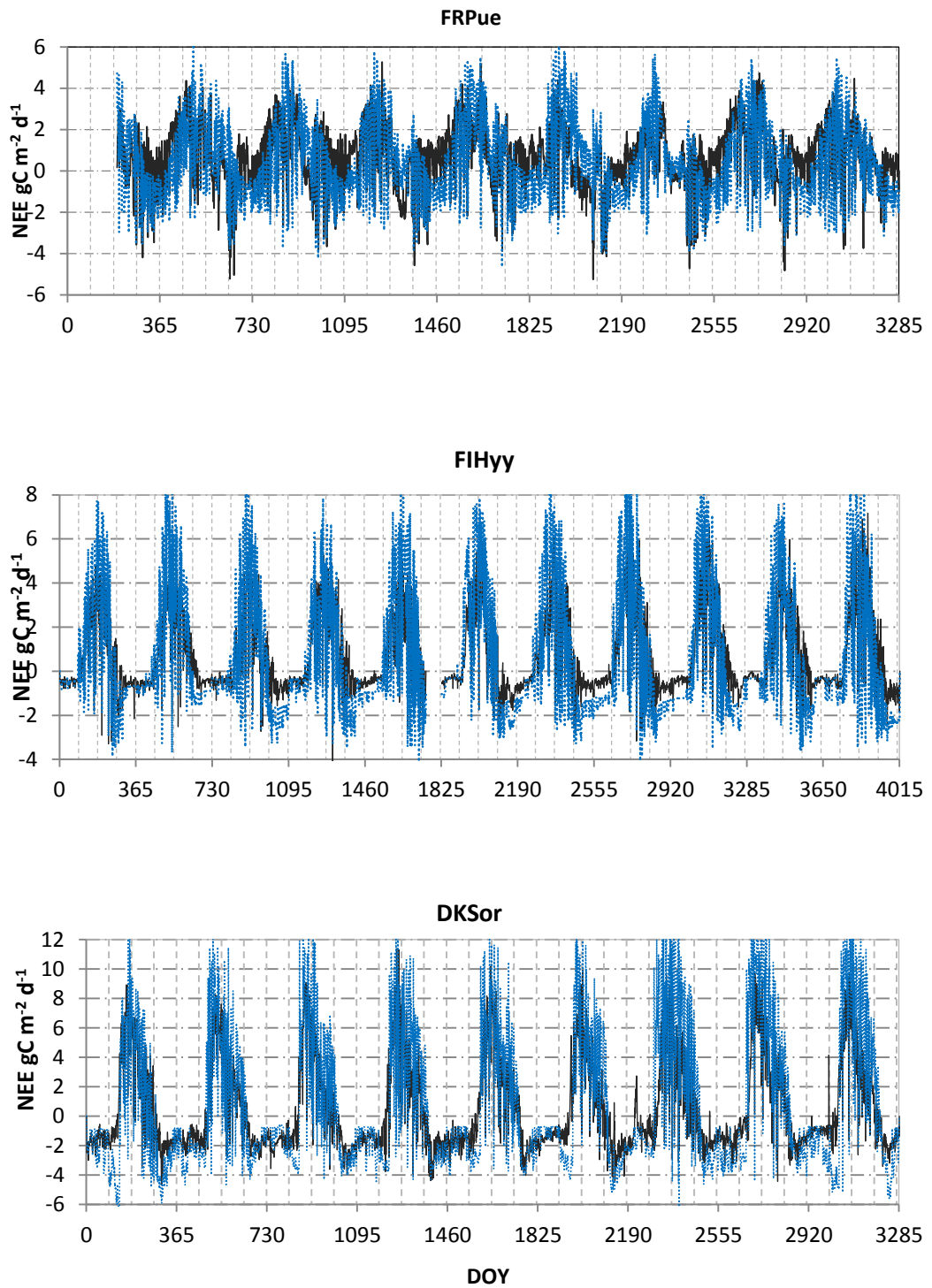


Fig. 5.41. Simulated (blue) and measured (black) NEE ($\text{gC m}^{-2} \text{d}^{-1}$) for each day of simulation (FRPue, FIHyy and DKSor study cases). XXX

RMSE ranged from 1.35 to 2.45 $\text{gC m}^{-2} \text{d}^{-1}$, with higher values associated to broadleaves and especially deciduous forests. On average the modeled daily GPP fluctuated among 28% of underestimation (ITRen) and 23% of overestimation, as inferred by the values of the “a” parameter.

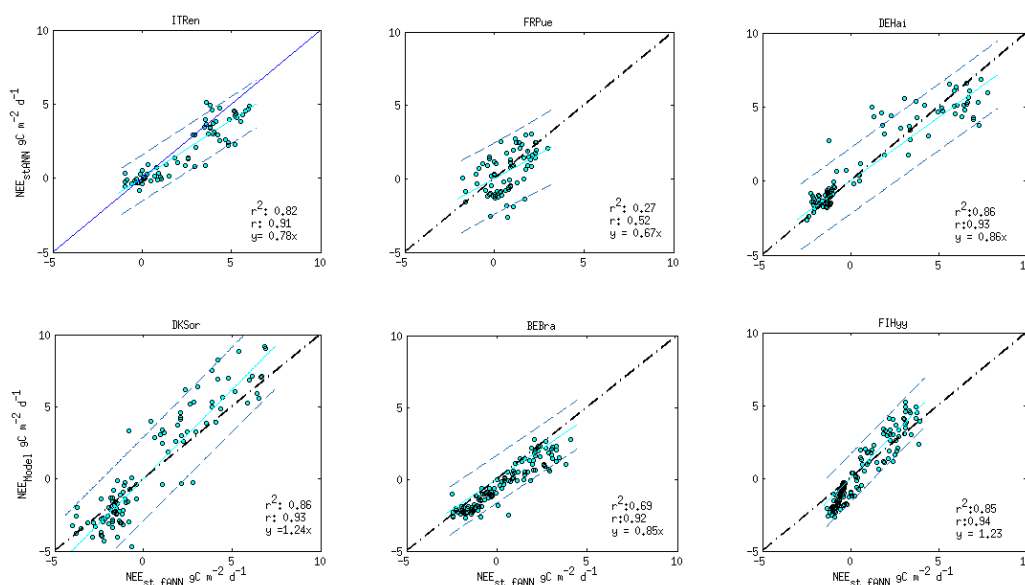


Fig. 5.42. Monthly simulated NEE plotted against monthly EC data for the six sites. The black dotted lines represent the 1:1 ratio (perfect fit), azure lines the actual mono parametric regression line. The slopes of these lines represent the average over/underestimation. Azure dotted lines are the 95% expected bonds. The r is the Pearson's correlation statistic.

The model showed significant improvement in the results reducing the temporal resolution to the monthly scale (Fig. 5.42). Excluding the bad exception of FRPue (r 0.52, r^2 0.25, NSE - 0.36), r values were always greater than 0.9. Goodness of fitness too was good, with r^2 greater than 0.83 except for BEBra, which anyway had a value of 0.69. RMSE values

were reduced of about a half relative to daily results. The variance of the fitting parameter “a” was reduced of about 9% ranging from -22 to 23% (Tab. 5.15).

Tab. 5.15 Statistics of the monthly observed-simulated NEE ($\text{gC m}^{-2} \text{d}^{-1}$). The table reports for each site: the regression goodness of fit estimator (r^2), the Pearson’s correlation estimator; the RMSE ($\text{gC m}^{-2} \text{d}^{-1}$); the Nash Sutcliffe model efficiency estimator; the slope of the mono parametric linear regression; the range of the parameter using a Levenberg-Marquardt algorithm.

Site	Var	r^2	r	RMSE	NSE	a	a-range
ITRen	NEE - Monthly	0.83	0.91	0.78	0.76	0.78	(0.72, 0.84)
FRPue	NEE - Monthly	0.25	0.51	1.21	-0.60	0.60	(0.98, 1.01)
DEHain	NEE - Monthly	0.86	0.93	1.12	0.93	0.87	(0.84, 0.90)
DKSor	NEE - Monthly	0.86	0.93	1.46	0.81	1.23	(1.15, 1.30)
BEBra	NEE - Monthly	0.69	0.92	0.84	0.86	1.07	(1.02, 1.10)
FIHy	NEE - Monthly	0.85	0.94	0.84	0.68	1.23	(1.18, 1.25)

5.3.3 3D-CMCC-Pheno FEM Performance for inter monthly, seasonal and annual variability of NEE

The magnitudes of modeled IAVs and IMVs in NEE flux were on average of the same order of the observed ones. Fig. 5.44 shows NEE annual anomalies for the six sites, Tab.5.16 their relative NRMSE. The model resulted to be able to capture about 64% of the anomalies for the total set of 52 years.

Tab. 5.16. Statistics of the NEE anomalies (IMVs, ISVs and IAVs). IMVs results of the statistic tests of normality (χ^2 GOF) and equivalency of the central tendency (CET). 0 values imply H0 acceptance, that is respectively that “the distribution of the IMVs is normal” and/or “the expected and observed distributions are statistically equal”. The CET t-test was performed for normally distributed IMVs, Mann–Whitney U if not. The CET H0 was automatically rejected if expected and observed IMVs had different χ^2 GOF outcome.

		ITRen	FRPue	DEHai	DKSor	BEBra	FIHy
NRMSE	Annual	1.13	0.34	1.22	1.82	0.74	0.95
NRMSE	Seasonal	0.96	0.93	1.48	1.8	0.99	1.23
NRMSE	Monthly	0.99	1.09	1.26	1.84	0.97	1.23
χ^2 GOF	Monthly	0	0	1	-	-	-
CET	Monthly	0	0	0	1	1	1

Despite of the results previously pointed out, the model remarkably reproduced IAVs in both FRPue (8/9) and DKSor (9/9). By contrast DEHai and FIHy inter annual anomalies were scarcely represented (respectively 29% and 27%).

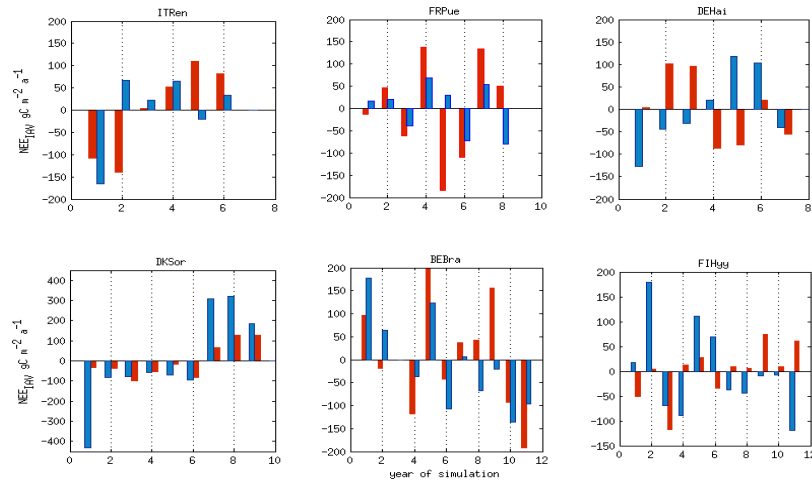


Fig. 5.44. Inter annual NEE variability for the 6 simulations ($\text{gC m}^{-2} \text{d}^{-1}$). Red bars represent EC based anomalies; blue ones the 3D-CMCC-FEM anomalies

NRMSEs evidenced that the highest errors were associated to DKSor, DEHai and FIHyy, mainly due to IMVs during spring (Tab. 5.17). NEE Anomalies variability was always higher in NEE than Reco, but lower than GPP ISVs and IMVs in the Mediterranean forest.

Tab. 5.17. Difference between NEE and GPP NRMSE (above dotted line) and between Reco and NEE (below dotted line). Positive values mean that NEE NRMSE is lower than the one it is compared to.

		ITRen	FRPue	DEHai	DKSor	BEBra	FIHyy
Δ NREMSE	IAVs	0.04	-0.28	-0.33	-0.16	-0.15	-0.93
Δ NREMSE	ISVs	-0.12	0.01	0.08	-0.08	0	-0.45
Δ NREMSE	IMVs	-0.05	0.05	-0.17	-0.43	-0.14	-0.38
Δ NREMSE	IAVs	0.03	-0.34	-0.96	-0.54	-0.13	-0.89
Δ NREMSE	ISVs	-0.12	-0.12	-0.61	-0.65	-0.21	-0.39
Δ NREMSE	IMVs	0.05	-0.17	-0.42	-0.9	-0.22	-0.45

The model often reproduced IMVs very similar in magnitude and density functions to the observed ones. DKSor and FIHyy PFEs showed wider distributions than expected, but similar skewness. ITRen on the contrary showed narrower distribution (Fig 5.45).

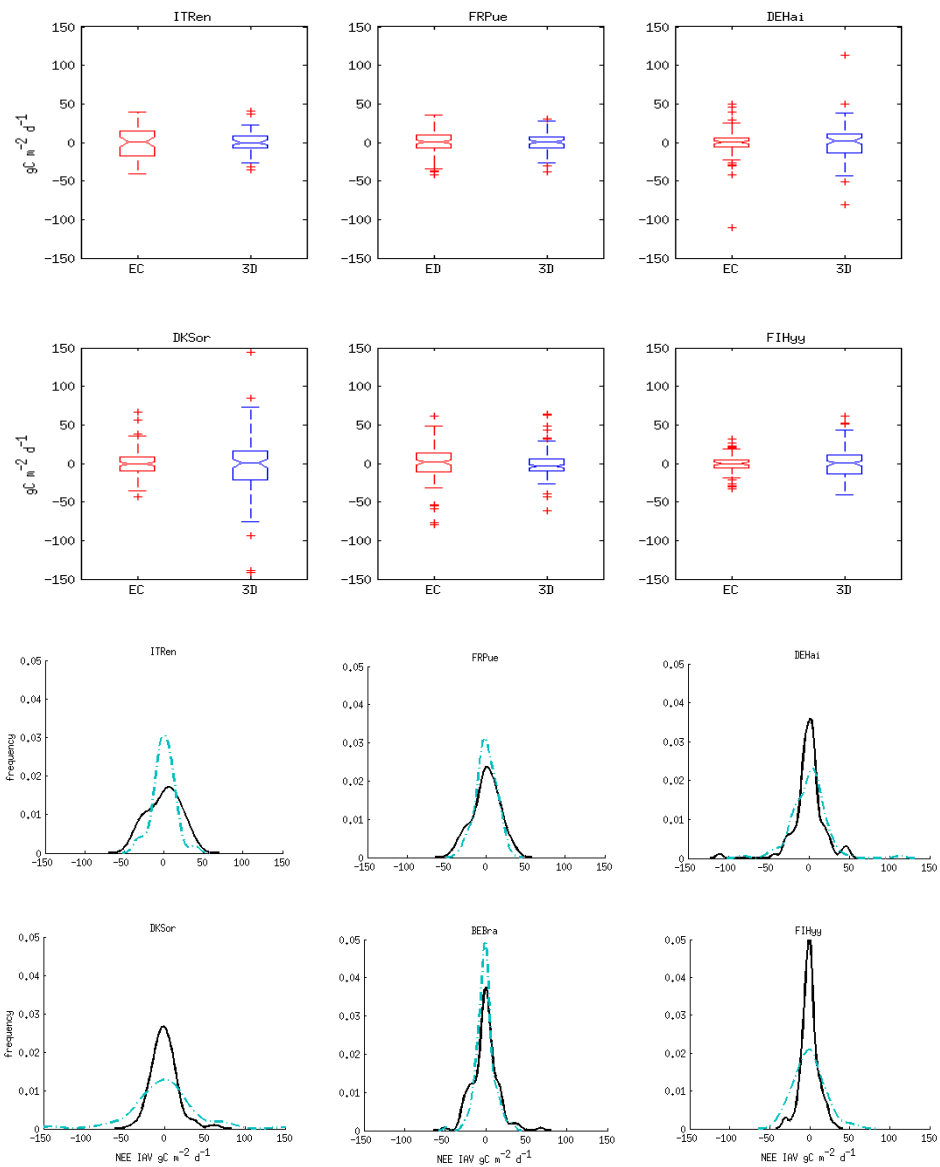


Fig. 5.45. IMVs of measured and simulated NEE for the 6 simulations. Boxplots in (a) (Red EC data, Blue 3D-CMCC simulations) represent median, upper-lower interquartile, lower and upper bounds. Red crosses represent IMVs extreme values. Graphs in (b) represent the distribution of the frequencies of GPP IMVs resulted from a kde estimation; yellow dotted lines represent simulated data, black lines EC data.

In general the model resulted to be able to capture about 64% of the biases for the months observed (384 over 600 months). Again evergreen forests showed better VRs and lower NRMSE, with the exception of

FIHyy spruce forest. The analysis of the VRs resulted in significant persistent positive biases in February and June at FRPue (Fig. 5.46).

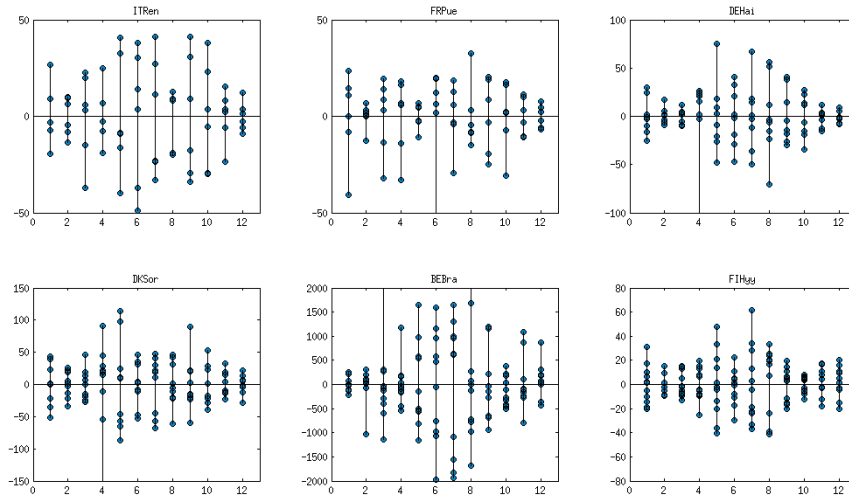


Fig. 5.46. Residuals (predicted-observed) of NEE monthly variability. Positive values indicate higher variability in the observations than in the model. When more than 90% of a specific month residuals were positive/negative systematic errors were detected.

The model showed its limits in simulating summer IMVs, especially in forests dominated or co-dominated by scots pines. As a matter of fact the model didn't perform well for the two forests of BEBra and FIHyy (about 18% of summer ISVs captured), while captured about 68% of the summer ISVs in the others (Fig. 5.47).

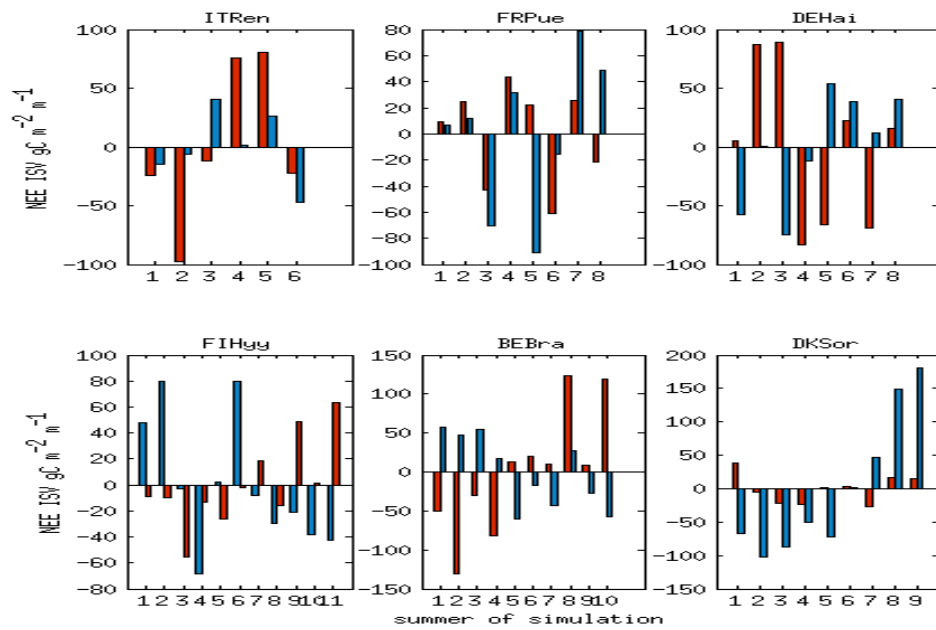


Fig. 5.47. Inter seasonal NEE variability for the 6 simulations during summer ($\text{gC m}^{-2} \text{d}^{-1}$). Red bars represent EC based anomalies; blue ones the 3D-CMCC-FEM anomalies.

The new Phenology routine gave excellent results for both spring (Fig 5.48) and autumn ISVs (Fig 5.49); the model captured about 69% of the anomalies during spring, and 79% during fall.

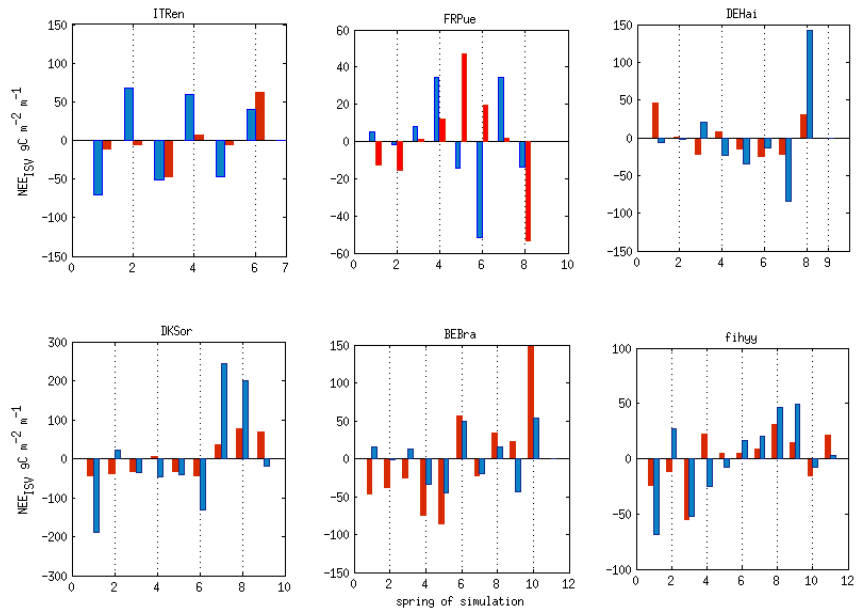


Fig. 5.48. Inter seasonal NEE variability for the 6 simulations during spring ($\text{gC m}^{-2} \text{d}^{-1}$). Red bars represent EC based anomalies; blue ones the 3D-CMCC-FEM anomalies.

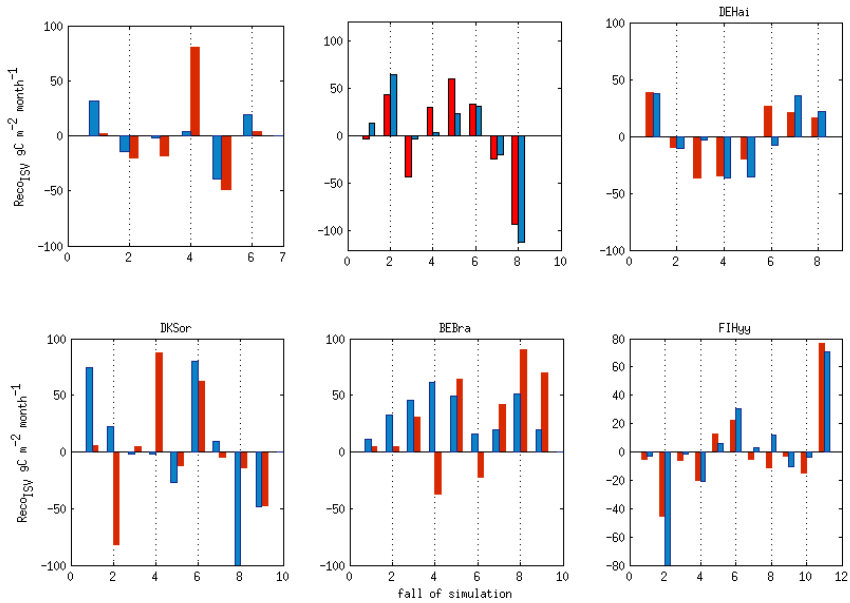


Fig. 5.49. Inter seasonal NEE variability for the 6 simulations during fall ($\text{gC m}^{-2} \text{d}^{-1}$). Red bars represent EC based anomalies; blue ones the 3D-CMCC-FEM anomalies.

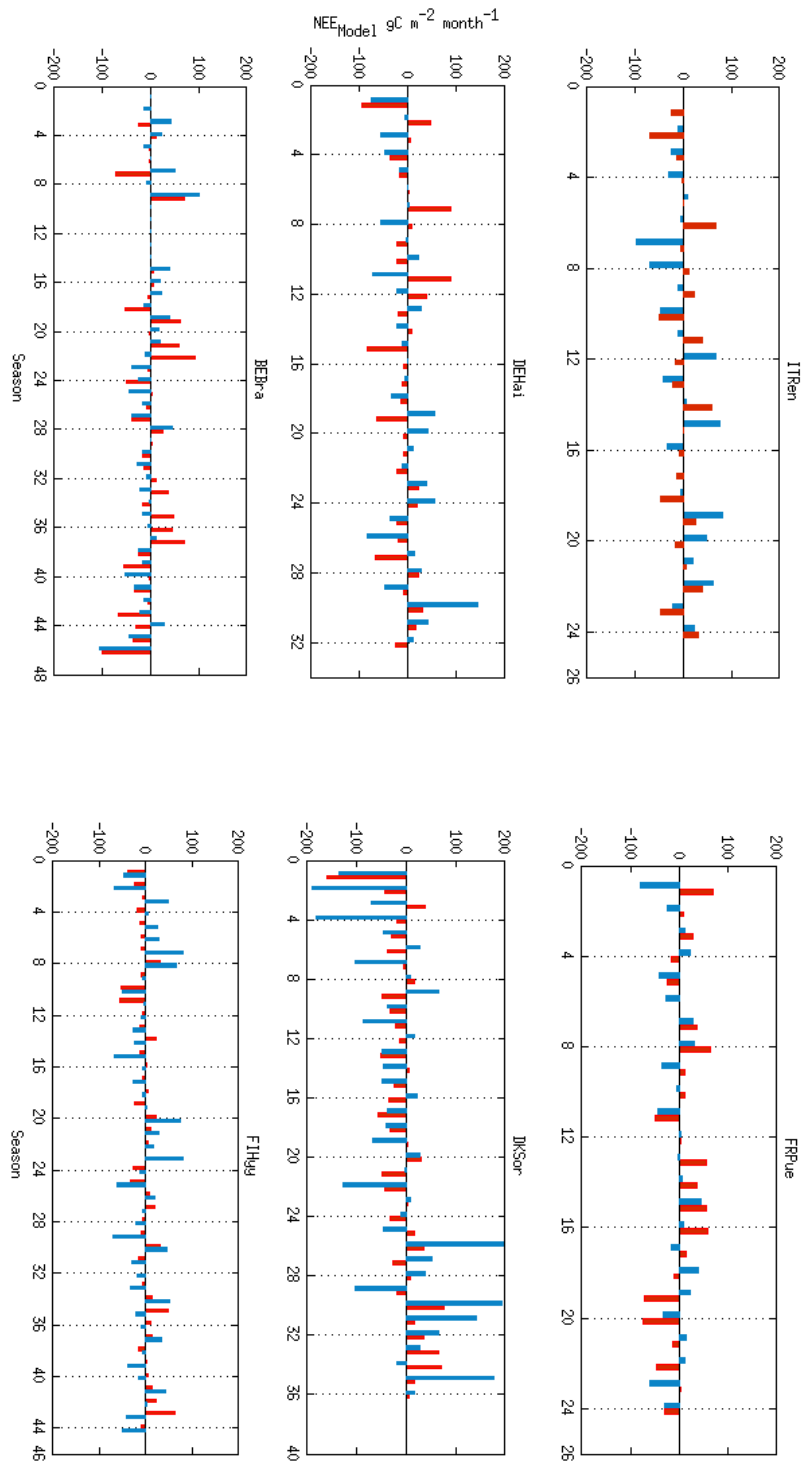


Fig. 5.50. Inter seasonal NEE variability for the 6 simulations ($\text{gC m}^{-2} \text{d}^{-1}$). Red bars represent EC based anomalies; blue ones the 3D-CMCC-FEM anomalies.

5.4. Soil Carbon dynamics

Fig. 5.51 shows the model's SOC dynamics among the three major soil C pools. The structure of the model allowed separating the two different soils beyond the two different stands in BEBra. The total SOC showed no significant difference between the first and the last year of simulation for any soil reproduced (Tab. 5.18). Initial SOC values were taken from literature or the CarboEurope sites' ancillary data. Unfortunately we lacked the data to validate C dynamics in the three C pools for the six sites.

Tab. 5.18. Soil Organic Carbon (SOC) general statistics (KgC m⁻²). Average, standard deviation SOC at the beginning and at the end of the simulation are represented. As expected no statistical significant difference was found between SOC₀ and SOC_{eos} (t-test p value always lower than 0.00001).

	ITRen	FRPue	DEHai	DKSor	BEBra - P	BEBra- Q	FIHyy
\overline{SOC}	2.04	4.44	3.8	9.09	15.66	7.53	5.21
σ	± 0.04	± 0.03	± 0.16	± 0.19	± 0.18	± 0.33	± 0.07
SOC ₀	2.01	4.46	3.65	9.62	16.15	6.93	5.37
SOC _{eos}	2.05	4.41	4.11	9.26	15.44	8.14	5.13
t-test p	<0.0001	<0.0001	<0.0001	<0.0001	<0.0001	<0.0001	<0.0001

The model has been initialized by having an amount of Microbial Biomass (B) of about 5% of the total Organic Carbon. At the end of the simulation Microbial biomass was about 6.33% of the total SOC, with

higher values for broadleaf forests (Tab.5.18). The model showed high values of Microbial Quotient (qMic) at the equilibrium. Evergreen forests showed lower qMic, as expected (Tab. 5.19). Significant increase of qMic occurred in the deciduous beech forests. qMic resulted significantly decreasing under the pine stand in Brasschat; that was mainly caused by the unbalanced high quantity of peat Humads laid by locals during the last centuries (Chiti et al., 2009).

Tab. 5.19. Fraction of Microbial Biomass over Total Organic Carbon (qMic). Average, standard deviation qMic at the beginning and at the end of the simulation are represented. Significant difference between qMic₀ and qMic_{eos} was found in any case.

	ITRen	FRPue	DEHai	DKSor	BEBra - P	BEBra - Q	FIHy
$\bar{B}_{\%}$	9.0%	2.5%	10.0%	7.7%	1.3%	8.8%	6.3%
$\sigma_{\%}$	1.7%	0.2%	3.0%	1.3%	0.4%	2.5%	0.3%
B%0	5.5%	2.0%	5.0%	5.0%	2.0%	5.0%	5.2%
B%eos	11.8%	2.1%	14.9%	10.0%	0.7%	12.1%	6.3%

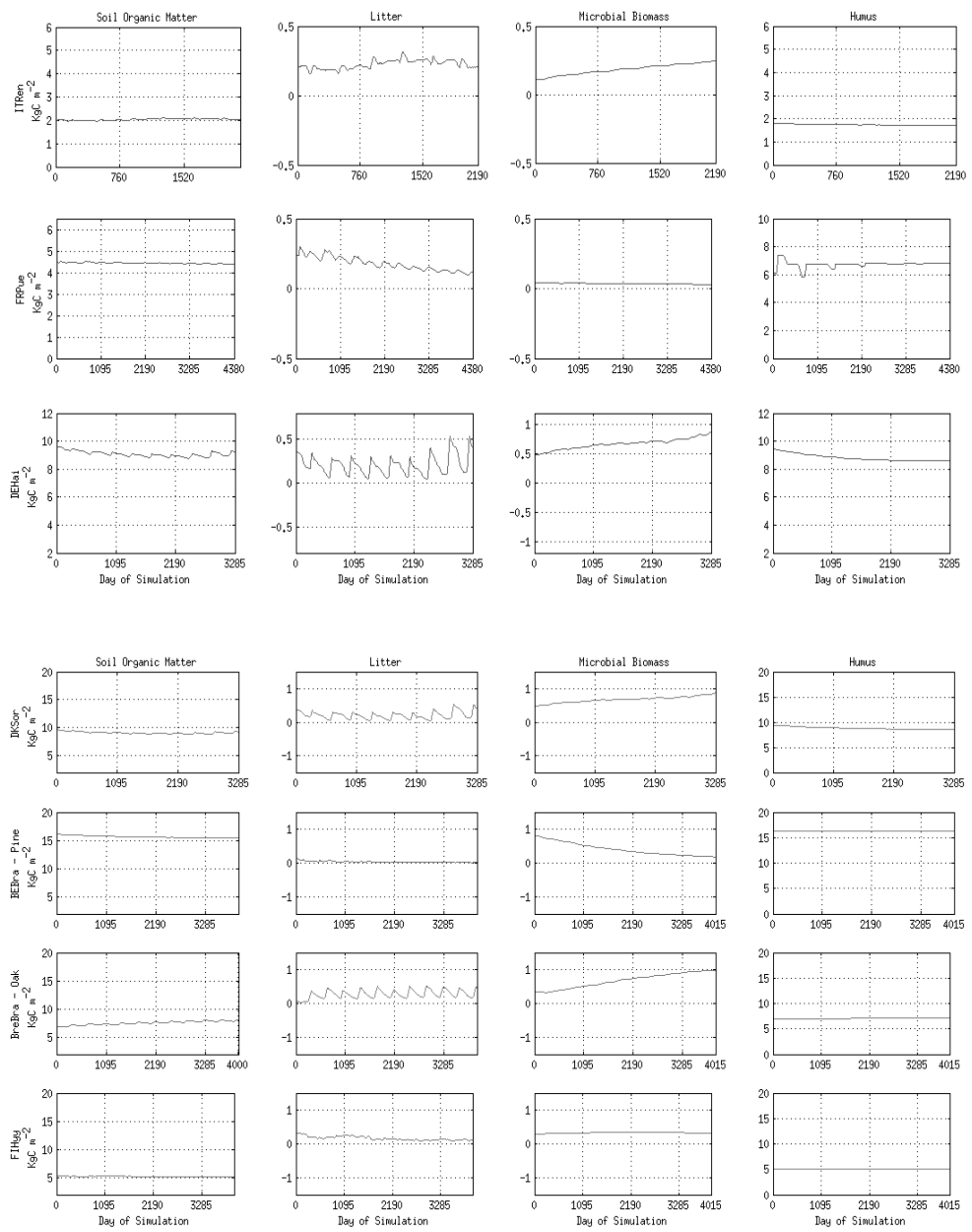


Fig. 5.51. Soil Organic matter (kgC m^{-2}). The first column represents TOC, the second residual OC, the third Microbial biomass, the fourth Humus C. Since they have a different story, the two soils of BEBra were considered separately.

CHAPTER 6: DISCUSSION

This work showed how the 6.1 version of 3D-CMCC-FEM was successfully parameterized and tested against field measurements of ecosystem performance, yielding a terrestrial ecosystem hybrid model able to reasonably predict regional scale variation in patterns of NEE, GPP and Reco. The new equations often resulted in significant improvements in representing C fluxes and/or their variability.

6.1. Phenology in the 6.1.v 3D-CMCC-FEM:

The ideas brought by the 6.1 version of 3D-CMCC overall appeared to grant good results in simulating C fluxes between the forest Ecosystem and the atmosphere.

The model validation against EC data gave encouraging results for both GPP and Reco; this work highlighted how simple improvements in Phenology may lead to significant improvement in the predictability of forest ecosystem gas exchange. In our opinion leaf phenology, turnover and ecology may considerably affect PBMs reliability. Differences in results could be especially noticed in inter temporal variability analysis. The integration of the evergreen turnover routine used in CLM (Oleson et al., 2010) and BIOME family models (Haxeltine and Prentice, 1996; Running and Hunt, 1993; Thornton, 2010) resulted in model's scarce plasticity and in low C:N FOM supply to the soil.

Similarly the use of the satellite data to represent deciduous leaf phenology (Zhang et al., 2003) could lead to excessive variations of LAI during summer, as inferred by the discrepancy between MODIS and

field based data. Moreover this method is data driven and could be ineffective under a prognostic viewpoint. For this reason we think that further attention should be invested in studying tree phenology and leaf/fineroot ecology. In the next future we aim to investigate on our suspects involving the relationship between the starting date of LAI reduction and vapor pressure at saturation peak, as a first step toward the development of an explicit deterministic model of leaf turnover.

Anyhow strong uncertainties still reside in the current phenology framework. Summer GPP ISVs scarce representation in deciduous forests was probably an effect of the use of the peak LAI throughout the season. The new framework already expects a reduction in summer LAI as a consequence of cavitation and loss of turgor, but still field information about the magnitude of the loss are missing and no validation has been possible. The use of the night length as a driver of senescence is justified by molecular ecology findings (Woo et al., 2010). However the use of a single parameter as threshold value is over simplistic, especially for regional studies, and could lead to bad tuning habits. The process of senescence is highly regulated and dependent upon concurrent increases in both synthesis and activity of some proteins as well as degradation or inactivation of others (Zwack and Rashotte, 2013). Thus in our opinion the yellowing and senescence function may somehow take into account the genotypic plasticity and temperature effects on the cytokinins transport (endogenous negative regulators of senescence) and positive regulators synthesis. Another source of uncertainty of our fall phenology equation resides in determining the length of the senescence period. We used the same method of Delpierre et al. (2009) which however not always returned

consistent results; it happened sometimes that the BIOME fractional approach (Running et al., 2006) gave better results.

As to spring phenology, the use of the GDD approach to determine the beginning of the vegetative period often returned inaccurate estimates of the bud burst. Even though several works proposed that one phase models (i.e. GDD) have higher probability to be correct than two phases ones (which consider both chilling and forcing temperatures) (Fu et al., 2012), the method may be imprecise for regional studies (Schaber & Badeck 2003). The problem in expliciting bud burst resides in the partially unknown processes triggering its timing (Linkosalo, 2008). Schaber & Badeck proposed a promoter-inhibitor rationale to simulate bud burst timing in France. Even though it appeared to be elastically able to reproduce climatic and phenological heterogeneity, it resulted over parameterized to an independent estimation of model parameters (Linkosalo, 2008).

The new evergreen leaf turnover rationale improved significantly the model's ability to represent temporal shifts and variability. Moreover it created the basis to further development of differential photosynthetic ability and respiration for leaves of different age. However the module still does not take into account any discrimination between species with or without secondary or even continuous growth. Thus species like *Quercus ilex* which exhibit secondary gem sprout in fall reported trends of reduced photosynthetic activity in fall and winter, especially in the Mediterranean ecosystem where winter temperatures are compatible with photosynthesis.

6.2. GPP in the 6.1.v 3D-CMCC-FEM:

The Carbon injection function allowed a better representation of the early spring C dynamics and solved several problems involving the Carbon Reserve pool of the 5.1 version. The old version in fact requested huge amounts of C for growth respiration (from 10 to 80 gC m⁻² d⁻¹) which had to be taken from Biomass Reserve; those unrealistic amounts could lead to the emptying of the Reserve pool and thus in anomalous low LAI and GPP year balance, activating an escalation which could determine unjustified stand collapse. With the introduction of this function the problem was mostly solved as inferred by spring results. Speaking of needle leaves species we suspect that gaps in early spring GPP may be related to the absence of other species understory in ITRen; as a matter of fact introducing the 17% of *Pinus cembra* cover, and treating it as a *Pinus sylvestris*, solved the reported underestimations in GPP and NEE, but implied a slight overestimation in spring Reco (unpublished data). Otherwise the significant overestimation in FIHy spring GPP may be attributable to the 3D-CMCC-FEM characteristics, since this problem appeared in both 5.1 and 6.1 versions. We think that it may be related to the absence of any limitation due to snow covering the needles, or to the inadequacy of 3PG limiting factors for daily temporal resolution in more stressing environments.

The model showed its weakness in representing the Mediterranean ecosystem. GPP was generally higher than expected in both spring and summer, lower in winter and fall. Our suspects in this context rely on the soil water budget over simplicity but also on the quality of the

initialization data. Published data describe the holm oak forest of FRPue as an overcrowded forest of 6150 trees with just 6cm average DBH and height of 7m. If that may be realistic in a coppice stand, it sounds strange for the 60 years old one, which in addition was converted to a timber forest. Moreover *Quercus ilex* is known to be strongly shade tolerant, and thus competition for light should be taken into account. Lack of initialization data however impeded to do that in the 3D-CMCC-FEM traditional way. In this context the development of a statistical way to upscale average biometric data using dendrometric models would be useful. As a matter of fact we could use them jointly with the PPA to initialize the canopy vertical structure at the beginning of each year as a function of both species and management and simulate light competition even for scarcely investigated sites.

That said another strong source of uncertainty in summer GPP may be held by the over simplicity of soil structure and thus of the soil water routine. For the very same reason we are already working on a multilayer approach to describe the physical chemical variability within soil profiles along with a deterministic soil water routine (Zhang et al. 2002). We also believe that the GPP soil water modifier should take into account soil-plant difference of water potential rather than merely soil water content.

The GPP variability improved significantly with the 6.1.v. Even though we couldn't verify if the model's standard error was placed within measured uncertainty variability, distributions of the anomalies were averagely consistent with EC data in both central tendency and variance. Discrepancies in IMVs variance were reduced but still too high for deciduous species; their worst representation occurred in summer,

suggesting that the use of a constant cover may be too simplistic. The NRMSE was averagely lower than in 5.1. and always lower than $1.3 \text{ gC m}^{-2} \text{ d}^{-1}$. These results were in line or even slightly better than those of other models in literature (Keenan et al., 2012; Kramer et al. 2002; Nolè et al. 2009; Keenan et al. 2007; Anav et al. 2010); however to test the statistical validity of this assumption further comparison analyses should be done.

6.3. Respiration in the 6.1.v 3D-CMCC-FEM

It was not always possible to individually validate the different components of respiration. However the results of Reco comparison with EC data, the reliable results of HR at ITRen and the NPP:GPP consistency with literature, showed that the new 3D-CMCC-FEM version was able to reproduce respiration processes quite well, especially on monthly timescale. Overall results were still inferior to the GPP ones, with the exception of the Mediterranean Ecosystem, where the new φ modifier determined impressive improvement in representing AR.

Anyway these results were expected. As a matter of fact higher uncertainties reside in modeling respiration processes. While GPP was directly calculated, the total ecosystem respiration was computed as the sum of independent processes, each one of which had its uncertainties. Thus the total Reco error resulted as the product of the singular cascade errors mining the goodness of fit and correlation with data.

Moreover parts of these errors reside in the simplistic depiction of the soil chemical physical structure; if it granted strong usability because of the very low quantity of parameters and initialization data, it apparently still was over simplistic.

The results also evidenced that the AR routine may strongly be influenced by uncertainties in MR estimation, which often resulted in AR overestimation. The MR is in fact simulated by a set of empirical relations which involve the use of the Q10 factor, whose usability is actually debated (Menge, personal communication). Moreover the rationale of Ryan's MR calculation (1995) requires that the specific tissue variation in N content may be correctly simulated; on the contrary PBMs as like as 3D-CMCC-FEM do it implicitly by using fixed C:N ratios. In a recent work, Thornley (2011) questioned the physical nature of the MR factor in the McCree's respiration model providing a new framework and interpretation, suggesting that MR as a specific process is not required and may be replaced with different approaches.

For all these reasons further investigation in tree respiration compartments may be further invested to better understand and explicitly model autotrophic respiration.

Reco variability was better represented than GPP's. Differences in variance or central tendency were never significant, the NRMSE was lower and the sign of the anomalies was captured 2 months on 3. The Reco having a smaller anomalies pattern seemed to confirm Kennan's assumption that models' inability to match the timing of observed variability in GPP is the main cause of errors in the simulation of interannual variability in NEE (2012).

6.4. NEE in the 6.1.v 3D-CMCC-FEM

The 6.1. version of 3D-CMCC-FEM is finally able to estimate net C fluxes between the forest ecosystem and the atmosphere which are particularly interesting because the ones actually measured by the EC towers. Even though summer fluxes may be averagely over or underestimated up to 25%, the model showed very good predictability. Clearly the uncertainties described above reduced the model's reliability. GPP anomalies especially determined the scarcity of the model in representing C fluxes at FRPue, whose simulation denoted how important is to discover the deterministic relations between Mediterranean forests and the environmental limiting factors. As a matter of fact the Mediterranean Biome strongly selects stress resistant species which however may compete in “relatively-limiting” conditions for about three quarters a year. Thus the canopy is dominated by evergreen species able to photosynthesize quite well during winter and to rapidly adapt to environmental stresses.

Even though the model captured about 2/3 of the anomalies signs, the NRMSE was always quite low (less than $2\text{gC m}^{-2} \text{d}^{-1}$) NEE variability was strongly affected by the GPP and Reco uncertainties and their distribution was poorly reproduced. Half of the sites showed significant difference in the anomalies frequency distribution. This was particularly true in the ecosystems where deciduous species were dominant or co-dominant; there GPP anomalies variance determined NEE IMVs twice as measured ones, especially in spring and summer. This again seems to

confirm that constancy in Summer LAI and the use of gross implicit environmental limiters may be sufficient in representing C fluxes (especially producing monthly outputs from daily simulations), but still not nearly perfect for deducing long term NEE patterns

Comparing model outputs with published works (Kramer et al. 2002; Nolè et al. 2009; Keenan et al. 2007) these defects were shared even with acclaimed PBMs, which in some cases resulted even more inert in representing NEE anomalies and fluxes. As a conclusion the 3D-CMCC-FEM 6.1.v validation remarked its flexibility and very good but not nearly perfect ability in predicting present and future long term NEE patterns for each northern hemisphere forest type. However, if it represents a good point, our ideas on how to reduce the model's sources of uncertainties aspire to make it just an always perfectible starting point.

6.5. SOC dynamics in the 6.1.v 3D-CMCC-FEM

Lack of data to validate the SOC dynamics reduced the spectrum of speculations which could be statistically analyzed. SOC didn't change its quantity in ten years; this result was consistent with the theoretical stability of the SOC, an indicator which rarely change within 10 years if no strong disturbance event (e.g. land use change) have occurred. Litter C was highly fluctuating within a year, but its quantity was stable if compared at the end of each year. This suggested that the model realistically represented litter turnover and decomposition, since residues

are degraded into humus labile substances about within a year (Dickinson et al., 2012.).

Microbial Biomass was highly variable as expected. As a matter of fact qMic (along with SR) is one of the most informative indicators of short term alterations in soil health and quality (Moscatelli, personal communication). However qMic changed too highly throughout the simulations. These results may suggest that (a) using a 5% qMic as default qMic quantity at the beginning of simulation may insufficiently represent different forest soil types' qMic at equilibrium; (b) that the tradeoffs within microbial growth and between the environmental conditions may be scarcely represented. The second hypothesis would be supported by the over simplicity of the chemical physical structure of the soil in a uni-layer representation. As a matter of fact the model as it is implied that microbes could find the same amount of C, O₂ and living space throughout the profile with no depth limitation. In conclusion Reco, RH and qMic modeled dynamics suggest that the single layer approach may be a good starting point to investigate the processes involved, but heterogeneity in soil horizons structure should be taken into account.

CHAPTER 7: CONCLUSIONS

The objectives of this work resided in theoretically and empirically investigate photosynthesis and ecosystem respiration to better understand C cycle in European forests. For this purpose we used a wide spectrum of means to create a physical based modeling framework able to represent past, present and future net C exchange with the atmosphere on a daily temporal resolution. Thus the aims of this work focused on improving an already existent Forest Ecosystem Model (Collalti et al., 2014) with a set of new theoretical or empirical intuitions, which led to new mathematical representation of canopy structure, leaves/fineroot turnover, leaf phenology, emergence and decay. We also integrated a new soil C dynamics routine, based on the mathematical framework of other well-known models (i.e. Century and DNDC). The new mathematical relations were written in C/C++ programming language, and integrated in 3D-CMCC-FEM, giving birth to the 6.1 version of the model. The results showed overall improvements in modeling the GPP; it also resulted to reliably estimate both Reco and NEE. TOC, litter C, microbial C and humus C dynamics could not be validated against field data. However their patterns resulted realistic. Even though microbial activity (HR) was consistent with literature, qMic resulted far from reaching the equilibrium; since no disturbance/erosion event was simulated in any case, we suspect it to be related to the over simplistic physical chemical description of the soil profile. For this reason we are already working in developing a multilayer approach able to discretize the soil in undefined amount of layers representing the several soil horizons.

The new Carbon injection function resolved artifacts in AR simulation during bud burst; the evergreen leaf turnover and deciduous leaves

yellowing functions resulted in better representation of inter temporal variability and FOM littering; the modified PPA resulted a very good automated estimator of dominance relations between canopy height classes.

The model showed its weakness in representing C cycle in the Mediterranean ecosystem, probably because of an over simplistic representation of soil water balance and water stress on GPP. This hypothesis was suggested also by the strong improvement in AR dynamics after including the water potential limiting factor on maintenance respiration.

In conclusion even though the 6.1. version of 3D-CMCC-FEM brought interesting improvements and novelties to the Ecosystem Modeling field, there is still much which needs to be done to achieve higher knowledge of terrestrial ecosystems biogeochemical cycle and their role in mitigating the Global Climate Change.

BIBLIOGRAPHY

- Adams, Thomas P, Drew W Purves, and Stephen W Pacala. (2007).** "Understanding Height-Structured Competition in Forests: Is There an R^* for Light?" *Proceedings. Biological Sciences / The Royal Society* 274 (1628): 3039–47. doi:10.1098/rspb.2007.0891.
- Almeida, A., Landsberg, J.J., Sands, P.J., 2004.** Parameterisation of 3-PG model for fast-growing *Eucalyptus grandis* plantations. *Forest Ecology and Management* 193, 179–195
- Ameztegui, Aitor, Lluís Coll, Raquel Benavides, Fernando Valladares, and Alain Paquette. (2012).** "Understory light predictions in mixed conifer mountain forests: Role of aspect-induced variation in crown geometry and openness." *Forest Ecology and Management* 276: 52-61.
- Amthor JS (1989).** *Respiration and Crop Productivity*, Springer-Verlag
- Amthor JS (2000).** "The McCree--de Wit--Penning de Vries--Thornley Respiration Paradigms: 30 Years Later", *Annals of Botany*, 86:1-20.
- Amthor JS, and 12 others (2001).** "Boreal forest CO₂ exchange and evapotranspiration predicted by nine ecosystem process models: intermodel comparisons and relationships to field measurements". *Journal of Geophysical Research* 106:33,623-33,648.
- Anav, Alessandro, Fabio D'Andrea, Nicolas Viovy, and Nicolas Vuichard. (2010).** "A Validation of Heat and Carbon Fluxes from High-Resolution Land Surface and Regional Models." *Journal of Geophysical Research* 115 (G4): G04016. doi:10.1029/2009JG001178.
- Arora, Vivek K., and George J. Boer. (2005).** "A Parameterization of Leaf Phenology for the Terrestrial Ecosystem Component of Climate Models." *Global Change Biology* 11 (1): 39–59. doi:10.1111/j.1365-2486.2004.00890.x.
- Baldocchi, Dennis D. (2003)** "Assessing the eddy covariance technique for evaluating carbon dioxide exchange rates of ecosystems: past, present and future." *Global Change Biology* 9, no. 4: 479-492.

- Bartelink, H. H. (1998).** "A model of dry matter partitioning in trees." *Tree Physiology* 18, no. 2: 91-101. Bellio and Pividori, 2009
- Bernetti, Giovanni. (1995).** *Selvicoltura speciale*. Unione Tipografico-Editrice Torinese.
- Berg, B., McClaugherty, C., (2007).** *Plant litter: decomposition, humus formation, carbon sequestration*, 2nd ed. Springer, 338 pp., ISBN 3-540-74922-5
- Binkley, Dan, and Richard Fisher, (2012).** *Ecology and management of forest soils*. John Wiley & Sons.
- Bourdeau, Philippe F. (1959)** "Seasonal variations of the photosynthetic efficiency of evergreen conifers." *Ecology*: 63-67.
- Breuer, L., Eckhardt, K., Frede, H.-G., (2003).** Review of plant parameter values for hydrological and soil-vegetation-atmosphere transfer (SVAT) models in temperate climates. Internet database: <http://www.uni-giessen.de/~gh1461/plapada/plapada.html>, January, 2003
- Brus, D. J., G. M. Hengeveld, D. J. J. Walvoort, P. W. Goedhart, A. H. Heidema, G. J. Nabuurs, and K. Gunia. (2012)** "Statistical mapping of tree species over Europe." *European Journal of Forest Research* 131, no. 1: 145-157.
- Bugmann, Harald. (2001).** "A REVIEW OF FOREST GAP MODELS The Description , Understanding and Prediction of the Long-Term Dynamics of Forest Ecosystems Has Fascinated Ecologists for a Long Time (Cf . Clements , 1916 ; Watt , 1925 ; Gleason , 1926 ; Tansley , 1936 ; Whittaker , 1953", 259–305.
- C. Michael Hogan. (2010).** Abiotic factor. *Encyclopedia of Earth*. eds Emily Monosson and C. Cleveland. National Council for Science and the Environment . Washington DC
- Campioli, Matteo, Hans Verbeeck, Joris Van den Bossche, Jian Wu, Andreas Ibrom, Ettore D'Andrea, Giorgio Matteucci, Roeland Samson, Kathy Steppe, and André Granier. (2013).** "Can decision rules simulate carbon allocation for years with

contrasting and extreme weather conditions? A case study for three temperate beech forests." *Ecological Modelling* 263: 42-55.

Cannell, M. G. R., and J. H.M. Thornley. (2000). "Modelling the Components of Plant Respiration: Some Guiding Principles." *Annals of Botany* 85: 45–54.

Carbone, Mariah S., Claudia I. Czimczik, Trevor F. Keenan, Paula F. Murakami, Neil Pederson, Paul G. Schaberg, Xiaomei Xu, and Andrew D. Richardson. (2013) "Age, allocation and availability of nonstructural carbon in mature red maple trees." *New Phytologist* 200, no. 4: 1145-1155.

Chabot, BF, and DJ Hicks. (1982). "The Ecology of Leaf Life Spans." *Annual Review of Ecology and Systematics* 13 (1982): 229–59. <http://www.jstor.org/stable/2097068>.

Chen B, Black TA, Coops NC, Krishnan P, Jassal R, Bru ¨mmer C, Nesic Z (2009) Seasonal controls on interannual variability in carbon dioxide exchange of a near-end- of rotation Douglas-fir stand in the Pacific Northwest, 1997-2006. *Global Change Biology*, 15, 1962–1981, doi: 10.1111/j.1365-2486.2008.01832.x.

Chiesi, M., Maselli, F., Moriondo, M., Fibbi, L., Bindi, M., Running, S.W., (2007). Application of BIOME-BGC to simulate Mediterranean forest processes. *Ecol. Model.* 206, 179–190.

Chiti, T., R.E.M. Neubert, I.a. Janssens, G. Certini, J. Curiel Yuste, and C. Sirignano. (2009). "Radiocarbon Dating Reveals Different Past Managements of Adjacent Forest Soils in the Campine Region, Belgium." *Geoderma* 149 (1-2): 137–42. doi:10.1016/j.geoderma.2008.11.030.

Chiti, Tommaso, Rolf E. M. Neubert, Ivan a. Janssens, Jorge Curiel Yuste, Carmina Sirignano, and Giacomo Certini. (2011). "Radiocarbon Based Assessment of Soil Organic Matter Contribution to Soil Respiration in a Pine Stand of the Campine Region, Belgium." *Plant and Soil* 344 (1-2): 273–82. doi:10.1007/s11104-011-0745-7.

- Cienciala, E., Cerny, M., Tatarinov, F., Apltauer, A., Exnerova, Z., (2006).** Biomass functions applicable to Scots pine. *Trees* 20, 483–495.
- Cienciala E, Tatarinov FA (2006)** Application of BIOME-BGC model to managed forests. 2. Comparison with long-term observations of stand production for major tree species. *For Ecol Manag* 237:252–266
- Clausnitzer, Falko, Barbara Köstner, Kai Schwärzel, and Christian Bernhofer. (2011).** "Relationships between canopy transpiration, atmospheric conditions and soil water availability—Analyses of long-term sap-flow measurements in an old Norway spruce forest at the Ore Mountains/Germany." *Agricultural and Forest Meteorology* 151, no. 8: 1023-1034.
- Coleman, K, and DS Jenkinson. (1999).** "ROTHC-26.3." A Model for the Turnover of Carbon in Soils ..., no. November 1999. http://www.uni-kassel.de/~w_dec/Modellierung/wdec-rothc_manual.pdf.
- Collalti A., Santini M., Marconi S., Mattiuzzi M., Candini A., Natali S., Nolè A., Valentini R. (2013)** "Application of the 3D-CMCC FEM (Three Dimension Forest Ecosystem Model) on multi-temporal NDVI satellite imagery and future scenarios". First annual conference, Società Italiana per le Scienze del Clima.
- Collalti, A., Perugini, L., Santini, M., Chiti, Nolè, A. , Matteucci, G., Valentini, R. (2014).** "A Process-Based Model to Simulate Growth in Forests with Complex Structure: Evaluation and Use of 3D-CMCC Forest Ecosystem Model in a Deciduous Forest in Central Italy." *Ecological Modelling* 272 (January). Elsevier B.V. 362–78. doi:10.1016/j.ecolmodel.2013.09.016.
- Collalti, Alessio. (2011)** "Sviluppo di un modello dinamico ecologico-forestale per foreste a struttura complessa." PhD diss., Tuscia University.
- Cox, D.R., Hinkley, D.V. (1974)** *Theoretical Statistics*, Chapman & Hall (Appendix 3) ISBN 0-412-12420-3

- Damesin, C., and C. Lelarge. (2003).** "Carbon isotope composition of current-year shoots from *Fagus sylvatica* in relation to growth, respiration and use of reserves." *Plant, Cell & Environment* 26, no. 2: 207-219.
- Davidson, Eric a., Ivan a. Janssens, and Yiqi Luo. (2006).** "On the Variability of Respiration in Terrestrial Ecosystems: Moving beyond Q10." *Global Change Biology* 12 (2): 154–64. doi:10.1111/j.1365-2486.2005.01065.x.
- Davies, Kevin M. (2004).** *Plant pigments and their manipulation.* Wiley-Blackwell. p. 6. ISBN 1-4051-1737-0.
- De Macedo, J.R., Do Amaral Meneguelli, N., Ottoni, T.B., Araujo de Sousa Lima, J., (2002).** Estimation of field capacity and moisture retention based on regression analysis involving chemical and physical properties in Alfisols and Ultisols of the state of Rio de Janeiro. *Communications in Soil Science and Plant Analysis*, 33: 2037–2055. doi:10.1081/CSS-120005747
- Delpierre, N., E. Dufrêne, K. Soudani, E. Ulrich, S. Cecchini, J. Boé, and C. François. (2009a).** "Modelling Interannual and Spatial Variability of Leaf Senescence for Three Deciduous Tree Species in France." *Agricultural and Forest Meteorology* 149 (6-7): 938–48. doi:10.1016/j.agrformet.2008.11.014.
- Devi, Athokpam Florida, and S. C. Garkoti. (2013).** "Variation in evergreen and deciduous species leaf phenology in Assam, India." *Trees* 27, no. 4: 985-997.
- Di Giovanni, C., Disnar, J.R., Bichet, V., Campy, M., (1998).** Sur la présence de matières organiques mésocénozoïques dans des humus actuels (bassin de Chaillexon, Doubs, France). *Comptes Rendus de l'Académie des Sciences de Paris, Series IIA, Earth and Planetary Science* 326:553–559 doi:10.1016/S1251-8050(98)80206-1
- Dickinson, Colin Hedley. 2012.** *Biology of plant litter decomposition.* Vol. 2. Elsevier,.
- Dungait, J. A.; Hopkins, D. W.; Gregory, A. S.; Whitmore, A. P. (2012).** "Soil organic matter turnover is governed by accessibility not

recalcitrance". *Global Change Biology* 18 (6): 1781–1796. doi:10.1111/j.1365-2486.2012.02665.x . Retrieved 30 August 2014.

Elo, S., Maunuksela, L., Salkinoja-Salonen, M., Smolander, A., Haahtela, K., (2006). Humus bacteria of Norway spruce stands: plant growth promoting properties and birch, red fescue and alder colonizing capacity. *FEMS Microbiology Ecology* 31:143–152 doi:10.1111/j.1574-6941.2000.tb00679.x

Federici, S., Vitullo, M., Tulipano, S., De Lauretis, M., Seufert, G., (2008). An approach to estimate carbon stocks change in forest carbon pools under the UNFCCC: the Italian case. *iForest*. 1, 86-95

Fumoto, Tamon, Kazuhiko Kobayashi, Changsheng Li, Kazuyuki Yagi, and Toshihiro Hasegawa. (2008a). “Revising a Process-based Biogeochemistry Model (DNDC) to Simulate Methane Emission from Rice Paddy Fields under Various Residue Management and Fertilizer.” *Global Change ...* 14 (2): 382–402. doi:10.1111/j.1365-2486.2007.01475.x.

Gifford, Roger M. (1995). "Whole plant respiration and photosynthesis of wheat under increased CO₂ concentration and temperature: long-term vs. short-term distinctions for modelling." *Global Change Biology* 1, no. 6: 385-396.

Glantz, Stanton A.; Slinker, B. K. (1990). *Primer of Applied Regression and Analysis of Variance*. McGraw-Hill. ISBN 0-07-023407-8.

González-Pérez, M., Vidal Torrado, P., Colnago, L.A., Martin-Neto, L., Otero, X.L., Milori, D.M.B.P., Haenel Gomes, F., (2008). ¹³C NMR and FTIR spectroscopy characterization of humic acids in spodosols under tropical rain forest in southeastern Brazil. *Geoderma* 146:425–433 doi:10.1016/j.geoderma.2008.06.018

Grace, James, (2012). *Perspectives on plant competition*. Elsevier.

Gunasekera, Dhammika, and Gerald A. Berkowitz. (1992). "Heterogenous stomatal closure in response to leaf water deficits is not a universal phenomenon." *Plant Physiology* 98, no. 2: 660-665.

- Hargitai, L., (1993).** The soil of organic matter content and humus quality in the maintenance of soil fertility and in environmental protection. *Landscape and Urban Planning* 27:161–167.doi:10.1016/0169-2046(93)90044-E
- Hashimoto, Hirofumi, Jennifer L. Dungan, Michael A. White, Feihua Yang, Andrew R. Michaelis, Steven W. Running, and Ramakrishna R. Nemani. (2008).** "Satellite-based estimation of surface vapor pressure deficits using MODIS land surface temperature data." *Remote Sensing of Environment* 112, no. 1: 142-155.
- Haxeltine, A., Prentice, C., (1996).** BIOME3: An equilibrium terrestrial biosphere model based on ecophysiological constraints, resource availability, and competition among plant functional types. *Global Biogeochemical Cycles* 10, 693–709.
- Hoff, C., S. Rambal, and R. Joffre. (2002).** "Simulating carbon and water flows and growth in a Mediterranean evergreen *Quercus ilex* coppice using the FOREST-BGC model." *Forest Ecology and Management* 164, no. 1: 121-136.
- Horie, Y.; Ito, H.; Kusaba, M.; Tanaka, R.; Tanaka, A. (2009).** "Participation of Chlorophyll b Reductase in the Initial Step of the Degradation of Light-harvesting Chlorophyll a/b-Protein Complexes in Arabidopsis" . *Journal of Biological Chemistry* 284 (26): 17449–56. doi:10.1074/jbc.M109.008912 . PMC 2719385 . PMID 19403948
- Horn, J. E., and K. Schulz. (2011).** "Identification of a general light use efficiency model for gross primary production." *Biogeosciences* 8, no. 4: 999-1021.
- Hortensteiner, S. (2006).** "Chlorophyll degradation during senescence". *Annual Review of Plant Biology* 57: 55–77. doi:10.1146/annurev.arplant.57.032905.105212 . PMID 16669755
- Huemmerich, Karl F. (2013)** "Simulations of seasonal and latitudinal variations in leaf inclination angle distribution: Implications for remote sensing." *Advances in Remote Sensing* 2: 93.

- Ichii, Kazuhito, Michael A. White, Petr Votava, Andrew Michaelis, and Ramakrishna R. Nemani. (2008).** "Evaluation of snow models in terrestrial biosphere models using ground observation and satellite data: impact on terrestrial ecosystem processes." *Hydrological processes* 22, no. 3: 347-355.
- Iovino, F., M. Borghetti, and A. Veltri. (2009).** "Foreste e ciclo dell'acqua." *Forest@-Journal of Silviculture and Forest Ecology* 6, no. 4: 256.
- James, Shelley A., and David T. Bell. (2000)** "Influence of light availability on leaf structure and growth of two *Eucalyptus globulus* ssp. *globulus* provenances." *Tree Physiology* 20.15: 1007-1018.
- Janssens, Ivan A., David A. Sampson, Jan Cermak, Linda Meiresonne, Francesca Riguzzi, Stijn Overloop, and Reinhart Ceulemans. (1999).** "Above-and belowground phytomass and carbon storage in a Belgian Scots pine stand." *Annals of Forest Science* 56, no. 2: 81-90.
- Kalliovirta, Jouni, and Timo Tokola. (2005).** "Functions for estimating stem diameter and tree age using tree height, crown width and existing stand database information." *Silva Fennica* 39, no. 2: 227-248.
- Karl Pearson (1895)** "Notes on regression and inheritance in the case of two parents," *Proceedings of the Royal Society of London*, 58 : 240–242.
- Keel, Sonja G., and Christina Schädel. (2010)** "Expanding leaves of mature deciduous forest trees rapidly become autotrophic." *Tree physiology* 30, no. 10: 1253-1259.
- Keenan, T.F., Ian Baker, Alan Barr, Philippe Ciais, Ken Davis, Michael Dietze, Danilo Dragoni, et al. (2012).** "Terrestrial Biosphere Model Performance for Inter-Annual Variability of Land-Atmosphere CO₂ Exchange." *Global Change Biology* 18 (6): 1971–87. doi:10.1111/j.1365-2486.2012.02678.x.
- Keenan, Trevor, Raquel Garcia, Santi Sabate, and Carlos A Gracia. (2007).** "Process Based Forest Modelling: A Thorough Validation

And Future Prospects For Mediterranean Forests In A Changing World” 92: 81–92.

Kikuzawa, K. (1991). “A Cost-Benefit Analysis of Leaf Habit and Leaf Longevity of Trees and Their Geographical Pattern.” *American Naturalist* 138 (5): 1250–63. <http://www.jstor.org/stable/2462519>.

Knicker, H., Almendros, G., González-Vila, F.J., Lüdemann, H.D., Martin, F., (1995). ¹³C and ¹⁵N NMR analysis of some fungal melanins in comparison with soil organic matter. *Organic Geochemistry* 23:1023–1028 doi:10.1016/0146-6380(95)00094-1

Köstner, B., E. Falge, and J. D. Tenhunen. (2002). "Age-related effects on leaf area/sapwood area relationships, canopy transpiration and carbon gain of Norway spruce stands (*Picea abies*) in the Fichtelgebirge, Germany." *Tree Physiology* 22, no. 8: 567-574.

Kramer, K, I Leinonen, H H Bartelink, P Berbigier, M Borghetti, E Cienciala, A J Dolman, et al. (2002). “Evaluation of Six Process-Based Forest Growth Models Using Eddy-Covariance Measurements of CO₂ and H₂O Fluxes at Six Forest Sites in Europe”, 213–30.

Krishnan P, Black TA, Barr AG, Grant NJ, Gaumont-Guay D, Nestic Z (2008). Factors controlling the interannual variability in the carbon balance of a southern boreal black spruce forest. *Journal of Geophysical Research*, 113,1–16, doi: 10.1029/ 2007JD008965.

Krishnan P, Black TA, Jassal RS, Chen B, Nestic Z (2009). Interannual variability of the carbon balance of three different-aged Douglas-fir stands in the Pacific Northwest. *Journal of Geophysical Research*, 114,1–18, doi: 10.1029/2008JG000912

Kucharik CJ, Barford CC, El Maayar M, Wofsy SC, Monson RK, Baldocchi DD (2006). A multiyear evaluation of a Dynamic Global Vegetation Model at three AmeriFlux forest sites: Vegetation structure, phenology, soil temperature, and CO₂ and H₂O vapor exchange. *Ecological Modelling*, 196, 1-31.

Kurz, Werner A., Sarah J. Beukema, and Michael J. Apps. (1996). "Estimation of root biomass and dynamics for the carbon budget

model of the Canadian forest sector." *Canadian Journal of Forest Research* 26, no. 11: 1973-1979.

Labandeira, C. C.; Dilcher, DL; Davis, DR; Wagner, DL (1994).

"Ninety-seven million years of angiosperm-insect association: paleobiological insights into the meaning of coevolution" . *Proceedings of the National Academy of Sciences* 91 (25): 12278–82. Bibcode:1994PNAS...9112278L . doi:10.1073/pnas.91.25.12278 . PMC 45420 . PMID 11607501 .

Lambers H, Szaniawski RK, de Visser R (1983). "Respiration for growth, maintenance and ion uptake. An evaluation of concepts, methods, values and their significance", *Physiologia Plantarum*, 58:556-563.

Landsberg, J.J., Waring, R.H., (1997). A generalised model of forest productivity using simplified concepts of radiation-use efficiency, carbon balance and partitioning. *Forest Ecology and Management* 95, 209–228.

Landsberg, Joe, Annikki Mäkelä, Risto Sievänen, and Mikko Kukkola. (2005). "Analysis of biomass accumulation and stem size distributions over long periods in managed stands of *Pinus sylvestris* in Finland using the 3-PG model." *Tree physiology* 25, no. 7: 781-792.

Lyr, Horst, and Volker Garbe. (1995). "Influence of root temperature on growth of *Pinus sylvestris*, *Fagus sylvatica*, *Tilia cordata* and *Quercus robur*." *Trees* 9, no. 4: 220-223.

le Maire G, Delpierre N, JungMet al. (2010). Detecting the critical periods that under- pin interannual fluctuations in the carbon balance of European forests. *Journal of Geophysical Research*, 115,1–16, doi: 10.1029/2009JG001244

Lee, D; Gould, K (2002). "Anthocyanins in leaves and other vegetative organs: An introduction". "Advances in Botanical Research Volume 37". *Advances in Botanical Research* 37. pp. 1–16. doi:10.1016/S0065-2296(02)37040-X . ISBN 978-0-12-005937-9.

- Lee, D.; Gould, K. (2002).** "Why Leaves Turn Red". *American Scientist* 90 (6): 524–531. Bibcode:2002AmSci..90..524L . doi:10.1511/2002.6.524 .
- Lehninger, Albert. (2008).** "Lehninger Principles Of Biochemistry & EBook Author: Albert Lehninger, David L. Nelson, Michael M. Cox, Publisher: W. H.": 1263.
- Levis SG, Bonan B, Vertenstein M, Oleson KW (2004).** The Community Land Model's Dynamic Global Vegetation Model (CLM-DGVM): Technical Description and User's Guide, NCAR Tech. Note TN-459+IA, 50 pp, National Center for Atmospheric Research, Boulder, Colorado.
- Levis, S., et al. (2004).**"The Community Land Model's dynamic global vegetation model (CLM-DGVM): Technical description and user's guide." NCAR Tech. Note TN-459+ IA 50.
- Li, Changsheng. (2007).** "Quantifying Soil Organic Carbon Sequestration Potential with Modeling Approach." Dndc.sr.unh.edu. http://www.dndc.sr.unh.edu/wp-content/papers/2008_Li_C_model.pdf.
- Liang, Chao, Guang Cheng, Devin L. Wixon, and Teri C. Balsler. (2011).** "An absorbing Markov chain approach to understanding the microbial role in soil carbon stabilization." *Biogeochemistry* 106, no. 3: 303-309.
- Lim, Pyung Ok, Hyo Jung Kim, and Hong Gil Nam. (2007).** "Leaf senescence." *Annu. Rev. Plant Biol.* 58: 115-136.
- Mäkelä, Annikki, Joe Landsberg, Alan R. Ek, Thomas E. Burk, Michael Ter-Mikaelian, Göran I. Agren, Chadwick D. Oliver, and Pasi Puttonen. (2000).** "Process-Based Models for Forest Ecosystem Management: Current State of the Art and Challenges for Practical Implementation." *Tree Physiology* 20 (5_6): 289–98. <http://www.ncbi.nlm.nih.gov/pubmed/12651445>.
- Manabe, S. (1969).** Climate and the ocean circulation, I, The atmospheric circulation and the hydrology of the Earth surface, *Mon. Weather Rev.*, 97, 739-774,

- Mann, Henry B.; Whitney, Donald R. (1947).** "On a Test of Whether one of Two Random Variables is Stochastically Larger than the Other". *Annals of Mathematical Statistics* 18 (1): 50–60. doi:10.1214/aoms/1177730491 . MR 22058 . Zbl 0041.26103 .
- Marconi, S., A. Collalti, M. Santini, and R. Valentini. (2013).** "Simulating Carbon cycle and phenology in complex forests using a multi-layer process based ecosystem model; evaluation and use of 3D-CMCC-Forest Ecosystem Model in a deciduous and an evergreen neighboring forests, within the area of Brasschaat (Be)." In *AGU Fall Meeting Abstracts*, vol. 1, p. 0473.
- Maxwell K, Johnson GN (2000).** "Chlorophyll fluorescence--a practical guide". *J. Exp. Bot.* 51 (345): 659–68. doi:10.1093/jexbot/51.345.659 . PMID 10938857
- McMurtrie, Ross E., Henry L. Gholz, Sune Linder, and Stith T. Gower. (1994)**"Climatic factors controlling the productivity of pine stands: a model-based analysis." *Ecological Bulletins*: 173-188.
- Medvigy, D., et al. (2009)** "Mechanistic scaling of ecosystem function and dynamics in space and time: Ecosystem Demography model version 2." *Journal of Geophysical Research: Biogeosciences* (2005–2012) 114.G1.
- Moffat, Antje M., Dario Papale, Markus Reichstein, David Y. Hollinger, Andrew D. Richardson, Alan G. Barr, Clemens Beckstein et al. (2007).** "Comprehensive comparison of gap-filling techniques for eddy covariance net carbon fluxes." *Agricultural and Forest Meteorology* 147, no. 3: 209-232.
- Mohren, G. M. J., and H. E. Burkhart. (1994).** "Preface." *Forest ecology and management* 69, no. 1: 1-5.
- Molina, J. A. E., C. E. Clapp, M. J. Shaffer, F. W. Chichester, and W. E. Larson. (1983).** "NCSOIL, A Model of Nitrogen and Carbon Transformations in Soil: Description, Calibration, and Behavior1." *Soil Science Society of America Journal* 47 (1): 85. doi:10.2136/sssaj1983.03615995004700010017x.

- Mollicone, Danilo, Frederic Achard, Luca Belelli Marchesini, Sandro Federici, Christian Wirth, Martina Leipold, Stefano Rosellini, E-Detlef Schulze, and Riccardo Valentini. (2002).** "A remote sensing based approach to determine forest fire cycle: case study of the Yenisei Ridge dark taiga." *Tellus B* 54, no. 5: 688-695.
- Monteith JL (1972)** Solar radiation and productivity in tropical ecosystems. *Journal of Applied Ecology*, 9, 747±766.
- Monteith JL (1977)** Climate and the efficiency of crop production in Britain. *Philosophical Transactions of the Royal Society of London*, B, 281, 277±294.
- Monteith, J.L. (1994)** Validity of the correlation between intercepted radiation and biomass. *Agricultural and Forest Meteorology* 68, 213-220.
- Morecroft, M.D., Stokes, V.J., Morison, J.I.L., (2003).** Seasonal changes in the photosynthetic capacity of canopy oak (*Quercus robur*) leaves: the impact of slow development on annual carbon uptake. *International Journal of Biometeorology* 47 (4), 221–226.
- Moorcroft, P. R., G. C. Hurtt, and Stephen W. Pacala. (2001).** "A method for scaling vegetation dynamics: the ecosystem demography model (ED)." *Ecological monographs* 71.4: 557-586.
- Moriasi, D N, J G Arnold, M W Van Liew, R L Bingner, R D Harmel, and T L Veith. (2007).** "Model Evaluation Guidelines for Systematic Quantification of Accuracy in Watershed Simulations" 50 (3): 885–900.
- Mott, K. A., and D. F. Parkhurst. (1991):** "Stomatal responses to humidity in air and helox." *Plant, Cell & Environment* 14, no. 5: 509-515.
- Muscoloa, A., Bovalob, F., Gionfriddob, F., Nardi, S., (1999).** Earthworm humic matter produces auxin-like effects on *Daucus carota* cell growth and nitrate metabolism. *Soil Biology and Biochemistry* 31:1303–1311doi:10.1016/S0038-0717(99)00049-8

- Nagy, Miklos T., Ivan a. Janssens, Jorge Curiel Yuste, Arnaud Carrara, and Reinhart Ceulemans. (2006).** "Footprint-Adjusted Net Ecosystem CO₂ Exchange and Carbon Balance Components of a Temperate Forest." *Agricultural and Forest Meteorology* 139 (3-4): 344–60. doi:10.1016/j.agrformet.2006.08.012.
- Nash, JEa, and J. V. Sutcliffe. (1970).** "River flow forecasting through conceptual models part I—A discussion of principles." *Journal of hydrology* 10, no. 3: 282-290.
- Nicolas Bernier and Jean-François Ponge (1994).** "Humus form dynamics during the sylvogenetic cycle in a mountain spruce forest" (PDF). *Soil Biology and Biochemistry* 26 (2): 183–220. doi:10.1016/0038-0717(94)90161-9
- Nightingale, J., Hill, M., Phinn, S., Davies, I., Held, A., Erskine, P., (2008).** Use of 3-PG and 3-PGS to simulate forest growth dynamics of Australian tropical rainforests. I. Parameterisation and calibration for old-growth, regeneration and plantation forests. *Forest Ecology and Management* 254, 107–121.
- Nitta, Ikuko, and Masahiko Ohsawa. (1997).** "Leaf dynamics and shoot phenology of eleven warm-temperate evergreen broad-leaved trees near their northern limit in central Japan." *Plant Ecology* 130, no. 1: 71-88.
- Nobel, PS. (1999).** *Physicochemical and Environmental Plant Physiology (leaves and Fluxes 8.1)*. http://books.google.com/books?hl=en&lr=&id=yW_pptyiMHoC&oi=fnd&pg=PR11&dq=Physicochemical+and+Environmental+Plant+Physiology&ots=Uzc35Cj8qr&sig=2882H823NjGl2KZ_qFa9W4_EkTk.
- Nolè, a., B. E. Law, F. Magnani, G. Matteucci, a. Ferrara, F. Ripullone, and M. Borghetti. (2009).** "Application of the 3-PGS Model to Assess Carbon Accumulation in Forest Ecosystems at a Regional Level." *Canadian Journal of Forest Research* 39 (9): 1647–61. doi:10.1139/X09-077.

- Oades, J. M. (1984).** "Soil organic matter and structural stability: mechanisms and implications for management" . *Plant and soil* 76: 319–337. doi:10.1007/BF02205590 . Retrieved 30 August 2014.
- Oerlemans & Vink (2010).** Rainfall Interception Experiments and Interception mapping using Remote Sensing. Master Thesis. Faculty of Geosciences, Department of Physical Geography Utrecht University.
- Oleson, Keith W., Yongjiu Dai, Gordon Bonan, Mike Bosilovich, Robert Dickinson, Paul Dirmeyer, Forrest Hoffman et al. (2004).** Technical description of the community land model (CLM). NCAR Technical Note NCAR/TN-461+ STR, National Center for Atmospheric Research, Boulder, CO.
- Pacala, S., Canham, C., Saponara, J., Silander, J., Kobe, R., Ribbens, E., (1996).** Forest models defined by field measurements: estimation, error analysis and dynamics. *Ecological Monographs* 66, 1–43.
- Pallardy, Stephen G. (2008).** *Physiology of Woody Plants*. Edited by Theodore T. Kozlowski. 3rd ed. Elsevier.
- Papale, D., M. Reichstein, M. Aubinet, E. Canfora, C. Bernhofer, W. Kutsch, B. Longdoz et al. (2006).** "Towards a standardized processing of Net Ecosystem Exchange measured with eddy covariance technique: algorithms and uncertainty estimation."
- Parker, GG, MD Lowman, and NM Nadkarni. (1995).** "Forest Canopies." *Forest Canopies*. http://www.cfc.umt.edu/courses/for330/Parker_1995.pdf.
- Parlange, Jean-Yves. (1971).** "Theory of water-movement in soils: I. One-dimensional absorption." *Soil science* 111, no. 2: 134-137.
- Penning de Vries FWT (1975).** "The cost of maintenance processes in plant cells", *Annals of Botany*, 39:77-92.
- Pilegaard, Kim, Teis N Mikkelsen, Claus Beier, Niels Otto Jensen, Per Ambus, and Helge Ro-poulsen. (2003).** "Field Measurements

of Atmosphere– Biosphere Interactions in a Danish Beech Forest”,
no. December: 315–33.

Pietsch S.A., Hasenauer H., Thornton P.E., (2005). BGC-model parameters for tree species growing in central European forests. *Forest Ecology and Management* 211(3), 264-295.

Pommerening, Arne, Valerie LeMay, and Dietrich Stoyan. (2011). "Model-based analysis of the influence of ecological processes on forest point pattern formation—A case study." *Ecological Modelling* 222, no. 3: 666-678.

Purves, Drew W., Jeremy W. Lichstein, Nikolay Strigul, and Stephen W. Pacala. (2008). "Predicting and understanding forest dynamics using a simple tractable model." *Proceedings of the National Academy of Sciences* 105, no. 44: 17018-17022.

Quiquampoix, H., Servagent-Noinville, S., Baron, M.-H., (2002). Enzyme adsorption on soil mineral surfaces and consequences for the catalytic activity. In: Burns, R.G., Dick, R.P. (Eds.), *Enzymes in the Environment*. Marcel Dekker, New York, pp. 285–306.

Raven PH, Evert RF, Eichhorn SE (2005). *Biology of Plants*, (7th ed.). New York: W.H. Freeman and Company Publishers. pp. 124–127. ISBN 0-7167-1007-2.

Reece J, Urry L, Cain M, Wasserman S, Minorsky P, Jackson R. *Biology* (International ed.). Upper Saddle River, NJ: Pearson Education. pp. 235, 244. ISBN 0-321-73975-2. "This initial incorporation of carbon into organic compounds is known as carbon fixation."

Richardson AD, Anderson RS, Arain MA et al. (2012) Terrestrial biosphere models need better representation of vegetation phenology: results from the North American Carbon Program Site Synthesis. *Global Change Biology*, 18, 566–584, doi: 10.1111/j.1365-2486.2011.02562.x

Richardson, Andrew D., Mariah S. Carbone, Trevor F. Keenan, Claudia I. Czimczik, David Y. Hollinger, Paula Murakami, Paul G. Schaberg, and Xiaomei Xu. (2013a). "Seasonal dynamics

and age of stemwood nonstructural carbohydrates in temperate forest trees." *New Phytologist* 197, no. 3: 850-861.

Richardson, Andrew D., Trevor F. Keenan, Mirco Migliavacca, Youngryel Ryu, Oliver Sonnentag, and Michael Toomey. (2013b). "Climate change, phenology, and phenological control of vegetation feedbacks to the climate system." *Agricultural and Forest Meteorology* 169: 156-173.

Running, S.W., Hunt, E.R., (1993). Generalization of a forest ecosystem model for other biomes, BIOME-BGC, and an application for global scale models. In: Ehleringer, J., Field, C.B. (Eds.), *Scaling Physiological Processes: Leaf to Globe*. Academic Press, San Diego, pp. 141–158.

Rupšys, Petras, and Edmundas Petrauskas. (2010). "The bivariate Gompertz diffusion model for tree diameter and height distribution." *Forest Science* 56, no. 3: 271-280.

Ryan, M. G., Dan Binkley, and James Henry Fownes. (1997). "Age-related decline in forest productivity: pattern and process." *Advances in ecological research* 27: 213-262.

Ryan, MG, ST Gower, and RM Hubbard. (1995). "Woody Tissue Maintenance Respiration of Four Conifers in Contrasting Climates." *Oecologia*, 133–40.
<http://link.springer.com/article/10.1007/BF00317276>.

Ryan, Michael G. (1991). "Effects of Climate Change on Plant Respiration." *Ecological Applications* 1 (2): 157.
doi:10.2307/1941808.

Ryu SR, Chen J, Noormets A, Bresee MK, Ollinger SV (2008) Comparisons between PnET-Day and eddy covariance based gross ecosystem production in two Northern Wisconsin forests. *Agricultural and Forest Meteorology*, 148, 247-256

Salk, Carl Frederick. (2011). "Will the Timing of Temperate Deciduous Trees' Budburst and Leaf Senescence Keep up." PhD diss., Duke University,

- Sands, P.J., Landsberg, J.J., (2002).** Parameterisation of 3-PG for plantation grown *Eucalyptus globulus*. *Forest Ecology and Management* 163, 273-292.
- Schaber, Jörg, and Franz-W Badeck. (2003).** "Physiology-Based Phenology Models for Forest Tree Species in Germany." *International Journal of Biometeorology* 47 (4): 193–201. doi:10.1007/s00484-003-0171-5.
- Schlichting, Carl D. (1986).** "The evolution of phenotypic plasticity in plants." *Annual review of ecology and systematics*: 667-693.
- Schulze, E-D., O. L. Lange, L. Kappen, U. Buschbom, and M. Evenari. (1973).** "Stomatal responses to changes in temperature at increasing water stress." *Planta* 110, no. 1: 29-42.
- Schulze, Ernst-detlef, Erwin Beck, and Klaus Muller-Hohenstein. (2002).** *Plant Ecology*. Jena: Springer.
- Seidl, S., Kroner, M., Dalgarno, P. A., Högele, A., Smith, J. M., Ediger, M., ... Warburton, R. J. (2005).** Absorption and photoluminescence spectroscopy on a single self-assembled charge-tunable quantum dot. *Physical Review B - Condensed Matter and Materials Physics*, 72. doi:10.1103/PhysRevB.72.195339
- Shao, Hong-Bo, Li-Ye Chu, Cheruth Abdul Jaleel, and Chang-Xing Zhao. (2008).** "Water-deficit stress-induced anatomical changes in higher plants." *Comptes rendus biologies* 331, no. 3: 215-225.
- Sirca, Costantino, Michele Salis, and Donatella Spano. (2014).** "A regional estimate of soil organic carbon content linking the RothC model to spatialised climate and soil database." In *EGU General Assembly Conference Abstracts*, vol. 16, p. 9923.
- Sitch S, Smith B, Prentice I C, Arneth A, Bondeau A, Cramer W, Kaplan J O, Levis S, Lucht W, Sykes M T, Thonicke K, Venevsky S. (2003).** Evaluation of ecosystem dynamics, plant geography and terrestrial carbon cycling in the LPJ dynamic global vegetation model. *Global Change Biology*.

- Sitch S, Smith B, Prentice IC, Arneth A, Bondeau A, Cramer W, Kaplan JO, Levis S, Lucht W, Sykes MT, Thonicke K, Venevsky S. (2003).** Evaluation of ecosystem dynamics, plant geography and terrestrial carbon cycling in the LPJ Dynamic Global Vegetation Model. *Global Change Biology* 9, 161-185.
- Sitch, S., Huntingford, C., Gedney, N., Levy, P E, Lomas, M, Piao, S L, Betts, R, Ciais, P, Cox et al. (2008).** Evaluation of the terrestrial carbon cycle, future plant geography and climate-carbon cycle feedbacks using five Dynamic Global Vegetation Models (DGVMs). *Global Change Biology*.
- Starr, Gregory, and Steven F. Oberbauer. (2003)** "Photosynthesis of arctic evergreens under snow: implications for tundra ecosystem carbon balance." *Ecology* 84, no. 6: 1415-1420.
- Strigul, Nikolay, Denis Pristinski, Drew Purves, Jonathan Dushoff, and Stephen Pacala. (2008).** "Scaling From Trees To Forests: Tractable Macroscopic Equations For Forest Dynamics." *Ecological Monographs* 78 (4): 523–45. doi:10.1890/08-0082.1.
- Suni, Tanja, Janne Rinne, Anni Reissell, Nuria Altimir, Petri Keronen, Miikka Dal Maso, Markku Kulmala, and Timo Vesala. (2003).** "Long-Term Measurements of Surface Fl Uxes above a Scots Pine Forest in Hyytiälä, Southern Finland, 1996–2001", no. December: 287–301.
- Szalay, A., (1964).** Cation exchange properties of humic acids and their importance in the geochemical enrichment of UO_2^{++} and other cations. *Geochimica et Cosmochimica Acta* 28:1605–1614. doi:10.1016/0016-7037(64)90009-2
- Terashima, Ichiro, Yuko T. Hanba, Danny Tholen, and Ülo Niinemets. (2011).** "Leaf functional anatomy in relation to photosynthesis." *Plant Physiology* 155, no. 1: 108-116.
- Thomas, H; Stoddart, J L. (1980).** "Leaf Senescence". *Annual Review of Plant Physiology* 31: 83–111. doi:10.1146/annurev.pp.31.060180.000503.

- Thornley JHM, France J. (2007).** *Mathematical Models in Agriculture*, CABI, Wallingford, UK.
- Thornley, John H M. (2011).** "Plant Growth and Respiration Re-Visited: Maintenance Respiration Defined - It Is an Emergent Property Of, Not a Separate Process Within, the System - and Why the Respiration : Photosynthesis Ratio Is Conservative." *Annals of Botany* 108 (7): 1365–80. doi:10.1093/aob/mcr238.
- Thornton, P., (2010).** *Biome BGC version 4.2: Theoretical Framework of Biome-BGC. Technical Documentation.*
- Thornton, Peter E, Steve W Running. (2002).** "User's Guide for Biome-BGC, Version 4.1.2", no. April.
- Tietjen, Todd, and Robert G. Wetzel. (2003).** "Extracellular enzyme-clay mineral complexes: enzyme adsorption, alteration of enzyme activity, and protection from photodegradation." *Aquatic Ecology* 37, no. 4: 331-339.
- Tilman, D, C L Lehman, and K T Thomson. (1997).** "Plant Diversity and Ecosystem Productivity: Theoretical Considerations." *Proceedings of the National Academy of Sciences of the United States of America* 94 (5): 1857–61. <http://www.pubmedcentral.nih.gov/articlerender.fcgi?artid=20007&tool=pmcentrez&rendertype=abstract>.
- Van Oijen, Marcel, Ad Schapendonk, and Mats Höglind. (2010).** "On the Relative Magnitudes of Photosynthesis, Respiration, Growth and Carbon Storage in Vegetation." *Annals of Botany* 105 (5): 793–97. doi:10.1093/aob/mcq039.
- Verbeeck, Hans, Kathy Steppe, Nadja Nadezhdina, M. Beeck, Gaby Deckmyn, Linda Meiresonne, Raoul Lemeur, J. Čermák, R. Ceulemans, and I. A. Janssens. (2007).** "Model analysis of the effects of atmospheric drivers on storage water use in Scots pine." *Biogeosciences* 4, no. 4 (2007): 657-671.
- Vitale, M., Mancini, M., Matteucci, G., Francesconi, F., Valenti, R., Attorre, F., (2012).** Model-based assessment of ecological adaptations of three forest trees species growing in Italy and impact

on carbon and water balance at national scale under current and future scenarios. *iForest*.

Vitasse, Yann, Christophe François, Nicolas Delpierre, Eric Dufrêne, Antoine Kremer, Isabelle Chuine, and Sylvain Delzon. (2011). "Assessing the Effects of Climate Change on the Phenology of European Temperate Trees." *Agricultural and Forest Meteorology* 151 (7): 969–80. doi:10.1016/j.agrformet.2011.03.003.

Vose, James M., et al. (1995). "Vertical leaf area distribution, light transmittance, and application of the Beer-Lambert law in four mature hardwood stands in the southern Appalachians." *Canadian Journal of Forest Research* 25.6: 1036-1043.

Vospertnik, Sonja, Robert A. Monserud, and Hubert Sterba. (2010). "Do individual-tree growth models correctly represent height:diameter ratios of Norway spruce and Scots pine?" *Forest ecology and management* 260, no. 10: 1735-1753.

Waksman, Selman Abraham. (1952). "Soil microbiology." *Soil microbiology*.

Wand, M.P; Jones, M.C. (1995). *Kernel Smoothing*. London: Chapman & Hall/CRC. ISBN 0-412-55270-1.

Wang, K-Y., S. Kellomäki, and T. Zha. (2003). "Modifications in photosynthetic pigments and chlorophyll fluorescence in 20-year-old pine trees after a four-year exposure to carbon dioxide and temperature elevation." *Photosynthetica* 41.2: 167-175.

Waring, R H, J J Landsberg, and M Williams. (1998). "Net Primary Production of Forests: A Constant Fraction of Gros", no. 1997.

Waring, R. H., P. E. Schroeder, and R. Oren. (1982). "Application of the pipe model theory to predict canopy leaf area." *Canadian Journal of Forest Research* 12, no. 3: 556-560.

White, M. A., P. E. Thornton, S. W. Running, and R. R. Nemani. (2000). Parameterization and sensitivity analysis of the BIOME-BGC terrestrial ecosystem model: net primary production controls. *Earth Interactions* 4:1–85.

- Whitehead, D. C.; Tinsley, J. (1963).** "The biochemistry of humus formation" . *Journal of the Science of Food and Agriculture* 14 (12): 849–857. doi:10.1002/jsfa.2740141201 . Retrieved 26 July 2014.
- Widlowski, J. L., M. M. Verstraete, B. Pinty, and N. Gobron. (2003).** "Allometric relationships of selected European tree species." Rep. EUR 20855 EN
- Willert, Dieter J. von; Eller, Benno M.; Werger, Marinus J. A.; Brinckmann, Enno; Ihlenfeldt, Hans-Dieter. (1992).** *Life Strategies of Succulents in Deserts.* Publisher: Cambridge University Press ISBN 978-0-521-24468-8.
- Williams, M., E. B. Rastetter, D. N. Fernandes, M. L. Gould-en, S. C. Wofsy, G. R. Shaver, J. M. Melillo, J.W. Munger, S.-M. Fan, and K. J. Nadelhoffer. (1996).** Modelling the soil–plant–atmosphere continuum in a *Quercus-Acer* stand at Harvard Forest: the regulation of stomatal conductance by light, nitrogen and soil/plant hydraulic properties. *Plant Cell and Environment* 19:911–927.
- Woo, Hye Ryun, Jin Hee Kim, Junyoung Kim, Jeongsik Kim, Ung Lee, In-Ja Song, Jin-Hong Kim, Hyo-Yeon Lee, Hong Gil Nam, and Pyung Ok Lim. (2010).** "The RAV1 transcription factor positively regulates leaf senescence in *Arabidopsis*." *Journal of experimental botany* 61, no. 14: 3947-3957.
- Xenakis, G., Ray, D., Mencuccini, M., (2008).** Sensitivity and uncertainty analysis from a coupled 3-PG and soil organic matter decomposition model. *Ecological Modelling.* 219, 1-16
- Xiao, Chun-wang, J Curiel Yuste, I A Janssens, P Roskams, L Nachtergale, A Carrara, B Y Sanchez, and R Ceulemans. (2003).** "Above- and Belowground Biomass and Net Primary Production in a 73-Year-Old Scots Pine Forest", 505–16.
- Yuste, J Curiel, I A Janssens, K Coenen, C W Xiao, and R Ceulemans. (2005).** "Contrasting Net Primary Productivity and Carbon Distribution between Neighboring Stands of", 701–12.

- Zelisko, A.; Garcia-Lorenzo, M.; Jackowski, G.; Jansson, S.; Funk, C. (2005).** "AtFtsH6 is involved in the degradation of the light-harvesting complex II during high-light acclimation and senescence". *Proceedings of the National Academy of Sciences* 102 (38): 13699–704. Bibcode:2005PNAS..10213699Z . doi:10.1073/pnas.0503472102
- Zhang, Xiaoyang, Mark a. Friedl, Crystal B. Schaaf, Alan H. Strahler, John C.F. Hodges, Feng Gao, Bradley C. Reed, and Alfredo Huete. (2003).** "Monitoring Vegetation Phenology Using MODIS." *Remote Sensing of Environment* 84 (3): 471–75. doi:10.1016/S0034-4257(02)00135-9.
- Zhang, Yu, Changsheng Li, Carl C Trettin, Harbin Li, and Ge Sun. (2002a).** "An Integrated Model of Soil, Hydrology, and Vegetation for Carbon Dynamics in Wetland Ecosystems" 16 (0). doi:10.1029/2001GB001838.
- Zhang, Yu, Changsheng Li, Carl C. Trettin, Harbin Li, and Ge Sun. (2002b).** "An Integrated Model of Soil, Hydrology, and Vegetation for Carbon Dynamics in Wetland Ecosystems." *Global Biogeochemical Cycles* 16 (4): 9–1–9–17. doi:10.1029/2001GB001838.

Appendix 1: Parameterization

A1.1. Pinus sylvestris (L.) parameters set

<u>Parameter</u>	<u>Value</u>	<u>Reference</u>	<u>Unit</u>	<u>Description</u>
Light_tol	3		-	Light tolerance
Phenology	1.2		-	Phenological habitus
Alpha	0.05	Landsberg et al., 2005	mol(C) mol(PAR)/	Canopy quantum efficiency
Epsilon_lcmj	-	-	gC mol(PAR)	Light use efficiency
K	0.54	Landsberg et al., 2005	-	Canopy PAR ext. coeff.
Albedo	0.095	Breuer et al., 2003	-	Canopy reflectance
<u>Leaf area</u>				
Laigcx	3.33	Landsberg et al., 2005	-	Max Canopy Conductance LAI
Laimaxintcpt	5	Landsberg et al., 2005	-	Max Canopy Rain Interception LAI
Maxintcptn	0.15	Landsberg et al., 2005	-	Max vapor from Rain Interception
<u>Specific leaf area</u>				
Sla	68	White et al., 2000	cm ² /gC	Specific Leaf Area
Sla_ratio	2.52	Mollicone et al., 2002	-	Shaded to sunlit projected SLA
<u>Mass density</u>				
Rhomin	0.502	Janssen et al., 1999	t /m ³	Min basic Density for young trees
Rhmax	0.502	Janssen et al., 1999	t m ³	Max basic Density for young trees
<u>Stomatal conductance</u>				
Coeffcond	0.05	Landsberg et al., 2005	mbar	Stomatal response to VPD
Blcond	0.2	Landsberg et al., 2005	m s ⁻¹	Canopy Boundary Layer Conductance
Maxcond	0.02	Landsberg et al., 2005	m s ⁻¹	Maximum Canopy Conductance
<u>Aging</u>				
Maxage	120	Xenakis et al., 2008	years	Age for physiological decline
Rage	0.75	Xenakis et al., 2008	-	Relative Age to halve age related limiting factor

<u>Parameter</u>	<u>Value</u>	<u>Reference</u>	<u>Unit</u>	<u>Description</u>
Nage	4	Landsberg et al., 2005	-	Power of relative Age in function for Age
<u>Temperature & photoperiod</u>				
Growthtmin	0	Xenakis et al., 2008	°C	Species specific biological 0
Growthtmax	35	Xenakis et al., 2008	°C	Maximum Temperature for growth
Growthtopt	22	Xenakis et al., 2008	°C	Optimal Growth Temperature
Growthstart	500	-	°C d	GDD for Bud Burst
Mindaylength	11.5	-	h	Photoperiod threshold for leaf fall activation
<u>Water potential</u>				
Swpopen	-0.5	Pietsch et al 2005	KPa	Min soil water potential to keep Stomata open
Swpclose	-2.2	Pietsch et al 2005	KPa	Min soil water potential to close Stomata
Swconst	1	-	-	Constant in Soil Water modifier vs Moist Ratio
Swpower	5	-	-	Power in Soil Water modifier vs Moist Ratio
<u>Allometry</u>				
<u>Allocation (CTEM)</u>				
Omega_ctem	0.5	Arora et al 2005	-	Environmental dependent Allocation factor
S0ctem	0.05	Arora et al 2005	-	Stem Allocation factor
R0ctem	0.89	Arora et al 2005	-	Root Allocation factor
F0ctem	0.06	Arora et al 2005	-	Foliage Allocation Factor
Fracbb0	0.29	Yuste et al., 2005	-	Branch/Bark at age 0
Fracbb1	0.1	Xenakis et al., 2008	-	Branch/Bark for mature
Fine_root_leaf	0.523	Pietsch et al., 2005	-	Fine roots to Leaf ratio
Stem_leaf	2.1225	White et al., 2000	-	Stem to Leaf ratio

<u>Parameter</u>	<u>Value</u>	<u>Reference</u>	<u>Unit</u>	<u>Description</u>
Coarse_root_stem	0.29	Pietsch et al., 2005	-	Coarse Roots to Stem ratio
Live_total_wood	0.05	P. Thornton (pers. comm.)	-	Sapwood to Hardwood ratio
<u>Sapwood</u>				
Sap_a	3.119	Verbeek et al., 2007	-	Sapwood Allometric Parameter
Sap_b	1.4544	Verbeek et al., 2007	-	Sapwood Allometric Exp Parameter
Sap_leaf	1500	Verbeek et al., 2007	-	Ratio Sapwood MaxLAI
<u>Stem biomass</u>				
Stemconst_p	0.1227	Cienciala et al., 2006	-	Allometric parameter to initialize stem Biomass
Stempower_p	2.3272	Cienciala et al., 2006	-	Allometric exp parameter to initialize stem Biomass
<u>Height (chapman richards)</u>				
Cra	32	Rupsys et al., 2010	m	Max height parameter
Crb	0.04	Rupsys et al., 2010	-	Exponential decay parameter
Crc	0.99	Rupsys et al., 2010	-	Shape parameter
<u>Nitrogen</u>				
Cn_leaves	33.1	Pietsch et al 2005	kg C kgN-1	Leaves C:N
Cn_fine_roots	38	Mollicone et al., 2002	kg C kgN-1	Fine roots C:N
Cn_live_woods	45	Mollicone et al., 2002	kg C kgN-1	Wood tissues C:N (live)
Cn_dead_woods	750	Chiesi et al., 2007	kg C kgN-1	Wood tissues C:N (dead)
<u>Phenology</u>				
Bud_burst	-	-	days	Max Budburst Days
Leaf_fall_frac_growin	-	-	-	Biome's leaffall time span
Leaf_life_span	0.33	White et al., 2000	years	Average Leaf longevity
<u>Turnover</u>				
Leaves_finerttover	0.18	Pietsch et al 2005	AIC / year	TURNOVER Fine roots turnover rate
Coarserttover	0.02	Kurz et al., 1996	AIC / year	Coarse roots turnover rate

Sapwoodtturnover	0.0025	Yuste et al., 2005	AIC / year	Sapwood turnover rate
Branchtturnover	0.01	Pietsch et al 2005	AIC / year	Branches turnover rate
Live_wood_turnover	0.7	Pietsch et al 2005	AIC / year	Woody tissues turnover rate
<u>Mortality</u>				
Wsx1000	550	Collalti et al., 2013	kg	Max stem mass per tree at 1000 trees
Thinpower	2	Landsberg et al., 2005	-	Self-Thinning Power Parameter
Dbhdcmin	0.14	Ameztegui et al., 2012	-	DBH:Crown Diameter ratio for high density stand
Dbhdcmax	0.2	Ameztegui et al., 2012	-	DBH:Crown Diameter ratio for low density stand
<u>Crowding competition</u>				
Hdmax	1.47	Vorspernik et al 2010	m cm ⁻¹	Max Height : DBH ratio
Hdmin	0.47	Vorspernik et al 2010	m cm ⁻¹	Min Height : DBH ratio
Denmax	0.4		trees ha ⁻¹	Maximum density
Denmin	0.01		trees ha ⁻¹	Minimum density

A1.2. Picea abies (L.) parameters set

<u>Parameter</u>	<u>Value</u>	<u>Reference</u>	<u>Unit</u>	<u>Description</u>
Light_tol	2		-	Light tolerance
Phenology	1.2		-	Phenological habitus
Alpha	0.068	Seidl et al., 2005	mol(C) mol(PAR)- 1	Canopy quantum efficiency
Epsilongcmj	-	-	gC mol(PAR)- 1	Light use efficiency
K	0.55	Pietsch et al., 2005	-	Canopy PAR ext. coeff.
Albedo	0.095	Breuer et al., 2003	-	Canopy reflectance
<u>Leaf area</u>				
Laigcx	3.33	Landsberg et al., 2005	-	Max Canopy Conductance LAI
Laimaxintcptn	5	Landsberg et al., 2005	-	Max Canopy Rain Interception LAI
Maxintcptn	0.15	Landsberg et al., 2005	-	Max vapor from Rain Interception

<u>Parameter</u>	<u>Value</u>	<u>Reference</u>	<u>Unit</u>	<u>Description</u>
<u>Specific leaf area</u>				
Sla	94	Pietsch et al., 2005	cm ² gC ⁻¹	Specific Leaf Area
Sla_ratio	2	Mollicone et al., 2002	-	Shaded to sunlit projected SLA
<u>Mass density</u>				
Rhomin	0.43	Seidl et al., 2012	t m ⁻³	Min basic Density for young trees
Rhomax	0.43	Seidl et al., 2012	t m ⁻³	Max basic Density for young trees
<u>Stomatal conductance</u>				
Coeffcond	0.06	Seidl et al., 2012	mbar	Stomatal response to VPD
Blcond	0.2	Seidl et al., 2012	m s ⁻¹	Canopy Boundary Layer Conductance
Maxcond	0.02	Seidl et al., 2012	m s ⁻¹	Maximum Canopy Conductance
<u>Aging</u>				
Maxage	200	Seidl et al., 2012	years	Age for physiological decline
Rage	0.95	Seidl et al., 2012	-	Relative Age to halve age related limiting factor
Nage	4	Seidl et al., 2012	-	Power of relative Age in function for Age
<u>Temperature & photoperiod</u>				
Growthtmin	0	Seidl et al., 2012	°C	Species specific biological 0
Growthtmax	35	Seidl et al., 2012	°C	Maximum Temperature for growth
Growthtopt	17.5	Seidl et al., 2012	°C	Optimal Growth Temperature
Growthstart	400	-	°C d	GDD for Bud Burst
Mindaylength	12	-	h	Photoperiod threshold for leaf fall activation
<u>Water potential</u>				
Swpopen	-0.5	Pietsch et al 2005	KPa	Min soil water potential to keep Stomata open
Swpclose	-2.2	Pietsch et al 2005	KPa	Min soil water potential to close Stomata
Swconst	1	-	-	Constant in Soil Water modifier vs Moist Ratio
Swpower	5	-	-	Power in Soil Water modifier vs Moist Ratio

<u>Parameter</u>	<u>Value</u>	<u>Reference</u>	<u>Unit</u>	<u>Description</u>
<u>Allometry</u>				
<u>Allocation (CTEM)</u>				
Omega_ctem	0.5	Arora et al 2005	-	Environmental dependent Allocation factor
S0ctem	0.05	Arora et al 2005	-	Stem Allocation factor
R0ctem	0.89	Arora et al 2005	-	Root Allocation factor
F0ctem	0.06	Arora et al 2005	-	Foliage Allocation Factor
Fracbb0	0.3	Yuste et al., 2005	-	Branch/Bark at age 0
Fracbb1	0.1	Xenakis et al., 2008	-	Branch/Bark for mature
Fine_root_leaf	0.762	Mollicone et al. 2002	-	Fine roots to Leaf ratio
Stem_leaf	3.42	White et al., 2000	-	Stem to Leaf ratio
Coarse_root_stem	0.23	White et al., 2000	-	Coarse Roots to Stem ratio
Live_total_wood	0.071	Mollicone et al. 2002	-	Sapwood to Hardwood ratio
<u>Sapwood</u>				
Sap_a	3.119	Clausnitzer et al., 2011	-	Sapwood Allometric Parameter
Sap_b	1.4544	Clausnitzer et al., 2011	-	Sapwood Allometric Exp Parameter
Sap_leaf	2600	Köstner et al. 2002	-	Ratio Sapwood MaxLAI
<u>Stem biomass</u>				
Stemconst_p	0.292	Yuste et al 2005	-	Allometric parameter to initialize stem Biomass
Stempower_p	2.0087	Yuste et al 2005	-	Allometric exp parameter to initialize stem Biomass
<u>Height (chapman richards)</u>				
Cra	56	Seidl et al., 2012	m	Max height parameter
Crb	0.0658	Pommerening et al., 2011	-	Exponential decay parameter
Crc	5.5289	Pommerening et al., 2011	-	Shape parameter
<u>Nitrogen</u>				
Cn_leaves	58.8	White et al., 2000	kg C kgN ⁻¹	Leaves C:N
Cn_fine_roots	46.7	White et al., 2000	kg C kgN ⁻¹	Fine roots C:N
Cn_live_woods	50	Pietsch et al 2005	kg C kgN ⁻¹	Wood tissues C:N (live)

<u>Parameter</u>	<u>Value</u>	<u>Reference</u>	<u>Unit</u>	<u>Description</u>
Cn_dead_wood	535	Pietsch et al 2005	kg C kgN-1	Wood tissues C:N (dead)
<u>Phenology</u>				LITTERFALL
Bud_burst	-	-	days	Max Budburst Days
Leaf_fall_frac_growing	-	-		Biome's leaffall time span
Leaf_life_span	0.2	White et al., 2000	years	Average Leaf longevity
<u>Turnover</u>				TURNOVER
Leaves_finertturnover	0.195	Pietsch et al 2005	AIC / year	Fine roots turnover rate
Coarsertturnover	0.02	Kurz et al., 1996	AIC / year	Coarse roots turnover rate
Sapwoodturnover	0.025	Yuste et al., 2005	AIC / year	Sapwood turnover rate
Branchturnover	0.01	Pietsch et al 2005	AIC / year	Branches turnover rate
Live_wood_turnover	0.7	Pietsch et al 2005	AIC / year	Woody tissues turnover rate
<u>Mortality</u>				
Wsx1000	550	Collalti et al., 2013	kg	Max stem mass per tree at 1000 trees
Thinpower	2	Landsberg et al., 2005	-	Self-Thinning Power Parameter
Dbhdcmin	0.14	Ameztegui et al., 2012	-	DBH:Crown Diameter ratio for high density stand
Dbhdcmax	0.18	Kalliovirta and Tokola 2005	-	DBH:Crown Diameter ratio for low density stand
<u>Crowding competition</u>				CROWDING COMPETITION FUNCTION
Hdmax	0.95	Seidl et al., 2012	m cm-1	Max Height : DBH ratio
Hdmin	0.47	Seidl et al., 2012	m cm-1	Min Height : DBH ratio
Denmax	0.4	Collalti (pers. Comm.)	trees ha-1	Maximum density
Denmin	0.01	Collalti (pers. Comm.)	trees ha-1	Minimum density

A1.3. Quercus ilex (L.) parameters set

<u>Parameter</u>	<u>Value</u>	<u>Reference</u>	<u>Unit</u>	<u>Description</u>
Light_tol	2		-	Light tolerance
Phenology	1.1		-	Phenological habitus

<u>Parameter</u>	<u>Value</u>	<u>Reference</u>	<u>Unit</u>	<u>Description</u>
Alpha	0.04	Vitale et al., 2012	mol(C) mol(PAR) -1	Canopy quantum efficiency
Epsilongcmj	-	-	gC mol(PAR) -1	Light use efficiency
K	0.72	Hoff et al., 2002	-	Canopy PAR ext. coeff.
Albedo	0.12	Hoff et al., 2002	-	Canopy reflectance
<u>Leaf area</u>				
Laigcx	3.3	Oerlemans & R.P. Vink 2010	-	Max Canopy Conductance LAI
Laimaxintcptn	5.8	Oerlemans & Vink 2010	-	Max Canopy Rain Interception LAI
Maxintcptn	0.25	Xenakis et al 2008	-	Max vapor from Rain Interception
<u>Specific leaf area</u>				
Sla	82	2002 Chiesi et al., 2007	cm2 gC-1	Specific Leaf Area
Sla_ratio	2	2002 Chiesi et al., 2007	-	Shaded to sunlit projected SLA
<u>Mass density</u>				
Rhomin	0.4	Federici et al., 2008	t m-3	Min basic Density for young trees
Rhomax	0.72	Federici et al., 2008	t m-3	Max basic Density for young trees
<u>Stomatal conductance</u>				
Coeffcond	0.05	Pietsch et al., 2005	mbar	Stomatal response to VPD
Blcond	0.01	Pietsch et al., 2005	m s-1	Canopy Boundary Layer Conductance
Maxcond	0.002 5	Hoff et al., 2002	m s-1	Maximum Canopy Conductance
<u>Aging</u>				
Maxage	120	Bernetti	years	Age for physiological decline
Rage	0.75	Collalti (pers. Com.)	-	Relative Age to halve age related limiting factor
Nage	4	Collalti (pers. Com.)	-	Power of relative Age in function for Age
<u>Temperature & photoperiod</u>				

<u>Parameter</u>	<u>Value</u>	<u>Reference</u>	<u>Unit</u>	<u>Description</u>
Growthtmin	1	Fares et al., 2013	°C	Species specific biological 0
Growthtmax	39	Fares et al., 2013	°C	Maximum Temperature for growth
Growthtopt	23	Fares et al., 2013	°C	Optimal Growth Temperature
Growthstart	450	-	°C d	GDD for Bud Burst
Mindaylength	12	-	h	Photoperiod threshold for leaf fall activation
<u>Water potential</u>				
Swpopen	-0.6	Mollicone et al., 2002	KPa	Min soil water potential to keep Stomata open
Swpclose	-3.2	Mollicone et al., 2002	KPa	Min soil water potential to close Stomata
Swconst	0.4	-	-	Costant in Soil Water modifier vs Moist Ratio
Swpower	3	-	-	Power in Soil Water modifier vs Moist Ratio
<u>Allometry</u>				
<u>Allocation (CTEM)</u>				
Omega_ctem	0.8	Arora et al 2005	-	Environmental dependent Allocation factor
S0ctem	0.1	Arora et al 2005	-	Stem Allocation factor
R0ctem	0.55	Arora et al 2005	-	Root Allocation factor
F0ctem	0.35	Arora et al 2005	-	Foliage Allocation Factor
Fracbb0	0.3	Yuste et al., 2005	-	Branch/Bark at age 0
Fracbb1	0.25	Xenakis et al., 2008	-	Branch/Bark for mature
Fine_root_leaf	1	Mollicone et al 2002	-	Fine roots to Leaf ratio
Stem_leaf	2.2	White et al., 2000	-	Stem to Leaf ratio
Coarse_root_stem	0.22	Mollicone et al 2002	-	Coarse Roots to Stem ratio
Live_total_wood	0.16	P. Thornton (pers. comm.)	-	Sapwood to Hardwood ratio
<u>Sapwood</u>				
Sap_a	0.674	Köstner et al. 2002	-	Sapwood Allometric Parameter
Sap_b	1.992	Köstner et al. 2002	-	Sapwood Allometric Exp Parameter
Sap_leaf	2600	Verbeek et al., 2007	-	Ratio Sapwood MaxLAI
<u>Height (chapman richards)</u>				

<u>Parameter</u>	<u>Value</u>	<u>Reference</u>	<u>Unit</u>	<u>Description</u>
Cra	34.597	Rupsys et al., 2010	m	Max height parameter
Crb	0.038	Rupsys et al., 2010	-	Exponential decay parameter
Crc	1.104	Rupsys et al., 2010	-	Shape parameter
<u>Nitrogen</u>				
Cn_leaves	42	Pietsch et al 2005	kg C kgN-1	Leaves C:N
Cn_fine_roots	42	Mollicone et al., 2002	kg C kgN-1	Fine roots C:N
Cn_live_woods	42	Mollicone et al., 2002	kg C kgN-1	Wood tissues C:N (live)
Cn_dead_woods	300	Chiesi et al., 2007	kg C kgN-1	Wood tissues C:N (dead)
<u>Phenology</u>				
Bud_burst	-	-	days	LITTERFALL Max Budburst Days
Leaf_fall_frac_growing	-	-		Biome's leaffall time span
Leaf_life_span	0.5	White et al., 2000	years	Average Leaf longevity
<u>Turnover</u>				
Leaves_finerttover	0.5	Pietsch et al 2005	AIC / year	TURNOVER Fine roots turnover rate
Coarserttover	0.02	Kurz et al., 1996	AIC / year	Coarse roots turnover rate
Sapwoodttover	0.01	Yuste et al., 2005	AIC / year	Sapwood turnover rate
Branchttover	0.03	Pietsch et al 2005	AIC / year	Branches turnover rate
Live_wood_turnover	0.7	Pietsch et al 2005	AIC / year	Woody tissues turnover rate
<u>Mortality</u>				
Wsx1000	550	Collalti et al., 2013	kg	Max stem mass per tree at 1000 trees
Thinpower	2	Landsberg et al., 2005	-	Self-Thinning Power Parameter
Dbhdcmin	0.18	Ameztegui et al., 2012	-	DBH:Crown Diameter ratio for high density stand
Dbhdcmax	0.24	Ameztegui et al., 2012	-	DBH:Crown Diameter ratio for low density stand
<u>Crowding competition</u>				
Hdmax	1.71	Portoghesi (pers. comm.)	m cm-1	CROWDING COMPETITION FUNCTION Max Height : DBH ratio
Hdmin	0.2	Portoghesi (pers. comm.)	m cm-1	Min Height : DBH ratio

<u>Parameter</u>	<u>Value</u>	<u>Reference</u>	<u>Unit</u>	<u>Description</u>
Denmax	0.8		trees ha-1	Maximum density
Denmin	0.01		trees ha-1	Minimum density

A1.4. Quercus robur (L.) parameters set

<u>Parameter</u>	<u>Value</u>	<u>Reference</u>	<u>Unit</u>	<u>Description</u>
Light_tol	2		-	Light tolerance
Phenology	0.1		-	Phenological habitus
Alpha	0.065	Morecroft et al 2003	mol(C) mol(PAR) -1	Canopy quantum efficiency
Epsilongcmj	1.05	Horn and Shulze 2011	gC mol(PAR) -1	Light use efficiency
K	-	-	-	Canopy PAR ext. coeff.
Albedo	0.2	-	-	Canopy reflectance
<u>Leaf area</u>				
Laigcx	8	-	-	Max Canopy Conductance LAI
Laimaxintcptn	5	-	-	Max Canopy Rain Interception LAI
Maxintcptn	0.038	Pietsch et al 2005	-	Max vapor from Rain Interception
<u>Specific leaf area</u>				
Sla	480	Pietsch et al 2005	cm2 gC-1	Specific Leaf Area
Sla_ratio	1.49	Mollicone et al., 2002	-	Shaded to sunlit projected SLA
<u>Mass density</u>				
Rhomin	0.5	Knopic et al., 2007	t m-3	Min basic Density for young trees
Rhmax	0.66	Knopic et al., 2007	t m-3	Max basic Density for young trees
<u>Stomatal conductance</u>				
Coeffcond	0.05	-	mbar	Stomatal response to VPD
Blcond	0.2	Pietsch et al 2005	m s-1	Canopy Boundary Layer Conductance
Maxcond	0.02	Nolè et al., 2002	m s-1	Maximum Canopy Conductance
<u>Aging</u>				
Maxage	300	Nolè et al., 2002	years	Age for physiological decline

<u>Parameter</u>	<u>Value</u>	<u>Reference</u>	<u>Unit</u>	<u>Description</u>
Rage	0.8	-	-	Relative Age to halve age related limiting factor
Nage	4	-	-	Power of relative Age in function for Age
<u>Temperature & photoperiod</u>				
Growthtmin	0	-	°C	Species specific biological 0
Growthtmax	35	-	°C	Maximum Temperature for growth
Growthtopt	17.66	Horn and Shulze 2011	°C	Optimal Growth Temperature
Growthstart	400	-	°C d	GDD for Bud Burst
Mindaylength	11	-	h	Photoperiod threshold for leaf fall activation
<u>Water potential</u>				
Swopen	-0.5	Cenciala and Tatarinov 2006	KPa	Min soil water potential to keep Stomata open
Swpclose	-2.5	Cenciala and Tatarinov 2006	KPa	Min soil water potential to close Stomata
Swconst	1	-	-	Constant in Soil Water modifier vs Moist Ratio
Swpower	5	-	-	Power in Soil Water modifier vs Moist Ratio
<u>Allometry</u>				
<u>Allocation (CTEM)</u>				
Omega_ctem	0.8	Arora et al 2005	-	Environmental dependent Allocation factor
S0ctem	0.1	Arora et al 2005	-	Stem Allocation factor
R0ctem	0.55	Arora et al 2005	-	Root Allocation factor
F0ctem	0.35	Arora et al 2005	-	Foliage Allocation Factor
Fracbb0	0.1	Yuste et al., 2005	-	Branch/Bark at age 0
Fracbb1	0.36	Yuste et al., 2005	-	Branch/Bark for mature
Fine_root_leaf	1.2	Pietsch et al., 2005	-	Fine roots to Leaf ratio
Stem_leaf	1.32	Mollicone et al 2002	-	Stem to Leaf ratio
Coarse_root_stem	0.26	Pietsch et al., 2005	-	Coarse Roots to Stem ratio

<u>Parameter</u>	<u>Value</u>	<u>Reference</u>	<u>Unit</u>	<u>Description</u>
Live_total_wood	0.05	-	-	Sapwood to Hardwood ratio
<u>Sapwood</u>				
Sap_a	0.043	Köstner et al. 2002	-	Sapwood Allometric Parameter
Sap_b	2.384	Köstner et al. 2002	-	Sapwood Allometric Exp Parameter
Sap_leaf	4000	Hickler et al 2012	-	Ratio Sapwood MaxLAI
<u>Stem biomass</u>				
Stemconst_p	0.065 4	Yuste et al 2005	-	Allometric parameter to initialize stem Biomass
Stempower_p	2.575 3	Yuste et al 2005	-	Allometric exp parameter to initialize stem Biomass
<u>Height (chapman richards)</u>				
Cra	21	Yuste et al 2005	m	Max height parameter
Crb	0.059 9	Yuste et al 2005	-	Exponential decay parameter
Crc	1.074	Yuste et al 2005	-	Shape parameter
<u>Nitrogen</u>				
Cn_leaves	16.16	Mollicone et al., 2002	kg C kgN-1	Leaves C:N
Cn_fine_roots	48	Mollicone et al., 2002	kg C kgN-1	Fine roots C:N
Cn_live_woods	50	Mollicone et al., 2002	kg C kgN-1	Wood tissues C:N (live)
Cn_dead_woods	451	Pietsch et al., 2005	kg C kgN-1	Wood tissues C:N (dead)
<u>Phenology</u>				
LITTERFALL				
Bud_burst	15	-	days	Max Budburst Days
Leaf_fall_frac_growing	0.3	Pietsch et al., 2005	-	Biome's leaffall time span
Leaf_life_span	1	-	years	Average Leaf longevity
<u>Turnover</u>				
TURNOVER				
Leaves_finerttover	1	Pietsch et al 2005	AIC / year	Fine roots turnover rate
Coarserttover	0.03	Pietsch et al 2005	AIC / year	Coarse roots turnover rate
Sapwoodttover	0.025	Pietsch et al 2005	AIC / year	Sapwood turnover rate
Branchttover	0.01	Pietsch et al 2005	AIC / year	Branches turnover rate
Live_wood_turnover	0.7	Pietsch et al 2005	AIC / year	Woody tissues turnover rate
<u>Mortality</u>				
Wsx1000	550	Collalti et al., 2013	kg	Max stem mass per tree at 1000 trees

<u>Parameter</u>	<u>Value</u>	<u>Reference</u>	<u>Unit</u>	<u>Description</u>
Thinpower	2	Landsberg et al., 2005	-	Self-Thinning Power Parameter
Dbhdcmin	0.2	Bellio and Pividori, 2009	-	DBH:Crown Diameter ratio for high density stand
Dbhdcmax	0.26	Bellio and Pividori, 2009	-	DBH:Crown Diameter ratio for low density stand
<u>Crowding competition</u>				
Hdmax	2.5	Bellio and Pividori, 2009	m cm-1	Max Height : DBH ratio
Hdmin	0.4	Bellio and Pividori, 2009	m cm-1	Min Height : DBH ratio
Denmax	0.3		trees ha-1	Maximum density
Denmin	0.02		trees ha-1	Minimum density

A1.5. Fagus sylvatica (L.) parameters set

<u>Parameter</u>	<u>Value</u>	<u>Reference</u>	<u>Unit</u>	<u>Description</u>
Light_tol	2		-	Light tolerance
Phenology	0.1		-	Phenological habitus
Alpha	0.0 55	Vitale et al., 2012	mol(C) mol(PAR)- 1	Canopy quantum efficiency
Epsilongcmj	-	-	gC mol(PAR)- 1	Light use efficiency
K	0.7 1	Vitale et al., 2012	-	Canopy PAR ext. coeff.
Albedo	0.0 1	-	-	Canopy reflectance
<u>Leaf area</u>				
Laigcx	8	-	-	Max Canopy Conductance LAI
Laimaxintcptn	5	Pietsch et al 2005	-	Max Canopy Rain Interception LAI
Maxintcptn	0.3 3	lovino et al., 2009	-	Max vapor from Rain Interception
<u>Specific leaf area</u>				
Sla	480	Pietsch et al 2005	cm2 gC-1	Specific Leaf Area

<u>Parameter</u>	<u>Value</u>	<u>Reference</u>	<u>Unit</u>	<u>Description</u>
Sla_ratio	2	Pietsch et al 2005	-	Shaded to sunlit projected SLA
<u>Mass density</u>				
Rhomin	0.6 4	D'andrea (pers. Comm.)	t m-3	Min basic Density for young trees
Rhomas	0.6 4	D'andrea (pers. Comm.)	t m-3	Max basic Density for young trees
<u>Stomatal conductance</u>				
Coeffcond	0.0 6	Pietsch et al 2005	mbar	Stomatal response to VPD
Blcond	0.0 1	Pietsch et al 2005	m s-1	Canopy Boundary Layer Conductance
Maxcond	0.0 2	Breuer et al, 2003	m s-1	Maximum Canopy Conductance
<u>Aging</u>				
Maxage	200		years	Age for physiological decline
Rage	0.7 5		-	Relative Age to halve age related limiting factor
Nage	10		-	Power of relative Age in function for Age
<u>Temperature & photoperiod</u>				
Growthtmin	0	Williams 1996	°C	Species specific biological 0
Growthtmax	40	Williams 1996	°C	Maximum Temperature for growth
Growthtopt	20	Lyr & Garbe, 1995	°C	Optimal Growth Temperature
Growthstart	480	-	°C d	GDD for Bud Burst
Mindaylength	12	-	h	Photoperiod threshold for leaf fall activation
<u>Water potential</u>				
Swopen	- 0.6	Mollicone et al., 2002	KPa	Min soil water potential to keep Stomata open
Swpclose	- 2.3	Mollicone et al., 2002	KPa	Min soil water potential to close Stomata
Swconst	1	-	-	Costant in Soil Water modifier vs Moist Ratio
Swpower	5	-	-	Power in Soil Water modifier vs Moist Ratio
<u>Allometry</u>				
<u>Allocation</u> <u>(CTEM)</u>				

<u>Parameter</u>	<u>Value</u>	<u>Reference</u>	<u>Unit</u>	<u>Description</u>
Omega_ctem	0.8	Arora et al 2005	-	Environmental dependent Allocation factor
S0ctem	0.1	Arora et al 2005	-	Stem Allocation factor
R0ctem	0.5 5	Arora et al 2005	-	Root Allocation factor
F0ctem	0.3 5	Arora et al 2005	-	Foliage Allocation Factor
Fracbb0	0.4		-	Branch/Bark at age 0
Fracbb1	0.1 25	Damesin et al., 2003	-	Branch/Bark for mature
Fine_root_leaf	1.5 45	Pietsch et al., 2005	-	Fine roots to Leaf ratio
Stem_leaf	1	White et al., 2000	-	Stem to Leaf ratio
Coarse_root_stem	0.3 6	Mollicone et al., 2002	-	Coarse Roots to Stem ratio
Live_total_wood	0.1 54	Pietsch et al., 2005	-	Sapwood to Hardwood ratio
<u>Sapwood</u>				
Sap_a	0.6 74	Köstner et al. 2002	-	Sapwood Allometric Parameter
Sap_b	1.9 92	Köstner et al. 2002	-	Sapwood Allometric Exp Parameter
Sap_leaf	341 0	Bartelink 1998	-	Ratio Sapwood MaxLAI
<u>Stem biomass</u>				
Stemconst_p	0.2 837	D'andrea (pers. Comm.)	-	Allometric parameter to initialize stem Biomass
Stempower_p	2.1 34	D'andrea (pers. Comm.)	-	Allometric exp parameter to initialize stem Biomass
<u>Height (chapman richards)</u>				
Cra	34. 597	-	m	Max height parameter
Crb	0.0 38	-	-	Exponential decay parameter
Crc	1.1 04	-	-	Shape parameter
<u>Nitrogen</u>				
Cn_leaves	18. 6	Campoli et al., 2013	kg C kgN- 1	Leaves C:N
Cn_fine_roots	48. 2	Mollicone et al., 2002	kg C kgN- 1	Fine roots C:N
Cn_live_woods	112	Mollicone et al., 2002	kg C kgN- 1	Wood tissues C:N (live)
Cn_dead_woods	375	Pietsch et al., 2005	kg C kgN- 1	Wood tissues C:N (dead)
<u>Phenology</u>				
Bud_burst	10	-	days	LITTERFALL Max Budburst Days

<u>Parameter</u>	<u>Value</u>	<u>Reference</u>	<u>Unit</u>	<u>Description</u>
Leaf_fall_frac_growing	0.3	Pietsch et al., 2005		Biome's leaffall time span
Leaf_life_span	-	-	years	Average Leaf longevity
<u>Turnover</u>				
				TURNOVER
Leaves_finertturnover	1	Pietsch et al 2005	AIC / year	Fine roots turnover rate
Coarsertturnover	0.0 2	Kurz et al., 1996	AIC / year	Coarse roots turnover rate
Sapwoodturnover	0.0 1	Bartelink 1998	AIC / year	Sapwood turnover rate
Branchturnover	0.0 5	Bartelink 1998	AIC / year	Branches turnover rate
Live_wood_turnover	0.7	-	AIC / year	Woody tissues turnover rate
<u>Mortality</u>				
Wsx1000	550	Collalti et al., 2013	kg	Max stem mass per tree at 1000 trees
Thinpower	2	-	-	Self-Thinning Power Parameter
Dbhdcmin	0.1 4	Ameztegui et al., 2012	-	DBH:Crown Diameter ratio for high density stand
Dbhdcmax	0.1 8	D'andrea (pers. Comm.)	-	DBH:Crown Diameter ratio for low density stand
				CROWDING COMPETITION FUNCTION
<u>Crowding competition</u>				
Hdmax	1.7 1	Portoghesi (pesr. Com)	m cm-1	Max Height : DBH ratio
Hdmin	0.2	Portoghesi (pesr. Com)	m cm-1	Min Height : DBH ratio
Denmax	0.1		trees ha-1	Maximum density
Denmin	-		trees ha-1	Minimum density

Appendix 2: Initialization sets

A1.1. ITRen initialization data

<u>Parameter</u>	<u>Value</u>	<u>Unit</u>	<u>Description</u>
Age	30	y	Cohort Age
	90		
	140		
N	501	trees	Cohort trees
	85		
	93		
Dbh	9.64	cm	Cohort average DBH
	24.11		
	45.14		
H	10.00	m	Cohort average H
	16.70		
	24.60		
Elev	1735	m a.s.l.	Elevation
Min_frac_maxasw	0.1		Max swc: min swc
Clay_perc	11.9	%	clay % content
Silt_perc	38.7	%	silt % content
Sand_perc	49.4	%	sand % content
Bulk_density	1.5	g/cm ³	Bulk density
Soil_depth	60	cm	profile depth
Soil_ph	4.2		soil pH
Insoc	2.2	KgC/m ²	TOC at day 0
Litfrac	0.1		TOC litter fraction at day 0
Humafract	0.417		TOC labile humus at day 0
Humufract	0.483		TOC recalcitrant humus at day 0
Biofract	0.05		qMic at day 0

A2.2. FRPue initialization data

<u>Parameter</u>	<u>Value</u>	<u>Unit</u>	<u>Description</u>
Age	59	y	Cohort Age
N	6149	trees	Cohort trees
Dbh	7.00	cm	Cohort average DBH
H	6.00	m	Cohort average H
Elev	270	m a.s.l.	Elevation
Min_frac_maxasw	0.18		Max swc: min swc
Clay_perc	38.8	%	clay % content
Silt_perc	35.2	%	silt % content
Sand_perc	26	%	sand % content
Bulk_density	1.17	g/cm ³	Bulk density
Soil_depth	50	cm	profile depth
Soil_ph	7.6		soil pH
Insoc	4.5	KgC/m ⁻²	TOC at day 0
Litfrac	0.01		TOC litter fraction at day 0
Humafract	0.025		TOC labile humus at day 0
Humufract	0.965		TOC recalcitrant humus at day 0
Biofract	0.05		qMic at day 0

A2.3. DEHai initialization data

<u>Parameter</u>	<u>Value</u>	<u>Unit</u>	<u>Description</u>
Age	120	y	Cohort Age
N	334	trees	Cohort trees
Dbh	30.80	cm	Cohort average DBH
H	23.10	m	Cohort average H
Elev	445	m a.s.l.	Elevation
Min_frac_maxasw	0.19		Max swc: min swc
Clay_perc	40	%	clay % content
Silt_perc	56	%	silt % content
Sand_perc	4	%	sand % content
Bulk_density	0.8	g/cm ³	Bulk density
Soil_depth	60	cm	profile depth
Soil_ph	5.4		soil pH
Insoc	3.681	KgC/m ⁻²	TOC at day 0
Litfrac	0.05		TOC litter fraction at day 0
Humafract	0.385		TOC labile humus at day 0
Humufract	0.605		TOC recalcitrant humus at day 0
Biofract	0.05		qMic at day 0

A2.4. DKSor initialization data

<u>Parameter</u>	<u>Value</u>	<u>Unit</u>	<u>Description</u>
Age	80	y	Cohort Age
N	283	trees	Cohort trees
Dbh	36.13	cm	Cohort average DBH
H	25.00	m	Cohort average H
Elev	40	m a.s.l.	Elevation
Min_frac_maxasw	0.1		Max swc: min swc
Clay_perc	17	%	clay % content
Silt_perc	40	%	silt % content
Sand_perc	43	%	sand % content
Bulk_density	1.05	g/cm ³	Bulk density
Soil_depth	150	cm	profile depth
Soil_ph	5		soil pH
Insoc	9.661	KgC/m ⁻²	TOC at day 0
Litfrac	0.04		TOC litter fraction at day 0
Humafract	0.546		TOC labile humus at day 0
Humufract	0.45		TOC recalcitrant humus at day 0
Biofract	0.05		qMic at day 0

A2.5. BEBra initialization data (Pedunculate Oak stand)

<u>Parameter</u>	<u>Value</u>	<u>Unit</u>	<u>Description</u>
Age	65	y	Cohort Age
	65		
N	130	trees	Cohort trees
	153		
Dbh	40	cm	Cohort average DBH
	15.03		
	27.87		
H	42.90	m	Cohort average H
	13.00		
	17.46		
Elev	20.44	m a.s.l.	Elevation
Min_frac_maxasw	16		Max swc: min swc
Clay_perc	0.1	%	clay % content

<u>Parameter</u>	<u>Value</u>	<u>Unit</u>	<u>Description</u>
Silt_perc	8	%	silt % content
Sand_perc	85	%	sand % content
Bulk_density	1.5	g/cm ³	Bulk density
Soil_depth	60	cm	profile depth
Soil_ph	4.5		soil pH
Insoc	7	KgC/m ²	TOC at day 0
Litfrac	0.01		TOC litter fraction at day 0
Humafract	0.025		TOC labile humus at day 0
Humufract	0.965		TOC recalcitrant humus at day 0
Biofract	0.05		qMic at day 0

A2.6. BEBra initialization data (Scot Pine stand)

<u>Parameter</u>	<u>Value</u>	<u>Unit</u>	<u>Description</u>
Age	72	y	Cohort Age
N	379	trees	Cohort trees
Dbh	28.65	cm	Cohort average DBH
H	21.33	m	Cohort average H
Elev	16	m a.s.l.	Elevation
Min_frac_maxasw	0.1		Max swc: min swc
Clay_perc	7	%	clay % content
Silt_perc	8	%	silt % content
Sand_perc	85	%	sand % content
Bulk_density	1.5	g/cm ³	Bulk density
Soil_depth	135	cm	profile depth
Soil_ph	3.8		soil pH
Insoc	16.3	KgC/m ²	TOC at day 0
Litfrac	0.01		TOC litter fraction at day 0
Humafract	0.025		TOC labile humus at day 0
Humufract	0.965		TOC recalcitrant humus at day 0
Biofract	0.05		qMic at day 0

A2.7. FIHy initialization data

<u>Parameter</u>	<u>Value</u>	<u>Unit</u>	<u>Description</u>
Age	39	y	Cohort Age
N	2500	trees	Cohort trees
Dbh	10.56	cm	Cohort average DBH
H	13.00	m	Cohort average H
Elev	181	m a.s.l.	Elevation
Min_frac_maxasw	0.07		Max swc: min swc
Clay_perc	11	%	clay % content
Silt_perc	19	%	silt % content
Sand_perc	70	%	sand % content
Bulk_density	1.15	g/cm ³	Bulk density
Soil_depth	75	cm	profile depth
Soil_ph	3.9		soil pH
Insoc	5.618	KgC/m ²	TOC at day 0
Litfrac	0.06		TOC litter fraction at day 0
Humafract	0.125		TOC labile humus at day 0
Humufract	0.825		TOC recalcitrant humus at day 0
Biofract	0.05		qMic at day 0

ACKNOWLEDGEMENTS

I thank all those involved in the CarboEurope Project and the PIs who provided the data on which this analysis is based. Special thanks go to Stefano Minerbi and Leonardo Montagnani, who gently provided soil data for the Renon forest. I greatly thank all the people of the CMCC (VT) IAFENT division, for having given me the opportunity to work with them, supported my ideas making me feel part of their Lab. I especially thank Alessio “the Dominus” Collalti, for having introduced me in the modeling world and having believed in my capabilities; it was a risk to put the versioned model in my hands, but I hope it worthed it. I thank him for the support, the advices, the jokes and the coral singing of Junk Roman humoristic music (he knows what I’m talking about); thank you, and give a kiss to your and Elisa daughter from me. I really thank Tommaso Chiti, for the everlasting kindness, congeniality and reliability; he has been a wonderful advisor. I thank Monia Santini, Antonio Bombelli, Sergio Noce, Arianna Di Paolo, Gaia V. Laurin, Lucia Perugini, Elisa Grieco and Francesca Pretto for their kindness, the opportunities, their advises, data, but especially for their congeniality and availability. I thank Riccardo Valentini to have formely accepted me as a thesist, always found a good word for me, and supported my interest in process oriented modeling. I thank Dario Papale for having me introduced in the field, maybe unconsciously, many years ago. I thank Andrea Borgia to have advised me on how always look for the brightest star, on aiming high and do not settle.

I thank my family, my Mother and Father, Brotheroni and Valerioni, for having supported me all these years, to have heard and advised me in the light and dark of these times. I thank Flavia, for having sustained my heaviness, my tours de force, my always speaking of how much modeling may be cool and the key to constrain Climate Change; I really thank you, and give you the bad new that maybe the next months I’m still going to have another tour. I thank all my friends, the new ones and the everlasting ones. May my bound with all of you never fade.